2020

HETEROGENEOUS UNCERTAINTY QUANTIFICATION FOR RELIABILITY-BASED DESIGN OPTIMIZATION

Mingyang Li

HETEROGENEOUS UNCERTAINTY QUANTIFICATION FOR RELIABILITY-BASED DESIGN OPTIMIZATION

By

Mingyang Li

A DISSERTATION

Submitted in partial fulfillment of the requirement for the degree of

DOCTOR OF PHILOSOPHY

In Mechanical Engineering – Engineering Mechanics

MICHIGAN TECHNOLOGICAL UNIVERSITY

2020

This dissertation has been approved in partial fulfillment of the requirements for the Degree of DOCTOR OF PHILOSOPHY in Mechanical Engineering-Engineering Mechanics.

Department of Mechanical Engineering – Engineering Mechanics

Dissertation Advisor:	*Dr. Zequn Wang.*
Committee Member:	*Dr. Trisha Sain*
Committee Member:	*Dr. Yongchao Yang*
Committee Member:	*Dr. Zhen Liu*
Department Chair:	*Dr. William Predebon.*

Table of Contents

PREFACE

Included in Chapter 4, Chapter 5, Chapter 6, Chapter 7, Chapter 8 are journal articles, respectively. Included in Chapter 3 is a journal article under review. They are reproduced in their entirety. I have written these journal papers as the lead contributor. As the co-author of all the articles, Dr. Zequn Wang has provided critical comments and important guidance.

ACKNOWLEDGEMENT

First and foremost, I would like to give my greatest appreciation to my advisor, Dr. Zequn Wang, for his constant encouragement, patient guidance, and generous support throughout my entire career at Michigan Tech. His creative mind and great passion for research inspired me to face the challenges I have encountered in my research. He is always generous to give me suggestions, and help me explore new research areas. I'm very grateful to Dr. Wang, without whose help I wouldn't make these remarkable progresses and gain such achievements. I would like to thank Dr. Trisha Sain, Dr. Yongchao Yang, and Dr. Zhen Liu for serving as my committee members and providing insightful feedback.

I want to express my thanks to all my teammates for their support, assistance, and friendship, especially Yunsheng, Narry, and Madhoo, who helped me dig into new research areas. I would like to give my sincere gratitude, Zhuyong Yang, Xin Wang, Haitao Cao, Zhihao Zhao, Xuebin Yang, Jiangyang Lyu, Jiajun Song, Xiang Zhou, Zhouquan Wu, Chong Cao, Jiongxun Zhang, Zhuo Xu, Yilin Wang, Zongjing Wu, and Shuaidong Zhao.

At last, I would like to express my deepest thanks to my mother Ming Sun, my father Jianjun Li, and my wife Mengjuan Ma for their unconditional love and support throughout my life.

ABSTRACT

Uncertainty is inherent to real-world engineering systems, and reliability analysis aims at quantitatively measuring the probability that engineering systems successfully perform the intended functionalities under various sources of uncertainties. In this dissertation, heterogeneous uncertainties including input variation, data uncertainty, simulation model uncertainty, and time-dependent uncertainty have been taken into account in reliability analysis and reliability-based design optimization (RBDO). The input variation inherently exists in practical engineering system and can be characterized by statistical modeling methods. Data uncertainty occurs when surrogate models are constructed to replace the simulations or experiments based on a set of training data, while simulation model uncertainty is introduced when high-fidelity simulation models are built through idealizations and simplifications of real physical processes or systems. Time-dependent uncertainty is involved when considering system or component aging and deterioration. Ensuring a high level of system reliability is one of the critical targets for engineering design, and this dissertation studies effective reliability analysis and reliability-based design optimization (RBDO) techniques to address the challenges of heterogeneous uncertainties.

First of all, a novel reliability analysis method is proposed to deal with input randomness and time-dependent uncertainty. An ensemble learning framework is designed by integrating the Long short-term memory (LSTM) and feedforward neural network. Time-series data is utilized to construct a surrogate model for capturing the time-dependent responses with respect to input variables and stochastic processes. Moreover, a RBDO

framework with Kriging technique is presented to address the time-dependent uncertainty in design optimization. Limit state functions are transformed into time-independent domain by converting the stochastic processes and time parameter to random variables, and Kriging surrogate models are then built and enhanced by a design-driven adaptive sampling scheme to accurately identify potential instantaneous failure events.

Secondly, an equivalent reliability index (ERI) method is proposed for handling both input variations and surrogate model uncertainty in RBDO. To account for the surrogate model uncertainty, a Gaussian mixture model is constructed based on Gaussian process model predictions. To propagate both input variations and surrogate model uncertainty into reliability analysis, the statistical moments of the GMM is utilized for calculating an equivalent reliability index. The sensitivity of ERI with respect to design variables is analytically derived to facilitate the surrogate model-based product design process, lead to reliable optimum solutions.

Thirdly, different effective methods are developed to handle the simulation model uncertainty as well as the surrogate model uncertainty. An active resource allocation framework is proposed for accurate reliability analysis using both simulation and experimental data, where a two-phase updating strategy is developed for reducing the computational costs. The framework is further extended for RBDO problems, where multi-fidelity design algorithm is presented to ensure accurate optimum designs while minimizing the computational costs. To account for both the bias terms and unknown parameters in the simulation model, Bayesian inference method is adopted for building a validated surrogate model, and a Bayesian-based mixture modeling method is developed to ensure reliable system designs with the consideration of heterogeneous uncertainties.

1 INTRODUCTION

1.1 Research Backgrounds

In the past decades, reliability analysis and reliability-based design optimization (RBDO) techniques have gained increasing attention in practical engineering applications. Reliability analysis aims at quantitatively measuring the probability that engineering systems successfully perform the intended functionalities under various sources of uncertainties. Uncertainty is inherent to real-world engineering systems, and reliability-based design optimization is utilized to provide optimum system designs that have the best compromise between cost and system reliability.

With the rapid development of computational power, computer simulations become more popular for representing physical processes. However, the computational costs limit the application of such simulation models in reliability analysis and RBDO. Surrogate modeling is a popular method to reduce the computational burden, which consists of replacing the expensive model by an easy-to-evaluate model fitted to a few data points called design of experiments (DoE). As a result, the accuracy of the surrogate model strongly affects the performance of reliability analysis and RBDO.

Performing an accurate yet efficient reliability analysis is of critical importance in RBDO as it involves repeatedly running expensive simulations. However, most of the existing reliability analysis and RBDO approached only accounts for the system input variations, which is also known as the aleatory uncertainty that inherently exists in practical engineering system such as material properties and manufacturing batch to batch

variations. Different types of heterogeneous uncertainties are summarized in Table 1.1. Given different combinations of these heterogeneous uncertainties, effective methods should be utilized for ensuring accurate reliability analysis or reliable optimum designs.

Table 1.1: Types of heterogeneous uncertainties

Type	Uncertainty	Description
A	Input uncertainty	Inherently exists in practical engineering system due to natural randomness
B	Surrogate model uncertainty	The prediction errors due to the lack of training data
C	Simulation model uncertainty (bias & parameter)	The response differences between real experiments and simulations, due to simplification and unknown parameters
D	Time-dependent uncertainty	Exist widely in the time-dependent performance degeneration processes of engineering systems

Model form uncertainty is also known as the simulation model uncertainty, which is introduced when high-fidelity simulation models are built through idealizations and simplifications of real physical processes or systems. Similarly, data uncertainty (or surrogate model uncertainty) occurs if low-fidelity surrogate models is constructed to replace the high-fidelity simulation models based on a set of simulations runs. The input variation, also known as aleatory uncertainty, inherently exists in practical engineering system such as material properties, and manufacturing batch to batch variations, which can be characterized by statistical modeling methods. A general formulation for quantifying the model form uncertainty is expressed as [1]

$$y^e(\mathbf{x}) = y^m(\mathbf{x}, \boldsymbol{\theta}) + \delta(\mathbf{x}) + \varepsilon \tag{1.1}$$

where $y^e(\mathrm{x})$ denotes the actual observations of a physical process, $y^m(\mathrm{x}, \theta)$ represents the simulation model response as a function of inputs x and unknown parameters θ, which

is also referred to as calibration parameter, θ_{ture} is the vector of true values for the unknown parameters, $\delta(x)$ represents the bias or discrepancy function that characterize the differences between simulation and experiment output. In this work, the experimental error is assumed to be neglectable as the model bias and unknown parameters are more dominant than experimental error in reality. As shown in Eq. (1.1), two main sources of model form uncertainties can be identified as: 1) the model parameters that fixed in real physics but is unknown in simulation model and 2) model discrepancy due to flawed understanding of the system. Inappropriate managing model form uncertainty may introduce significant errors in predicting system responses, resulting in inaccurate reliability assessment and untrustworthy optimal designs. Surrogate models can be constructed based on simulations and experimental data to further reduce the computational costs. However, the data uncertainty is introduced due to the limited number of training. As a result, errors are inevitable when using surrogates to predict the actual performance of the physical system.

1.2 Research Objectives

1.2.1 Efficient time-dependent reliability analysis and RBDO

Time-variant RBDO, referred to as "tRBDO", seeks optimum system designs with a high reliability level over time under time-variant uncertainties such as stochastic operation condition and system aging. Thus, the time-variant reliability analysis in tRBDO often involves stochastic processes and time parameters and thus is technically difficult and computationally expensive. Though vast efforts have been investigated for time-variant reliability assessment, a rigorous formulation is still lacking for generic time-variant reliability-based design optimization (tRBDO) and it remains a grand challenge to handle

such complexity associated with both stationary and non-stationary stochastic processes in tRBDO. Moreover, how to efficiently conduct the time-dependent reliability analysis for problems involving stochastic processes still remains a challenge.

Research solution 1: A LSTM-based Ensemble Learning Framework for Time-Dependent Reliability Analysis. To be specific, multiple long short-term memory networks are employed to learn the random behavior of the system response with respect to the stochastic process while fixing the random variables. The benefit of constructing the LSTM models lies in that they can accurately predict system responses given any new random realizations of the stochastic process. With the LSTM models, a set of artificial data is collected according to different random realizations of the stochastic process. To quantify the uncertainty due to the random variables as well as the stochastic process, a deep feedforward neural network (DFN) is employed. The artificial data set is utilized to train the DFN, which is served as a surrogate model of the time-dependent limit state function. By employing the Gaussian process (GP) regression, the number of neurons of the DFN is determined through an approximated response surface. As a result, the well trained DFN can be utilized to make predictions of the minimum value of time-dependent response given any random realizations of variable and stochastic process. By employing the Monte Carlo simulation, the proposed approach can be directly utilized for estimating the time-dependent reliability without incurring extra computational costs.

Research solution 2: Time-variant reliability-based design optimization using sequential kriging modeling. This approach employs a transformation scheme for dimension reduction of performance functions with stochastic process. A Kriging surrogate model is developed based on the transformed random variables and a sequential sampling

update method is adopted for increasing the fidelity of the surrogate model. Time-variant probability of failure is accurately estimated by applying the MCS method based on the updated Kriging model. For the design process, stochastic sensitivity is approximated by the first-order score function without incurring any extra computational cost.

1.2.2 Surrogate model uncertainty quantification in RBDO

Surrogate modeling methods have been widely used to replace the computationally expensive simulations using a set of training data, and thus alleviate the computational burden of simulation-based reliability assessment. The accuracy of response predictions using surrogates varies over the input domain, and highly depends on the amount and locations of training data points. The major issue of surrogate modeling lies in that there is no rigorous means of quantifying and propagating the surrogate model uncertainty due to the lack of training data, which may result in less confidence in predicting the probability of failure. Ignoring surrogate model uncertainty in simulation-based design optimization with insufficient training data may lead to inaccurate predictions and unreliable system design.

Research solution 3: Surrogate model uncertainty quantification for reliability-based design optimization. An equivalent reliability index (ERI) method is presented for handling both input variation and surrogate model uncertainty in RBDO. The ERI first employs Gaussian process (GP) regression to build surrogates of expensive simulations for predicting the performances of system at unobserved points within input domain as normal distributed random variables. Then a Gaussian mixture model (GMM) will be formed to propagate both the input variations and surrogate model uncertainty simultaneously in

characterizing the stochastic behavior of system performance. With the development of GMM, an equivalent reliability index is derived based on the statistical moments of the GMM to approximate the probability of failure. To facilitate the ERI-based RBDO, we also derive the sensitivity of ERI with respect to design variables analytically without requiring extra training data.

1.2.3 Simulation model uncertainty quantification in reliability analysis and RBDO

Most reliability analysis methods are performed purely based on simulation models, which are assumed to be able to accurately represent the real physics. However, simulation models are often established based on idealization and simplification of the physical process. Therefore, conventional reliability analysis methods may be unreliable as they lack the capability to account for the model bias, which is referred to as the differences in simulation results and actual physical observations. To validate the simulation model, data are needed from both the simulations and experimental observations, and surrogate models can be constructed for predicting experiment responses. Therefore, the simulation and experimental data used for simulation model validation highly affects the accuracy of the response predictions from the surrogate model. In most existing model bias correction methods, design of experiments using random sampling approach is employed for obtaining simulation results and experimental observations. As a result, resources including both simulations and experiments are not well allocated, resulting in inaccurate reliability approximations and unfordable costs. In reality, the experimental data is often limited as the cost dramatically increases with the number of experiments, and the cost of running high-fidelity simulations cannot be ignored. Therefore, an efficient resource allocation approach needs to be developed for smartly choosing the best input sites for both

simulations and experiments, and hence balance the tradeoff between costs and accuracy of reliability assessment.

With the rapid development of computational power, computer simulations become more popular for representing physical processes and RBDO is often conducted based on predictive simulation models. However, a simulation model is often established based on approximations and simplifications of a physical process, and most of existing RBDO methods assume that simulation models are accurate, resulting in risky designs due to the ignorance of model form uncertainty (aka simulation model uncertainty). Therefore, simulation models have to be validated using experimental observations before it is utilized for engineering design under uncertainty. Mixture uncertainties due to model imperfection, lack of training data, and input variations coexist in practical simulation-based design applications. Despite the development of advanced approaches in managing different types of uncertainties individually, it remains challenging to handle the heterogeneity of different sources of uncertainties in uncertainty propagation and system design process.

Research solution 4: Active resource allocation for reliability analysis with model bias correction. Instead of randomly allocating resources, the proposed ARA approach introduces a two-phase strategy for sequentially identifying the important samples for running simulations and conducting experiments. In ARA, Gaussian process modeling technique is employed for correcting the model bias and quantifying the sufficiency of data. Based on a set of initial simulation data, GP model is first built for replacing the simulation model, then an adaptive sampling method is employed for updating the simulation data in phase I of ARA. To determine the experimental data that can effectively correct the simulation model, a new sample insertion criterion is proposed in phase II for iteratively

identifying the best input site for experiment. At each iteration, the available experimental data and simulation data are combined for model bias correction, and a hybrid GP model for the actual experimental response can be constructed accordingly. Then the Monte Carlo simulation method is employed for reliability analysis while the response is predicted by the GP model. The updating process in phase II is iteratively performed to enhance the fidelity of the hybrid GP model until the reliability approximations converge.

Research solution 5: Reliability-based multi-fidelity optimization using adaptive hybrid learning. In this work, we propose a reliability-based multi-fidelity design optimization (RBMO) framework to deal with design problems involving low- and high-fidelity data. In RBMO, the costs of running low- and high-fidelity models are reduced by introducing an adaptive hybrid learning (AHL) algorithm, which identifies new training samples for low- and high-fidelity model in a sequential manner. With available low- and high-fidelity data, a hybrid GP model can be constructed using GP-based multi-fidelity data fusion technique. Then the updated hybrid GP model is utilized for reliability and sensitivity analysis in solving an RBDO problem, leading to a pseudo optimal solution. At each iteration of RBMO, the adaptive hybrid learning and RBDO processes are sequentially performed until the pseudo optimal design is validated as a reliable optimal design. Therefore, the RBMO framework provides an efficient way to achieve accurate optimal solutions.

Research solution 6: Bayesian mixture modeling for reliability-based design optimization under heterogeneous uncertainties. To aggregate the mixture uncertainties in reliability analysis, a Bayesian model inference approach is first employed to calibrate unknown parameters and capture the bias of the high-fidelity simulation model. By fusing

the simulation results and experimental observations, a validated Bayesian model is constructed for predicting the responses of the actual physical system. Monte Carlo simulation method is employed for propagating the input variations while the response at each MCS sample is predicted by the Bayesian model as a random variable that follows a normal distribution. With the resultant Gaussian mixtures, mixture uncertainties can be properly aggregated concurrently to obtain the distributions of stochastic system responses. A new concept, referred to as "aggregative reliability index", is then defined based on the Gaussian mixtures to approximate the probability of failure under mixture uncertainties. The proposed Bayesian mixture modeling (BMM) approach is further integrated into the RBDO framework to search for the optimal solutions that can provide the best compromise balance the design coat and risks due to mixture uncertainties.

2 LITERATURE REVIEW

2.1 Reliability analysis approaches

In practical engineering applications, reliability analysis aims at quantitatively measuring the probability that engineering systems successfully perform the intended functionalities under various sources of uncertainties. In past decades, vast research efforts [2-4] have been devoted to developing advanced approaches for systemically treating uncertainties in reliability analysis. For example, the Bayesian inference method [5, 6] has been integrated into reliability analysis for handling the epistemic uncertainty due to the insufficient statistical information of the input variables. In order to consider system degradation and stochastic operation condition, time-dependent reliability analysis approaches [3, 7, 8] have been developed to calculate the reliability level of an engineering system during a specific time period. In addition, attention has been focused on rare event probability estimation [9-11] to improve the capability of estimating extremely small probability of failure.

In the literature, both analytical- and simulation-based methods have been proposed for reliability assessment. As representatives of most probable point (MPP) based method, the first-order reliability method (FORM) [12, 13] and second-order reliability method (SORM) [14, 15] estimate the reliability by using the Taylor expansion to approximate the limit state function at the MPP. These approaches rely on iterative MPP searching process and require accurate sensitivity information of limit state function with respect to random variables. However, it is technically difficult to obtain the sensitivity information in practice. Moreover, significant errors may be introduced when dealing with highly nonlinear

problems. In reliability analysis, the ultimate purpose is to compute a multi-dimensional integral over a failure region, and univariate dimension reduction methods [16, 17] focus on decomposing the multi-dimensional integration into multiple one-dimensional integrations. To estimate the reliability, the moment-based integration rule is utilized for approximating the statistical moments of the limit state function based on the moments of each random variable. However, errors may be introduced due to the numerical integration using the Gaussian quadrature method. Simulation-based methods [18-20] such as direct Monte Carlo simulation is capable of providing more accurate reliability estimations than using analytical-based methods. Nevertheless, the extensive evaluations of the limit state function are computationally prohibitive in practical engineering applications.

2.2 Reliability-based design optimization

For decades, reliability-based design optimization (RBDO) [21-25] has been extensively studied to obtain a reliable solution under input variations in the early stage of product development. The goal of RBDO is to minimize the objective function while meeting predefined probabilistic constraints, and different RBDO methods have been investigated for specific concerns. To handle the epistemic uncertainty due to the unknown statistical information of the input variable, Bayesian inference is integrated with reliability analysis in Bayesian reliability-based design optimization (BRBDO) [26-28]. Reliability and robustness-based design optimization (RRBDO) [29-31] has gained more attention for seeking optimal designs, where the variability in the system performance due to the input variation is minimized. Dynamic reliability analysis approaches have been developed in time-dependent RBDO methods [32, 33] for ensuring high system reliability level

throughout a specific time period, leading to optimal solutions considering time-dependent uncertainties such as system deterioration and stochastic loading.

In the literature, sophisticated optimization strategies such as double-loop [34], decoupled-loop [35, 36], and single-loop approaches [37, 38] have been developed to improve the computational efficiency of RBDO. In the double-loop approaches, reliability analysis is performed for every design iterations, resulting a nesting of two distinct levels of optimization. In contrast, single-loop approaches replace the probabilistic constraint with optimality conditions and solve the RBDO in a single loop procedure, while decoupled-loop methods transform the RBDO problem into a sequence of deterministic optimization problems. Despite the development of optimization strategies, implementing RBDO for large-scale industry applications remains challenging, as it requires a significant number of computationally intensive simulations in reliability analysis.

2.3 Time-dependent reliability analysis and RBDO

Recently, time-variant RBDO [39, 40] has gain an increasing attention for engineering system design. Time-variant RBDO, referred to as "tRBDO", seeks optimum system designs with a high reliability level over time under time-variant uncertainties such as stochastic operation condition and system aging. Thus, the time-variant reliability analysis in tRBDO often involves stochastic processes and time parameters and thus is technically difficult and computationally expensive. In the literature, many methods have been developed for the time-variant reliability analysis. In the extreme value based approaches [41, 42], the worst scenario of system performance over a time interval is extracted to identify system failures. A time-variant reliability model can be transformed to a time-

independent counterpart by only focusing on extreme system performances, and static reliability analysis tools are employed to estimate the time-variant probability of failure. Chen and Li [43] proposed an approach to evaluate the structural reliability based on the distribution of extreme value, where the virtual stochastic process is created to capture the probability density function of the extreme value. Hu and Du [44] proposed a sampling method to evaluate the extreme values of stochastic processes, and approximate the time-variant reliability using the first-order reliability method. As analytical-based approaches, the out-crossing rate-based approaches [45, 46] evaluate the time-variant probability of failure by the integration of an out-crossing rate. Kuschel and Rackwitz [47] approximated the out-crossing rate by asymptotic second-order reliability methods while Andrieu-Renaud et al. [48] proposed a PHI2 approach to obtain time-invariant reliability indices using FORM and compute the outcrossing rate based on the correlation of reliability indices at two successive time instants. To solve the first passage problem in time-variant reliability analysis involving stationary random processes, Singh et al. [49] developed an importance sampling approach to calculate the cumulative probability of failure. Recently, some researchers have utilized metamodeling techniques [50-52] to alleviate the computational burden of time-variant reliability analysis. With the consideration of parametric uncertainty, Hu et al. [53] construct surrogate models for evaluating the time-instantaneous reliability index, and then identify the time-instantaneous most probable points using the fast integration method. Wang and Wang [54] proposed a double-loop adaptive sampling approach for efficient time-variant reliability analysis. In detail, Gaussian process regression is adopted to build surrogate models for predicting extreme system responses over time while the double loop sampling scheme searches for input

variables and time concurrently for updating the surrogate model until a pre-defined confidence target is satisfied. Hu and Du [55] developed a simulation method to evaluate the time-variant reliability based on the first order approximation and series expansions, where the stochastic process of the system performance is mapped into a Gaussian process for efficiently approximating time-variant reliability.

In general, the performance of an engineering system is modeled by a limit state function $G(\mathrm{x}, \mathrm{z}(t), t)$, where $\mathrm{x} \in \mathrm{R}^{nr}$ denotes the time-independent random variables, $\mathrm{z}(t)$ represents the stochastic processes, and t is the time parameter. For time-dependent reliability analysis, failure event occurs if system performance at any time instant falls below a threshold, written as

$$g(\mathbf{x}, \mathbf{z}(t), t) < 0, \exists t \in [0, T_L] \tag{2.1}$$

where $[0, T_L]$ represents the system life cycle. Therefore, the probability of failure over a given time period $[0, T]$ is defined as

$$P_f(0,T) = P(g(\mathbf{x}, \mathbf{z}(t), t) < 0, \exists \mathrm{t} \in [0,T]), 0 \le T \le T_L \tag{2.2}$$

As shown in Eqs. (2.1) and (2.2), stochastic processes are involved in the limit state function, thus, random realizations for the stochastic processes are required for computing the time-dependent system performances and reliability. For a Gaussian process $z_G(t)$, it can be fully characterized by three time-dependent functions, including the mean function $\mu_Y(t)$, standard deviation function $\sigma_Y(t)$, and auto correlation function $\rho_Y(t)$. By discretizing the overall time interval into s time nodes, the covariance between two time nodes is defined as

$$Cov(t_i, t_j) = \sigma_Y(t_i)\sigma_Y(t_j)\rho_Y(t_i, t_j) \tag{2.3}$$

Therefore, a covariance matrix with respective to each two time nodes can be obtained as

$$\sum = \begin{pmatrix} Cov(t_1,t_1) & Cov(t_1,t_2) & \cdots & Cov(t_1,t_s) \\ Cov(t_2,t_1) & Cov(t_2,t_2) & \cdots & Cov(t_2,t_s) \\ \vdots & \vdots & \ddots & \vdots \\ Cov(t_s,t_1) & Cov(t_s,t_2) & \cdots & Cov(t_s,t_s) \end{pmatrix} \tag{2.4}$$

By employing Eigen decomposition, the covariance matrix can be decomposed as $\Sigma = QIQ^T$, where $Q = [Q_1, Q_2, \ldots, Q_s]$ represents the matrix of eigenvectors and I is a diagonal matrix with eigenvalues. Given a specified criterion, the number of dominated eigenfunctions *m* can be determined, then the original Gaussian process $z_G(t)$ can be simulated as

$$z_G(t) \approx \mu_y(t) + \sum_{i=1}^{m} \sqrt{I_i} Q_i(t) p_i \tag{2.5}$$

where *p* is the number of dominated eigenfunctions and $p = [p_1, p_2, \ldots, p_m]$ are a set of uncorrelated standard normal random variables.

- Out-crossing rated based approach

A crossing event is defined as the phenomenon when time-variant system performance exceeds the safety zone. Therefore, time-variant reliability is approximated by the integration of the rate of reliability change with respect to time, referred to as out-crossing rate. Assuming all crossing events are independent, the crossing rate at time instant *t* is derived by

$$\lambda(t) \approx \lim_{\Delta t \to 0} \frac{\Pr\{g(X,Y(t),t) < 0 \cap g(X,Y(t+\Delta t),t+\Delta t) > 0\}}{\Delta t} \tag{2.6}$$

and the probability of failure within a time interval [*0*, *T*] is defined as

$$P_f(0,T) = 1 - (1 - P_{f0}) \exp\left\{-\int_0^T \lambda(t)dt\right\} \tag{2.7}$$

where P_{f0} is the probability of failure at the initial state with $t = 0$. As shown in Eq. (2.7), the time-variant reliability can be directly estimated once the crossing rate $\lambda(t)$ is obtained. To approximate the crossing rate with consideration of stochastic processes, Stephen O. Rice published a formula in 1944 [56] that is widely used with the first-order reliability method (FORM). The specified time interval is discretized into many time instants, and stochastic processes Y(t) are translated to random variables at each time node. The corresponding discretized limit state functions are transformed into a standard normal space and FORM is employed for searching the most probable point (MPP). Reliability index of each time node are evaluated by FORM, and the crossing rate can be approximated by the reliability indices of two successive time node and the correlation of stochastic process Y(t).

- Extreme values based approach

Another category of time-variant reliability analysis is the extreme value-based approach, which focuses on the worst performance of an engineered system over a time period. Assuming failure is defined as $g(\mathrm{X},\mathrm{Y}(t),t) < 0$, the worst system performance $g_e(\mathrm{X},T_L)$ over a period is the minimum of time-variant limit state functions,

$$\mathrm{g}_e(\mathbf{X}, T_L) = \min\ g(\mathbf{X}, Y(t), t), t \in [0, \mathrm{T}_L] \tag{2.8}$$

Thus the probability of failure within a time interval is described as the probability that extreme value falls below the threshold ($g_e < 0$). In practice, it is intractable to analytically obtain the probabilistic characterization of the extreme value, and simulation-based methods are often used to obtain the extreme value distribution and then approximate the

time-variant probability of failure. However, the computational cost is extremely high due to the inevitable large number of evaluations. To alleviate the computational burden of simulation-based methods, Wang et al. [57] developed a nested extreme response surface (NERS) method to efficiently extract the worst performance within a time interval. In NERS framework, a response surface is constructed for predicting the time instant corresponding to the extreme response within a specified time interval [0, T], which is described by,

$$T_e(X) = \left\{ t \middle| \min\ g(X,t), t \in [0,\mathrm{T}] \right\} \tag{2.9}$$

$$g_e = g(X, T_e(X)) \tag{2.10}$$

An efficient global optimization (EGO) approach [58] is utilized to efficiently extract extreme events for constructing a time response surface. Furthermore, an adaptive response prediction and model maturation mechanism (ARPMM) is employed to update the time response surface iteratively. After the updating process, the original time-variant reliability analysis can be converted to the time-independent one and the probability of failure within [0, T_L] is derived as

$$P_f(0,T_L) = P_r(g(X,T_e(X)) < 0) \tag{2.11}$$

Consequently, time-independent reliability analysis tools such as FORM can be used for reliability-based design optimization.

2.4 Surrogate model-based approaches

Surrogate modeling methods [59-61] such as artificial neural networks (ANN) [62-64], radial basis functions (RBF) [65-67], and Kriging [68-70] have been developed to replace

the computationally expensive simulations using a set of training data, and thus alleviate the computational burden of simulation-based reliability assessment and RBDO. The accuracy of response predictions using surrogates varies over the input domain, and highly depends on the amount and locations of training data points. The major issue of surrogate modeling lies in that there is no rigorous means of quantifying and propagating the surrogate model uncertainty due to the lack of training data, which may result in less confidence in predicting the probability of failure. To improve the fidelity of surrogate models, adaptive updating schemes [71-74] have been integrated with reliability analysis to identify important points sequentially in the local critical regions for updating the surrogates. For instance, Deng, J. [75] adopted the radial basis function network to build surrogates for reliability analysis and adaptively update the parameters of the RBF to minimize the sum squared error. Wang and Wang proposed a cumulative confidence level (*CCL*) concept to quantify the fidelity of surrogates for reliability analysis, and then developed a sequential sampling scheme to improve the *CCL* in RBDO. Dubourg et al. [76] developed a population-based adaptive refinement technique to sequentially reduce the error, where the Kriging model can be updated by adding multiple training samples simultaneously. Even though the accuracy of surrogate models can be significantly improved with these adaptive sampling schemes, the remaining surrogate model uncertainty can still be significant, especially for cases when the computational resource is limited. Ignoring surrogate model uncertainty in simulation-based design optimization with insufficient training data may lead to inaccurate predictions and unreliable system design. To compensate the surrogate model uncertainty without adding new training data, conservative surrogate modeling methods [77-79] utilized safety margin concepts in

predicting system performance. Luna and Young [80] used the bootstrapping method to construct the conservative surrogate model, where the prediction interval is estimated by considering the uncertainty from the correlation parameter used in Kriging covariance function. Zhao et al. [81] employed the corrected Akaike information criterion (AICc) to assess the accuracy of the Kriging surrogate model and calculate the weighted prediction variance, and a conservative surrogate model is developed by using the percentile value of the prediction interval.

- Conservative surrogate modeling

Given a set of training points, a surrogate model $\hat{g}(\mathrm{x})$ can be constructed after evaluating the responses of all the training points. By adding a safety margin to the surrogate model, a conservative surrogate model $\hat{g}_c(\mathrm{x})$ can be obtained as

$$\hat{g}_c(\mathbf{x}) = \hat{g}(\mathbf{x}) - s \tag{2.12}$$

where x is a vector of system input parameters and s is the safety margin used to bias the predicted response from the original surrogate model $\hat{g}(\mathrm{x})$. The safety margin s is always a constant and its sign depends on the definition of failure event. Assuming a failure event occurs if the system performance is less than zero, the safety margin will always be positive. As shown in Eq. (2.12), determining a suitable safety margin is of critical importance in compensating the surrogate model uncertainty due to the lack of data in reliability analysis.

In the literature, the prediction errors between the surrogate model and the origin performance function are calculated for computing the safety margin, given as

$$e(\mathbf{x}_t) = \hat{g}(\mathbf{x}_t) - g(\mathbf{x}_t) \tag{2.13}$$

where x_t is the vector of a large number of test samples within the design space. Accordingly, the cumulative distribution function of the prediction errors F_e can be calculated and the fraction of the errors can be obtained by

$$c = 1 - F_e(0) \tag{2.14}$$

where c is referred to as the conservativeness level of the surrogate model. For a given conservativeness level, the safety margin can be estimated in terms of the cumulative distribution function F_e as

$$s = -F_e^{-1}(1-c) \tag{2.15}$$

where F_e^{-1} is the inverse cumulative distribution function of the prediction errors. Obviously, the number of test samples determines the accuracy of the inverse CDF in Eq. (2.15) and affects the obtained safety margin. Therefore, obtaining an accurate estimation of the inverse CDF is extremely important in ensuring the performance of conservative estimations. By using a large number of test samples, an accurate safety margin for achieving a given conservativeness level can be obtained by Eq. (2.15). However, it is not applicable in practice due to the lack of training data. To alleviate the computational burden, Vianna et al. [82] employed the cross validation method to approximate the prediction errors. For a surrogate model constructed with p training samples, cross validation is a process of constructing new surrogate model without one of the p points and calculating the error respectively. After repeating the leave-one-out strategy for all the p samples, the corresponding cross validation errors can be obtained and used as the prediction errors of the origin surrogate model.

3 AN LSTM-BASED ENSEMBLE LEARNING FRAMEWORK

FOR TIME-DEPENDENT RELIABILITY ANALYSIS

3.1 Introduction

This section presents a Long short-term memory (LSTM)-based ensemble learning framework for time-dependent reliability analysis. To deal with the time-dependent uncertainties, an LSTM network is first adopted to capture the relationship between the stochastic processes and the time-dependent system behavior. As a result, time-dependent system responses given any new random realizations of the stochastic process can be accurately predicted by the LSTM. By using different realizations of the time-independent random variables and stochastic process, multiple LSTMs are trained to model conditional limit state functions with fixed random variables, where a set of artificial data is collected according to random realizations of the stochastic processes. To quantify the uncertainty due to the random variables, Gaussian process modeling (GP) technique is employed for building surrogate models for the specified stochastic processes and time instant. With the GP models, the time-dependent system reliability can be directly approximated by using the Monte Carlo simulation. Two case studies are introduced to demonstrate the efficiency and accuracy of the proposed approach.

3.2 LSTM-Based Ensemble Learning Framework

The proposed framework aims at dealing with time-dependent reliability analysis problems involving stochastic processes and time parameter. To address the uncertainty due to the stochastic processes and time parameter, multiple LSTM models are first constructed by using sets of random realizations of the input variables and the stochastic process, where the inputs variables are used to introduce conditional limit state functions.

For each LSTM model, random realizations of the stochastic processes are provided for predicting the time-dependent system responses for the conditional limit state functions. Though these estimated system responses are not obtained by directly evaluating the actual time-dependent limit state function, the accuracy is ensured due to the benefits of LSTM. To specifically quantify the uncertainty due to the time-independent random variables, the Gaussian process modeling technique is adopted in the proposed ensemble learning framework. Based on the response predictions collected from multiple LSTM models, a set of Gaussian process models are constructed at the specified random realization of stochastic processes and time instant. With the GP models, the time-dependent reliability can be approximated by employing the Monte Carlo simulation (MCS) method.

3.2.1 Long Short-Term Memory (LSTM) Neural Network

In past decades, neural networks have seen great development in solving machine learning problems such as classification and regression. For problems with time series data, recurrent neural network (RNN) has been utilized, which has a feed-back loop to store past input information. A major challenge remains that it cannot provide accurate predictions when the data has long-term dependencies. To tackle the problem of long-term dependencies, LSTM was designed for processing and predicting on the basis of time series data.

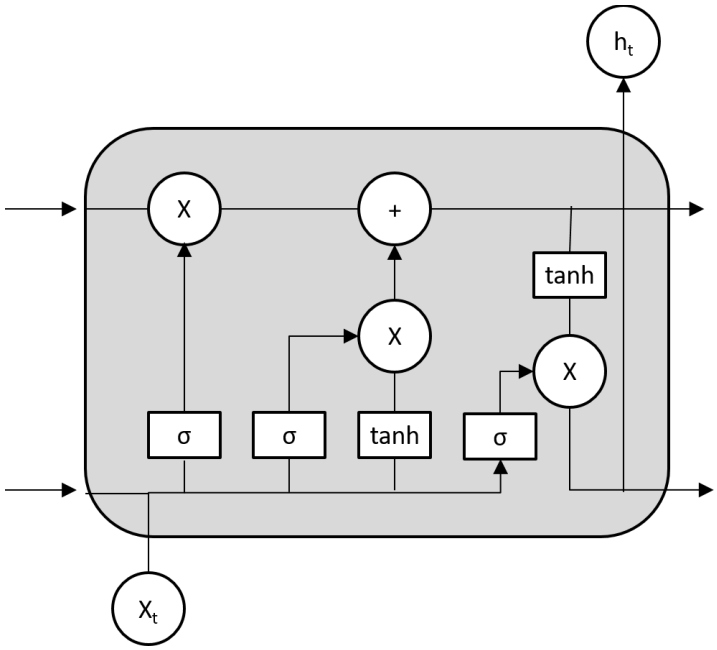

Figure 3.1: Repeating modules of LSTM

All recurrent neural networks have the form of a chain of repeating modules. To ensure LSTM is able to remember information for long periods of time, three gated unites are used in the repeating modules, including an input gate, output gate, and forget gate. The core idea of LSTM lies in that the information flow is represented by the cell state, which is shown as the top horizontal line in Fig. 3.1. LSTM has the capability of removing or adding information to the cell state by using the gated units. The information that no longer useful is removed with the forget gate. The inputs at the particular time instant x_t and the previous cell output y_{t-1} are provided to the forget gate, which are multiplied with weight matrices and followed by bias, expressed as

$$f_t = \sigma\left(\mathbf{W}_f z_t + \mathbf{R}_f y_{t-1} + b_f\right) \tag{3.1}$$

where f_t represents the forget gate output, W_f, R_f, and b_f represents the input weights, recurrent weights, and bias, respectively, and $\sigma(.)$ stands for the activation function. Usually

the sigmoid function is adopted as the activation function of the forget gate. Next, we need to decide what new information should be stored in the cell state based on two parts. First, the input gate determines which state will be updated, meanwhile a hyperbolic tangent layer creates a vector candidate values that should be added to the state. The computation process can be summarized as

$$\begin{aligned} i_t &= \sigma\left(\mathbf{W}_i z_t + \mathbf{R}_i y_{t-1} + b_i\right) \\ \tilde{C}_t &= \tanh\left(\mathbf{W}_C z_t + \mathbf{R}_C y_{t-1} + b_C\right) \end{aligned} \tag{3.2}$$

where (W_i, R_i, and b_i) and (W_C, R_C, and b_C) are the input weights, recurrent weights, and bias of the input gate and the cell state, respectively. Then all the outputs from Eqs. (1) and (2) are utilized to update the old cell state, written as

$$C_t = f_t C_{t-1} + i_t \tilde{C}_t \tag{3.3}$$

As shown in Eq. (3.3), useless information is removed by multiplying the old state with the forget gate output, and the second term represents the new candidate values that scaled by how much we would like to update. At the end, the output gate is used to decide which part of the cell state should be utilized as the output y_t. By applying the hyperbolic tangent function to the cell state, the output y_t of LSTM at time instant t can be achieved as

$$\begin{aligned} o_t &= \sigma\left(\mathbf{W}_o z_t + \mathbf{R}_o y_{t-1} + b_o\right) \\ h_t &= o_t \cdot \tanh(C_t) \end{aligned} \tag{3.4}$$

where o_t represents the results of output gate, and W_o, R_o, and b_o represents the input weights, recurrent weights, and bias, respectively. Based on the LSTM structure that introduced above, the gradients of weights and biases term can be computed accordingly. Therefore, optimization algorithms such as stochastic gradient descent, Root Mean Square

Propagation (RMS prop), and Adam can be utilized for determining the weight matrices and biases of the LSTM, where the mean square error (MSE) between the training labels and the LSTM outputs is minimized by employing the back-propagation through time (BPTT) algorithm.

Tremendous research works have illustrated the effectiveness of LSTM network when handling time-dependent problems, however, LSTM lacks the capability of directly dealing with the time-independent random variables as it requires time-series training data. Therefore, instead of modeling the limit state function $G(\mathrm{x}, \mathrm{z}(t), t)$, the concept of conditional limit state functions are introduced for LSTM modeling. In the proposed approach, n random realizations of the input variables and the stochastic process are generated for multiple LSTM training data preparation, denoted as $\mathrm{X} =[\mathrm{x}_1, \mathrm{x}_2, \ldots, \mathrm{x}_n]$ and $\mathrm{Z} = [\mathrm{z}_1(t), \mathrm{z}_2(t), \ldots, \mathrm{z}_n(t)]$, respectively. Given the random samples X, n conditional limit state functions $g_i(\mathrm{z}(t), t)$ are used for building multiple LSTM models, which is expressed as

$$g_i(z(t),t) = G(\mathbf{x}_i, z(t), t), \qquad i = 1,2,...,n \tag{3.5}$$

where x_i represents the i^{th} realizations of the random variables x. As shown in Eq. (3.5), each conditional limit state function is a simplified version of the original limit state function with fixed random variables. For the i^{th} conditional limit state function, the time-dependent system responses y_i are evaluated by giving the inputs $[\mathrm{x}_\mathrm{i}, \mathrm{z}_\mathrm{i}(t), t]$. To train an LSTM model for this conditional limit state function, the training input is expressed as a matrix

$$\begin{bmatrix} \mathbf{z}_i(t_1) & t_1 \\ \mathbf{z}_i(t_2) & t_2 \\ \vdots & \vdots \\ \mathbf{z}_i(t_s) & t_s \end{bmatrix} \tag{3.6}$$

where $z_i(t_j)$ represents the stochastic processes value at the j^{th} time instant. Accordingly, the training labels for the LSTM is a vector with s elements, expressed as $y_i = [y_i(t_1), y_i(t_2), \ldots, y_i(t_s)]$. Given the training data set, the LSTM can be trained by minimizing the MSE loss function. Following the same procedure, n LSTM models can be constructed, which respectively capture the relationship between the stochastic processes and time-dependent system behaviors of the conditional limit state functions. For each LSTM model, time-dependent response predictions can be achieved given any realizations of the stochastic processes. Indeed, results are very accurate since the LSTM is capable of capturing the relationship between the stochastic processes and the system responses. However, how to quantify the uncertainty due to the random variables still remains a challenge.

3.2.2 Instantaneous Response Modeling Using Gaussian Process

As aforementioned, LSTM lacks the capability of dealing with the time-independent random variables. Therefore, Gaussian process modeling technique is employed for modeling the random system responses at each time instant. Gaussian process modeling technique is known as a nonparametric, Bayesian approach for tasks of both supervised and unsupervised learning. By using the GP model, a function with input parameters η can be modeled as

$$\hat{g}(\boldsymbol{\eta}) \sim GP\left(\mathbf{h}(\boldsymbol{\eta})\boldsymbol{\beta}, \sigma^2 R(\boldsymbol{\eta}_i, \boldsymbol{\eta}_j)\right) \tag{3.7}$$

where the response is assumed to be a stationary Gaussian process with mean function h(η)β and covariance function $V(\eta, \eta') = \sigma^2 R(\eta, \eta')$. The term h(η) is the vector of predefined polynomial functions and β is the vector of corresponding coefficients. In this work, a constant mean function is adopted, which is sufficient for engineering applications. In the GP model, the covariance function $V(\eta, \eta')$ is expressed as

$$V(\boldsymbol{\eta}, \boldsymbol{\eta}') = \sigma^2 R(\boldsymbol{\eta}, \boldsymbol{\eta}') = \sigma^2 \exp\left[-\sum_{p=1}^{d} \omega_p \left| \boldsymbol{\eta}_p - \boldsymbol{\eta}_p' \right|^2 \right] \tag{3.8}$$

where $\omega = [\omega_1, \omega_2, \ldots, \omega_k]$ is the vector of roughness parameters that capture the nonlinearity of the process, d is the dimension of the input η, and σ^2 is an unknown variance. Therefore, the unknown hyperparameters β, σ^2, and ω a fully characterize a GP model, which can be approximated by maximum likelihood estimation (MLEs) method based on a training data set. Once the hyperparameters are achieved, the GP model is capable of predicting the response at any point η' as a normal distribution with mean

$$\mu_{gp}(\boldsymbol{\eta}') = \mathbf{h}(\boldsymbol{\eta})\boldsymbol{\beta} + \mathbf{r}^T \mathbf{R}^{-1} (\mathbf{Y}_t - \mathbf{H}\boldsymbol{\beta}) \tag{3.9}$$

and variance,

$$v_{gp}(\boldsymbol{\eta}') = \sigma^2 \left\{ 1 - \mathbf{r}^T \mathbf{R}^{-1} \mathbf{r} + \left[\mathbf{h}^T(\boldsymbol{\eta}) - \mathbf{H}^T \mathbf{R}^{-1} \mathbf{r} \right]^T \left(\mathbf{H}^T \mathbf{R}^{-1} \mathbf{H} \right)^{-1} \left[\mathbf{h}^T(\boldsymbol{\eta}) - \mathbf{H}^T \mathbf{R}^{-1} \mathbf{r} \right] \right\} \tag{3.10}$$

where Y_t denotes output training data, r is the correlation vector between η' and the existing training points, H is an unit vector if the prior mean function is a constant. In this work, the GP model is adopted to construct the surrogate models based on the artificial data.

As aforementioned, the constructed LSTMs can be used to make time-dependent response predictions of the conditional limit state functions. For data preparation, N

random realizations of the stochastic process $Z^{mcs}(t) = [z_1^m(t), z_2^m(t), \ldots, z_N^m(t)]$ are generated according to the stochastic properties, which are provided to each LSTM model for predicting the overall time-dependent responses. As a result, the collected responses data from the i^{th} LSTM model are expressed as

$$\hat{\mathbf{Y}}^i = \left[\hat{\mathbf{y}}_1^i, \hat{\mathbf{y}}_2^i, ..., \hat{\mathbf{y}}_N^i\right]^T = \begin{bmatrix} \hat{y}_1^i(t_1) & \cdots & \hat{y}_1^i(t_s) \\ \vdots & \ddots & \vdots \\ \hat{y}_N^i(t_1) & \cdots & \hat{y}_N^i(t_s) \end{bmatrix} \tag{3.11}$$

where the time-dependent responses $\hat{y}_j^i$ are the predictions of the conditional limit state function g_i as

$$\hat{\mathbf{y}}_j^i \approx g_i(\mathbf{z}_j^m(t), t), t = t_1, ..., t_s \tag{3.12}$$

Though the responses predictions $\hat{Y} = \{\hat{Y}^i, i=1, 2, ..., n\}$ are very accurate due to the benefits of LSTM, they are not directly obtained based on the actual limit state functions. To distinguish the difference, they are denoted as artificial data in this work. With all the constructed n LSTM models, the responses of each conditional limit state function given the random realizations $Z^{mcs}(t)$ can be achieved. Therefore, given a specified time instant t_k and a random realization of stochastic processes $z_j^m(t_k)$, the collected response predictions $\hat{y}_j(t_k) = \{\hat{y}_j^i(t_k), i=1, 2, ..., n\}$ can be treated as instantaneous responses for limit state function with fixed stochastic processes and time instant, expressed as

$$\hat{y}_j^i(t_k) \approx G(\mathbf{x}_i)\left|\mathbf{z}_j^m(t_k), t_k\right. \tag{3.13}$$

Given the n training inputs $X = [x_1, x_2, \ldots, x_n]$ and set the corresponding response predictions $\hat{y}_j(t_k)$ as the training outputs, a GP model can be constructed for predicting the responses with different input x. In other words, the constructed GP model is utilized to

specifically quantify the random variables x. With the identical training inputs X, a GP model M_j^k can be constructed with the training outputs $\hat{y}_j(t_k)$ determined by specified j = 1, ..., N and k =1, ..., s.

3.2.3 Time-Dependent Reliability Analysis

In this work, the Monte Carlo simulation (MCS) method is employed to calculate the time-dependent probability of failure based on the GP models. According to the statistical information of the input variables and the stochastic process, N random realizations are generated as the MCS samples, denoted as $U^{mcs} = [X^{mcs}, Z^{mcs}(t)]$, where $X_{mcs} = [x_1^m, x_2^m, \ldots, x_N^m]$ and $Z^{mcs}(t) = [z_1^m(t), z_2^m(t), \ldots, z_N^m(t)]$. Based on the constructed GP models, the response for the j^{th} MCS sample at time instant t_k can be predicted as

$$y_j^{mcs}(t_k) = G(\mathbf{x}_j^{mcs}, \mathbf{z}_j^{mcs}(t_k), t_k) \approx M_j^k(\mathbf{x}_j^{mcs}) \tag{3.14}$$

Once all the time-dependent response predictions have been obtained, the minimum response corresponding to each MCS sample is extracted for reliability analysis. The MCS sample will be classified as failure or safe by an indicator function, given as

$$I_f(\mathbf{U}_j^{mcs}) = \begin{cases} 1, \min\limits_{1 \le k \le s} y_j^{mcs}(t_k) < 0 \\ 0, \quad otherwise \end{cases} \tag{3.15}$$

In Eq. (3.15), it shows that a failure event occurs when the worst performance over the given time period is less than zero. After evaluating all the MCS samples, the time-dependent reliability can be approximated by

$$P_f(0,T) \approx \frac{N_f}{N} \tag{3.16}$$

where N_f represents the number of failure samples classified by the indicator function.

3.3.4 Numerical Procedure

The procedure of employing the proposed ensemble learning framework is summarized in a flowchart as shown in Fig. 3.2. Firstly, N MCS samples $U^{mcs} = [X^{mcs}, Z^{mcs}(t)]$ are generated according to the statistic properties of the time-independent random variables and stochastic processes. To prepare the data for training multiple LSTM models, Latin hypercube sampling (LHS) is employed to generate n random samples of the time-independent variables as $X = [x_1, x_2, \ldots, x_n]$, lead to n conditional limit state functions. With n random realizations of the stochastic processes $Z = [z_1(t), z_2(t), \ldots, z_n(t)]$, the corresponding time-dependent responses are directly evaluated based on the actual limit state functions. For modeling the conditional limit state functions, the i^{th} LSTM model can be constructed based on the input $[z_i(t), t]$ and output y_i. In the proposed approach, the LSTM models are constructed based on the "Keras" library in Python 3.6. The mean square error is used as the loss function, where the "Adam" optimizer with default learning rate 0.001 is adopted for training process of all LSTM models.

For each LSTM model, random realizations of stochastic processes Z^{mcs} are provided to achieve the time-dependent response predictions. Once all the artificial data is collected, GP models are constructed to model the instantaneous response with respect to the random variable x. For j^{th} random realization and time instant t_k, the obtained response data $\hat{y}_j(t_k)$ is utilized as the training outputs of GP model M_j^k, where the training inputs are the LHS samples X. The same procedure is repeated with different training outputs specified by j and k. By providing the MCS samples X^{mcs} to each GP model, the time-dependent response prediction corresponding to U^{mcs} can be calculated. With an indicator function shown in Eq. (3.15), the minimum responses are utilized to determine if a MCS sample is classified

as failure or safe. Eventually, the time-dependent system reliability can be approximated according to Eq. (3.16).

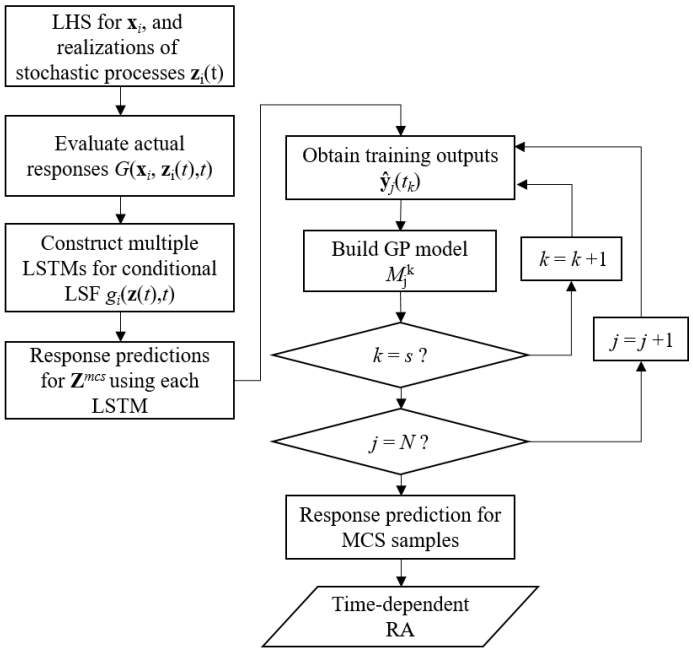

Figure 3.2: Flowchart of the proposed ensemble learning framework

3.3 Case Studies

In this section, two examples are used to demonstrate the effectiveness of the proposed approach for solving the time-dependent reliability analysis problems.

3.3.1 Case Study I: A Mathematical Problem

In the first case study, a limit state function with two random variables and three stochastic processes is utilized, which can be formulated as

$$G(\mathbf{x},\mathbf{z}(t)) = 0.5x_1^2 z_2(t) z_3(t) - 8 z_1(t) z_2(t) + (x_2+1)^2 - 20 \tag{3.17}$$

where each time-independent random variable in x = [x_1, x_2] follows a normal distribution,

and the each stochastic process $z(t)$ is assumed to follow a stationary Gaussian process. The autoeocrrelation for the i^{th} stochastic process can be expressed as

$$\rho_i\left(t_1,t_2\right)=\exp\left(-\frac{\left(t_2-t_1\right)^2}{\lambda_i}\right) \tag{3.18}$$

where the coefficients λ are assigned to be 0.01, 0.005, 0.005, respectively. The statistical information of the random variables and the stochastic process are summarized in Table 3.1. The time interval [0, 1] for this example is discretized into 60 nodes evenly, and 10^5 random realizations of the stochastic process are generated for time-dependent reliability analysis.

Table 3.1: Stochastic properties of the random variables

Random variable	Distribution	Mean	Standard deviation
x_1	Normal	5	0.5
x_2	Normal	6	0.5
$z_1(t)$	Stationary Gaussian	5	0.3
$z_2(t)$	Stationary Gaussian	2	0.1
$z_3(t)$	Stationary Gaussian	4	0.2

The first step of employing the proposed approach is to prepare the training data for the LSTM models. As introduced in subsection 3.3.4, the Latin hypercube sampling is employed to generated 10 samples of random variables x. Each LHS sample is combined with a random realization of the stochastic processes z(t), and then evaluate the corresponding time-dependent responses based on Eq. (3.17). Given the training data sets, 10 LSTM models can be constructed respectively. For each LSTM model, 10^5 MCS

samples of stochastic processes are provided for predicting the time-dependent system responses of the conditional limit state functions. Based on the achieved time-dependent response predictions, GP models can be constructed to estimate the instantaneous response at each time instant for a specified realization of the stochastic processes. Eventually, the time-dependent responses corresponding to the 10^5 MCS samples can be obtained based on the GP models, which are further utilized for estimating the time-dependent reliability.

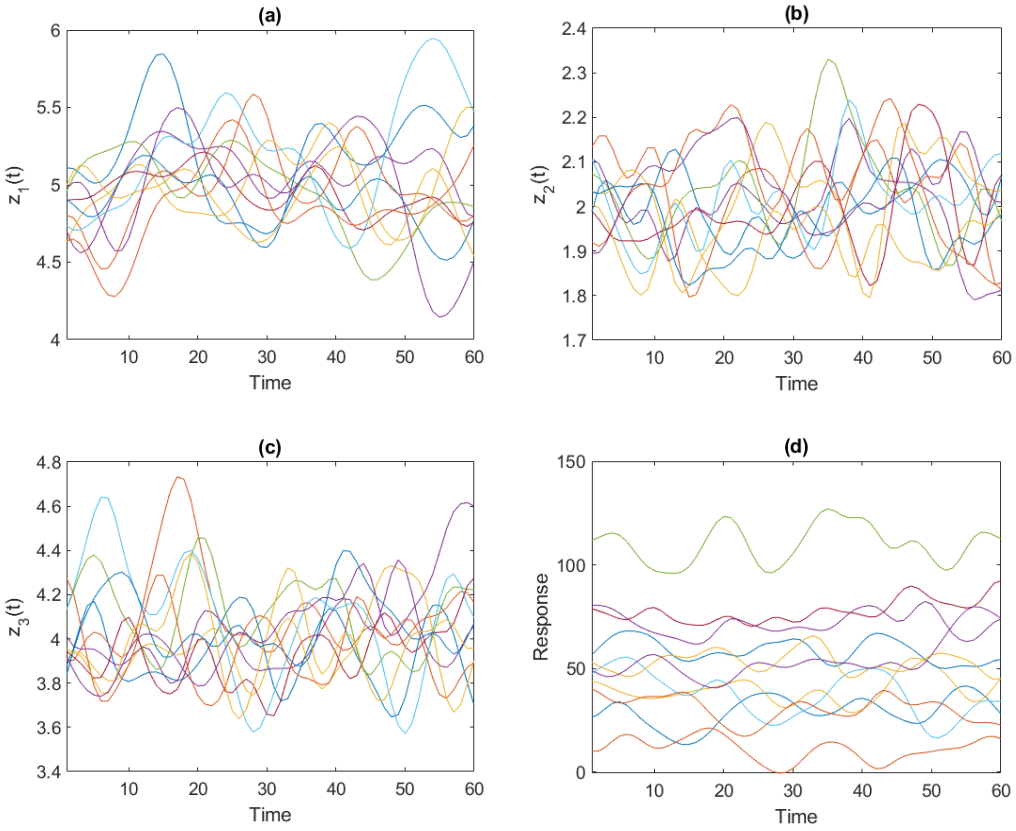

Figure 3.3: 10 random realizations of the stochastic processes and the resultant time-dependent responses

The 10 random realizations of stochastic processes that are used to multiple LSTMs are shown in Fig. 3.3, where a), b), and c) respectively plots the random realizations for each stochastic process, and the resultant time-dependent responses are depicted in Fig.

3.3d). Ten LSTM models are trained based on these training data, where the number of neurons for each LSTM model is set to 40. All the LSTM models are well trained by using the Adam optimizer to minimize the MSE with 3000 maximum epochs, and the convergence curve for the 1st LSTM is shown in Fig. 3.4. To demonstrate that the LSTM is capable of accurately capturing the relationship between the stochastic processes and the time-dependent response. The comparison of the actual and predicted time-dependent responses is depicted in Fig. 3.5, where a) shows the response comparison of the 1st test sample using the 1st LSTM, and b) shows the response comparison of the 10th test sample using the 10th LSTM. The results demonstrated that the LSTM models have been well trained, which are capable of accurately predicting the time-dependent responses given any realizations of the stochastic processes.

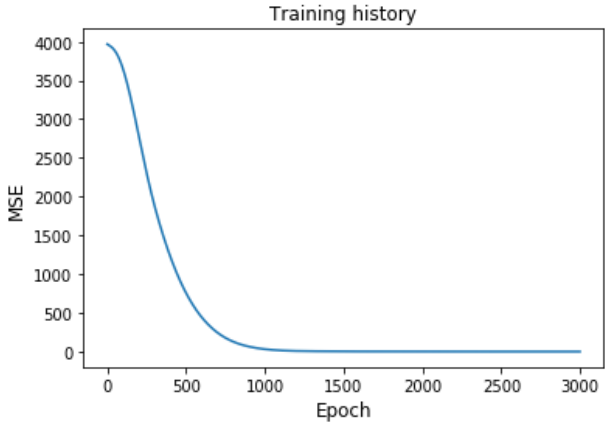

Figure 3.4: Convergence of the loss function for the 1st LSTM model

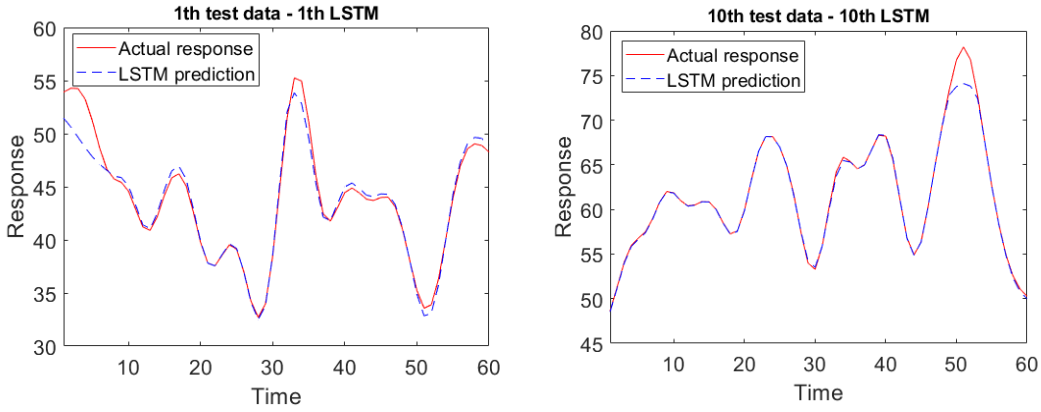

Figure 3.5: Comparisons between actual responses and estimations from LSTMs

To demonstrate the accuracy of time-dependent response predictions using GP models, Figure 3.6 shows the comparison of the accurate and predicted time-dependent responses for the 25th and 75th MCS sample, respectively. The results demonstrate that the constructed GP models can effectively handle the randomness of the time-independent variables, and they can provide accurate response predictions for the whole time-series data.

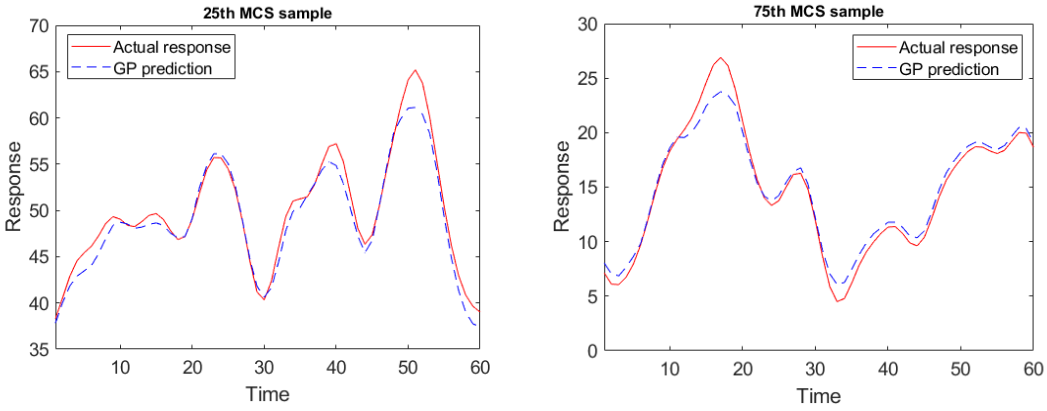

Figure 3.6: Comparisons between the actual and estimated time-dependent responses

For comparison purpose, the "equivalent stochastic process transformation (eSPT)" method [8] is adopted for approximating the time-dependent reliability of the mathematical example. To validate the accuracy of reliability estimation, the actual time-dependent

system responses for the 10^5 MCS samples are calculated, and the resultant accurate reliability 0.9754 is treated as a reference. The reliability approximations achieved by the proposed approach and eSPT are given as 0.9732 and 0.9726 respectively. By converting the stochastic processes into time-independent variables, the eSPT method requires 88 function evaluations to obtain the reliability estimation, which assumes the time-dependent response can be directly evaluated given stochastic processes values at any time instant. For practical time-dependent problems, it is intractable to directly achieve the response at a specified time instant. Thus, the required number of function evaluations for eSPT considering all the necessary evaluations is recalculated as 2512. In the proposed approach, we constructed multiple LSTM models by using 10 time series data, where the time interval consist of 60 time instant. Therefore, the number of function evaluations for the proposed approach is given as 600. By specifying different time intervals within [0, 1], time-dependent reliability at different time period can be approximated based on the predicted responses. The comparison between the reliability approximations and accurate results computed by direct MCS is summarized in Table 3.2, which indicates that the proposed approach is capable of accurately capturing the variation of time-dependent reliability with respect to time.

Table 3.2: Time-dependent reliability within different time intervals

Time Interval	Time nodes	Estimated R	Accurate R
[0, 0.2]	$t_1 \sim t_{12}$	0.9856	0.9858
[0, 0.4]	$t_{12} \sim t_{24}$	0.9826	0.9820
[0, 0.6]	$t_{25} \sim t_{36}$	0.9800	0.9784
[0, 0.8]	$t_{36} \sim t_{48}$	0.9780	0.9760

[0, 1]	$t_{48} \sim t_{60}$	0.9758	0.9736

3.3.2 Case Study II: A Corroded Beam Problem

A beam corrosion problem is considered as the second case study, where the geometry of the beam is shown in Fig. 3.7. The cross section is rectangular with an initial width b_0 and height h_0. Due to the corrosion, the size the of cross section decrease with time, where the time-dependent behavior can be modeled as

$$\begin{cases} b(t) = b_0 - 2kt \\ h(t) = h_0 - 2kt \end{cases} \tag{3.19}$$

According to Eq. (3.19), $b(t)$ and $h(t)$ are two time-dependent random variables at any time. A stochastic load $F(t)$ is applied at the middle span, which follows a stationary Gaussian process. The yield strength of the material is denoted by σ_y, and the failure event occurs when the maximum stress exceeds the yielding limit of the beam. Therefore, the limit state function of the corroded beam problem is expressed as

$$G(\mathbf{X}, F(t), t) = \frac{b(t)h(t)^2}{4}\sigma_y - \left(\frac{F(t)L}{4} + \frac{\rho b(t)h(t)L^2}{8} \right) \tag{3.20}$$

In this case, three random variables, one stochastic process, and time parameter is involved in the limit state function. The statistical information of the variables is summarized in Table 3.3, where the autoencorrelation function for the stochastic load is given as

$$\rho_Y(t_1, t_2) = \exp\left(\left(t_2 - t_1 \right)^2 \right) \tag{3.21}$$

The time interval is given as [1, 30] month, which is evenly divided into 59 time nodes. Following the numerical procedure, the proposed approach is employed to solve the corroded beam problem. For reliability analysis, 10^5 MCS samples are generated according to the stochastic properties of the random variables and the stochastic process. Fifteen training data sets are utilized for training the LSTM models, and the artificial data is obtained by using the LSTM models to predict the time-dependent responses given the 10^5 random realizations of the stochastic process. Accordingly, GP models can be constructed to model the instantaneous response corresponding to each random realization of $F(t)$. As a result, time-dependent response predictions for the MCS samples are obtained based on the GP models.

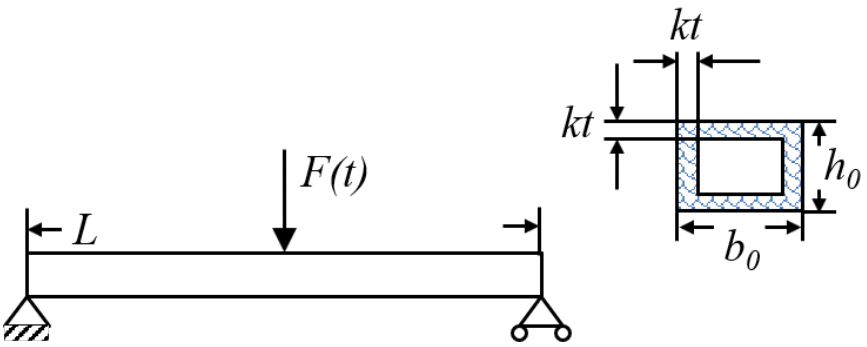

Figure 3.7: Geometry and corroded cross section of the beam

Table 3.3: Variables of the corroded beam example

Design variable	Distribution	Mean	Standard deviation
Yield stress, σ (MPa)	Normal	250	24
Breadth, b_0 (m)	Normal	0.6	0.01
Height, h_0 (m)	Normal	0.06	0.004

Load, F(t) (N)	Stationary Gaussian.	3500	700
Corrosion rate, k, (m/month)	/	5e-5	/
Length, L (m)	/	5	/
Material Density, ρ (g/cm^3)	/	7.85	/

For comparison purpose, the eSPT method is employed for time dependent reliability analysis with a predefined cumulative confidence level 0.999. The reliability calculated by direct MCS, proposed approach, and eSPT are given as 0.9756, 0.9748, and 0.9778, respectively. The results shows that both eSPT and the proposed approach can achieve an accurate time dependent reliability estimation. In eSPT, 84 function evaluations are utilized for updating process, which is calculated based on an assumption that the system response at any time instant can be directly evaluated and requires only one function evaluation. However, evaluating responses at all previous time instant are necessary and should be considered into the number of function evaluations. Thus, the actual number of function evaluations when employing eSPT for practical problems is calculated as 2946. The proposed approach requires 15 time series data, corresponding to 885 function evaluations.

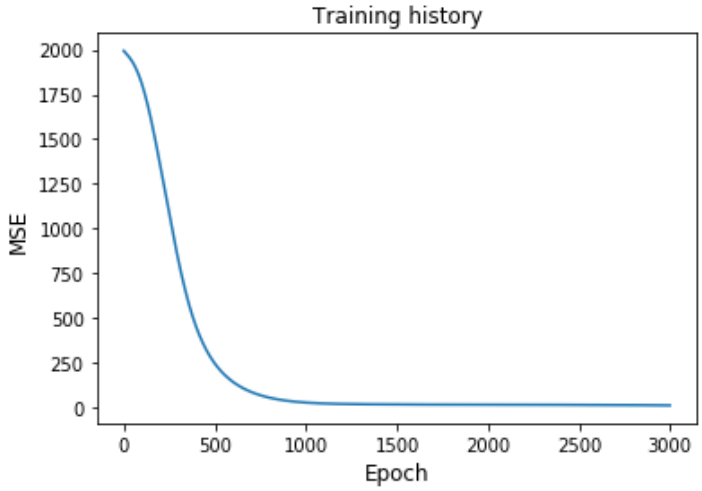

Figure 3.8: Convergence of the loss function for the 1st LSTM model

In this study, the LSTM models are trained with a maximum epochs 3000, and the convergence of the MSE loss function for the first LSTM is shown in Fig. 3.8. It has been observed that all the LSTM models have similar convergence curves. To validate the effectiveness of the LSTM, the comparison of the actual and predicted responses using LSTMs is shown in Fig. 3.9, where the title shows the information of specified LSTM and test sample. The results demonstrate that the LSTM can make accurate response predictions for the conditional limit state functions with any random realization of the stochastic process. Thought the artificial data is not collected by directly evaluating the limit state function, the accuracy is guaranteed due to the benefits of using the LSTM.

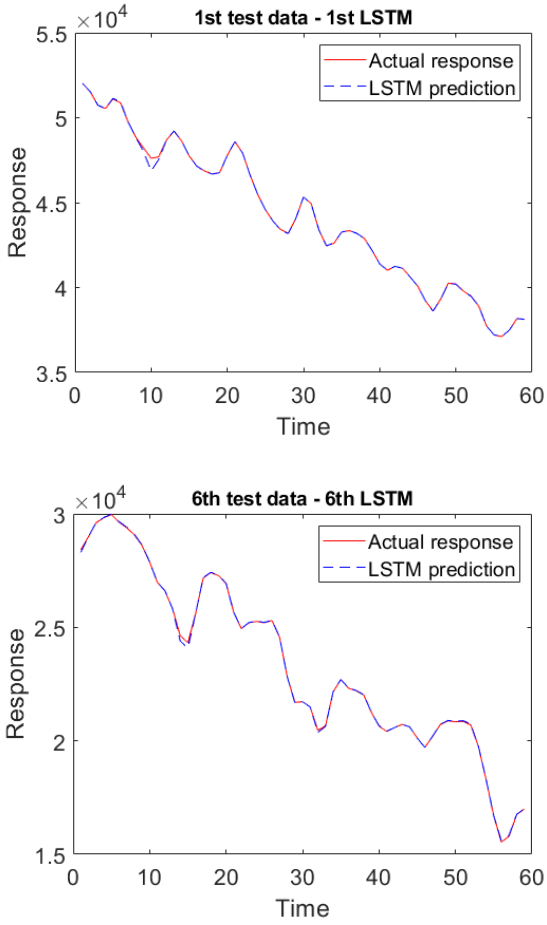

Figure 3.9: Comparisons between actual responses and estimations from LSTMs

Samples

Once all the artificial data has been collected from the multiple LSTM, GP models for modeling the instantaneous response can be constructed as introduced in subsection 3.3.2. As a result, the time-dependent responses corresponding to each MCS sample can be predicted based on the GP models. Similarly, the actual minimum responses for the first 50 MCS samples are compared to the minimum responses extracted from the GP predictions. As shown in Fig. 3.10, the estimated minimum responses are ensured to be accurate, which almost overlap the actual one. Considering all the 10^5 MCS samples, Figure 3.11 shows the comparison between the PDFs of the actual and estimated minimum responses. The results reveal that the proposed ensemble learning framework can provide accurate predictions of the minimum value of the time-dependent responses within the time interval, thus lead to accurate time-dependent reliability approximation. By specifying different time intervals, time-dependent reliability can be approximated based on the collected overall time-dependent response predictions. The comparison between the approximations and accurate results computed by direct MCS is summarized in Table 3.4, which indicates that the proposed approach is capable of accurately predicting the time-dependent reliability within any interested time intervals $[0, T_I]$, $T_I \leq T$.

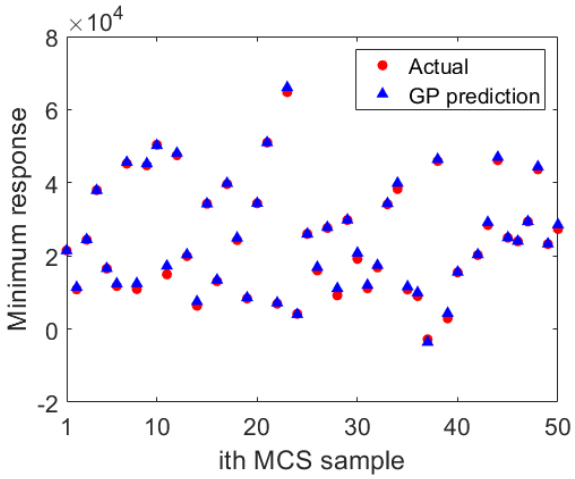

Figure 3.10: Minimum responses comparison of the first 50 MCS samples in the beam example

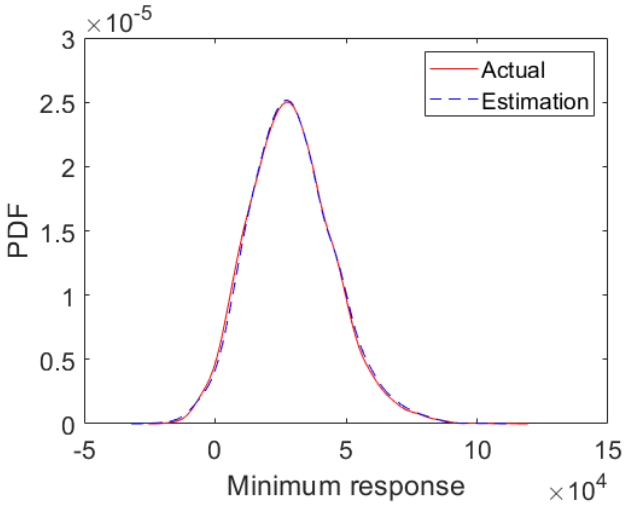

Figure 3.11: PDF curve of the actual and estimated minimum responses of all MCS

Table 3.4: Time-dependent reliability within different time intervals

Time Interval	Time nodes	Estimated R	Accurate R
[1, 6]	$t_1 \sim t_{11}$	0.9952	0.9962
[1, 12]	$t_{11} \sim t_{23}$	0.9924	0.9932
[1, 18]	$t_{23} \sim t_{35}$	0.9862	0.9864

[1, 24]	$t_{35} \sim t_{47}$	0.9824	0.9820
[1, 30]	$t_{47} \sim t_{59}$	0.9748	0.9756

To test the robustness of the proposed approach, time-dependent reliability estimations are performed for the corroded beam problem with different modifications. Four different scenarios are introduced according to the detailed configurations shown in Table 3.5. With the identical settings and procedure as previous, the proposed LSTM-based ensemble learning framework is employed for estimating the time-dependent reliability for each scenario. To demonstrate the accuracy of the proposed approach, direct MCS method is also adopted for accurate reliability analysis, and all the results are presented in Table 3.5. For different scenarios, the performances of the proposed approach are quite stable as accurate reliability approximations can always be achieved with small relative errors. The results demonstrate that the proposed approach is capable of solving time-dependent reliability analysis problems involving stochastic process and time parameter.

Table 3.5: Robustness test results for corroded beam example

Scenarios	Modification	MCS Reliability	Estimated Reliability	Relative Error
1	$h_0 \sim N(0.06, 0.008)$	0.9022	0.9014	0.0887%
2	$b_0 \sim N(0.4, 0.01)$	0.9579	0.9543	0.3758%
3	$u_F = 5500$, $\sigma_F = 800$ $b_0 \sim N(0.4, 0.01)$	0.9207	0.9222	0.1629%
4	$u_F = 4500$, $\sigma_F = 800$ $h_0 \sim N(0.055, 0.004)$	0.8538	0.8554	0.1874%

3.4 Conclusion

In this work, an LSTM-based ensemble learning framework has been established, where Monte Carlo simulation is adopted for estimating the time-dependent reliability based on the combination of LSTM network and GP modeling technique. To employ the LSTM network for learning the relationship between stochastic processes and time-dependent system responses, conditional limit state functions are introduced by fixing the time-independent random variables. Based on one time-series data, a LSTM model can be constructed for modeling a specific conditional limit state function, which can provide accurate response predictions given any random realizations of the stochastic processes. The time-dependent response predictions collected from multiple LSTM models are reorganized according to the realizations of stochastic processes and time instant. Gaussian process models are constructed to specifically model the instantaneous response with respect to random variables. As a result, time-dependent response predictions for the MCS samples can be achieved based on the GP models. The results from two case studies demonstrate that the proposed approach can handle complex problems involving multiple stochastic processes. The proposed approach is capable of accurately predicting the overall time-dependent responses, which ensures the accuracy of reliability estimation and enables the capability of depicting the change of reliability with respect to time. The proposed approach only requires a small number of time-series data for estimating the time-dependent reliability, thus it is convenient to apply the proposed ensemble learning for practical problems.

4 TIME-VARIANT RELIABILITY-BASED DESIGN OPTIMIZATION USING SEQUENTIAL KRIGING MODELING[83]

4.1 Introduction

Though vast efforts have been investigated for time-variant reliability assessment, a rigorous formulation is still lacking for generic time-variant reliability-based design optimization (tRBDO) and it remains a grand challenge to handle such complexity associated with both stationary and non-stationary stochastic processes in tRBDO. In this section, a sequential Kriging modeling approach (SKM) is proposed to effectively search for optimal designs with the desired system time-variant reliability level over a time period under uncertainty. The major contribution of the proposed work lies in developing a simulation-based framework for efficiently handling the complexity and high dimensionality of generic stochastic processes in time-variant reliability-based design optimization. The SKM approach involves a transformation scheme for the dimension reduction of performance functions with stochastic processes, and thus enables the development of time-independent Kriging models in the transformed space to evaluate time-variant system reliability. A design-driven sequential sampling method is then developed for managing the surrogate model uncertainty due to lack of data in tRBDO.

4.2 Sequential Kriging Modeling Approach

4.2.1 Time-variant RBDO Framework

In engineering design, various sources of uncertainties must be considered to ensure a

high-level of system reliability; however, time-related uncertainties such as stochastic operating conditions and component deteriorations have not been taken into account in RBDO. Therefore, time-variant RBDO (tRBDO) is introduced to obtain optimum solutions with the minimum cost while satisfying system reliability requirements over a time period. Generally, a time-variant RBDO with stochastic processes Y(t) and time parameter t can be formulated as

$$\begin{aligned} &\textit{Minimize}: \quad \textit{Cost}(\mathbf{X},\mathbf{d}) \\ &\textit{subject to}: \quad P_f(0,T) = \Pr(\exists t \in [0,T], G_i(\mathbf{X},\mathbf{d},\mathbf{Y}(t),t) \le 0) \le 1 - R_t, \quad i = 1,....,nc \\ &\qquad\qquad \mathbf{Y}(t) = [Y_1(t), Y_2(t),..., Y_{ns}(t)] \\ &\qquad\qquad \mathbf{d}^{\mathrm{L}} \le \mathbf{d} \le \mathbf{d}^{\mathrm{U}}, \mathbf{d} \in R^{nd} \text{ and } \mathbf{X} \in R^{nr} \end{aligned} \tag{4.1}$$

where *Cost* (X, d) is the object function and [0, T] is the projected lifetime; Y(t) represents a vector of stochastic processes; G_i(X, d, Y(t), t) ≤ 0 is defined as the i^{th} failure mode and P_f(0, T) is the time-variant probability of failure at time interval [0, T]; d is a vector of design variables and X is a vector of random variables; d^L and d^U are the lower and upper boundaries of the design variables; *nc*, *nd*, *ns,* and *nr* are the numbers of constraints, design variables, stochastic processes, and random variables, respectively.

The proposed sequential Kriging modeling framework aims to handle tRBDO involving stochastic processes, which mainly consists of four critical components: (1) stochastic processes modeling, (2) stochastic equivalent transformation to handle the high dimensionality associated with temporal uncertainty, (3) design-driven adaptive sampling, and (4) stochastic sensitivity analysis. To solve a tRBDO problem, a deterministic design optimization problem is first solved to obtain the initial design point. Starting with the deterministic optimum design as shown in Fig. 4.1, the SKM first generates realizations of

stochastic processes according to their probabilistic characterizations, and then translates time-variant reliability models to time-independent counterparts through the stochastic equivalent transformation. It is worth noting that the resulting time-independent reliability model can predict time-variant system performance and thus is capable of capturing time-variant failures in time domain. Kriging surrogate model is then constructed for the time-independent reliability model and updated by identifying important samples across time-design domain. To evaluate the time-variant reliability, the resulting Kriging models will be mapped back to time-variant space for predicting time-variant system performance, which eventually yields the extreme distributions of system performance and time-variant probability of failure. The sensitivity of time-variant reliability with respect to design variables is approximated based on the first-order score function, and then utilized in the optimizer to search for optimum designs iteratively.

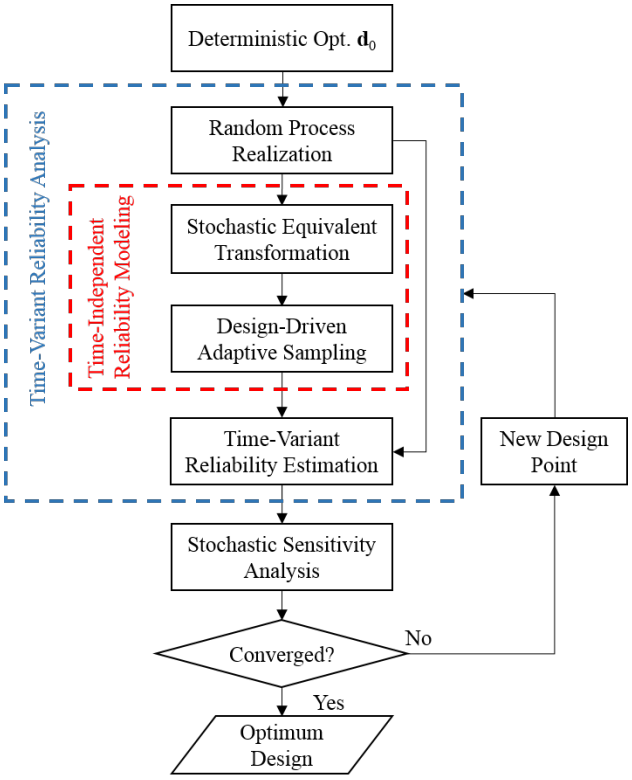

Figure 4.1: Flowchart of SKM framework for tRBDO

4.2.2 Random Processes Realization

In SKM, the first step is to generate random realizations of stochastic processes, including Gaussian/non-Gaussian and/or stationary/non-stationary random processes. For a stochastic process such as Gaussian process $Y_G(t)$, it can be prescribed by three functions with respect to time t, mean function $\mu_Y(t)$, standard deviation function $\sigma_Y(t)$, and auto correlation function $\rho_Y(t)$. In the literature, various methods [84-86] can be used to simulate a Gaussian process, such as the Expansion Optimal Linear Estimation method (EOLE) [87], and the Orthogonal Series Expansion method [88] (OSE). Assuming the time interval is discretized by s time nodes, the covariance between two time nodes is calculated by

$$Cov(t_i, t_j) = \sigma_Y(t_i)\sigma_Y(t_j)\rho_Y(t_i, t_j) \tag{4.2}$$

then the corresponding covariance matrix is derived as

$$\sum = \begin{pmatrix} Cov(t_1,t_1) & Cov(t_1,t_2) & \cdots & Cov(t_1,t_s) \\ Cov(t_2,t_1) & Cov(t_2,t_2) & \cdots & Cov(t_2,t_s) \\ \vdots & \vdots & \ddots & \vdots \\ Cov(t_s,t_1) & Cov(t_s,t_2) & \cdots & Cov(t_s,t_s) \end{pmatrix} \tag{4.3}$$

The covariance matrix can be decomposed as $\Sigma = QIQ^T$ by using Eigen decomposition where $Q = [Q_1, Q_2, \ldots, Q_s]$ is the matrix of eigenvectors and I is a diagonal matrix with the corresponding eigenvalues. Then the Gaussian process $Y_G(t)$ can be expressed as

$$Y_G(t) \approx \mu_y(t) + \sum_{i=1}^{p} \sqrt{I_i} Q_i(t) Z_i \tag{4.4}$$

where p is the number of dominated Eigen functions and $Z = [Z_1, Z_2, \ldots, Z_p]$ are a set of uncorrelated standard normal random variables.

For non-Gaussian processes, Polynomial Chaos Expansion (PCE) and Karhunen-Loeve (KL) expansion are adopted in this work to generate random realizations. According to the methodology in Sakamoto and Ghanem [84], a non-Gaussian process $Y_{NG}(t)$ can be approximated by Hermite orthogonal polynomials, which is expressed as

$$Y_{NG}(t) = \sum_{s=0} b_s(t) \Psi_s\left(\xi(t)\right) \tag{4.5}$$

where the Hermite polynomials $\Psi_s(\xi(t))$ are expressed as

$$\Psi_s\left(\xi(t)\right) = (-1)^s \frac{\phi^s\left(\xi(t)\right)}{\phi\left(\xi(t)\right)} \tag{4.6}$$

where $\phi^s(\xi(t))$ is the s^{th} derivative of probability density function of the standard normal process $\xi(t)$. Then, the approximation of $Y_{NG}(t)$ can be written as

$$Y_{NG}(t) = \sum_{s=0} b_s(t) \Psi_s\left(\xi(t)\right) = b_0(t) + b_1(t)\xi(t) + b_2(t)\left(\xi^2(t) - 1\right) + b_3(t)\left(\xi^3(t) - 3\xi(t)\right) + \cdots \tag{4.7}$$

where $b_s(t)$, $s = 0, 1, 2, 3$ are expansion coefficients corresponding to the first four moments of the non-Gaussian process $Y_{NG}(t)$. For a given non-Gaussian process, the mean $\mu_{NG}(t)$, standard deviation $\sigma_{NG}(t)$, skewness $Sk_{NG}(t)$, and kurtosis $K\mu_{NG}(t)$ are used to calculate the expansion coefficients $b_s(t)$. Assuming that a non-Gaussian process $Y_{NG}(t)$ is expanded in a four-terms series ($s = 3$), the first coefficient $b_0(t)$ is equal to $\mu_{NG}(t)$ as the mean values of the Hermite polynomials are zero. According to the orthonormality properties of the Hermite polynomials, the i^{th} central moments ($i = 2, 3, 4$) can be expressed as,

$$gg_i(b_1(t), b_2(t), b_3(t)) = E\left[\left(Y_{NG}(t) - b_0\right)^i\right], i = 2,3,4 \tag{4.8}$$

The values of $b_1(t)$, $b_2(t)$, and $b_3(t)$ is obtained by minimizing the difference between the gg_i values and the given moments, expressed as

$$\min_{b_1,b_2,b_3} \sum_{i=2}^{4} (gg_i(b_1(t), b_2(t), b_3(t)) - M_i) \tag{4.9}$$

where M_i are the i^{th} central moments of the given non-Gaussian process $Y_{NG}(t)$. It is worth noting that the expansion coefficients $b_s(t)$ are time independent if the non-Gaussian process is stationary. Using the orthogonality properties of the Hermite polynomials, the relationship between covariance matrix $C_{NG}(t_i, t_j)$ of $Y_{NG}(t)$ and covariance matrix $C_\xi(t_i, t_j)$ of $\xi(t)$ can be written as

$$C_{NG}(t_i, t_j) = \sum_{s=1}^{3} b_s^2(t) \cdot (s!) \cdot \left(C_\xi(t_i, t_j)\right)^s \tag{4.10}$$

Given that $C_{NG}(t_i, t_j)$ can be analytically determined based on the autocorrelation of random process $Y_{NG}(t)$, the covariance matrix of the standard normal process $C_\xi(t_i, t_j)$ can be computed according to Eq. (10). A KL expansion is then able to represent $\xi(t)$ as

$$\xi(t) = \sum_{i=1}^{p} \sqrt{\lambda_i} f_i(t) \xi_i \tag{4.11}$$

where p is the number of dominant eigenvalues, λ_i and $f_i(t)$ are the eigenvalues and eigenvectors of covariance matrix $C_\xi(t_i, t_j)$, and ξ_i are independent standard normal random variables.

A stationary non-Gaussian process $Y_{NG}(t)$ following a Weibull marginal PDF with the shape parameter 1.5 and scale parameter 3 is simulated to generate fifteen random realizations as shown in Fig. 4.2. The autocorrelation function is expressed as

$$\rho_{NG}(\Delta t) = e^{-\left(\frac{\Delta t}{0.3}\right)^2} \tag{4.12}$$

where the given time interval [0, 1] is discretized into 100 time nodes. With the first four moments $\mu_{NG} = 2.7082$, $\sigma_{NG} = 1.8388$, $Sk_{NG} = 1.0720$, and $K\mu_{NG} = 1.3904$, a series of Hermite polynomials is used to represent the stochastic process with the four expansion coefficients estimated by Eq. (9), expressed as

$$Y_{NG}(t) = 2.7082 + 0.9662\xi(t) + 0.5652\left(\xi^2(t) - 1\right) - 0.0575\left(\xi^3(t) - 3\xi(t)\right) \tag{4.13}$$

With the obtained four expansion coefficients, the covariance matrix of $\xi(t)$ is calculated by Eq. (4.10). Through employing the Eigen analysis, the standard normal process $\xi(t)$ is then generated from the KL expansion with five dominate Eigen values as shown in Fig. 4.3.

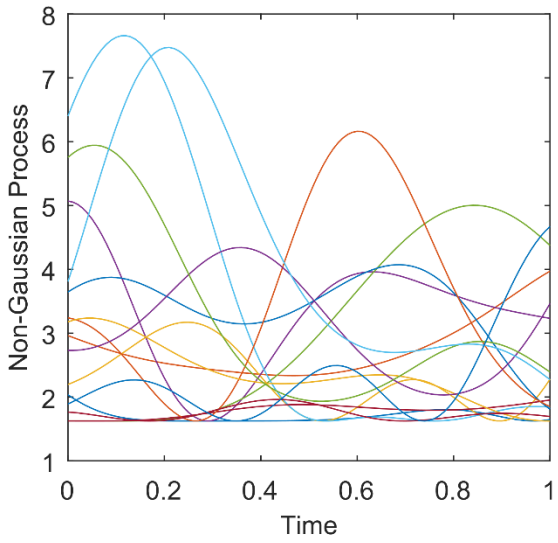

Figure 4.2: Fifteen random realizations of the non-Gaussian process

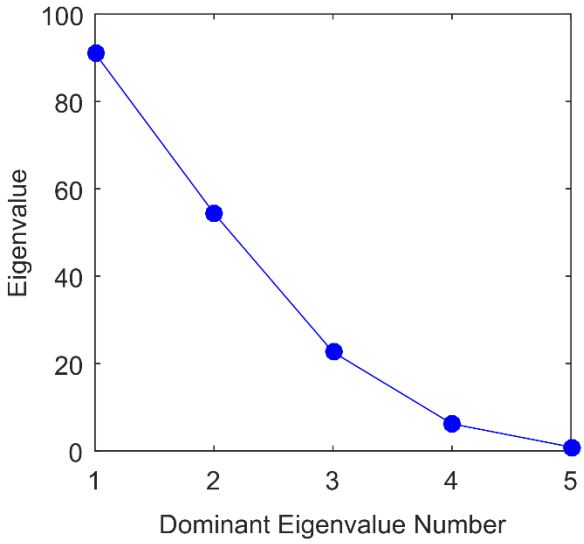

Figure 4.3: Five dominate eigenvalues in the KL expansion

4.2.3 Stochastic Equivalent Transformation

In the time-variant reliability analysis, the limit state is a function of random inputs X, stochastic processes Y(t), and time parameter t. In SKM, stochastic equivalent process

transformation [8] transforms the origin time-variant limit state function $G(\mathrm{X}, \mathrm{Y}(t), t)$ to a time-independent domain, and instantaneous failure events are described as

$$g(\mathbf{X}, \mathbf{Y}', t') < 0 \tag{4.14}$$

where continuous random variables Y *'* and *t'* are translated from stochastic processes $\mathrm{Y}(t)$ and time *t* respectively, random variables X remain the same in the transformed input space. As shown in Fig. 4.4, with the multiple realizations of the stochastic process $Y(t)$, the probability density function (PDF) of *Y*' is then obtained by averaging the PDFs of $Y(t)$ over the time of interest [0, *T*]. At each time node, the stochastic process is converted to a random variable, and thus the transformed random parameter *Y'* is a mixture model constructed with random distributions at a set of time nodes. By discretizing the time interval into *s* time nodes, *s* probability density function can be obtained for the distribution of $Y(t_i)$, $i = 1, 2, \ldots, s$. The probability density function of the *Y'* is then expressed as

$$f_{pdf}(Y') \approx \frac{1}{s}\sum_{i=1}^{s} f_{pdf}(Y(t_i)) \tag{4.15}$$

For stationary Gaussian processes, the probabilistic characteristics of *Y'* can be obtained analytically as the mean and standard deviation functions remain the same over time. In terms of general random processes, the realizations of stochastic processes $Y(t)$ in subsection 4.2.2 is readily merged to form a set of random sample points that follow the distribution of random parameter *Y'*. In the transformed input space, the random variable *t'* is treated as a uniform distributed variable over the time interval [0, *T*] as a failure event at any time instant will lead to a system failure.

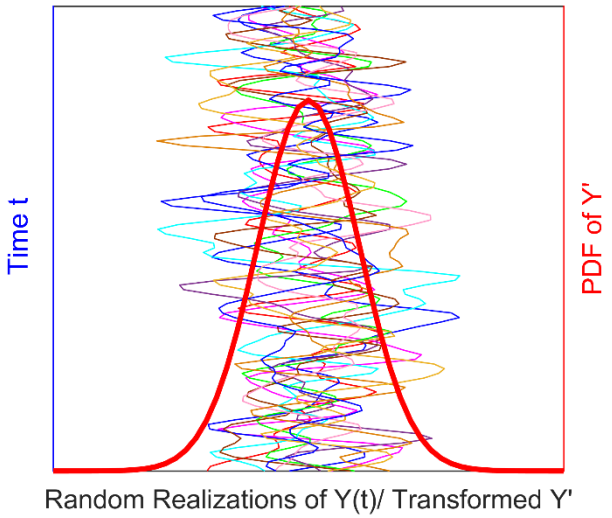

Figure 4.4: Transformation of stochastic process Y(t)

With the transformed random parameters X, Y', and t', the probability of failure in the transformed space is defined as

$$P_{f-ave} = \Pr\left[g(\mathbf{X}, \mathbf{Y}', t') < 0\right] \tag{4.16}$$

where the $P_{f\text{-}ave}$ is the average of the instantaneous probability of failure over the time interval [0, T]. It is worth noting that the time-independent model in Eq. (4.16) is able to capture time-variant failure events by nature.

4.2.4 Design-Driven Adaptive Sampling

With the stochastic equivalent transformation, surrogate modeling techniques are employed to predict the time-independent limit state function g(X, Y', t'). Though a variety of surrogate modeling techniques are available, a confidence-based adaptive sampling scheme [50] is utilized in the proposed approach to construct metamodels for the time-independent limit state function mainly due to its ability of efficiently handling surrogate model uncertainty. Let W = [X, Y', t'] denotes the input variables of transformed limit state

function g(X, Y*'*, *t'*), and w is a random realization of input W, the probability of failure is then expressed as

$$P_{f-ave} = \Pr(g(\mathbf{w}) < 0) = \int ... \int_{g(\mathbf{w})<0} f_x(\mathbf{w}) d\mathbf{w} \tag{4.17}$$

where f_x(w) is the joint probability density function. By defining the failure region $\Omega_f = \{w \mid g(w) < 0\}$, the probability of failure can be expressed as

$$P_{f-ave} = \Pr(\mathbf{w} \in \Omega_f) = \int_{\Omega} I_f(\mathbf{w}) f_x(\mathbf{w}) d\mathbf{w} = E[I_f(\mathbf{w})] \tag{4.18}$$

where Ω represents the transformed random input space. E[.] is the expectation operator and I_f(w) is an indicator function to classify success and failure points, defined as

$$I_f(\mathbf{w}) = \begin{cases} 1, & \mathbf{w} \in \Omega_f \\ 0, & otherwise \end{cases} \tag{4.19}$$

Let *nr* and *ns* denote the number of random variables in X and Y' respectively, then $k = nr + ns + 1$ is the number of input variables in W. With the training data set D = [W, G] consisting of n input points W and the corresponding responses G, the general form of Kriging model is described as

$$g_K(\mathbf{w}) = f(\mathbf{w}) + S(\mathbf{w}) \tag{4.20}$$

where g_K(w) is the approximation of the performance function g(w) at the point w. The first term f(w) is a polynomial term which can be substituted by a constant value μ. S(w) is a Gaussian stochastic process with zero mean and a covariance matrix given by

$$\mathbf{Cov}_{(i,j)} = \sigma^2 \mathbf{R} \tag{4.21}$$

where i and j represent input points w_i and w_j, respectively, and R is a $n \times n$ correlation matrix. Various correlation functions are available in the literature, such as Gaussian,

rational quadratic, Matern, and exponential correlation function. According to Stein [89], the impact on the Kriging prediction from not using the suitable covariance structure is asymptotically negligible if the Kriging model can be updated by having more observations. In this study, the Kriging surrogate will be iteratively updated by the adaptive sampling scheme. Thus, the selection of the Kriging covariance structure will not have significant impact on the response prediction, and a stationary and isotropic Gaussian correlation function is adopted in this work, expressed as

$$R(\mathbf{w}_i, \mathbf{w}_j) = \exp\left[-\sum_{q=1}^{k} a_q \left| \mathbf{w}_{i,q} - \mathbf{w}_{j,q} \right|^{b_q} \right] \tag{4.22}$$

With n initial samples [W, G], the log likelihood function is given by

$$LogLikelihood = -\frac{1}{2}\left[n\ln(2\pi) + n\ln\sigma^2 + \ln|\mathbf{R}| + \frac{1}{2\sigma^2}(\mathbf{G} - \mathbf{A}\mu)^T \mathbf{R}^{-1}(\mathbf{G} - \mathbf{A}\mu) \right] \tag{4.23}$$

where A is an $n \times 1$ unit vector. All the hyper parameters can be obtained by maximizing the likelihood function, and then the correlation matrix R can be computed according to Eq. (4.22). Let r denotes the correlation vector between a new point w *'* and training samples, the response and mean square error predicted by the Kriging model are obtained as

$$g_k(\mathbf{w}') = \mu + \mathbf{r}^T \mathbf{R}^{-1}(\mathbf{G} - \mathbf{A}\mu) \tag{4.24}$$

$$e(\mathbf{w}') = \sigma^2 \left[1 - \mathbf{r}^T \mathbf{R}^{-1}\mathbf{r} + \frac{(1 - \mathbf{A}^T \mathbf{R}^{-1}\mathbf{r})^2}{\mathbf{A}^T \mathbf{R}^{-1}\mathbf{A}} \right] \tag{4.25}$$

To handle the surrogate model uncertainty $e(.)$ due to the lack of data, adaptive sampling scheme should be employed for identifying most useful point and updating Kriging for probability analysis in Monte Carlo simulation (MCS).

In MCS, N Monte Carlo samples are generated based on the randomness of the input

variables, denoted as

$$\mathbf{w}_{m,i} = [\mathbf{x}_i, \mathbf{y}_i^{mcs}, t_i], i = 1, 2, ...N \tag{4.26}$$

where y_i^{mcs} is the i^{th} Monte Carlo samples of Y'. For the point $w_{m,i}$, the limit state function $g(w_{m,i})$ can be approximated by Kriging as a normally distributed random variable, given by $g(w_{m,i}) \sim N(g_K(w_{m,i}), e(w_{m,i}))$. The indicator function is thus derived as

$$I_f(\mathbf{w}_{m,i}) = \begin{cases} 1, \ g_k(\mathbf{w}_{m,i}) < 0 \quad \text{(failure)} \\ 0, \ g_k(\mathbf{w}_{m,i}) \geq 0 \quad \text{(success)} \end{cases} \tag{4.27}$$

The average probability of failure $P_{f\text{-}ave}$, over the time period [0, T] is thus calculated in MCS. The confidence level (CL) at the point $w_{m,i}$ is defined as the probability of correct classification, which is expressed as

$$CL(\mathbf{w}_{m,i}) = \Phi\left(\frac{|g_k(\mathbf{w}_{m,i})|}{\sqrt{e(\mathbf{w}_{m,i})}}\right) \tag{4.28}$$

where $\Phi(.)$ is a standard normal cumulative distribution function. After evaluating the CL for all the points in MCS, the cumulative confidence level (CCL) is obtained as

$$CCL = \frac{1}{N}\sum_{i=1}^{N} CL(\mathbf{w}_{m,i}) \tag{4.29}$$

The CCL indicates the accuracy of Kriging model in predicting $P_{f\text{-}ave}$ in MCS. To enhance the fidelity of Kriging model, the most useful point will be identified by maximizing the importance measure, which is defined as

$$\mathrm{H}(\mathbf{w}_{m,i}) = (1 - CL(\mathbf{w}_{m,i})) * f_x(\mathbf{w}_{m,i}) * \sqrt{e(\mathbf{w}_{m,i})} \tag{4.30}$$

where $f_x(.)$ is the joint probability density function of input variables, and $e(.)$ is the estimated mean square error of Kriging model prediction. The limit state value at the

selected point will be evaluated and then incorporated in the training data set for updating the Kriging model. As shown in Fig. 4.5, the design-driven adaptive updating procedure will be triggered at each design iteration to search for the important sample points.

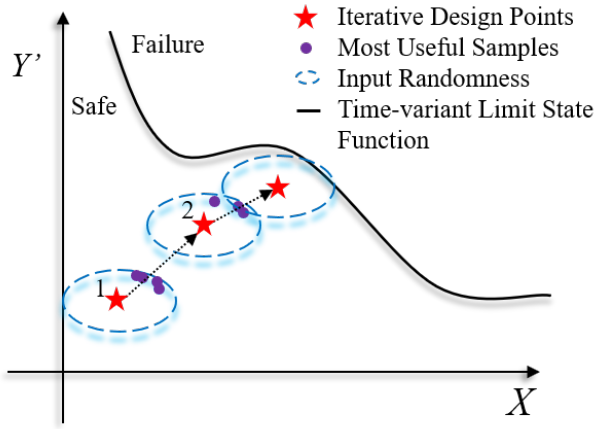

Figure 4.5: Illustration of the design-driven adaptive sampling

4.2.5 Time-variant Reliability Analysis

With the Kriging surrogate model, the time-variant probability of failure within the time interval [0, T] can be approximated by

$$P_f(0,T) \approx \Pr(\exists t \in [0,T], g_k(\mathbf{X}, \mathbf{Y}(t), t) < 0) \tag{4.31}$$

where $g_k(.)$ is the time-variant limit state prediction using the Kriging model. Monte Carlo simulation (MCS) method is employed in this work to calculate the time-variant probability of failure in Eq. (4.31). In MCS, the first step is to generate N random realizations of X and Y(t) as introduced in section 4.2.2 by discretizing the time interval [0, T] with s nodes. For the i^{th} realization of random parameter and the stochastic process (x_i, y_i), the instantaneous limit state function g(x_i, $y_{i,(j)}$, t_j) at the j^{th} time node is predicted directly by the Kriging model, and a time-variant failure event occurs if

$$\min_{1\le j\le s} g_K(\mathbf{x}_i, y_{i,(j)}, t_j) < 0 \tag{4.32}$$

Clearly, the distribution of the worst performance over time period [0, T] can be obtained in Eq. (4.32), and the time-variant probability of failure is then approximated by

$$P_f(0,T) \approx \frac{N_f}{N} \tag{4.33}$$

where N_f is the number of time-variant failure samples within the time interval [0, T].

4.2.6 Sensitivity Analysis of Time-variant Reliability

In sensitivity analysis, a general form of the time-variant probability of failure is rewritten as

$$P_f(0,T) \equiv \int_{R^N} I_{f-t}(\mathbf{X}) f_x(\mathbf{X}) d\mathbf{X} = E[I_{f-t}(\mathbf{X})] \tag{4.34}$$

where X is the vector of input random variables, f_x(X) is the joint probability density function, and $I_{f\text{-}t}$(X) is the indicator function expressed as

$$I_{f-t}(x_i) = \begin{cases} 1, & \min\limits_{1\le j\le s} g_K(x_i, y_j, t_j) < 0 \ \text{(failure)} \\ 0, & \text{otherwise (success)} \end{cases} \tag{4.35}$$

The partial derivative of the probability of failure with respect to the i^{th} design variable d_{i} is thus derived [47] as

$$\frac{\partial P_f(0,T)}{\partial d_i} = \frac{\partial}{\partial d_i} \int_{R^N} I_{f-t}(\mathbf{X}) f_x(\mathbf{X}) d\mathbf{X} = \mathrm{E}\left[I_{f-t}(\mathbf{X}) \frac{\partial \ln f_x(\mathbf{X})}{\partial d_i} \right] \tag{4.36}$$

For independent random variables, the joint probability density function of X is expressed

as multiplication its marginal PDFs as

$$f_x(\mathbf{X}) = \prod_{i=1}^{nr} f_{x_i}(x_i) \tag{4.37}$$

where *nr* is the dimension of input variables X. With the time-variant reliability and its sensitivity information, the sequential quadratic programming (SQP) [90] is adopted as an optimizer to search for optimum solutions iteratively in tRBDO.

4.3 Case Studies

In this section, three examples are used to demonstrate the effectiveness of the proposed approach for solving the time-variant reliability-based design optimization problems.

4.3.1 Case Study I: A Mathematical Design Problem

A two dimensional mathematical time-variant reliability-based design optimization problem [11] is formulated as

$$\begin{aligned}
&\text{Minimize}: \ Cost(\mathbf{d}) = 10 - X_1 + X_2 \\
&\text{subject to:} \ P_f(0,1) = \Pr(\exists t \in [0,1], G_i(\mathbf{d}, Y_1(t), Y_2(t)) \le 0) \le 1 - R_t, \ i = 1 \sim 3 \\
&\qquad \mathbf{d} \ = \ [X_1, X_2], \ 0 \le X_1 \ \& \ X_2 \le 10 \\
&\text{where} \qquad G_1 = \frac{X_1^{\,2} X_2}{20} - 1 \\
&\qquad G_2 = \frac{(X_1 + X_2 - 5)^2}{30} + \frac{(X_1 - X_2 - 12)^2}{120} - 1 - Y_1(t) + 0.01 * Y_2(t) \\
&\qquad G_3 = \frac{80}{(X_1^{\,2} + 8X_2 - 5)} - 1
\end{aligned} \tag{4.38}$$

where the two random design variables X_1 and X_2 follow normal distributions as $X_1 \sim N(\mu_1, 0.3464^2)$ and $X_2 \sim N(\mu_2, 0.3464^2)$. The target reliability is set to $R_t = 0.985$ for all three probabilistic constraints. To maintain a high-fidelity Kriging model during the design

optimization, a high-level target cumulative confidence level CCL_t = 0.999 is set as a criterion in updating Kriging models adaptively, as introduced in subsection 4.2.4. The tRBDO problem involves two stochastic processes Y(t)=[$Y_1(t)$, $Y_2(t)$], including a non-stationary Gaussian process $Y_1(t)$ and a stationary process $Y_2(t)$ with a Weibull marginal PDF. The Gaussian process $Y_1(t)$ is fully characterized by its mean function $\mu_Y(t)$, standard deviation function $\sigma_Y(t)$ and the autocorrelation function $\rho_Y(t)$, given as

$$\mu_Y(t) = 0.1 * t \tag{4.39}$$

$$\sigma_Y(t) = 0.05 * t \tag{4.40}$$

$$\rho_Y(t_1, t_2) = \exp\left(-\frac{(t_2 - t_1)^2}{0.001}\right) \tag{4.41}$$

The scale and shape parameters of the non-Gaussian process $Y_2(t)$ are set to 2 and 1.2, thus the first four moments can be directly obtained as mean μ_{NG} = 1.8813, standard deviation σ_{NG} = 1.5745, skewness Sk_{NG} = 1.5211, and kurtosis $K\mu_{NG}$ =3.2357. The autocorrelation function of $Y_2(t)$ is given by

$$\rho_{NG}(t_1, t_2) = \exp\left(-\frac{(t_2 - t_1)^2}{0.01}\right) \tag{4.42}$$

Following the procedure outlined in subsection 4.2.2, the time interval [0, 1] is discretized into 100 nodes evenly, and 10^6 random realizations for each stochastic process are generated for the time-variant reliability analysis. The first fifty realizations of $Y_1(t)$ and $Y_2(t)$ are shown in Fig. 4.6.

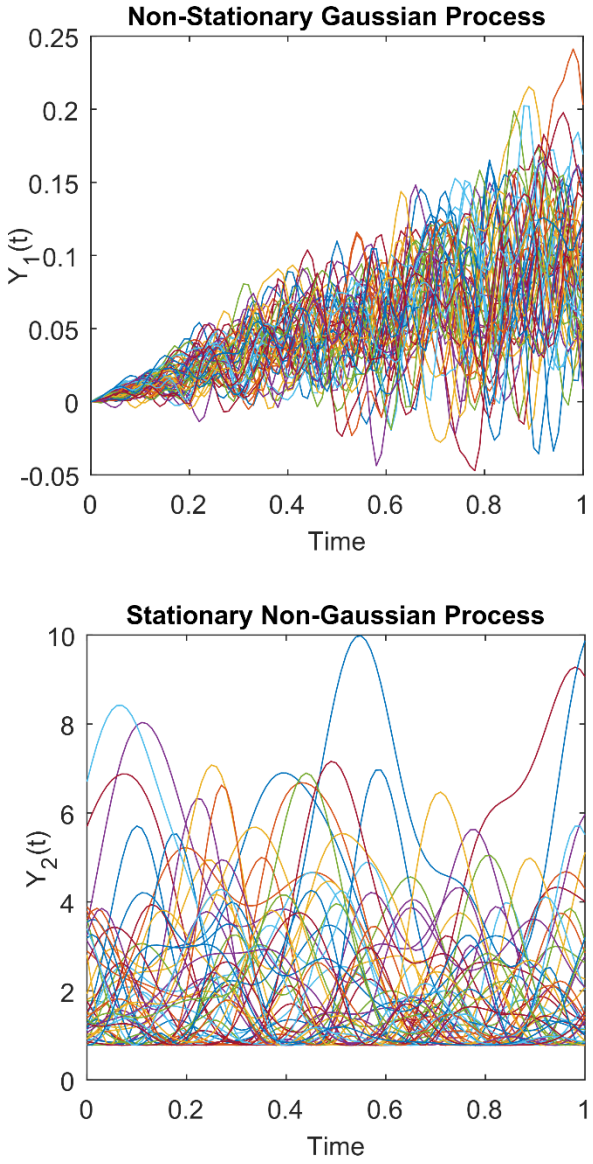

Figure 4.6: 50 realizations of the $Y_1(t)$ and $Y_2(t)$

The first step of the SKM approach is to obtain an initial design point by solving the corresponding deterministic optimization problem, where the stochastic processes in G_2 are fixed to its mean. The deterministic design optimization starts with $d_0 = [5, 5]$, and approaches the deterministic optimum design $d_d = [8.5770, 1.4294]$ after seven iterations. As the second constraint G_2 contains stochastic processes, the time-variant limit state

function of G_2 is converted to the time-independent one using stochastic equivalent transformation. The input domains of three Kriging models g_{K1}, g_{K2}, and g_{K3} are defined as $W_1 = W_3 = [X_1, X_2,]$, $W_2 = [X_1, X_2, Y_1', Y_2']$, respectively, where the PDFs of Y_1' and Y_2' are obtained as introduced in subsection 4.2.3. Then the Latin Hypercube sampling method (LHS) is utilized to generate 20 initial sample points, and they are combined with seven sample points that evaluated during deterministic design for constructing initial Kriging models. By setting the deterministic optimum design d_d as the initial design point in tRBDO, the optimum design d_{opt} = [6.7733, 3.3718] is obtained after 8 iterations. The iterative history of reliabilities for three constraints, design points, and cost function values are summarized in Table 4.1. It is worth noting that the reliabilities are estimated by the updated Kriging models, denoted by R_1^{SKM}, R_2^{SKM}, and R_3^{SKM}, respectively.

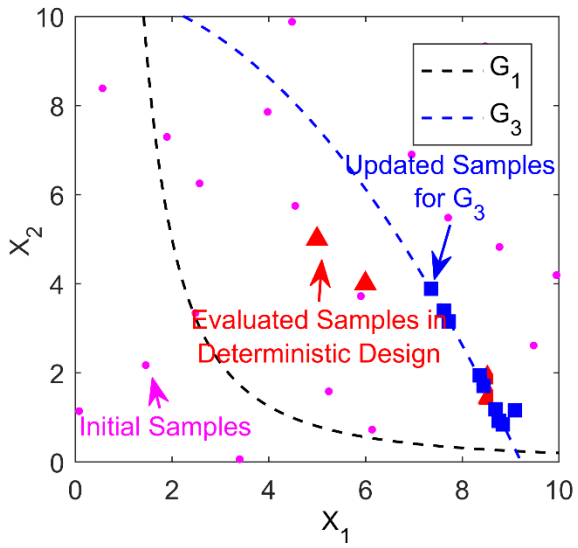

Figure 4.7: Samples for constructing g_{K1} and g_{K3} Kriging models

During the tRBDO process, the design-driven adaptive sampling scheme is triggered to identify 57 samples and 9 samples for updating the Kriging model g_{K2} and g_{K3}, respectively. There is no need to update g_{K1} since the target CCL_t can always be satisfied

in the design optimization process. Figure 4.7 shows the sample points for constructing the Kriging models, including 20 LHS samples, 7 samples evaluated during deterministic design optimization, and the additional nine samples identified through design-driven adaptive sampling for g_{K3}. The comparison between true limit state functions (dashed lines) and estimated results (solid lines) by updated Kriging models is shown in Fig. 4.8, where the time-variant limit state function G_2 is depicted at $Y_1(t) = 0$ and $Y_2(t) = 1.8813$. A high accuracy level of Kriging model g_{K2} can be obtained in the area near to the optimum design d_{opt} = [6.7733, 3.3718] because the most useful samples selected by the design-driven adaptive sampling scheme are located in the critical area of interest as needed.

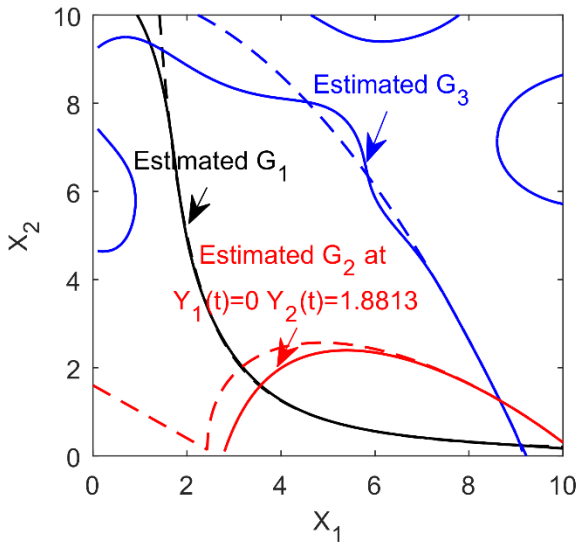

Figure 4.8: Approximated limit state functions by Kriging model vs. true limit state functions

The overall tRBDO process is shown in Fig. 4.9, where the first three designs are marked with numbers and point '1' is the deterministic optimum design point. The

convergence of design points with respect to design iterations is detailed in Fig. 4.10 while the time-variant reliabilities for three constraints also converge to the target reliability 0.9850 within 8 design iterations as shown in Fig. 11.

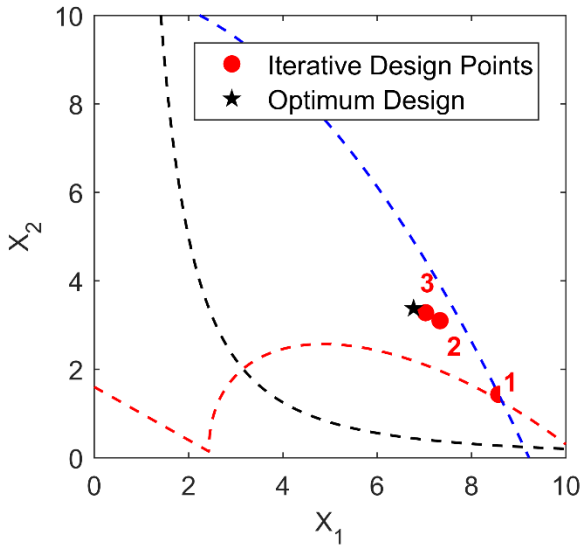

Figure 4.9: Iterative design points in tRBDO

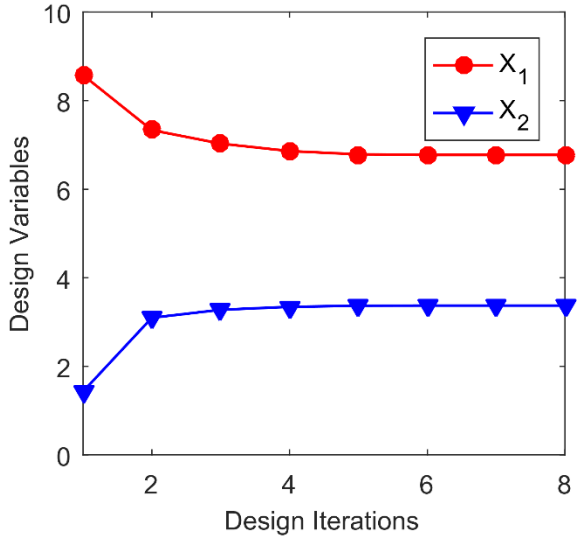

Figure 4.10: Design history at each iteration

For the purpose of comparison, the simulation-based time-variant reliability analysis approach SPCE [91], together with the first-order score function method (SF) for sensitivity analysis, are employed to solve the same tRBDO problem, denoted as SPCE&SF. Furthermore, direct Monte Carlo simulation is utilized to verify the accuracy of the proposed method. As shown in Table 4.2 where the reliability R_1, R_2, and R_3 are verified through direct MCS, the SPCE&SF approach obtains an optimum design after 17 iterations while requiring 459 function evaluations in total. However, the resulting optimum design violates the probabilistic constraints as the reliability R_2 and R_3 are less than the target 0.985 and the error of time-variant reliability for performance function G_2 is 6.36%. With the proposed SKM approach, the optimum design is close to the optimum solution obtained from direct MCS and satisfies the reliability requirements. In addition, it is observed that the proposed SKM approach only needs 147 function evaluations to obtain an accurate optimum design, including 27, 84, and 36 function calls for Kriging model g_{K1}, g_{K2}, and g_{K3}, respectively. The results demonstrate that the proposed approach can efficiently handle stochastic processes and solve time-variant RBDO problems effectively.

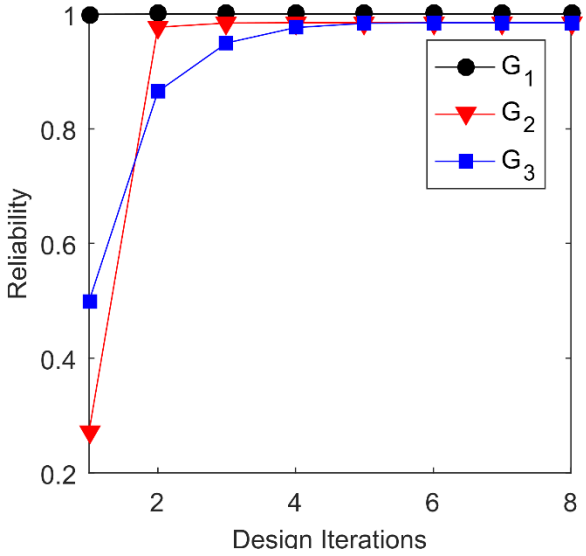

Figure 4.11: Reliabilities of three constraints at each design iteration

Table 4.1: tRBDO design history for case study I

Iterations	Design Variables		Reliabilities			Cost
	X_1	X_2	R_1^{SKM}	R_2^{SKM}	R_3^{SKM}	
1	8.5770	1.4294	0.9995	0.2714	0.4990	2.8524
2	7.3334	3.0961	1	0.9771	0.8649	5.7627
3	7.0291	3.2763	1	0.9844	0.9497	6.2472
4	6.8607	3.3431	1	0.9851	0.9765	6.4824
5	6.7868	3.3676	1	0.9850	0.9839	6.5807
6	6.7732	3.3721	1	0.9850	0.9849	6.5989
7	6.7732	3.3720	1	0.9850	0.9849	6.5988
8	6.7733	3.3718	1	0.9850	0.9849	6.5985

Table 4.2: Comparison of optimum results for case study I

	Optimum	R_1	R_2	R_3	Cost	#F
SKM	[6.7733, 3.3718]	1	0.9839	0.9849	6.5984	147
SPCE&SF	[6.9540, 3.0661]	1	0.9224	0.9831	6.1122	459

MCS	[6.7634, 3.3883]	1	0.9850	0.9850	6.6249	$3*10^6$

4.3.2 Case Study II: A Cantilever Beam Design Problem

In the second study, a cantilever beam under an external load is introduced as shown in Fig. 4.12. The material of the beam is assumed to be SAE-1008, a standard grade carbon steel which is widely used in auto manufacture, oil drum, and transformer's tank panel. The length L is fixed to 500 mm while height h and width b are treated as two design variables, denoted as d = [h, b]. An external load $F(t)$ is applied on the tip of this beam and depicted as a stationary Gaussian stochastic process with 170 kN mean and 10 kN standard deviation. The time interval of interest is [0, 1], and all random variables and stochastic process are detailed in Table 4.3.

Table 4.3: Cantilever beam specifications

Random variable	Distribution	Mean value	Standard deviation
Length, L	/	500 mm	/
Width, b	Normal	b	3.436 mm
Height, h	Normal	h	3.436 mm
External Load F(t)	Normal	170 kN	10 kN

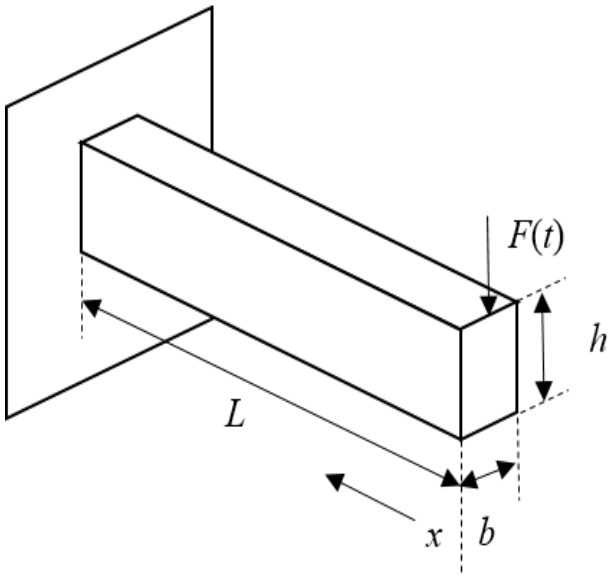

Figure 4.12: Cantilever beam geometry

For this cantilever beam, the stress at position x can be expressed as

$$S(x) = \frac{6 \cdot F(t) \cdot (L - x)}{bh^2} \tag{4.43}$$

According to the geometry of the beam, the maximum stress at $x = 0$ can be expressed as

$$S_{\max} = S(0) = \frac{6F(t)L}{bh^2} \tag{4.44}$$

Given the yield strength of SAE-1008 $S_y = 275$ MPa, the limit state function of this beam is defined as

$$G(\mathbf{d}, F(t)) = S_y - S_{\max} \tag{4.45}$$

Thus, for any time instant t within [0, 1], $G(\mathrm{d}, F(t)) < 0$ indicates failure due to plastic deformation. The size of cross section is formulated as an objective function, and the boundaries of the two design variables are given as 1) the height h should be within [140,

180] in millimeters and 2) the width b should be within [50, 150] in millimeters. Therefore, the cantilever beam tRBDO problem is formulated as

$$\begin{aligned} &\text{Minimize}: && \text{Cost}(\mathbf{d}) = h + b \\ &\text{subject to}: && P_f(0,1) = \Pr(\exists t \in [0,1], G(\mathbf{d}, F(t)) \le 0) \le 1 - R_t \\ & && \mathbf{d} = [h,\ b] \\ &\text{where} && G = S_y - \frac{6000 \cdot F(t) \cdot 500}{h^2 \cdot b} \end{aligned} \tag{4.46}$$

In this study, a target reliability is set to R_t = 0.985 and a target cumulative confidence level CCL_t is set to 0.999. The deterministic design starts with the mean value of the design variables d_0 = [160, 100] and terminates at the deterministic optimum design d_d = [154.7946, 77.3973], while 11 points are evaluated during the deterministic optimization process. By employing the stochastic equivalent transformation, the stochastic process $F(t)$ is transformed to a random variable F', which follows a normal distribution with 170 kN mean and 10 kN standard deviation since $F(t)$ is a stationary Gaussian process. By discretizing the time interval into 100 time nodes, 10^6 random realizations are obtained as introduced in section 4.2.2. To solve the tRBDO problem, a total number of 20 initial samples points are generated by Latin hypercube sampling scheme and evaluated for the performance function. The initial Kriging model is then constructed based on the available 31 samples, and 10^6 random realizations of the stochastic process $F(t)$ are generated for the time-variant reliability analysis. The tRBDO process starts with the deterministic optimum design d_d, and it converges to an optimum design d_{opt} = [166.1193, 87.4383] after 14 iterations. As shown in Fig. 4.13, the approximated limit state function is compared with the true responses while the stochastic load is fixed to 170 kN. It shows that the high-fidelity Kriging model is able to accurately approximate limit state functions.

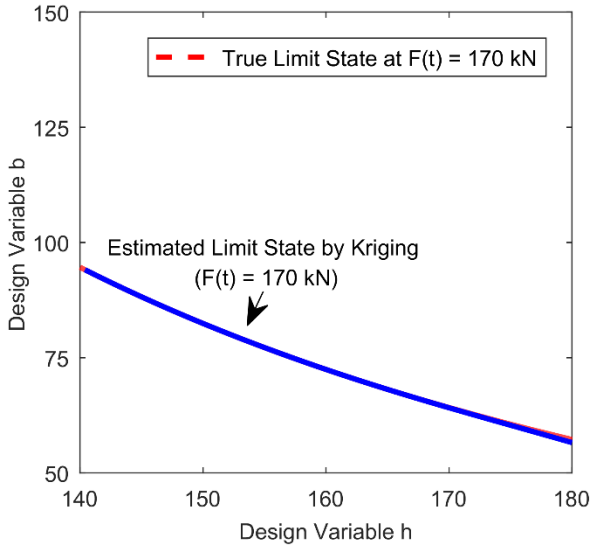

Figure 4.13: High fidelity of the updated Kriging model at *h*, *b* design space.

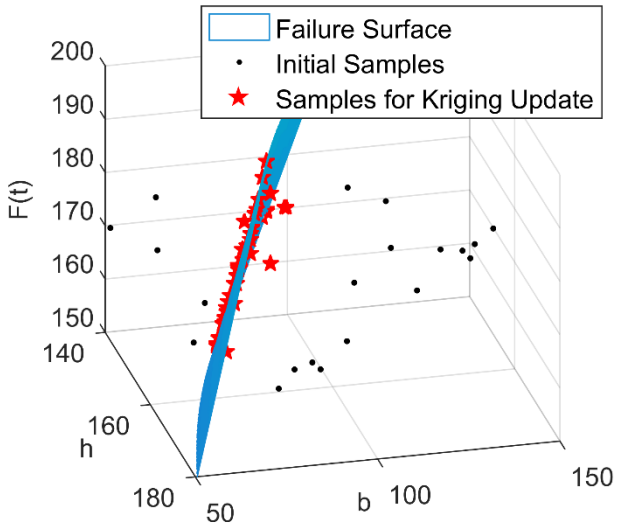

Figure 4.14: Sample points for constructing Kriging model.

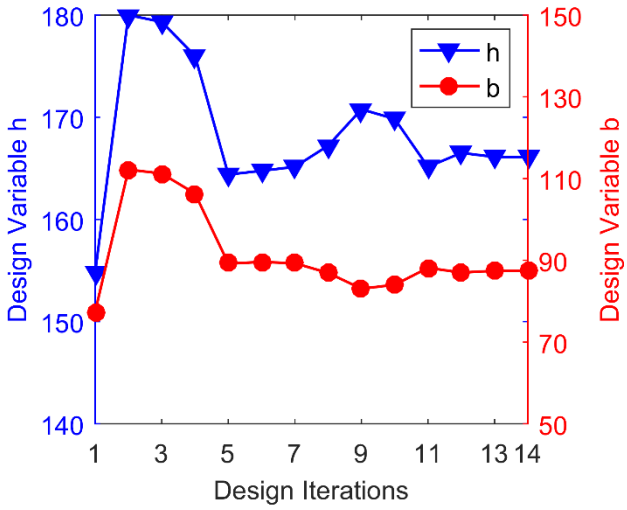

Figure 4.15: Design history at each iteration.

In the SKM approach, the Kriging model is automatically updated through the design-driven adaptive sampling at each design iteration and a total number of 35 most useful sample points are identified during the overall tRBDO process. All the selected samples for constructing the Kriging model are plotted in Fig. 4.14, where black nodes represent the initial points and red stars denote the most useful samples. As shown in the figure, almost all the selected samples are located on the failure surface, ensuring an efficient Kriging updating procedure. Figure 4.15 shows the iterative history of design variables during tRBDO process while Table 4.4 provides the reliabilities R^{SKM}, design points, and cost at each design iteration.

For the comparison purpose, the SPCE&SF method and direct MCS method are also employed to solve the tRBDO problem for the cantilever beam case study, and the optimum solutions and number of function evaluations from three methods are listed in Table 4.5. To verify the optimum designs obtained by the SKM and SPCE&SF, MCS with 10^6

samples is employed as the reference to compute the reliabilities. An optimum design is obtained after 40 iterations by SPCE&SF as [167.7387, 85.6917], while 400 function evaluations are required to construct a SPCE model in design optimization. The result shows that both SKM and SPCE&SF approach can accurately solve the time-variant reliability-based design optimization problem involving stationary Gaussian process. However, the SKM approach is more efficient as it only requires 66 functions evaluations for achieving the optimum design.

Table 4.4: tRBDO design history for case study II

Iterations	Design Variables		R^{SKM}	Cost
	h	b		
1	154.7946	77.3973	0.0363	232.1919
2	180.0000	112.2090	1.0000	292.2090
3	179.3359	111.2309	1.0000	290.5669
4	176.0155	106.3408	1.0000	282.3563
5	164.3941	89.2254	0.9789	253.6194
6	164.7613	89.5981	0.9841	254.3594
7	165.1484	89.3034	0.9848	254.4517
8	167.2207	86.9177	0.9852	254.1384
9	170.7791	83.0660	0.9840	253.8451
10	169.8417	84.0105	0.9849	253.8523
11	165.1435	88.1642	0.9830	253.3078
12	166.5170	87.0030	0.9847	253.5200
13	166.1181	87.4380	0.9850	253.5561
14	166.1193	87.4383	0.9850	253.5576

Table 4.5: Comparison of optimum results for case study II

	Optimum	Reliability	Cost	#F
SKM	[166.1193, 87.4383]	0.9856	253.5576	66
SPCE&SF	[167.7387, 85.6917]	0.9848	253.4304	400
MCS	[168.4629, 84.9994]	0.9850	253.4623	10^6

4.3.3 Case Study III: Aircraft Tubing Design

In industry, tubing assemblies have been widely integrated in many subsystems, for example, fuel system and hydraulic system. Catastrophic system failure can be caused by the potential failure of aircraft tubing, and determining the optimized geometry of tubing under the time-variant uncertainties becomes extremely important in the early design stage. In this study, a twisted tubing design problem is solved by employing the proposed SKM approach.

A twisted tube made of steel (E = 200 GPa, v = 0.27) is shown in Fig. 4.16. The inner diameter D, thickness T, the radius of bending for two bended tube R_1 and R_2 are design variables that follow normal distributions, detailed in Table 4.6.

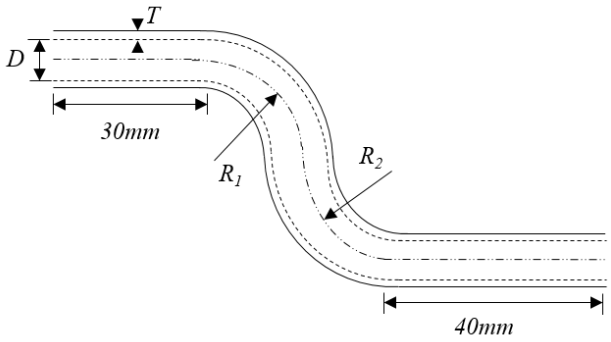

Figure 4.16: Geometry of twisted aircraft tubing.

Table 4.6: Aircraft tubing specifications

Design variable	Distribution	Mean value	STD	Boundary
Inner diameter, D	Normal	μ_D	0.1 mm	[14mm, 16mm]
Thickness, T	Normal	μ_T	0.05 mm	[2mm, 2.6mm]
Radius of bending, R_1	Normal	μ_{R1}	0.1 mm	[14mm, 16mm]
Radius of bending, R_2	Normal	μ_{R2}	0.1 mm	[14mm, 16mm]

The tube will experience time-variant pressure $P(t)$ during the operation, which is applied on the inner surface of the twisted tube. The inner pressure is modeled as a stationary Gaussian process with 30 MPa the mean and 1 MPa standard deviations respectively. The time interval of interest is [0, 1] and the autocorrelation function of $P(t)$ is the same as shown in Eq. (4.41). A finite element model has been developed in ANSYS to obtain the maximum von Mises stress of the tube. A failure is defined as the maximum von Mises stress is greater than the yield strength σ_y = 235 MPa, and the design objective is to minimize the total volume of the twisted tube, expressed as

$$\text{Cost}(D,T,R_1,R_2)=\pi\left\{\left(\frac{D}{2}+T\right)^2-\left(\frac{D}{2}\right)^2\right\}\left(30+40+\frac{2\pi R_1}{4}+\frac{2\pi R_2}{4}\right) \quad (4.47)$$

Thus, the tRBDO problem for the aircraft tubing design is formulated as,

$$\begin{aligned}
&\text{Minimize}: && \text{Cost}(\mathbf{d})\\
&\text{subject to}: && P_f(0,1)=\Pr(\exists t\in[0,1], G(\mathbf{d},P(t))\le 0)\le 1-R_t,\\
& && \mathbf{d}\ =\ [D,T,R_1,R_2]\\
&\text{where} && G(\mathbf{d},P(t))=\sigma_y-Max_{stress}(\mathbf{d},P(t))
\end{aligned} \quad (4.48)$$

In this study, both the targets of reliability and the cumulative confidence level are set to 0.98. Starting with the design [15, 2.3, 15, 15], a deterministic design optimization problem is first solved to obtain the initial design point for tRBDO. By using the finite

difference method to provide the sensitivity, the deterministic solution d_d = [14, 2, 14.5420, 14.4637] is obtained after 10 iterations, and 50 samples points are evaluated during the deterministic design process. In the SKM approach, the time-variant limit state function with stochastic processes is first converted into time-independent counterpart through the stochastic equivalent transformation. To construct surrogate model for the finite element simulation, an Kriging model is trained based on the 50 sample points that evaluated in deterministic optimization and 40 random samples generated by Latin hyper cube sampling. The time interval [0, 1] is evenly discretized into 100 time nodes, then 10^6 random realizations of the stochastic process $P(t)$ is generated for time-variant reliability analysis. The optimum design is achieved after 14 iterations as d_{opt} = [14.0000, 2.2215, 15.7457, 15.7297], and the iterative design history for the four design variables is shown in Fig. 4.17. The convergence of the time-variant reliability and the total volume of the twisted tube are plotted in Figure 4.18.

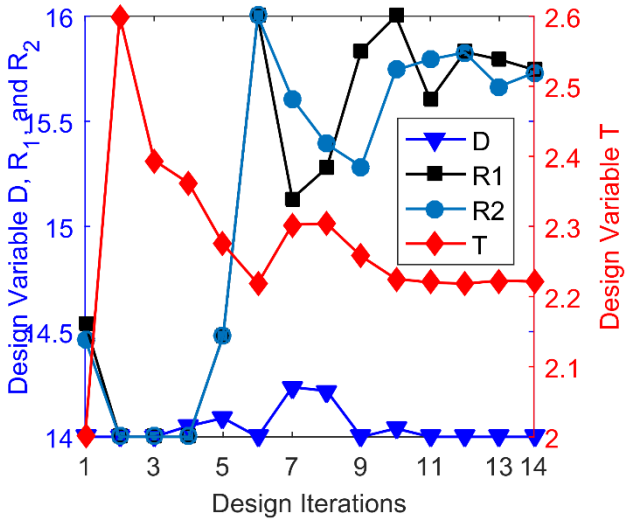

Figure 4.17: Design variables at each design iteration.

The design-driven adaptive sampling scheme is employed in the tRBDO to ensure that the *CCL* of the Kriging model satisfies the target value, and 145 most useful samples are identified until the optimum design is obtained. With a total number of 235 function evaluations in the tRBDO, the total volume of the twisted tube is minimized to 13522.173 mm^3 while the reliability is approximated as 0.9803. Figure 4.19 shows the stress contour of the optimum design in ANSYS while the inner stress is set to 30 MPa.

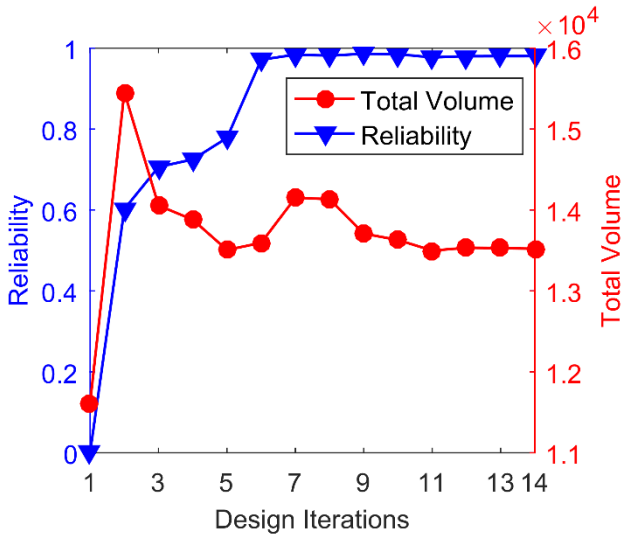

Figure 4.18: Reliability and total volume at each design iteration.

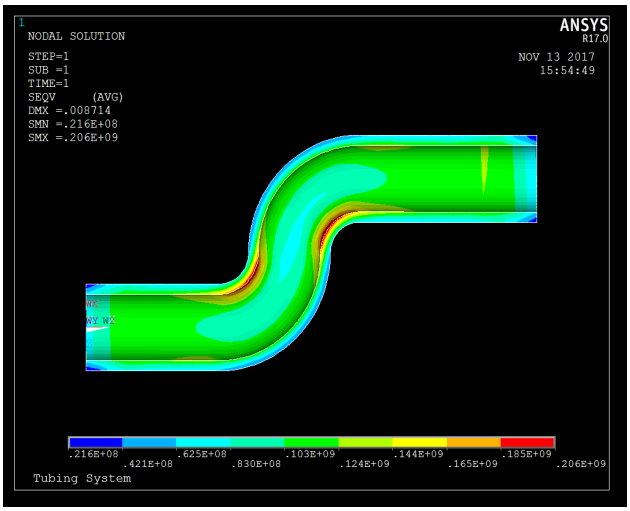

Figure 4.19: Stress contour given by ANSYS (cutting plane is normal to view).

4.4 Conclusion

This work presents a sequential Kriging modeling approach to accurately evaluate time-variant reliability and efficiently carry out the time-variant RBDO involving stochastic processes. To reduce the high dimensionality associated with time-variant uncertainties, the SKM approach first converts time-variant limit state functions to time-independent counterparts using stochastic equivalent transformation, and then build Kriging surrogate models to predict the responses of time-variant limit state functions. To enhance the accuracy of time-variant reliability approximations in tRBDO, a design-driven adaptive sampling scheme is developed to update surrogate models by identifying most useful sample points within time-variant random space. As a result, the system failures can be captured with the high-fidelity Kriging models to predict the time-variant reliability in MCS. With the sensitivity information obtained by the first-order score function, sequential quadratic programming (SQP) is adopted as an optimizer to search for optimal solutions

iteratively. The results of three case studies indicate that the sequential Kriging modeling approach is capable of effectively handling tRBDO problems involving stochastic processes.

5 SURROGATE MODEL UNCERTAINTY QUANTIFICATION FOR RELIABILITY-BASED DESIGN OPTIMIZATION[92]

5.1 Introduction

Surrogate models have been widely employed as approximations of expensive physics-based simulations to alleviate computational burden in reliability-based design optimization. Ignoring the surrogate model uncertainty due to lack of training samples will lead to untrustworthy designs in product development. This work addresses surrogate model uncertainty in reliability analysis using equivalent reliability index (ERI) and further develops a new smooth sensitivity analysis approach to facilitate the surrogate model-based product design process. Based on the Gaussian process modeling, Gaussian mixture model is constructed for reliability analysis using Monte Carlo simulation. To propagate both input variation and surrogate model uncertainty, the probability of failure is approximated by calculating the equivalent reliability index using the first and second statistical moment of the GMM. The sensitivity of ERI with respect to design variables is analytically derived based on the GP predictions. Three case studies are used to demonstrate the effectiveness and robustness of the proposed approach.

5.2 Equivalent Reliability Index Method

Reliability analysis aims to evaluate the probability that engineering system successfully performs functionality under input variations. The system fails if the limit state value is less than zero, and the probability of failure P_f can be defined as a multi-dimensional integral

$$P_f = \Pr\left[G(\mathbf{x}) < 0\right] = F_G(0) = \int \cdots \int_{G(\mathbf{x})<0} f_x(\mathbf{x}) d\mathbf{x} \tag{5.1}$$

where G(x) is the limit state function, x represents the vector of random input variables, f_x(x) represents the joint probability density function of the input variables, and F_G(.) represents the cumulative distribution function of G(x). As it is challenge to obtain the exact value of the probability of failure for complex systems in Eq. (5.1), simulation-based methods such as MCS are often utilized to approximate the probability of failure as

$$P_f = \int_{\Omega} I_f(\mathbf{x}) f_x(\mathbf{x}) d\mathbf{x} = E\left[I_f(\mathbf{x})\right] \tag{5.2}$$

where Ω_f represents the failure region in the input space Ω, E[.] is the expectation operator, and the indicator function I_f(x) is defined as

$$I_f(\mathbf{x}) = \begin{cases} 1, & G(\mathbf{x}) < 0 \\ 0, & otherwise \end{cases} \tag{5.3}$$

To reduce the tremendous computational cost of the limit state function evaluations, surrogate modeling techniques are generally employed to represent the limit state function. Thus, the performance function in Eq. (5.3) is replaced by the surrogate model predictions, and the predicted response will be used to identify potential system failures. Inappropriate managing surrogate model uncertainty may introduce significant errors in predicting system reliability and searching for optimal designs, especially for cases when only a limited number of training data is available for construing surrogate models. In this work, Gaussian process (GP) modeling is employed to construct the surrogate model for reliability-based design optimization. As a typical nonparametric regression technique, GP modeling is one of the most common methods that has been widely used in engineering

design applications. By using the GP model to represent the limit state function, system performance at any given point can be predicted with a mean squared error (MSE) that gives an estimation of the prediction accuracy. For a performance function $G(\mathrm{x})$, a GP model can be developed based on an training data set D = [X, Y], where $\mathrm{X} = [\mathrm{x}_1, \mathrm{x}_2, \ldots, \mathrm{x}_n]$, and x_i (i=1, 2, …, n) represents the random realizations of input variables x, and $\mathrm{Y} = [G(\mathrm{x}_1), G(\mathrm{x}_2), \ldots, G(\mathrm{x}_n)]$ represents the evaluated performances corresponding to each random sample in X. In the GP model, the system performance is assumed to follow a multivariate Gaussian distribution, which is expressed as

$$\hat{g}(\mathbf{x}) \sim GP\left(\mathbf{h}(\mathbf{x})\boldsymbol{\beta}, R(\mathbf{x}_i, \mathbf{x}_j)\right) \tag{5.4}$$

where h(x)β is the prior mean function, h(x) is a row vector of regression functions (i.e., constant, linear, etc.), β is a column vector of the coefficients, and $R(\mathrm{x}_i, \mathrm{x}_j)$ is the covariance function that characterizes the correlation between the responses at points x_i and x_j, expressed as

$$R(\mathbf{x}_i, \mathbf{x}_j) = \sigma^2 \exp\left[-\sum_{p=1}^{k} \omega_p \left|\mathbf{x}_{i,p} - \mathbf{x}_{j,p}\right|^2\right] \tag{5.5}$$

where $\mathrm{x}_{i,p}$ represents the p^{th} input variable in the i^{th} random realization, k is the dimension of x, $\omega = [\omega_1, \omega_2, \ldots, \omega_k,]$ is the roughness parameter to capture the nonlinearity of the process, and σ^2 is an unknown variance. A GP model can be fully characterized by all the aforementioned unknown hyperparameters β, σ^2, and ω, while the maximum likelihood estimation (MLEs) method can be used to estimate the values of those hyperparameters based on the given data set D. Once obtaining the hyperparamaters, the GP model is capable of predicting the response at any point x' as a conditional Gaussian distribution,

given as

$$\hat{g}(\mathbf{x}')\big|\mathbf{Y} \sim N\left(\mu_{gp}(\mathbf{x}')\big|\mathbf{Y}, v_{gp}(\mathbf{x}')\big|\mathbf{Y}\right) \tag{5.6}$$

where the prediction mean is

$$\mu_{gp}(\mathbf{x}')\big|\mathbf{Y} = \mathbf{h}(\mathbf{x})\boldsymbol{\beta} + \mathbf{r}^T\mathbf{R}^{-1}(\mathbf{Y} - \mathbf{H}\boldsymbol{\beta}) \tag{5.7}$$

where r is the correlation vector between x' and the existing training points, H = [h(x_1), h(x_2), …, h(x_n)] is a $n \times 1$ unit vector if the prior mean function is a constant. The prediction variance is written as

$$v_{gp}(\mathbf{x}')\big|\mathbf{Y} = \sigma^2\left\{1 - \mathbf{r}^T\mathbf{R}^{-1}\mathbf{r} + \left[\mathbf{h}^T(\mathbf{x}) - \mathbf{H}^T\mathbf{R}^{-1}\mathbf{r}\right]^T\left(\mathbf{H}^T\mathbf{R}^{-1}\mathbf{H}\right)^{-1}\left[\mathbf{h}^T(\mathbf{x}) - \mathbf{H}^T\mathbf{R}^{-1}\mathbf{r}\right]\right\} \tag{5.8}$$

In the GP model, the surrogate model uncertainty is quantified by the prediction variance as shown in Eq. (5.8), which is also known as the mean squared error of the prediction. Ignoring surrogate model uncertainty in RBDO may result in underestimating the probability of failure and potentially infeasible solutions. In this work, the probability of failure is reformulated by concurrently incorporating input variation and surrogate model uncertainty in uncertainty propagation, which is expressed as

$$\Pr(G(\mathbf{x}) < 0) \approx \Pr\left[\hat{g}\left(\mathbf{x}\right)\big|\mathbf{Y} < 0\right] = F_{\hat{g}(\mathbf{x})|\mathbf{Y}}(0) = \int_{-\infty}^{0} p(\hat{g}\left(\mathbf{x}\right)\big|\mathbf{Y})d\hat{g}\left(\mathbf{x}\right) \tag{5.9}$$

where $\hat{g}$(x)|Y represents the conditional probability distribution of system performance obtained by the GP model; $F_{\hat{g}(\mathbf{x})|\mathbf{Y}}(.)$ represents the cumulative distribution function of the $\hat{g}$(x)|Y ; Y is the vector of the observations; $p(.)$ represents the probability density function,

and x is an input vector contains k random variables x_i, i = 1, 2, …, k. It is worth noting that the GP model prediction $\hat{g}(.)|\mathrm{Y}$ for a single point is a normal random variable given the observation Y, and $\hat{g}^{\mathrm{Y}}(.)$ is adopted to represent the conditional probability distribution $\hat{g}(.)|\mathrm{Y}$ for the sake of simplicity. By treating the GP model predictions as normal distributed random variables, a point-to-distribution mapping relationship can be obtained to take surrogate model uncertainty into account in uncertainty propagation as shown in Fig. 5.1. Given the randomness of the input x, the conditional PDF of the response prediction for a random realization $\mathrm{x_r}$ is given by

$$p\left(\hat{g}^{\mathbf{Y}}(\mathbf{x}_r)\right) = N\left(\mu_{gp}(\mathbf{x}_r), v_{gp}(\mathbf{x}_r)\right) \tag{5.10}$$

where $\mu_{gp}(.)$ and $v_{gp}(.)$ are the mean and variance of GP model prediction, which vary over the input domain. To concurrently propagate input variation and surrogate model uncertainty, a Gaussian mixture model (GMM) is developed to capture the probability density function of system performance, which is expressed as

$$p(GMM) = \lim_{N\to\infty} \sum_{i=1}^{N} \pi_i p\left[\hat{g}^{\mathbf{Y}}(\mathbf{x}_{\mathbf{r}i})\right] = \lim_{N\to\infty} \sum_{i=1}^{N} \pi_i N\left(\mu_{gp}(\mathbf{x}_{\mathbf{r}i}), v_{gp}(\mathbf{x}_{\mathbf{r}i})\right) \tag{5.11}$$

where $\mathrm{x_{r}}_i$ represents the random realizations of the input x, π_i is the weight of the i^{th} component normal distribution, and the summary of π_i is equal to one. As shown in Eq. (5.11), the prediction at a given point $\hat{g}^{\mathrm{Y}}(\mathrm{x_{r}}_i)$ is treated as a component normal distribution of the GMM, and the Gaussian mixture model consists of infinite number of normal distributions.

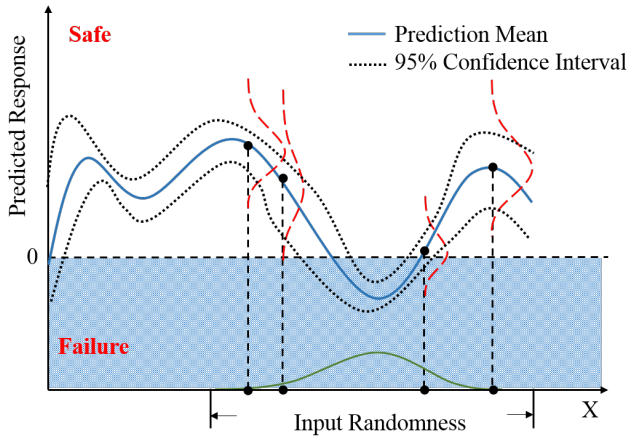

Figure 5.1: Point-to-distribution mapping relationship

In this study, we employ the MCS to approximate the PDF of the GMM according to the response predictions from GP models. In MCS, N Monte Carlo samples are first generated according to input randomness, denoted as $\mathrm{X_m} = (\mathrm{x}_{m,1}, \mathrm{x}_{m,2}, \ldots, \mathrm{x}_{m,N})$. The performance prediction of the GP model at the i^{th} sample point $\mathrm{x}_{m,i}$ is a normally distributed random variable given by $\hat{g}^{\mathrm{Y}}(\mathrm{x}_{m,i}) \sim N(\mu_{gp}(\mathrm{x}_{m,i}),v_{gp}(\mathrm{x}_{m,i}))$. Thus, a total number of N normal distributions can be obtained after predicting the responses of all the MCS samples, where the prediction mean and variance for the i^{th} distribution are denoted as $\mu_i = \mu_{gp}(\mathrm{x}_{m,i})$ and $v_i = v_{gp}(\mathrm{x}_{m,i})$ for simplicity. According to Eq. (5.11), the probability density function of the GMM can be rewritten as

$$p(GMM) \cong \sum_{i=1}^{N} \pi_i N\left(\mu_i, v_i\right) \tag{5.12}$$

In reliability analysis, all MCS samples are equally important since they are simultaneously generated from the same joint PDF and represent the random realizations of the given input x. Therefore, the weight π_i of each component normal distribution in the

GMM is actually the same, as $\pi_1 = \pi_2 = \ldots = \pi_i = 1/N$. The mean and variance of the GMM can be directly calculated based on the statistical moments of the N component normal distributions. Assuming that each normal distribution is fully characterized by M random samples, denoted as s_1, s_2, …, s_M, where M is a sufficient large number. The mean and variance of the i^{th} normal distribution can be characterized as

$$\mu_i = \frac{1}{M}\sum_{j=1}^{M} s_j, i = 1,2,...,N \tag{5.13}$$

and

$$v_i = \frac{1}{M}\sum_{j=1}^{M} s_j^2 - \mu_i^2, i = 1,2,...,N \tag{5.14}$$

Since the Gaussian mixture model is constructed by the N normal distributions, the total number of samples is $N \times M$, and mean and variance of the GMM can be calculated as

$$\mu_{GMM} = \frac{1}{N\times M}\sum_{j=1}^{N\times M} s_j = \frac{1}{N}\sum^{N}\left(\frac{1}{M}\sum_{j=1}^{M} s_j\right) = \frac{1}{N}\sum_{i=1}^{N}\mu_i \tag{5.15}$$

$$\begin{aligned} v_{GMM} &= \frac{1}{N\times M}\sum_{j=1}^{N\times M} s_j^2 - \mu_{GMM}^2 = \frac{1}{N}\sum^{N}\left(\frac{1}{M}\sum_{j=1}^{M} s_j^2\right) - \mu_{GMM}^2 \\ &= \frac{1}{N}\sum_{i=1}^{N}\left(v_i + \mu_i^2\right) - \mu_{GMM}^2 \end{aligned} \tag{5.16}$$

Assuming that the resulting GMM follows a normal distribution with mean μ_{GMM} and variance v_{GMM}, an equivalent reliability index β_e is defined in this work as

$$\beta_e = \frac{\mu_{GMM}}{\sqrt{v_{GMM}}} = \frac{\mu_{GMM}}{\sigma_{GMM}} \tag{5.17}$$

where σ_{GMM} represents the standard deviation. Therefore, the reliability estimation with the consideration of both input variation and surrogate model uncertainty is expressed as

$$R \approx \hat{R} = \Phi(\beta_e) \tag{5.18}$$

The procedure of reliability analysis using the proposed ERI method is summarized in Table 5.1.

Table 5.1: Procedure of reliability analysis using ERI approach

Steps	Procedure
Step 1:	Identify initial data set D, generate N MCS samples X_m according to input randomness.
Step 2:	Develop a Gaussian process model based on the data set D;
Step 3:	Predict the responses for all the N samples and collect the mean μ_i and variance v_i of each normal distribution;
Step 4:	Calculate the mean and variance of the Gaussian mixture model using Eq. (15) and (16), respectively:
Step 5:	Estimate the reliability using the equivalent reliability index.

5.3 Stochastic Sensitivity Analysis

In RBDO process, gradient-based optimization methods require the sensitivity information to search for optimal solutions, such as the sequential linear programming (SLP) [93] and the sequential quadratic programming (SQP) [94]. Sensitivity information of reliability with respect to design variables affects the convergence process, thus an

accurate sensitivity analysis is essential for RBDO. The existing simulation-based sensitivity analysis methods such as first-order score function method [95] lack the capability of handling surrogate model uncertainty. To facilitate the RBDO process, this work presents a new method to calculate the sensitivity of ERI with respect to design variables.

In RBDO, the reliability index should be greater than a predefined target, expressed as

$$\Pr(G(\mathbf{x}) \geq 0) \geq \Phi(\beta_t) \tag{5.19}$$

In the ERI approach, the reliability is estimated as the standard normal cumulative distribution function of the ERI, denoted as $\Phi(\beta_e)$. Thus, the probabilistic constraint in Eq. (19) can be transformed to an equivalent form, expressed as

$$\beta_e \geq \beta_t \tag{5.20}$$

where β_e is the equivalent reliability index and β_t is the target reliability index. Instead of using the sensitivity of reliability, the sensitivity of ERI with respect to design variables is required for design optimization. Taking the partial derivative of the ERI with respect to the design variable d yields

$$\frac{\partial \beta_e}{\partial \mathbf{d}} = \frac{\partial\left(\frac{\mu_{GMM}}{\sqrt{v_{GMM}}}\right)}{\partial \mathbf{d}} = \frac{1}{\sqrt{v_{GMM}}}\frac{\partial \mu_{GMM}}{\partial \mathbf{d}} - \frac{\mu_{GMM}}{2\sqrt{v_{GMM}}^3}\frac{\partial v_{GMM}}{\partial \mathbf{d}} \tag{5.21}$$

where the sensitivity is decomposed by the gradient of the mean μ_{GMM} and the variance v_{GMM}. According to the Eq. (5.15) and (5.16), the two gradient terms can be further derived as

$$\frac{\partial \mu_{GMM}}{\partial \mathbf{d}} = \frac{1}{N}\sum_{i=1}^{N}\frac{\partial \mu_i}{\partial \mathbf{d}} \tag{5.22}$$

while the gradient for the variance of the GMM can be written as

$$\begin{aligned}\frac{\partial v_{GMM}}{\partial \mathbf{d}} &= \frac{1}{N}\sum_{i=1}^{N}\left(\frac{\partial v_i}{\partial \mathbf{d}} + \frac{\partial \mu_i^2}{\partial \mathbf{d}}\right) - \frac{\partial \mu_{GMM}^2}{\partial \mathbf{d}} \\ &= \frac{1}{N}\sum_{i=1}^{N}\left(\frac{\partial v_i}{\partial \mathbf{d}} + 2\mu_i\frac{\partial \mu_i}{\partial \mathbf{d}}\right) - 2\mu_{GMM}\frac{\partial \mu_{GMM}}{\partial \mathbf{d}}\end{aligned} \tag{5.23}$$

According to Eq. (5.22) and (5.23), the two gradient terms can be directly calculated based on the first-order derivative of the prediction mean and variance. In the GP model, the prediction mean and variance are functions of the given point and the initial data set, as shown in Eq. (5.7) and (5.8). Taking the derivative of the prediction mean and variance with respect to design variable x, we can obtain

$$\frac{\partial \mu_{GP}(\mathbf{x})}{\partial \mathbf{x}} = \mathbf{J}_h\boldsymbol{\beta} + \mathbf{J}_r\mathbf{R}^{-1}(\mathbf{Y} - \mathbf{H}\boldsymbol{\beta}) \tag{5.24}$$

and

$$\frac{\partial v_{gp}(\mathbf{x})}{\partial \mathbf{x}} = 2\sigma^2\left[-\mathbf{R}^{-1}\mathbf{J}_r + \left(\mathbf{H}^T\mathbf{R}^{-1}\mathbf{H}\right)^{-1}\left(\mathbf{H}^T\mathbf{R}^{-1}\mathbf{J}_r - \mathbf{J}_h\right)\right] \tag{5.25}$$

where H is a unit vector, r(x) represents the correlation vector between the point x and the training sample points, and J_h and J_r are the Jacobian of h(x) and r(x). As a result, the values of the first-order derivative of the prediction mean and variance can be easily obtained through the GP model. After evaluating all the MCS samples, the required gradient information can be obtained based on Eq. (5.22) and (5.23), and finally, the sensitivity for the current design point can be derived accordingly.

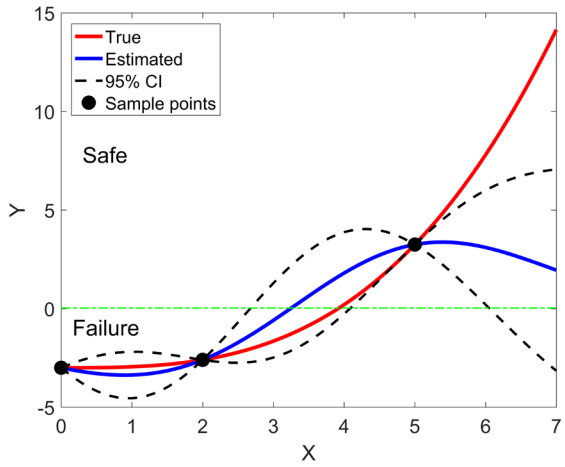

Figure 5.2: GP modeling of the limit state function

A limit state function $G(x) = x^3/20 - 3$ is employed to demonstrate the effectiveness of the proposed sensitivity analysis approach. Three samples $x = 0, 2, 5$ are used to construct the surrogate model, as shown in Fig. 5.2. The design variable x is treated as a normally distributed random variable with 0.12 standard deviation while the failure is defined as the function value is less than zero. For a given design point, 10^6 MCS samples are generated for reliability analysis using ERI approach. According to the gradient of prediction mean and variance of each MCS sample as calculated in Eq. (5.24) and (5.25), the sensitivity of ERI with respect to x can be obtained by Eq. (5.21). For comparison purpose, the first-order score function method is employed to compute the sensitivity for the probability of failure with respect to the input x, as shown in Fig. 5.3a, where the red dashed line represents the zero approximation. It is observed that the sensitivity approximated by SF method is zero when x is within the range [2, 2.8] and [3.6, 6], where the reliability approximation is either zero or one. On the contrary, the smooth sensitivity evaluated by the proposed method can avoid the zero estimation as shown in Fig. 5.3b. Therefore, the

stability of RBDO using ERI approach is ensured by the proposed sensitivity analysis.

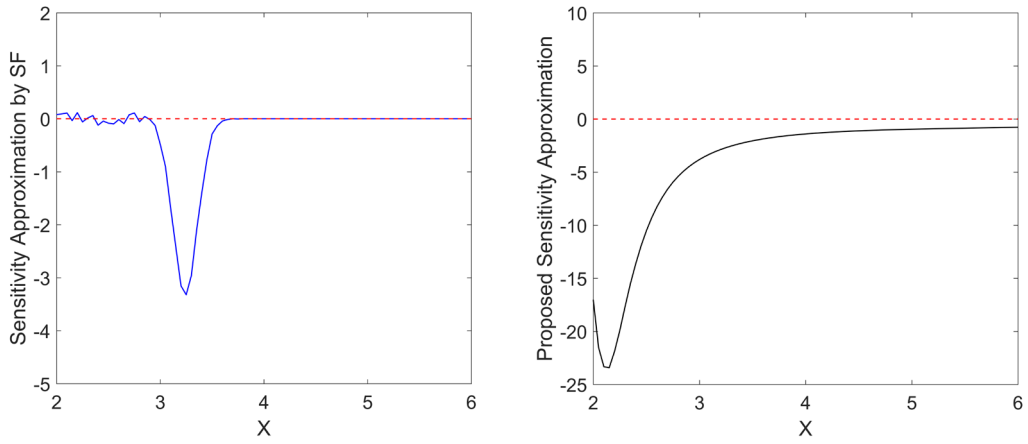

Figure 5.3: Approximated sensitivity by a) first-order score function method and b) proposed approach.

5.4 RBDO Using Equivalent Reliability Index

In this section, the ERI approach will be integrated with sensitivity analysis approach for RBDO to achieve a reliable optimal system design. The design objective is to minimize the cost while ensuring a target reliability index, and the formulation of RBDO using ERI approach is given as

$$\begin{aligned} &\textit{Minimize}: \quad \textit{Cost}(\mathbf{d}) \\ &\textit{subject to}: \quad \beta_e^i \geq \beta_t^i, \;\; i = 1,....,nc \\ &\qquad\qquad \mathbf{d}^{\mathbf{L}} \leq \mathbf{d} \leq \mathbf{d}^{\mathbf{U}}, \quad \mathbf{d} \in R^{nd} \;\text{ and }\; \mathbf{X} \in R^{nr} \end{aligned} \tag{5.26}$$

where β_e^i represents the equivalent reliability index of the i^{th} limit state function G_i(X, d), β_t^i is the corresponding reliability target; *Cost*(d) is the objective function; d is the vector of design variables and X is the vector of random variables; and *nc*, *nd*, and *nr* are the number of constraints, design variables, and random variables, respectively.

As shown in Fig. 5.4, the first step of employing RBDO using ERI approach is to construct a GP model corresponding to each limit state function. For a design problem with k random variables, a set of n initial samples within the design domain are first generated according to the Latin hypercube sampling scheme, denoted as $X = [x_1, x_2, \ldots, x_n]$, where each initial sample is a vector of k random variables. Then the training data set corresponding to each limit state function can be obtained after evaluating the true performances of the initial samples, denoted as $D_j = [X, Y_j]$, where $j = 1, 2, \ldots, nc$ represents the j^{th} limit state function. Consequently, nc GP models can be constructed accordingly as discussed in section 5.2, and the RBDO will be performed iteratively staring at an initial design. To provide a reliable optimal design with the consideration of surrogate model uncertainty, the proposed ERI approach is employed to estimate the reliability in each design iteration. In reliability analysis, N Monte Carlo samples are first generated according to the randomness of the current design point, denoted as $X_m = [x_{m,1}, x_{m,2}, \ldots, x_{m,N}]$. For each limit state function, the constructed GP model is used to predict the response of the MCS samples, while the prediction is treated as a normally distributed random variable as shown in Eq. (5.7) and (5.8). After predicting the responses for all MCS samples, the obtained N normal distributions are combined to form a Gaussian mixture model, which represents the estimated random output of the current design. The GMM is assumed to follow a normal distribution with the mean μ_{GMM} and variance $v_{GMM,}$ which can be calculated based on the means and variances of the component normal distributions, as illustrated in Eq. (5.15) and (5.16). An equivalent reliability index β_e can be calculated as the ratio of the mean μ_{GMM} to the standard deviation $\sigma_{GMM,}$ and the reliability R is approximated by the standard normal cumulative distribution function of the ERI. In the

proposed work, the sensitivity of ERI with respect to design variables is required in each design iteration. First, the gradient information of the prediction mean and variance for each MCS sample are first calculated according to Eq. (5.24) and (5.25). Then the two gradient terms of the mean μ_{GMM} and variance v_{GMM} can be calculated and used to derive the sensitivity of ERI as shown in Eq. (5.21). Then the sequential quadratic programming (SQP) technique is employed as the optimizer to generate the new design point, and the iterative design process will be repeated until an optimal design is achieved.

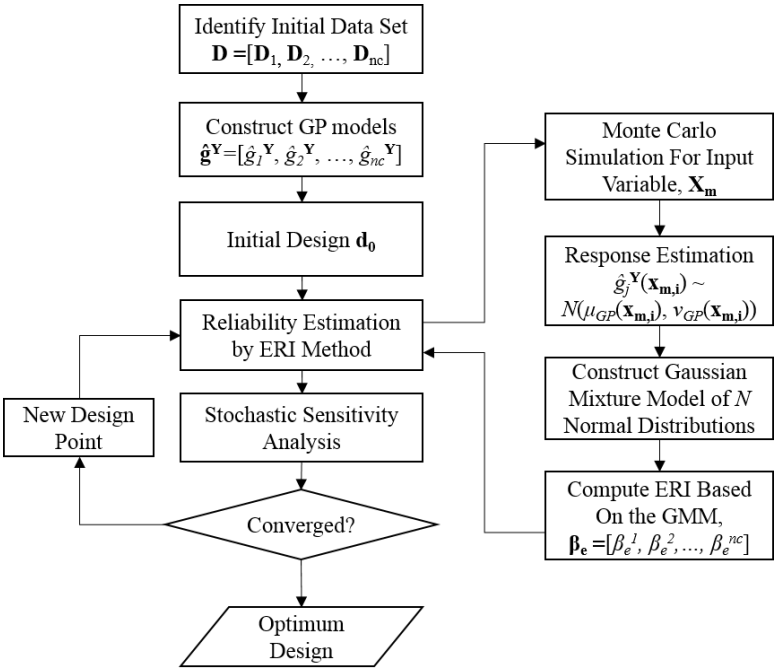

Figure 5.4: Flowchart of the RBDO using ERI

5.5 Case Studies

In this section, three examples are used to demonstrate the effectiveness of the reliability-based design optimization using ERI approach, including a mathematical design problem, a vehicle side crash design and an aircraft tubing design problem.

5.5.1 Case Study I: A Mathematical Design Problem

The first case study considers a benchmark mathematical problem involving two random design variables and three constraints. The RBDO problem is formulated as

$$\begin{aligned} &\text{Minimize}: \ Cost = 10 - X_1 + X_2 \\ &\text{subject to}: \ \beta_e^i = \Phi^{-1}\left(\Pr\left(G_i(\mathbf{d}) \geq 0\right)\right) \geq \beta_t^i, \ \ i = 1 \sim 3 \\ &\qquad\qquad \mathbf{d} \ = \ [X_1, X_2]; 0 \leq d_1 \ \& \ d_2 \leq 10 \\ &\text{where} \qquad G_1 = \frac{X_1^2 X_2}{20} - 1 \\ &\qquad\qquad G_2 = \frac{(X_1 + X_2 - 5)^2}{30} + \frac{(X_1 - X_2 - 12)^2}{120} - 1 \\ &\qquad\qquad G_3 = -0.05 X_1^2 - X_1 - X_2 + 14 \end{aligned} \tag{5.27}$$

where two random design variables d =[μ_1, μ_2] are both normally distributed as $X_1 \sim N(\mu_1, 0.3464^2)$ and $X_2 \sim N(\mu_2, 0.3464^2)$. The target reliability level is set to 0.985 for all three constraints, thus the target reliability index β_t^i, (i = 1, 2, 3) can be calculated as 2.1701. To investigate the effectiveness and robustness of the proposed approach, the design problem is solved in two different scenarios. In the first scenario, the RBDO using ERI approach is performed while only 6 initial training samples are used to construct the GP model. The goal is to test the performance of the ERI approach for solving RBDO problems with limited data. In the second scenario, the number of initial training samples has been increased to 15, aiming to investigate if the proposed approach is applicable for RBDO when the training data is sufficient.

5.1.1 First scenario: Insufficient data. The first step of employing the proposed ERI method in RBDO is to build the surrogate GP model for each probabilistic constraint. 6 initial samples are first generated by using Latin hypercube sampling within the design domain, and evaluated for the limit state values. Consequently, three GP models can be

constructed based on the obtained data sets D_1, D_2, and D_3. Following the procedure introduced in section 5.4, RBDO using ERI approach is performed by setting an initial design point $d_0 = [5, 5]$. In each design iteration, 10^6 MCS samples are generated based on the randomness of the current design point to conduct the reliability analysis using ERI approach, while the design sensitivity can be accurately obtained as introduced in section 5.3. Therefore, an optimal design $d_{opt} = [6.4965, 3.5679]$ is achieved after 12 iterations. The iterative design history of reliabilities, design points, and cost function values are detailed in Table 5.2, where the values of reliabilities for the three constraints are estimated from the corresponding GP models, denoted by R_1^{ERI}, R_2^{ERI}, and R_3^{ERI}, respectively. Figure 5.5 plots the six training points, the accurate limit state function, and the GP predictions with 95% confidence intervals.

Table 5.2: Design history for case study I (First scenario)

Iteration	Design Point	R_1^{ERI}	R_2^{ERI}	R_3^{ERI}	Cost
1	[5.0000, 5.0000]	0.9970	1.0000	0.9999	10.0000
2	[5.6381, 4.1544]	0.9999	0.9997	0.9999	8.5163
3	[6.4504, 3.3397]	0.9995	0.9481	0.9922	6.8892
4	[6.3399, 3.4610]	0.9998	0.9716	0.9956	7.1211
5	[6.0443, 3.7471]	1.0000	0.9955	0.9991	7.7028
6	[6.4766, 3.6329]	1.0000	0.9901	0.9849	7.1563
7	[6.3200, 3.6526]	1.0000	0.9913	0.9943	7.3326
8	[6.4630, 3.5853]	0.9999	0.9865	0.9873	7.1224
9	[6.4722, 3.5835]	0.9999	0.9864	0.9867	7.1112
10	[6.4961, 3.5694]	0.9999	0.9851	0.9850	7.0733
11	[6.4965, 3.5678]	0.9999	0.9850	0.9850	7.0713

12	[6.4965, 3.5679]	0.9999	0.9850	0.9850	7.0714

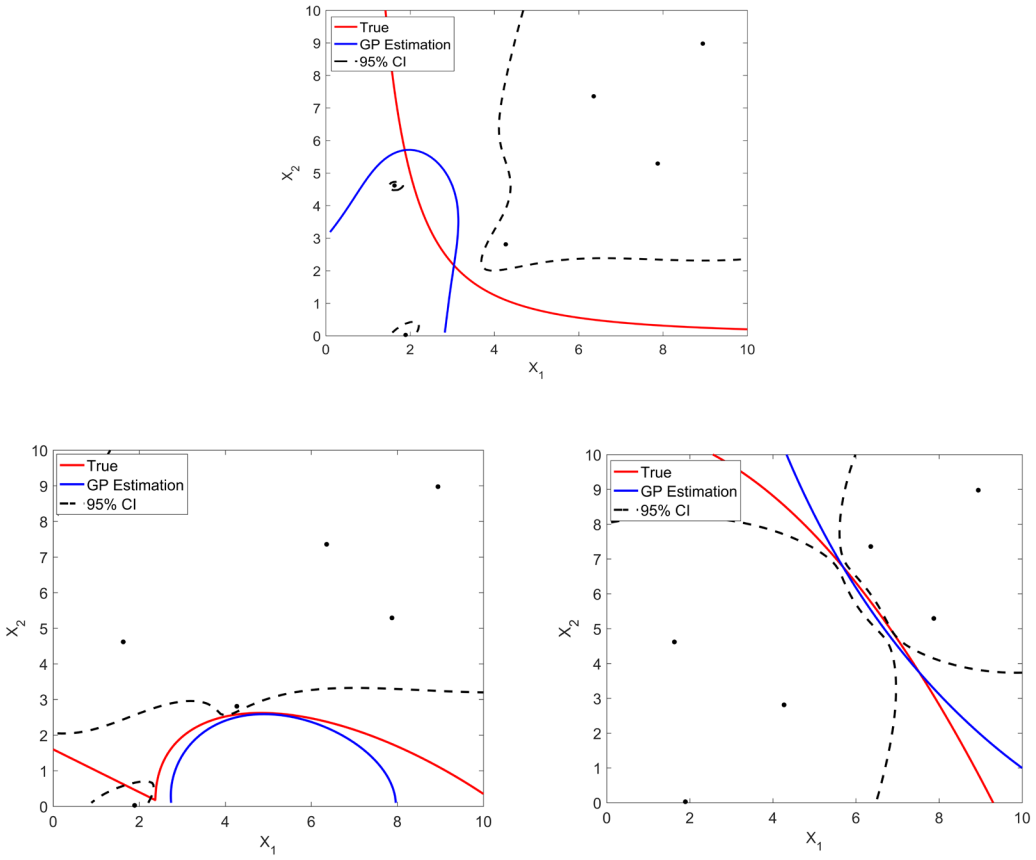

Figure 5.5: Accurate and estimated limit state functions for scenario 1

For the purpose of comparison, existing methods have been employed to solve the same design problem while the first-order score function method is used for sensitivity analysis, including 1) traditional RBDO using GP model without the consideration of surrogate model uncertainty, 2) safety margin method using 50 test sample to determine the magnitude of the safety margin, denoted SM(TS), 3) safety margin method using cross validation to determine the magnitude of the safety margin, denoted as SM(CV) [82], and 4) direct MCS method with 10^6 sample points. The conservativeness level is set to 90% for

both SM(TS) and SM(CV). The optimal results obtained from different methods are shown in Fig. 5.6 and Table 5.3, where the reliabilities at the optimal designs obtained through different methods are verified by direct MCS using 10^6 samples. The safety margin using the cross validation method failed to provide an optimal solution because the estimated safety margin is too large when the initial data is limited. On the contrary, the safety margin method using test samples can provide an optimal design that satisfies the target reliability, however, it requires extra 150 function evaluations to determine the magnitude of safety margin. Without the consideration of surrogate model uncertainty, the traditional RBDO offers an optimal design located in the failure region, where the reliabilities of three constraints are given as 0.2828, 0.2026, and 0.1095, respectively. The optimal design using the proposed approach is near to the actual optimal, while the reliabilities satisfy the target value 0.985.

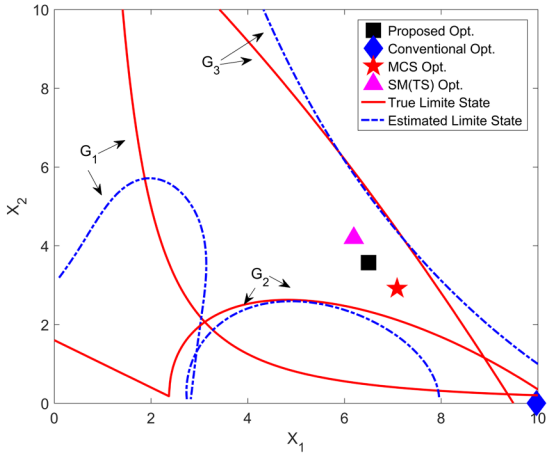

Figure 5.6: Comparison of optimal designs obtained by different methods

Table 5.3: Comparison of optimal results (scenario 1)

	Optimum	R1	R2	R3	Cost	#F

MCS	[7.0891, 2.9153]	1	0.9850	0.9850	5.8262	$3*10^6$
Traditional	[9.9701, 0.0018]	0.2828	0.2026	0.1095	0.0317	3*6
SM(TS)	[6.1948, 4.1961]	1	1	0.9947	8.0013	3*(6+50)
SM(CV)	/	/	/	/	/	3*6
Proposed	[6.4965, 3.5679]	1	0.9997	0.9975	7.0714	3*6

6.1.2 Second scenario: Sufficient data. In this scenario, 15 initial sample points are used to construct the surrogate GP model. Following the same procedure as introduced in previous section, an optimal design d_{opt} = [7.0701, 2.9678] is obtained after 10 iterations, and the iterative design history of design points, estimated reliabilities for three constraints, cost function values are detailed in Table 5.4. As shown in Fig. 5.7, the estimated limit state functions from the GP models are close to the accurate counterparts. As indicated by the width of the 95% confidence interval, the surrogate model uncertainties can be significantly reduced by constructing GP models using more training samples.

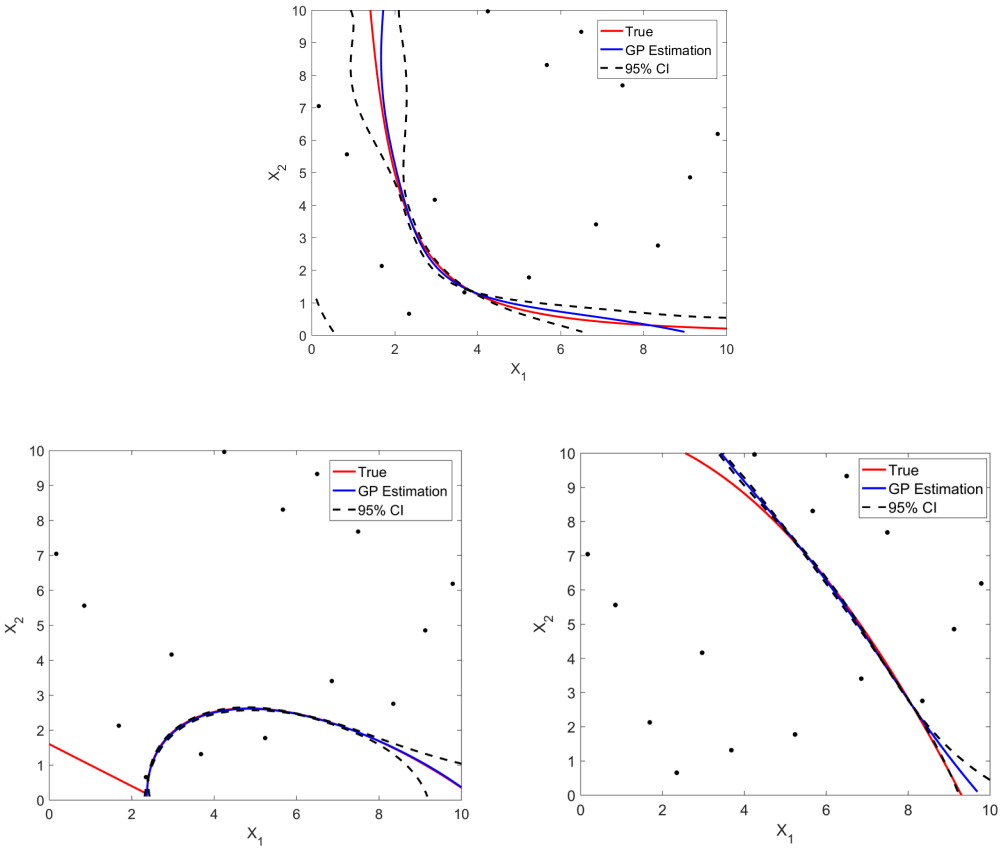

Figure 5.7: Accurate and estimated limit state functions for three constraints, G_1, G_2, and G_3, respectively (scenario 2)

Table 5.4: Design history for case study I (Second layout)

Iteration	Design Point	R_1^{ERI}	R_2^{ERI}	R_3^{ERI}	Cost
1	[5.0000, 5.0000]	1.0000	1.0000	1.0000	10.0000
2	[5.7901, 4.1184]	1.0000	1.0000	1.0000	8.3283
3	[6.8115, 3.0967]	1.0000	0.9883	0.9963	6.2852
4	[7.0449, 3.0330]	1.0000	0.9894	0.9841	5.9882
5	[6.9501, 3.0627]	1.0000	0.9891	0.9907	6.1126
6	[7.0472, 2.9902]	1.0000	0.9864	0.9862	5.9429
7	[7.0530, 2.9817]	1.0000	0.9858	0.9861	5.9287

8	[7.0525, 2.9824]	1.0000	0.9859	0.9861	5.9300
9	[7.0701, 2.9677]	1.0000	0.9852	0.9852	5.8976
10	[7.0701, 2.9678]	1.0000	0.9852	0.9852	5.8977

Similarly, four optimal designs are obtained by using traditional RBDO, SM(TS), SM(CV), and direct MCS methods, where the results are detailed in Fig. 5.8 and Table 5.5. It is observed that all the optimal solutions converge to the same. In the second scenario, with three high-fidelity GP models, the traditional RBDO is capable of offering a reliable optimal design. Both the SM(TS) and SM(CV) method can provide a reliable optimal design, while SM(TS) requires 195 functions evaluations. With the consideration of the surrogate model uncertainty, the proposed approach offers an optimal design near to the MCS optimal. The results demonstrate that the proposed approach can provide reliable yet accurate optimal design for RBDO with sufficient training data.

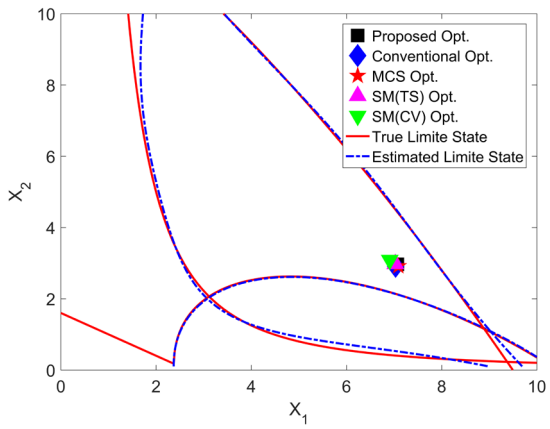

Figure 5.8: Optimum designs of proposed method and other existing approaches (scenario *2*)

Table 5.5: Comparison of optimal results (scenario *2*)

	Optimum	R1	R2	R3	Cost	#F

MCS	[7.0891, 2.9153]	1	0.9850	0.9850	5.8262	$3*10^6$
Tradition	[7.0307, 2.9102]	1	0.9826	0.9921	5.8795	3*15
SM(TS)	[7.0255, 2.9754]	1	0.9895	0.9871	5.9499	3*(15+50)
SM(CV)	[6.9092, 3.0864]	1	0.9932	0.9902	6.1772	3*15
Proposed	[7.0701, 2.9678]	1	0.9894	0.9871	5.8977	3*15

5.5.2 Case Study II: Vehicle Side Crash Problem

According to the European Enhanced Vehicle-Safety Committee (EEVC) criterion, ten vehicle performances must satisfy the safety regulations, including the constraint of abdomen load (G_1), rib deflection (upper G_2, middle G_3, and lower G_4), viscous criterion (upper G_5, middle G_6, and lower G_7), public symphysis force (G_8), velocity of B-pillar at middle point (G_9), and velocity of front door at B-pillar (G_{10}), which are expressed as

$$F_{Abdom} = 1.16 - 0.3717 d_2 d_4 - 0.00931 d_2 x_1 - 0.484 d_3 d_9 + 0.01343 d_6 x_1 \quad (5.28)$$

$$\begin{aligned} Deflection_{rib\_u} = {} & 28.98 + 3.818 d_3 - 4.2 d_1 d_2 + 0.0207 d_5 x_1 + 6.63 d_6 d_9 \\ & - 7.7 d_7 d_8 + 0.32 d_9 x_1 \end{aligned} \quad (5.29)$$

$$\begin{aligned} Deflection_{rib\_m} = {} & 33.86 + 2.95 d_3 + 0.1792 x_1 - 5.057 d_1 d_2 - 11 d_2 d_8 \\ & - 0.0215 d_5 x_1 - 9.98 d_7 d_8 + 22 d_8 d_9 \end{aligned} \quad (5.30)$$

$$Deflection_{rib\_l} = 46.36 - 9.9 d_2 - 12.9 d_1 d_8 + 0.1107 d_3 x_1 \quad (5.31)$$

$$\begin{aligned} VC_{upper} = {} & 0.261 - 0.0159 d_1 d_2 - 0.188 d_1 d_8 - 0.019 d_2 d_7 + 0.0144 d_3 d_5 \\ & + 0.0008757 \mathrm{d}_5 x_1 + 0.08045 d_6 d_9 + 0.00139 d_8 x_2 + 0.00001575 x_1^2 \end{aligned} \quad (5.32)$$

$$\begin{aligned} VC_{middle} = {} & 0.214 + 0.00817 d_5 - 0.131 d_1 d_8 - 0.0704 d_1 d_9 + 0.03099 d_2 d_6 \\ & - 0.018 d_2 d_7 + 0.0208 d_3 d_8 + 0.121 d_3 d_9 - 0.00364 d_5 d_6 \\ & + 0.0007715 d_5 x_1 - 0.0005354 d_6 x_1 + 0.00121 d_8 x_2 + 0.00184 d_9 x_1 \\ & - 0.018 d_2^2 \end{aligned} \quad (5.33)$$

$$VC_{lower} = 0.74 - 0.61d_2 - 0.163d_3d_8 + 0.001232d_3x_1 - 0.166d_7d_9 + 0.227d_2^2 \tag{5.34}$$

$$Force_{public} = 4.72 - 0.5d_4 - 0.19d_2d_3 - 0.0122d_4x_1 + 0.009325d_6x_1 + 0.000191x_2^2 \tag{5.35}$$

$$Velocity_{B-pillar} = 10.58 - 0.674d_1d_2 - 1.95d_2d_8 + 0.02054d_3x_1 - 0.0198d_4x_1 + 0.028d_6x_1 \tag{5.36}$$

$$Velocity_{door} = 16.45 - 0.489d_3d_7 - 0.843d_5d_6 + 0.0432d_9x_1 - 0.0556d_9x_1 - 0.000786x_2^2 \tag{5.37}$$

As shown in Eq. (5.28) ~ (5.37), a total number of nine design variables d and two non-design random variables x are considered in this case study. All of the random variables are assumed to follow normal distributions, as detailed in Table 5.6.

Table 5.6: Properties of random variables for vehicle side impact

Design variables	Standard deviation	d_L	d_0	d_U
d_1(B-pillar inner)	0.03	0.5	1	1.5
d_2(B-pillar reinforce)	0.03	0.5	1	1.5
d_3(Floor side inner)	0.03	0.5	1	1.5
d_4(Cross member)	0.03	0.5	1	1.5
d_5(Door beam)	0.03	0.5	1	1.5
d_6(Door belt line)	0.03	0.5	1	1.5
d_7(Roof rail)	0.03	0.5	1	1.5
d_8(Mat. floor side inner)	0.006	0.192	0.3	0.345
d_9(Mat. floor side)	0.006	0.192	0.3	0.345
x_1(Barrier height)	10	/	0	/
x_2(Barrier hitting)	10	/	0	/

The design objective is to reduce the weight while maintaining the reliability of the vehicle during a side impact, the function of total weight is expressed as

$$\text{Cost}(\mathbf{d}) = 1.98 + 4.90d_1 + 6.67d_2 + 6.98d_3 + 4.01d_4 + 1.78d_5 + 2.73d_7 \quad (5.38)$$

Thus, the RBDO problem for case side crash is formulated as

$$\begin{aligned}
\text{Minimize}: \quad & \text{Cost}(\mathbf{d}) \\
\text{subject to:} \quad & \beta_e^i = \Phi^{-1}\left(\Pr\left(G_i(\mathbf{d}) < 0\right)\right) \le \beta_t^i, \ i = 1 \sim 10 \\
& G_1 = 1 - F_{Abdom} \\
& G_{2/3/4} = 32 - Deflection_{rib_u} / Deflection_{rib_m} / Deflection_{rib_l} \\
& G_{5/6/7} = 0.32 - VC_{upper} / VC_{middle} / VC_{lower} \\
& G_8 = 4 - Force_{public} \\
& G_9 = 9.9 - Velocity_{B-pillar} \\
& G_{10} = 15.7 - Velocity_{door} \\
& \mathbf{d}_L \le \mathbf{d} \le \mathbf{d}_U
\end{aligned} \quad (5.39)$$

By setting the target reliability index as β_t = 1.7507 (R_t = 0.9600) for all the ten constraints, the design problem is solved by RBDO using ERI approach. The first step is to construct ten GP models for the limit state functions based on 300 random samples generated by Latin hypercube sampling. Starting with an initial design d_0 = [1, 1, 1, 1, 1, 1, 1, 0.3, 0.3], an optimal design d_{opt} = [0.7414, 1.3368, 0.7654, 1.2920, 0.8565, 1.3110, 0.6870, 0.2838, 0.2902] is obtained after 32 iterations. Figure 5.9 shows the iterative design history for the nine design variables. In each design iteration, the ERI approach is employed to conduct the reliability analysis under both input variation surrogate model uncertainty, and the estimated reliability history of ten probabilistic constraints is provided in Fig. 5.10.

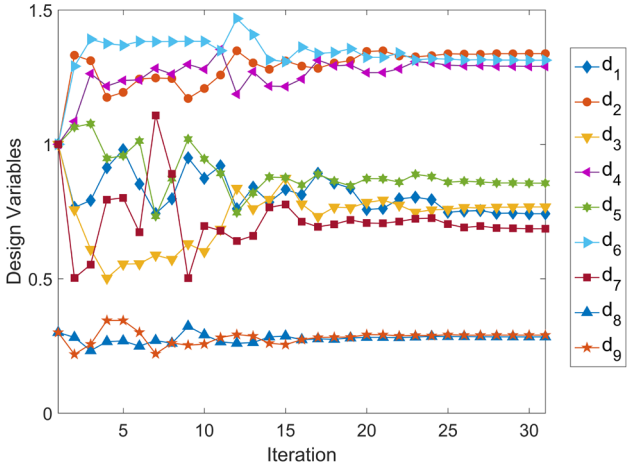

Figure 5.9: Iterative design history for nine design variables

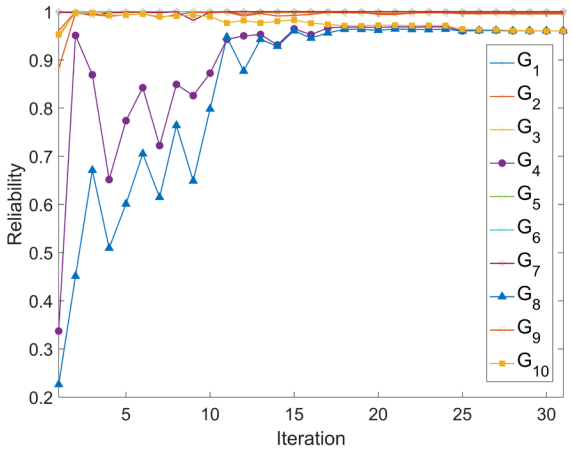

Figure 5.10: Reliability history for vehicle side impact

For comparison purpose, the traditional RBDO, SM(TS) using 50 test samples, SM(CV) and direct MCS method are employed to solve the same RBDO problem. The optimal solutions and the corresponding minimized weights are listed in Table 5.7. We employed direct MCS using 10^6 samples to verify the reliabilities of these optimal solutions as shown in Table 5.8. It is observed that the traditional RBDO method failed to provide a reliable optimal design due to the lack of data, as the reliability of the forth constraint 0.6008 and

tenth constraint 0.6611 cannot satisfy the target reliability requirement. With 500 more function evaluations than other approaches, the SM(TS) method offers an unreliable optimal design because the reliability of G_{10} is less than 0.96. As shown in Tables 5.7 and 5.8, both the SM(CV) and proposed method can provide reliable optimal designs with 300 function evaluations while the proposed ERI approach obtains a less weight of the design.

Table 5.7: Comparison of optimal designs from different methods

	d_1	d_2	d_3	d_4	d_5	d_6	d_7	d_8	d_9	Weight
MCS	0.502	1.347	0.501	1.374	0.626	1.497	0.502	0.339	0.193	24.8644
RBDO	0.681	1.229	0.666	1.365	0.503	1.437	0.519	0.273	0.277	25.9502
SM(TS)	0.803	1.363	0.858	1.353	0.607	1.359	0.504	0.258	0.277	28.8782
SM(CV)	0.883	1.420	0.891	1.339	0.859	1.364	0.580	0.246	0.266	30.4720
Proposed	0.742	1.337	0.767	1.290	0.855	1.313	0.686	0.284	0.290	28.4548

Table 5.8: True reliabilities for the optimal designs

	R_1	R_2	R_3	R_4	R_5	R_6	R_7	R_8	R_9	R_{10}
RBDO	1	0.9922	0.9888	0.6008	1	1	1	0.9746	0.9759	0.6611
SM(TS)	1	0.9976	0.9980	0.9633	1	1	1	0.9952	0.9947	0.8909
SM(CV)	1	0.9999	1	0.9920	1	1	1	0.9970	0.9978	1
Proposed	1	0.9976	0.9990	0.9621	1	1	1	0.9748	0.9962	0.9994

5.5.3 Case Study III: Aircraft Tubing Design

Tubing assemblies have been widely integrated in many subsystems, such as hydraulic system in aircraft systems. Ensuring the reliability of tubing assemblies is important to the safety and reliability of aircrafts. This case study employs the RBDO using ERI approach for the design of a twisted tube. A twisted tube is made of steel with Young's modulus 200 GPa and Poisson's ratio 0.27. As shown in Fig. 5.11, the geometry of the twisted tube is fully characterized by four design variables listed in Table 5.9, including the inner diameter *D*, thickness *T*, radius of bending R for two bended tube, and the length *L*.

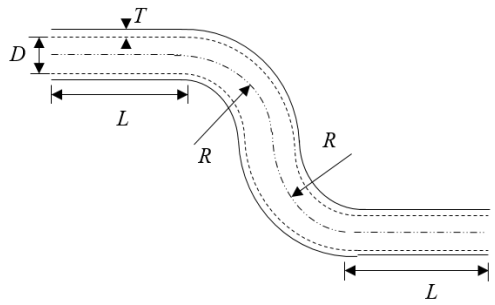

Figure 5.11: Geometry of twisted aircraft tubing

Table 5.9: Aircraft tubing design variables

Design variable	Distribution	Standard deviation	Boundary
Inner diameter, D	Normal	0.2 mm	[17mm, 20mm]
Thickness, T	Normal	0.05 mm	[2.5mm, 3.5mm]
Radius of bending, R	Normal	0.2 mm	[17mm, 20mm]
Length, L	Normal	0.4 mm	[35mm, 40mm]

A finite element model of the twisted model has been developed in ANSYS to obtain the maximum total deformation δ_{max} of the tube. A failure is defined as the maximum total deformation is greater than the critical threshold 0.01 mm, and the design objective is to minimize total volume of the twisted tube. By setting a target reliability as 0.985 and the

target reliability index β_t as 2.1701, the RBDO problem for the aircraft tubing is formulated as

$$\begin{aligned} &\text{Minimize}: && \mathrm{V}(\mathbf{d}) \\ &\text{subject to}: && \beta_e = \Phi^{-1}\left(\Pr\left(G(\mathbf{d}) \geq 0\right)\right) \geq \beta_t \\ & && \mathbf{d} = [D, T, R, L] \end{aligned} \tag{5.40}$$

The ERI-based RBDO starts with an initial design d_0 = [18.5000, 3.0000, 18.5000, 37.5000], and then constructs a surrogate model using 40 training data points for reliability assessment and sensitivity analysis using the proposed ERI approach. An optimal design d_{opt} = [17.0000, 2.9983, 18.2228, 35.0000] is achieved after 15 iterations as shown in Fig. 5.12 and Fig. 5.13. The total volume is reduced from 258383.236 mm^3 to 23970.199 mm^3. In this case study, the maximum total deformation is evaluated by finite element analysis using ANSYS. Thus, it is intractable to verify the optimal design by direct MCS method due to the extremely expensive computational cost. Therefore, a high-fidelity GP model constructed with 400 samples is used to provide accurate prediction of the maximum total deformation approximations. Then the MCS with 10^6 samples is utilized by using the high-fidelity GP model to verify the reliability at the obtained optimal solution as shown in Table 5.10. For comparison purpose, the aircraft tubing design problem is also solve by employing direct MCS method based on the high-fidelity GP model. As shown in Table 5.10, with only 40 evaluations of finite element analysis, the optimal design obtained by the proposed work is near to the optimal solution achieved by direct MCS with high-fidelity GP model. Figure 5.14 shows deformation contour for the optimal design. Moreover, the static structure analysis is conducted in ANSYS for both the initial and the optimal design, while the maximum total deformations are 0.011295mm and 0.009222 mm, respectively.

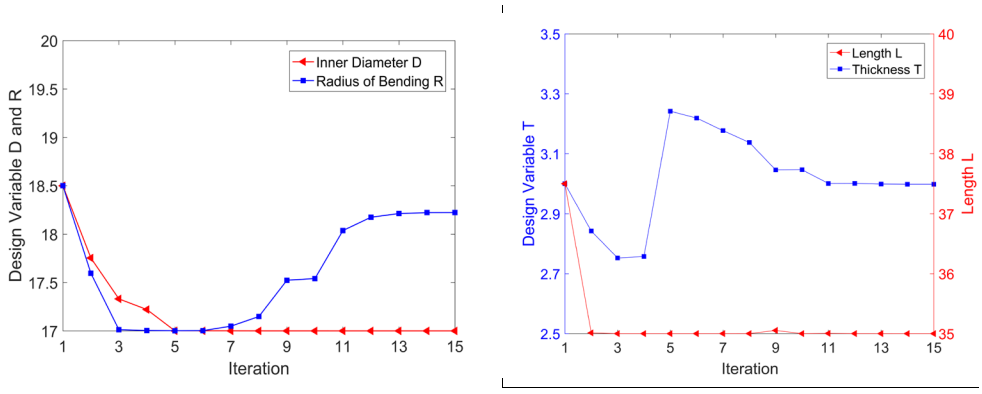

Figure 5.12: Design variables at each design iteration

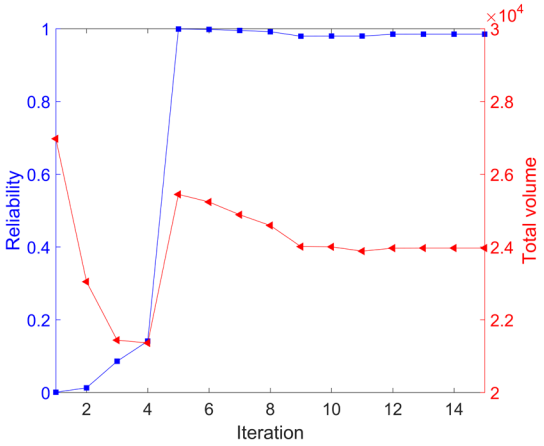

Figure 5.13: Design history of reliability and total volume

Table 5.10: Comparison of the optimal designs

	Optimum	Reliability	Volume
High-fidelity GP	[17.0000, 2.9280, 18.7827, 35.0000]	0.9850	23648.300
Proposed	[17.0000, 2.9983, 18.2228, 35.0000]	0.9913	23970.199

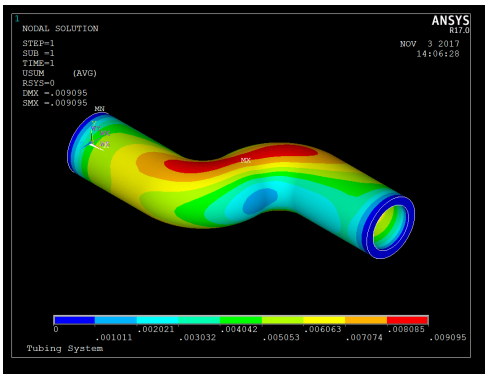

Figure 5.14: Maximum total deformation given by ANSYS

5.6 Conclusion

This work presents an equivalent reliability index (ERI) approach to ensure reliable optimal designs for reliability-based design optimization problems with limited data. The Gaussian process modeling technique is used for constructing surrogate models of limit state functions. By employing the Monte Carlo simulation for reliability analysis, the predictions from GP model are treated as component normal distributions to form a Gaussian mixture model (GMM), which is capable of handling both input variation and the surrogate model uncertainty due to the lack of data. Then the reliability is approximated based on the first two statistical moments of the GMM and an equivalent reliability index can be computed through the cumulative distribution function. To facilitate the RBDO process, the smooth sensitivity of ERI is analytically derived based on the constructed GMM and the predictions from GP model. Comparison results from three case studies demonstrated the proposed approach outperforms existing RBDO approaches when the training data is limited.

6 ACTIVE RESOURCE ALLOCATION FOR RELIABILITY ANALYSIS WITH MODEL BIAS CORRECTION[96]

6.1 Introduction

Though various methods have been developed for validating simulation models with experimental data, it still lacks a strategy to actively seek critical information from both sources for effective reliability assessment. This work presents an active resource allocation approach (ARA) for reliability analysis by iteratively identifying important simulations and experiments for evaluations. With both the simulation data and experimental observations, predictive models are constructed in ARA using the Gaussian process modeling technique (GP) to capture the model bias. To improve the fidelity of predictive models, a two-phase strategy is proposed to actively search for most valuable points within the input space for managing the uncertainty due to lack of data and model bias. As a result, an enhanced Gaussian process model is obtained to predict the actual response of system and accurately approximate the reliability using Monte Carlo simulation while reducing the overall costs. The effectiveness of the proposed approach is demonstrated through four case studies.

6.2 Active Resources Allocation

6.2.1 Problem Statement

In reliability analysis, simulation models and surrogate modeling techniques have been widely used for reducing the costs of evaluating the limit state function. As a substitution of actual physical process, simulation models constructed through idealization and simplification can capture some fundamental features of the underlying physics. However,

most reliability analysis methods assume the simulations are perfectly accurate and construct surrogate models purely based on simulation data. Generally, random sampling approaches are first used to collect the simulation training data, and then adaptive sampling approaches are utilized for building surrogate models with iterative updating process. Despite the sampling strategy, surrogate models constructed by using only simulation data are not capable of addressing the intrinsic differences between simulations and experiments, leading to inevitable errors in reliability assessment of the actual physical system.

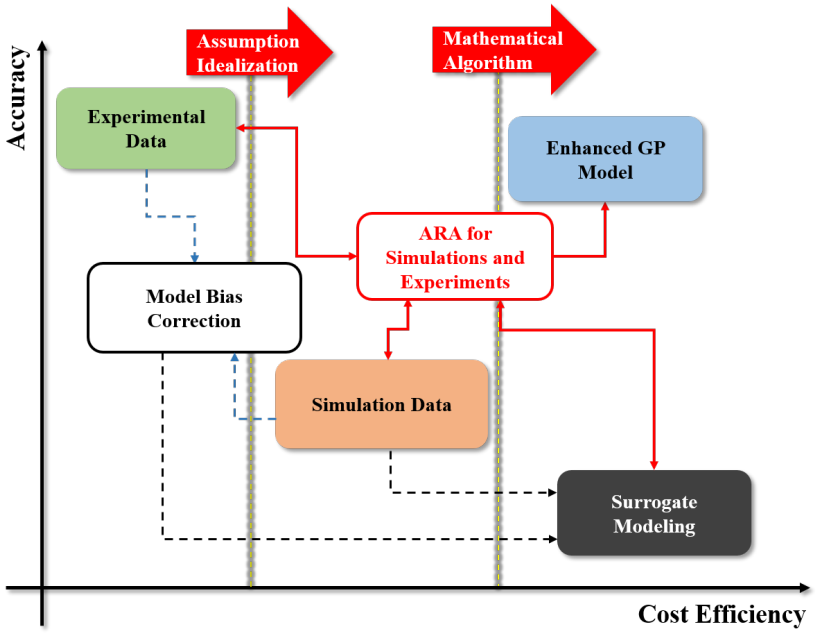

Figure 6.1: Illustration of active resource allocation for enhancing surrogate model fidelity and reducing cost

Consequently, research efforts have been made to validate the simulation model by integrating both simulation and experimental data. Among the various sources of uncertainties that existed in simulation models [97], a simulation model validation problem has gained lots of attention, formulated as

$$y^e(\mathbf{x}) = y^m(\mathbf{x}) + \delta(\mathbf{x}) + \varepsilon \tag{6.1}$$

where y^e(x) denotes experimental response, y^m(x) represents the simulation model response as a function of inputs x, δ(x) represents the discrepancy function that characterizes the differences between simulation outputs and experimental results, and ε stands for the experimental errors, which is often assumed to follow a normal distribution ~ $N(0, \lambda)$. In this work, the experimental error is assumed to be neglectable. Eq. (6.1) is often referred to as a problem of model bias correction and the goal is to estimate the model bias δ(x) for adjusting the simulation results to be closer to the experiment responses. With given sets of simulation and experimental data, conventional simulation model validation approaches correct the model bias by using Eq. (6.1), and then construct surrogate models to predict the experimental responses. Though the prediction is more accurate than using a surrogate model constructed purely based on simulation data, the prediction accuracy is not guaranteed as it highly depends on the strategy of choosing the input sites for conducting simulations and experiments.

The fidelity of surrogate models can be improved by adding more training samples, however, collecting experimental data is extremely expensive due to the labor and time cost. In addition, though running simulations is not as expensive as conducting experiments, the computational costs also post a grand challenge while running a large number of simulations in reliability analysis. Despite the total numbers of the overall data including simulations and experiments, the locations of these sample points also affect the fidelity of the surrogate model constructed after model bias correction. For example, more prediction errors may be introduced within the area that sample points are sparsely distributed.

Conventional methods lack the capability of identifying new simulation and experimental samples for improving the fidelity of the surrogate models and a major challenge remains that it still lacks an effective means for maintaining the accuracy of reliability analysis while reducing the total costs including both computational and experimental cost. In this work, we use the term "resource" to define the layout of simulations and experiments that used for model bias correction and construction of an enhanced surrogate model. The challenge can be potentially solved by a resource allocation framework, which is formulated as

$$\begin{aligned} \min_{\mathbf{X}_m, \mathbf{X}_e} \quad & cost = f_r\left(N_m, N_e\right) \\ s.t. \quad & F\left(R_{est} \mid \mathbf{X}_m, \mathbf{X}_e, N_m, N_e\right) > F_t \end{aligned} \tag{6.2}$$

where N_m and N_e represent the number of simulations and experiments, $\mathrm{X_m}$ and $\mathrm{X_e}$ represent the input sites for simulations and experiments, respectively, and R_{est} represents the estimated system reliability given the simulation results and experimental observations. As shown in Eq. (6.2), the goal is to ensure that the fidelity of the reliability analysis $F(.)$ is greater than a high level target F_t while minimizing the computational and experimental costs.

It is technically impossible to analytically solve the resources allocation problem involving both simulations and experiments. Therefore, we proposed an active resources allocation approach that aims at approaching the best solution of balancing the tradeoff between costs and accuracy of reliability analysis. As shown in Fig. 6.1, the goal is to construct an enhanced surrogate model by smartly distributing the simulations and experiments, and the constructed model is ensured to possess a high prediction accuracy.

As the flowchart shown in Fig. 6.2, the ARA updates the simulation and experimental data in a two-phase manner.

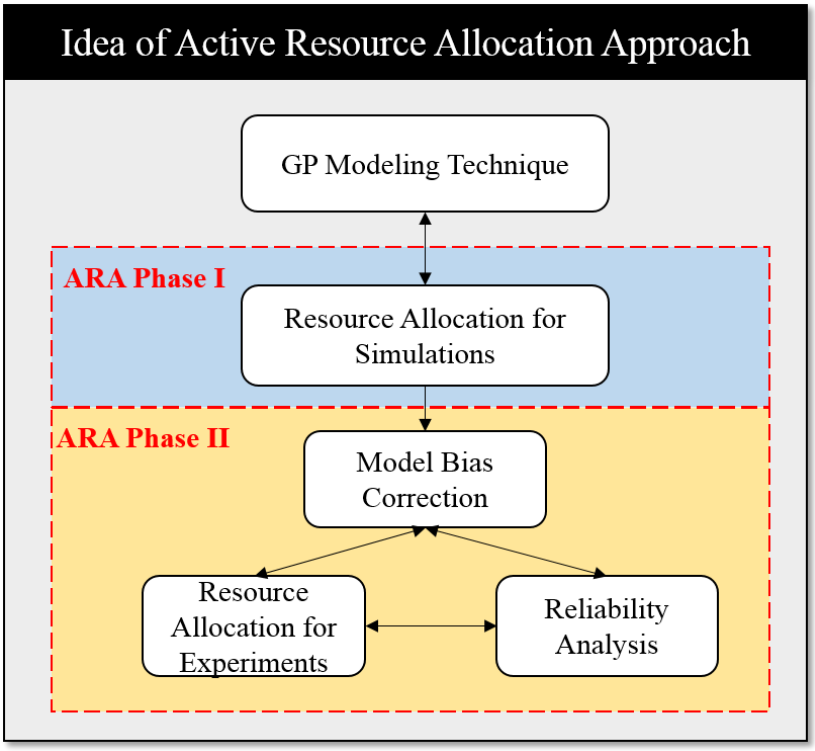

Figure 6.2: Idea of the proposed ARA approach

6.2.2 Model Bias Correction Using Gaussian Process Modeling

In this subsection, we briefly review the Gaussian process modeling technique and its application for model bias correction using simulation and experimental data. Generally, a performance function $G(\mathrm{x})$ can be characterized by a Gaussian process model as

$$G(\mathbf{x}) \sim GP\left(\mathbf{h}(\mathbf{x})\boldsymbol{\beta}, \sigma^2 R(\mathbf{x}, \mathbf{x}')\right) \tag{6.3}$$

where the response of $G(\mathrm{x})$ at point x is assumed to be a stationary Gaussian process with mean function $\mathrm{h(x)}\beta$ and covariance function $V(\mathrm{x}, \mathrm{x}') = \sigma^2 R(\mathrm{x}, \mathrm{x}')$. The term $\mathrm{h(x)}$ is the vector of predefined polynomial functions and β is the vector of corresponding coefficients.

Typically, a constant mean function is sufficient for engineering applications, in which case a constant value 1 is used to replace the polynomial term h(x). In the GP model, the covariance function $V(x, x')$ is expressed as

$$V(\mathbf{x}, \mathbf{x}') = \sigma^2 R(\mathbf{x}, \mathbf{x}') = \sigma^2 \exp\left[-\sum_{p=1}^{k} \omega_p \left| \mathbf{x}_p - \mathbf{x}'_p \right|^2 \right] \tag{6.4}$$

where $\omega = [\omega_1, \omega_2, \ldots, \omega_k]$ is the vector of roughness parameters that capture the nonlinearity of the process. Given a data set D = [X, Y], where X represents n training input sites and Y denotes the evaluated performance function value at these inputs, the responses Y is treated as a multivariate normal distribution by using the Gaussian process modeling technique, denoted as

$$\mathbf{Y} \sim N(\mathbf{H\beta}, \mathbf{V}) \tag{6.5}$$

where $H = [h^T(x_1), \ldots, h^T(x_n)]$ and $H\beta$ represents the mean vector, V represents the $n*n$ covariance matrix whose i^{th} row, j^{th} column element is $\sigma^2 R(x_i, x_j)$. Based on the data set D, the hyperparameters σ^2, β, and ω that characterize the GP model can be estimated by using the Maximum Likelihood Estimation method. After obtaining the hyperparameters, the Gaussian process model of the performance function $G(x)$ can be constructed for predicting the responses at any input site, and the prediction follows a normal distribution with mean $\mu(x)$ and variance $v(x)$, written as

$$\mu(\mathbf{x}) = \mathbf{h}(\mathbf{x})\boldsymbol{\beta} + \mathbf{r}^T \mathbf{V}^{-1} (\mathbf{Y} - \mathbf{H}\boldsymbol{\beta}) \tag{6.6}$$

and

$$v(\mathbf{x}) = \sigma^2 \left\{ 1 - \mathbf{r}^T \mathbf{V}^{-1} \mathbf{r} + \left[\mathbf{h}(\mathbf{x}) - \mathbf{H}^T \mathbf{V}^{-1} \mathbf{r} \right]^T \left(\mathbf{H}^T \mathbf{V}^{-1} \mathbf{H} \right)^{-1} \left[\mathbf{h}(\mathbf{x}) - \mathbf{H}^T \mathbf{V}^{-1} \mathbf{r} \right] \right\} \tag{6.7}$$

where r represents the correlation vector between the input point x and all training sample points in X. In conventional reliability analysis methods, GP models are constructed purely based on simulation training data set. To account for the model bias, the Gaussian process modeling technique is extended for model bias correction [98] as the flowchart shown in Fig. 6.3, where the simulation model $y^m(\mathrm{x})$ is first assumed to be replaced by a GP model, expressed as

$$\begin{aligned} y^m(\mathbf{x}) &\sim GP\left(\mathbf{h}^m(\mathbf{x})\boldsymbol{\beta}^m, \sigma_m^2 R^m(\mathbf{x},\mathbf{x}')\right) \\ R^m(\mathbf{x},\mathbf{x}') &= \exp\left[-\sum_{p=1}^{k} \omega_p^m \left|\mathbf{x}_p - \mathbf{x}_p'\right|^2\right] \end{aligned} \tag{6.8}$$

Similarly, the bias function $\delta(\mathrm{x})$ can be modeled by a GP model as

$$\begin{aligned} \delta(\mathbf{x}) &\sim GP\left(\mathbf{h}^\delta(\mathbf{x})\boldsymbol{\beta}^\delta, \sigma_\delta^2 R^\delta(\mathbf{x},\mathbf{x}')\right) \\ R^\delta(\mathbf{x},\mathbf{x}') &= \exp\left[-\sum_{p=1}^{k} \omega_p^\delta \left|\mathbf{x}_p - \mathbf{x}_p'\right|^2\right] \end{aligned} \tag{6.9}$$

For simplicity, we use $\hat{g}^m$ and $\hat{g}^\delta$ to represent the GP models of simulation model and bias function, respectively. Accordingly, $\mathrm{h}^m(\mathrm{x})$ and $\mathrm{h}^\delta(\mathrm{x})$ stand for the polynomial regression functions, β^m and β^δ represents the corresponding coefficients, and $V^m(.,.) = \sigma_m{}^2 R^m(.,.)$ and $V^\delta(.,.) = \sigma_\delta{}^2 R^\delta(.,.)$ represents the covariance functions of the two GP models. It should be mentioned that the polynomial regression functions for both GP models are assumed to be a constant 1 in this study. Assuming two data sets have been respectively collected from simulation models and experimental observations, where the N_m simulation data is denoted as

$$\begin{aligned} &\mathbf{D}^m = [\mathbf{X}^m, \mathbf{Y}^m] \\ &\mathbf{X}^m = [\mathbf{x}_1^m, ..., \mathbf{x}_{Nm}^m]; \mathbf{Y}^m = [y^m(\mathbf{x}_1^m), ..., y^m(\mathbf{x}_{Nm}^m)] \end{aligned} \tag{6.10}$$

and N_e experimental observations are written as

$$\begin{aligned}&\mathbf{D}^e = [\mathbf{X}^e, \mathbf{Y}^e] \\ &\mathbf{X}^e = [\mathbf{x}_1^e, ..., \mathbf{x}_{Ne}^e]; \mathbf{Y}^e = [y^e(\mathbf{x}_1^e), ..., y^e(\mathbf{x}_{Ne}^e)]\end{aligned} \tag{6.11}$$

As the experiment responses are the combination of simulation results and bias function, the overall collected responses $Y^{all} = [Y^m, Y^e]$ follow a multivariate normal distribution by assuming the independency between $y^m(x)$, $\delta(x)$, and experimental error ε, expressed as

$$\begin{bmatrix} y^m(\mathbf{x}_1^m) \\ \vdots \\ y^m(\mathbf{x}_{Nm}^m) \\ y^e(\mathbf{x}_1^e) \\ \vdots \\ y^e(\mathbf{x}_{Ne}^e) \end{bmatrix} \sim N\left(\begin{bmatrix} \mathbf{H}^m(\mathbf{X}^m) & 0 \\ \mathbf{H}^m(\mathbf{X}^e) & \mathbf{H}^\delta(\mathbf{X}^e) \end{bmatrix} \begin{bmatrix} \boldsymbol{\beta}^m \\ \boldsymbol{\beta}^\delta \end{bmatrix}, \mathbf{V}^{all} \right) \tag{6.12}$$

Since the constant regression functions is used, $H^m(X^m)$ is a $N_m \times 1$ unit vector and $H^\delta(X^\delta)$ is also a unit vector with N_e components. The covariance matrix is given as

$$\mathbf{V}^{all} = \begin{bmatrix} V^m\left(\mathbf{X}^m, \mathbf{X}^m\right) & V^m\left(\mathbf{X}^e, \mathbf{X}^m\right)^T \\ V^m\left(\mathbf{X}^e, \mathbf{X}^m\right) & \lambda\mathbf{I} + V^m\left(\mathbf{X}^e, \mathbf{X}^e\right) + V^\delta\left(\mathbf{X}^e, \mathbf{X}^e\right) \end{bmatrix} \tag{6.13}$$

where I represents an identity matrix and λ represents the standard deviation of the experimental error. Both $V^m(.,.)$ and $V^\delta(.,.)$ have the same formulation as shown in Eq. (4), however, the hyperparameters are different as they represent the covariance function of simulation GP model and bias GP model, respectively. As indicated by Eqs. (6.12) and (6.13), a GP model for the experimental responsecan be constructed if all the unknown hyperparameters $\varphi = [\sigma_m, \beta^m, \omega^m, \sigma_\delta, \beta^\delta, \omega^\delta]$ can be determined. Based on the overall data set $D = [D^m, D^e]$, the likelihood function of the hyperparameters is formulated as

$$L(\mathbf{Y}^{all}\left|\phi\right.) = p(\phi\left|\mathbf{Y}^{all}\right.) \propto$$
$$\left|\mathbf{V}^{all}\right|^{-1/2}\left|\mathbf{H}_e^T\mathbf{V}_{all}{}^{-1}\mathbf{H}_e^T\right|^{-1/2}\exp\left[-\frac{1}{2}\left(\mathbf{Y}^{all}-\mathbf{H}_e^T\boldsymbol{\beta}_e\right)^T\mathbf{V}_{all}{}^{-1}\left(\mathbf{Y}^{all}-\mathbf{H}_e^T\boldsymbol{\beta}_e\right)\right] \quad (6.14)$$

where H_e and β_e are expressed as

$$\mathbf{H}_e=\begin{bmatrix}\mathbf{H}^m(\mathbf{X}^m) & 0\\ \mathbf{H}^m(\mathbf{X}^e) & \mathbf{H}^\delta(\mathbf{X}^e)\end{bmatrix},$$
$$\boldsymbol{\beta}_e=\begin{bmatrix}\boldsymbol{\beta}^m\\ \boldsymbol{\beta}^\delta\end{bmatrix} \quad (6.15)$$

The hyperparameters can be estimated by maximizing the log-likelihood function, which is expressed as

$$\log L(\mathbf{Y}^{all}\left|\phi\right.) = -\frac{1}{2}\left[\log\left|\mathbf{V}^{all}\right| + \log\left|\mathbf{H}_e^T\mathbf{V}_{all}{}^{-1}\mathbf{H}_e^T\right| + \left(\mathbf{Y}^{all}-\mathbf{H}_e^T\boldsymbol{\beta}_e\right)^T\mathbf{V}_{all}{}^{-1}\left(\mathbf{Y}^{all}-\mathbf{H}_e^T\boldsymbol{\beta}_e\right)\right]$$

(6.16)

Various optimization methods can be utilized to solve the optimization problem, and all the hyperparameters can be determined accordingly. As a result, a GP model $\hat{g}^e$ can be obtained for predicting the experimental response $y^e(.)$, expressed as

$$y^e(\mathbf{x}) \sim GP\left(\mathbf{h}_e(\mathbf{x})\boldsymbol{\beta}_e, V^{all}(\mathbf{x},\mathbf{x}')\right) \quad (6.17)$$

Accordingly, the GP models $\hat{g}^m$ and $\hat{g}^\delta$ can be obtained after estimating the hyperparameters. Therefore, the simulation response, bias prediction, and experimental response at any given input can be predicted by using the three GP models.

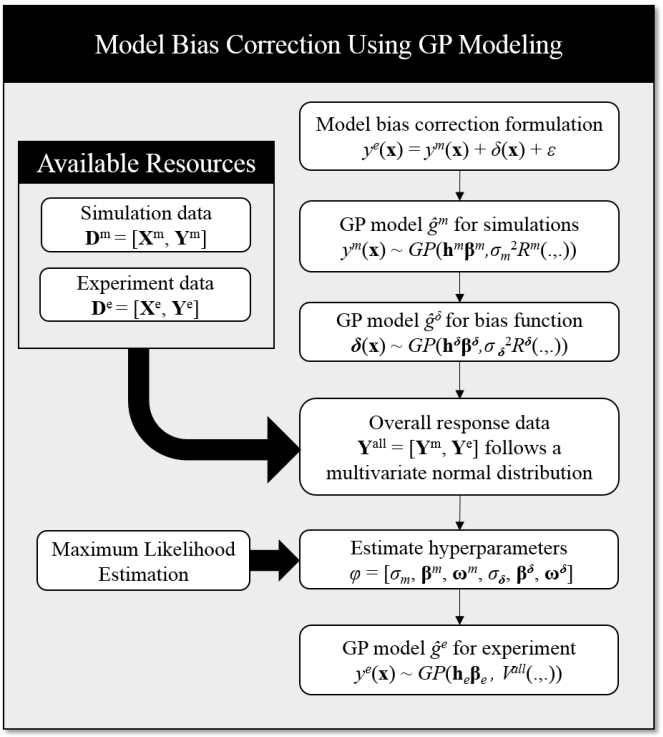

Figure 6.3: Flowchart of the model bias correction using Gaussian process modeling

6.2.3 Two-Phase Strategy for Active Resource Allocation

To effectively allocate recourses for both simulations and experiments, a two-phase strategy is introduced in this subsection. The resource allocation for simulation data is first addressed in phase I and the experiment is then iteratively conducted by fixing the updated simulation data in the second phase.

Phase I: Resource allocation for simulation. With an initial simulation data set $D^{mi} = [X^{mi}, Y^{mi}]$, where X^{mi} represents N_{mi} random input sample points and Y^{mi} represents the corresponding simulation responses, a GP model can be constructed, denoted as $\hat{G}^m(x) \sim N(\mu_m(x),\sigma_m(x))$, where $\mu_m(x)$ and $\sigma_m(x)$ represents the prediction mean and standard deviation, respectively. It should be mentioned that this GP model is different from the GP model $\hat{g}^m$ as the hyperparameters are estimated purely based on simulation data. The

simulation response at any input can be predicted by the GP model $\hat{G}^m$ and the prediction accuracy has to be quantified to check if current simulation data is sufficient or still needs to be updated for characterizing the simulation model. Therefore, a maximum confidence-based adaptive sampling method [99] is utilized in the proposed approach for updating the simulation data.

According to the randomness of the given input, the Monte Carlo simulation method is employed for generating N random realizations of the input variable, denoted as $\mathrm{X}_{\mathrm{mcs}} = [\mathrm{x}_{mcs,1}, \mathrm{x}_{mcs,2}, \ldots, \mathrm{x}_{mcs,N}]$. For each MCS sample, an indicator function is used for classification, expressed as

$$I_f(\mathbf{x}_{mcs,i}) = \begin{cases} 1, & \mu_m(\mathbf{x}_{mcs,i}) < 0 \\ 0, & otherwise \end{cases} \tag{6.18}$$

Note the prediction mean may not be the same as the actual simulation response y^m.x), and the sign of prediction mean μ_m(.) and y^m(.) can be different due to the prediction error. Therefore, the confidence level of GP model $\hat{G}^m$ (.) at the point $\mathrm{x}_{mcs,i}$ is defined as the probability of correct classification, meaning that the prediction mean has the same sign with the actual simulation response. The confidence level can be calculated as

$$CL_m(\mathbf{x}_{mcs,i}) = \Phi\left(\frac{\left|\mu_m(\mathbf{x}_{mcs,i})\right|}{\sigma_m(\mathbf{x}_{mcs,i})}\right) \tag{6.19}$$

where Φ(.) is the standard normal cumulative distribution function. As a result, a cumulative confidence level (CCL_m) of $\hat{G}^m$ can be obtained after evaluating the CL_m for all the MCS samples, expressed as

$$CCL_m = \frac{1}{N}\sum_{i=1}^{N} CL_m(\mathbf{x}_{mcs,i}) \tag{6.20}$$

According to the definition of CL_m, it can be found that the CCL_m represents the accuracy of the GP model $\hat{G}^m$ in classifying the MCS samples. More MCS samples can be correctly classified if a higher CCL_m is achieved, which indicates the higher-fidelity of the GP model. Otherwise, additional simulation samples are required for improving the fidelity of the GP model. An importance measurement (IM) of the MCS samples IM^m is used to identify new training sample, written as

$$IM^m(\mathbf{x}_{mcs,i}) = (1 - CL_m(\mathbf{x}_{mcs,i})) * f_x(\mathbf{x}_{mcs,i}) * \sigma_m(\mathbf{x}_{mcs,i}) \tag{6.21}$$

where $f_x(.)$ is the joint probability density function of input variables. The MCS sample with the highest value of IM^m will be selected as the most important point, which will be evaluated by the actual simulation model and added into the training data set for updating the GP model. By setting a high target cumulative confidence level as the stopping criterion, the updating process is repeated until the current CCL_m is greater than the target. In phase I of the ARA approach, the Gaussian process modeling technique is employed for constructing a surrogate model of the simulation, and the accuracy of the surrogate model is treated as a measurement of the sufficiency of simulation data. Eventually, an accurate GP model can be achieved, which demonstrates that the collected simulation data is capable of representing the actual simulation model. For consistency and simplicity, we assume that a total number of N_m simulation data have been evaluated during the updating process at phase I.

Phase II: Recourse allocation for experiment. After determining the simulation data set, the experimental observations need to be collected for capturing the model bias. At the last updating iteration of phase I, the identified most important point is used as the input

site for obtaining the first experiment response. With the collected N_m simulation data and the available experimental data, model bias correction using GP modeling technique is performed, and an enhanced GP model $\hat{g}^e$ can be constructed as introduced in subsection 6.2.2. The enhanced model is utilized for predicting the experimental response, and it can be directly used for estimating the reliability of the actual physical system. With the N MCS samples, the probability of failure can be approximated as

$$P_f = \Pr\left(G(\mathbf{x}) < 0\right) = \int_{\Omega} I_{fe}(\mathbf{x}) f_x(\mathbf{x}) d\mathbf{x} = E[I_{fe}(\mathbf{x})] \tag{6.22}$$

where x is the vector of random variables, f_x(x) is the corresponding joint probability density function, E[.] is the expectation operator and I_{fe}(x) is a failure indicator function. Assuming the failure event occurs when the limit state function response is smaller than zero, the failure indicator function I_{fe}(x) is used to identify failure samples, expressed as

$$I_{fe}(\mathbf{x}_{mcs,i}) = \begin{cases} 1, & \mu_e(\mathbf{x}_{mcs,i}) < 0 \quad \text{failure} \\ 0, & \mu_e(\mathbf{x}_{mcs,i}) \geq 0 \quad \text{safe} \end{cases} \tag{6.23}$$

where μ_e(x$_{mcs,i}$) represents the prediction mean of the i^{th} MCS sample that obtained by using the GP model $\hat{g}^e$. Based on Eqs. (6.22) and (6.23), the probability of failure can be approximated based on the ratio of the number of failure samples N_f to the number of total MCS samples, given as

$$P_f \approx \frac{1}{N} \sum_{i}^{N} I_f(\mathbf{x}_{mcs,i}) = \frac{N_f}{N} \tag{6.24}$$

There is no doubt that the estimated probability of failure lacks accuracy when only one experimental observation is used to construct the enhanced GP model. Therefore, a new updating procedure is introduced for iteratively adding experimental data.

Based on the same MCS samples that generated in phase I, the concept of confidence level is used to quantify the accuracy of the GP model $\hat{g}^e$, formulated as

$$CL_e(\mathbf{x}_{mcs,i}) = \Phi\left(\frac{\left|\mu_e(\mathbf{x}_{mcs,i})\right|}{\sigma_e(\mathbf{x}_{mcs,i})}\right) \tag{6.25}$$

where $\sigma_e(.)$ represents the prediction standard deviation from the enhanced model. Accordingly, the cumulative confidence level for $\hat{g}^e$ can be obtained by averaging the CL_e for all the MCS samples. Since we have already updated the simulation data in Phase I, the accuracy of predicting the bias function is of critical importance in selecting the experimental data. Therefore, a new importance measurement for experiment IM^e is proposed to find the best location of evaluating the next experiment response, written as

$$IM^e(\mathbf{x}_{mcs,i}) = (1 - CL_e(\mathbf{x}_{mcs,i})) * f_x(\mathbf{x}_{mcs,i}) * \sigma^\delta(\mathbf{x}_{mcs,i}) \tag{6.26}$$

Compared to Eq. (6.26), the confidence level CL_e is used and the last term is replaced by the standard deviation of the bias prediction that calculated by the GP model $\hat{g}^\delta(.)$. As a result, the sample points with larger bias prediction variance are tends to be selected for improving the fidelity of the enhanced GP model. Similarly, the point with largest IM^e will be iteratively selected as the input for conducting the next experiment. With the updated experimental data set and N_m simulation data that determined in phase I, a new enhanced GP model can be obtained by following the same procedure. The iterative updating process will be repeated until the target cumulative confidence level is achieved.

At the first few iterations, the model bias prediction might contain significant errors due to the lack of experimental data, leading to extremely small prediction variance $\sigma_e(.)$. As a result, the cumulative confidence level may falsely satisfy the target. To enhance the

stability of the updating process, the reliability assessment is performed at each updating iteration in phase II, and the relative error for estimated P_f^i and P_f^{i-1} are treated as an additional stopping criterion, given as

$$\varepsilon = \left| \frac{P_f^i - P_f^{i-1}}{P_f^i} \right| \leq \varepsilon_t \tag{6.27}$$

where i represents the i^{th} iteration in phase II, and ε_t is a pre-defined threshold. Therefore, the experimental data updating process will be repeated until the estimated probability of failure converges. By iteratively adding the experimental data for correcting the model bias, the accuracy of experimental responsepredictions using the enhanced model can be increased and the estimated reliability tends to converge to the actual value.

6.2.4 Numerical Procedure

The procedure of employing the proposed active resource allocation approach for reliability analysis is summarized in Fig. 6.4. According to the randomness of the given input variables x, MCS samples are first generated as $X_{mcs} = [x_{mcs,1}, \ldots, x_{mcs,N}]$. Then the active resource allocation is performed in a two-phase strategy. For the simulation model y^m, N_{mi} initial samples are first generated by using Latin hypercube sampling (LHS), and a GP model $\hat{G}^m$ is constructed after obtaining the simulation results of these initial samples. According to the author's experience, the number is suggested to be around 10*(n_r - 1), where n_r represents the total number of random variables. After predicting the simulation response at each MCS sample, the fidelity of the simulation GP model is quantified by the cumulative confidence level CCL_m. The sample point that can maximize the improvement of the accuracy of the GP model is iteratively identified as the new simulation sample until

the target *CCL* is satisfied, and then all the evaluated simulation samples will be collected as the finalized simulation data set. To allocate the resource for experiments, the last important sample that identified in phase I will be used to conduct the first experiment. Following the procedure introduced in subsection 6.2.3, the model bias correction is performed based on the current data sets and an enhanced GP model $\hat{g}^e$ can be constructed accordingly. With model bias correction, the experimental response at each MCS point can be predicted by using the GP model $\hat{g}^e$. By identifying the failure samples, the probability of failure can be directly approximated as the ratio of the number of failure samples to the total number of the MCS samples, and the CCL_e and IM^e can be calculated based on Eqs. (6.25) and (6.26). Both the estimated probability of failure and CCL_e are used for determining if it is needed to add more experimental data. At each iteration during phase II, the sample point with maximum IM_e will be selected as the input for conducting new experiment. Consequently, we are able to observe the convergence of the estimated probability of failure. The iterative updating process will automatically stop when both stopping criterions are satisfied, and the accurate estimation of probability of failure can be achieved simultaneously.

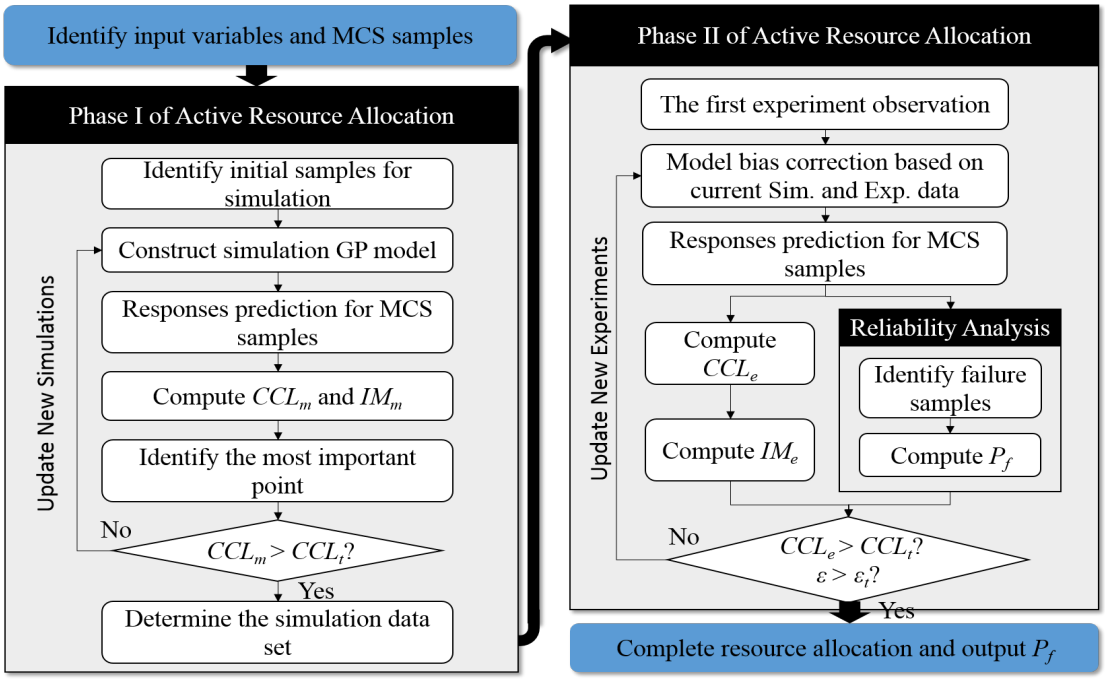

Figure 6.4: Flowchart of the proposed active resource allocation approach

6.3 Case Studies

In this section, four case studies will be introduced to demonstrate the effectiveness of the ARA approach for reliability analysis with model bias correction.

6.3.1 Case Study I: A 2D Mathematical Problem

A 2D mathematical problem is first introduced to test the performance of the proposed ARA approach, where the limit state functions are given as

$$G^m(x_1,x_2)=\frac{(x_1+x_2-5)^2}{30}+\frac{(x_1-x_2-12)^2}{120}-1$$
$$G^e(x_1,x_2)=G^m(x_1,x_2)+\delta(x_1,x_2);\quad \delta(x_1,x_2)=0.05x_1x_2 \tag{6.28}$$

where G^m and G^e represent the simulation model and experiment, respectively. The input variable is given as x = [5, 2], where both x_1 and x_2 follow a normal distribution with a

standard deviation 0.45. In this study, the experimental error is assumed neglectable. To apply the proposed ARA approach, the target *CCL* is set to 0.99 while the threshold ε_t is set to 3%.

As outlined in subsection 6.2.4, 10^6 MCS samples are first generated according to the randomness of the input variable. Then the ARA approach is performed for model bias correction and reliability analysis. By employing the Latin hypercube sampling scheme, four initial samples are generated within the input range [x – 3σ, x + 3σ], and a GP model is constructed after evaluating the corresponding simulation responses. At phase I of ARA, 4 samples have been identified to satisfy the target *CCL*, where the iterative updating history of the simulation data is shown in Fig. 6.5. During the phase I of ARA, the estimated limit state function (LSF) of G^m gradually approaches to the actual G^m, and a total number of eight simulations are determined which will be further used in phase II updating process.

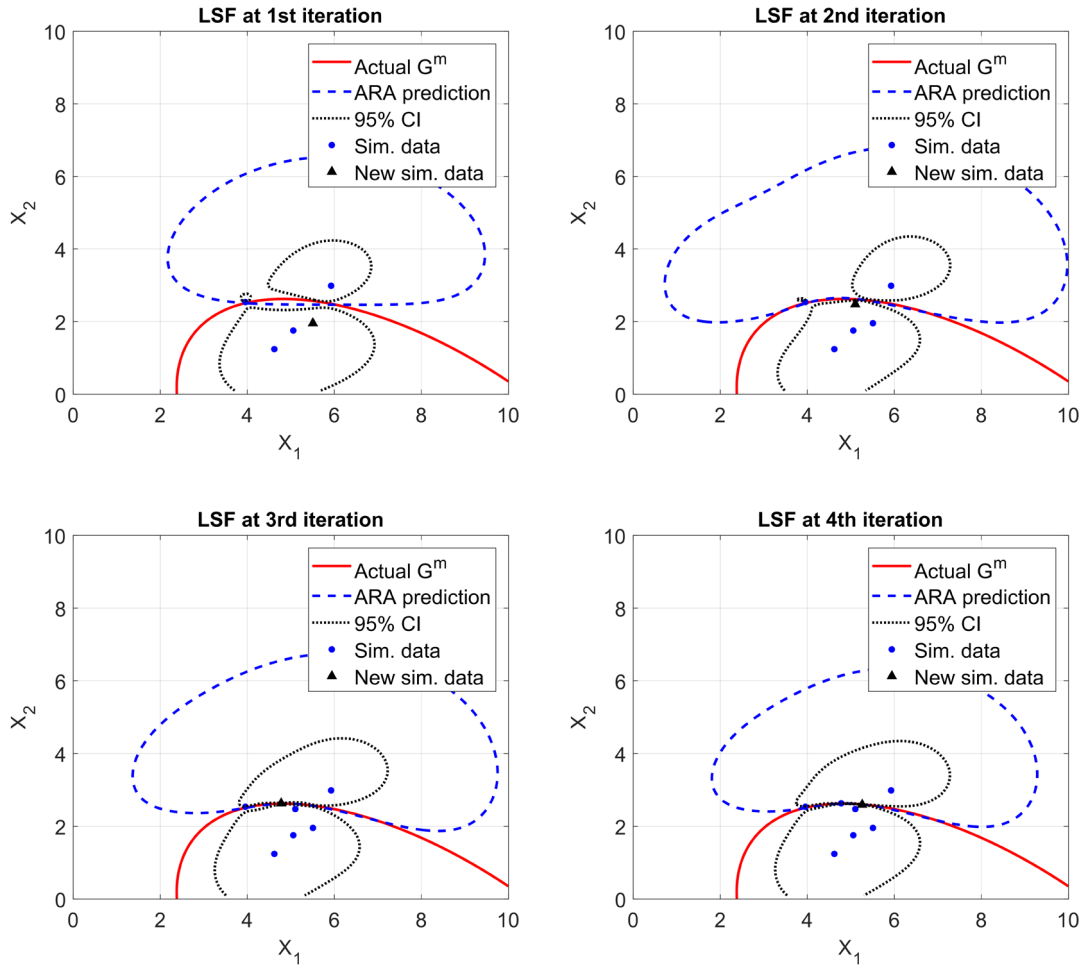

Figure 6.5: Iterative updating process for simulations

As introduced in subsection 6.2.2, the eight simulation data and one experimental data are used for model bias correction at the first iteration of phase II. With the available data sets, the hyperparameters of the GP models $\hat{g}^m$ and $\hat{g}^\delta$ can be simultaneously estimated, and the enhanced GP model $\hat{g}^e$ can be obtained accordingly. The enhanced GP model is used for predicting the experimental response of each MCS sample, and the failure samples are identified for reliability analysis. Meanwhile, the CCL_e are calculated for quantifying the accuracy of the current GP model $\hat{g}^e$, and the prediction variance of the bias function that

obtained from GP model $\hat{g}^{\delta}$ is involved in finding the next location for experimental observation. Eventually, a total number of four experimental sample points have been selected for updating the enhanced GP model. The estimated hyperparameters of the final GP models in phase I are given as σ = 0.0424, w_1 = 0.1, and w_2 = 0.2, while the hyperparameters of the simulation and bias GP model in Phase II are estimated as σ_m = 2.1975, w_{m1} = 0.7183, w_{m2} = 0.4421, and σ_δ =1.1045, $w_{\delta 1}$ = 0.9020, and $w_{\delta 2}$ = 1.6373, respectively. Figure 6.6 shows the comparisons of the predicted and the actual limit state function G^e during the phase II updating process. At the last iteration, accurate experimental response predictions can be obtained by the enhanced GP model $\hat{g}^e$. The simulations and experiments updating history is shown in Table 6.1, including the iterative new sample points, reliability analysis results, and CCL_m and CCL_e history. To verify the accuracy of reliability analysis using ARA, MCS with 10^6 samples is directly employed for reliability analysis based on the actual limit state functions G^m and G^e, given as 0.9058, and 0.0833, respectively. By allocating the resource for both simulations and experiments, the proposed approach is capable of providing an accurate reliability assessment by only using eight simulations and four experiments, where the error of estimated probability of failure is calculated as 0.12%.

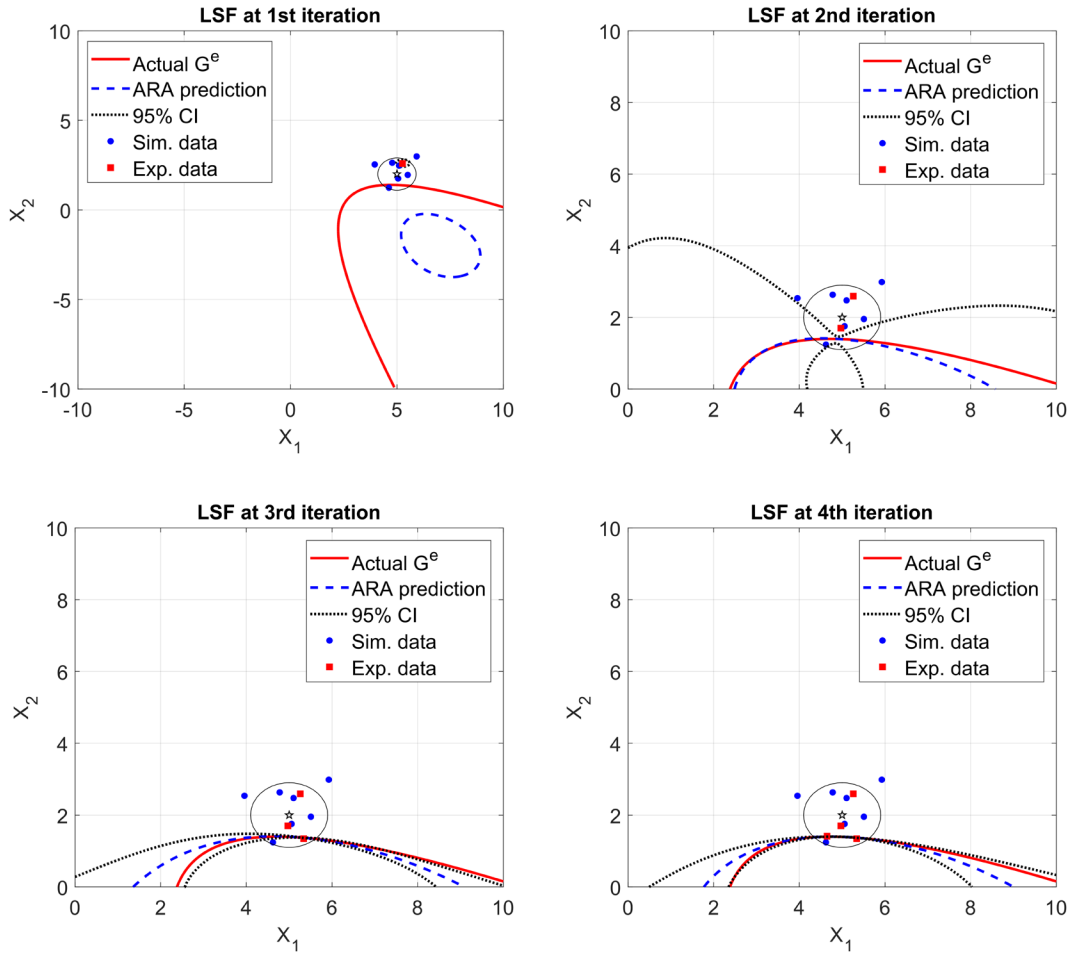

Figure 6.6: Iterative updating process for experiments

Table 6.1: ARA history for updating simulations and experiments

	Ite.	Input	Sim. Response	Exp. Response	CCL_m /CCL_e	Estimated P_f
Initial Sim. Sample	/	[5.9262, 2.9864]	0.1944	/	/	/
	/	[5.0563, 1.7541]	-0.2603	/	/	/
	/	[3.9561, 2.5373]	0.0073	/	/	/
	/	[4.6215, 1.2407]	-0.3561	/	/	/
	1	[5.5073, 1.9541]	-0.2035	/	0.9115	0.8578

ARA Phase I	2	[5.1025, 2.4749]	-0.0465	/	0.8866	0.8972
	3	[4.7781, 2.6322]	0.0028	/	0.9800	0.9055
	4	[5.2602, 2.5917]	-0.0032	/	0.9934	0.9052
ARA phase II	1	[5.2602, 2.5917]	/	0.6784	0.7052	0.0000
	2	[4.9708, 1.6996]	/	0.1504	0.9546	0.0820
	3	[5.3394, 1.3441]	/	-0.0127	0.9951	0.0854
	4	[4.6463, 1.4097]	/	0.0047	0.9993	0.0834

In addition, the same mathematical problem with uniformly distributed input variables has been solved to test the performance of the proposed approach, where the boundaries for both input variables are set to $[X_{1,2} - 2*0.45, X_{1,2} + 2*0.45]$. Similarly, four LHS samples are generated and evaluated as the initial simulation data set. By employing the ARA approach, four simulation samples and four experimental data have been identified until the estimated probability of failure converges. Figures 6.7 and 6.8 show the iterative updating history for ARA phase I and II, respectively. The overall ARA history is detailed in Table 6.2, including all the evaluated simulation and experimental samples and the iterative CCL_m/CCL_e history. The actual probability of failure that estimated by directly employing MCS on the G^e limit state function is given as 0.1510. The results show that an accurate reliability estimation with 0.3311% error can be obtained by using the proposed approach, which demonstrates that the ARA approach is applicable for reliability analysis problems with non-Gaussian distributed random variables.

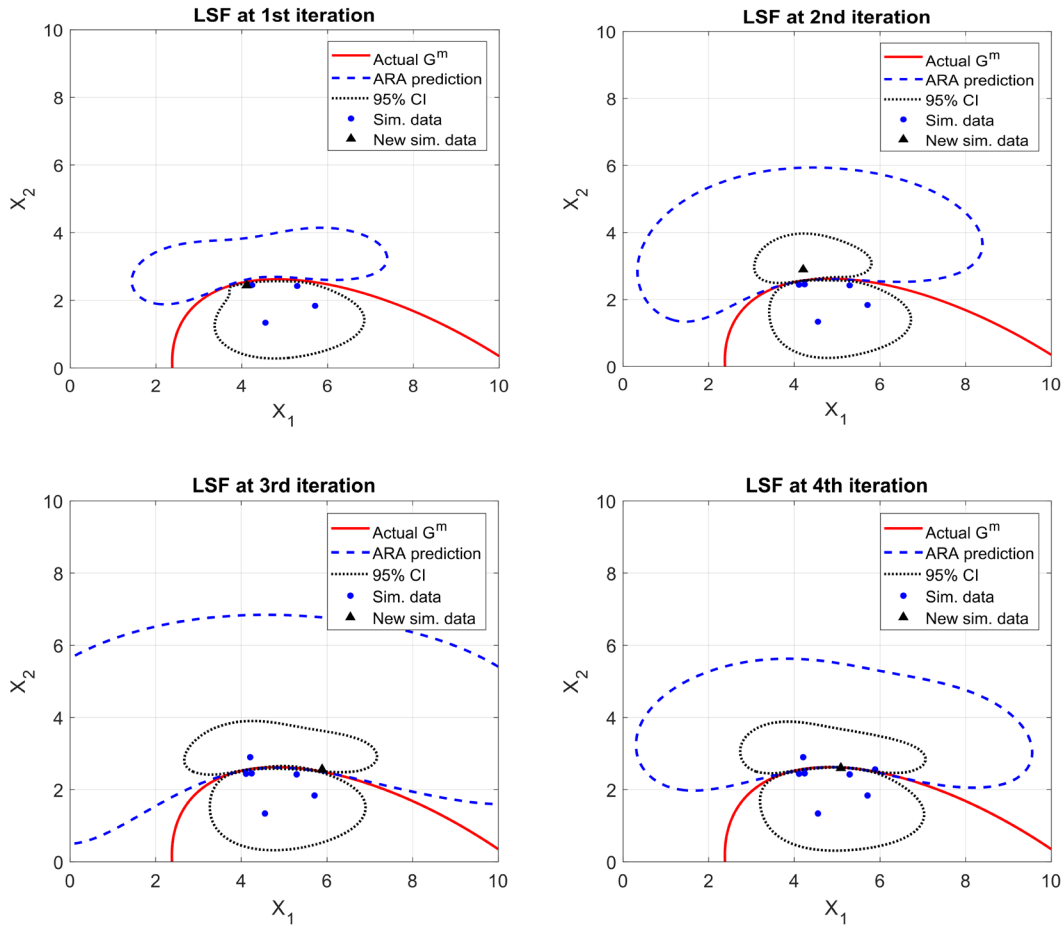

Figure 6.7: Iterative updating process for simulations (uniform distribution)

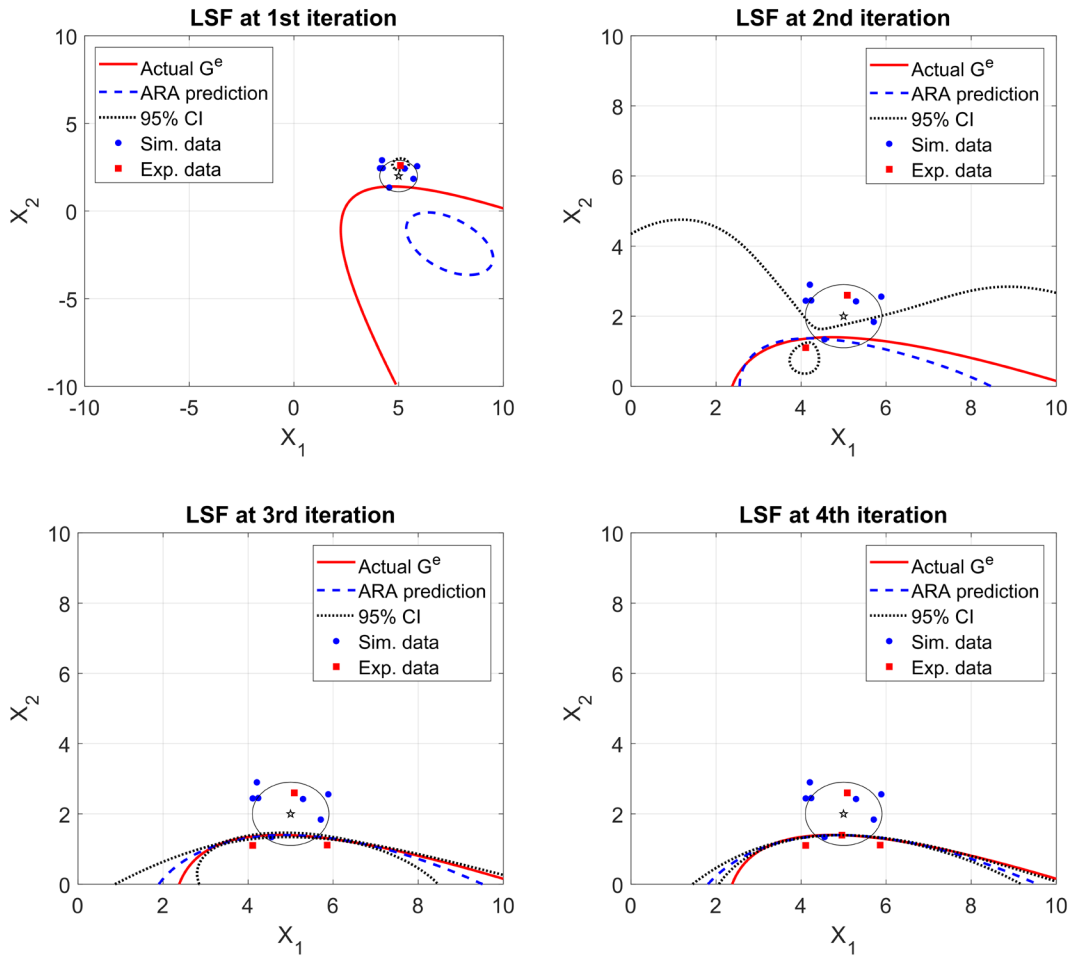

Figure 6.8: Iterative updating process for experiments (uniform distribution)

Table 6.2: ARA history for updating simulations and experiments (uniform distribution)

	Ite.	Input	Sim. Response	Exp. Response	CCL_m /CCL_e	Estimated P_f
Initial Sim. Sample	/	[5.2920, 2.4230]	-0.0595	/	/	/
	/	[4.5511, 1.3385]	-0.3301	/	/	/
	/	[4.2391, 2.4508]	-0.0358	/	/	/
	/	[5.7090, 1.8378]	-0.2332	/	/	/
	1	[4.1094, 2.4411]	-0.0303	/	0.8891	0.8670

ARA Phase I	2	[4.2063, 2.8988]	0.1004	/	0.9361	0.8192
	3	[5.8860, 2.5580]	0.0221	/	0.9843	0.8248
	4	[5.0867, 2.5997]	-0.0053	/	0.9944	0.8264
ARA phase II	1	[5.0867, 2.5997]	/	0.6559	0.7602	0.0000
	2	[4.1076, 1.1014]	/	-0.0983	0.9065	0.0948
	3	[5.8600, 1.1117]	/	-0.1064	0.9873	0.1515
	4	[4.9603, 1.3953]	/	2.36e-4	0.9995	0.1515

6.3.2 Case Study II: A Vehicle Disc Brake System

In this section, a vehicle disc brake system [100] consisting of a brake disc and a pair of brake pads is considered to test the performance of ARA approach. During the working process, strong vibration may occur when the brake system gets into an unstable state. To express the limit state function of the damping ratio, a quadratic polynomial response surface approximation model that constructed by 35 finite element simulations is treated as the simulation model in this work, given as

$$\begin{aligned} G^m(\mathbf{x}) &= 0.046287 + 0.20458u - 0.059821p - 0.00036549h_1 - 0.010037h_2 \\ &+0.013836h_3 + 0.24308up - 0.0037884uh_1 + 0.0023358uh_2 - 0.016918uh_3 \\ &+0.029287ph_1 - 0.015872ph_2 - 0.0028333ph_3 + 0.0007175h_1h_2 \\ &-0.00046158h_1h_3 - 0.0003648h_2h_3 - 0.39076u^2 - 0.015968p^2 - 0.0011936h_1^2 \\ &+0.000269h_2^2 + 0.00062638h_3^2 + 0.01; \end{aligned} \tag{6.29}$$

The input variables x = [h_1, h_2, h_3, μ, p] are assumed to be normally distributed as shown in Table 6.3, where h_1 represents friction material thickness, h_2 represents the disc thickness,

h_3 is the back plate thickness, μ is the friction coefficient, and p is the brake pressure. We assume the actual experimental limit state function G^e is formulated as

$$\begin{aligned} G^e(x) &= G_m(x) + \delta(x); \\ \delta(x) &= 0.25h_1 p - \frac{h_2}{h_3} - u \end{aligned} \tag{6.30}$$

The proposed ARA approach is employed to estimate the reliability of the actual vehicle disc brake system, where the target cumulative confidence level is set to 0.99, and the threshold for relative error of estimated probability of failure is set to 3%. Monte Carlo simulation with 10^6 samples are used in the two-phase updating process and reliability analysis. Starting with 60 initial simulation samples that generated by Latin hypercube sampling, 14 samples have been iteratively updated in phase I of ARA. Therefore, a total number of 74 simulations are determined for model bias correction and reliability analysis. In the second phase of ARA, 10 experiments have been identified until the stopping criterions are satisfied. The iteratively identified new experiments, corresponding actual experiment responses, and estimated P_f during the ARA phase II updating process are shown in Table 6.4. The actual probability of failure that evaluated based on the G^e limit state function is given as 0.0970. The two-phase updating history for both simulations and experiments are depicted in Figure 6.9, where the red dash line represents the actual reliability $R = 0.9030$ that calculated based on the actual experiment G^e. It is observed that the estimated reliability converges to the accurate value at the last iteration of phase II.

Table 6.3: Properties of input variables

Variable	Distribution Type	Mean	Standard Deviation
h_1	Normal	14.5 mm	0.8 mm
h_2	Normal	15 mm	0.8 mm
h_3	Normal	12 mm	0.8 mm
μ	Normal	0.35	0.01
p	Normal	0.5 MPa	0.02 MPa

Table 6.4: ARA history in phase II

Ite.	Experiment Input	Exp. Response	Estimated P_f
1	[14.9809, 13.8920, 11.5052, 0.3494, 0.5132]	0.3654	0.0000
2	[14.4833, 15.0998, 12.2422, 0.3513, 0.4957]	0.2183	0.0000
3	[15.3672, 16.9097, 12.8724, 0.3541, 0.4640]	0.1044	0.0000
4	[14.6035, 15.0355, 12.0434, 0.3403, 0.4964]	0.2302	0.0001
5	[12.6778, 16.5355, 12.4197, 0.3494, 0.4651]	-0.1784	0.1288
6	[14.4128, 15.4669, 11.0770, 0.3495, 0.5018]	0.0616	0.0858
7	[14.1931, 16.1508, 11.8956, 0.3500, 0.5077]	0.1022	0.0895
8	[14.3713, 14.8596, 11.0610, 0.3516, 0.4742]	0.0053	0.1202
9	[13.3826, 14.8894, 11.5931, 0.3504, 0.5040]	0.0721	0.0969
10	[14.4270, 15.0624, 10.4762, 0.3558, 0.5022]	0.0124	0.0958

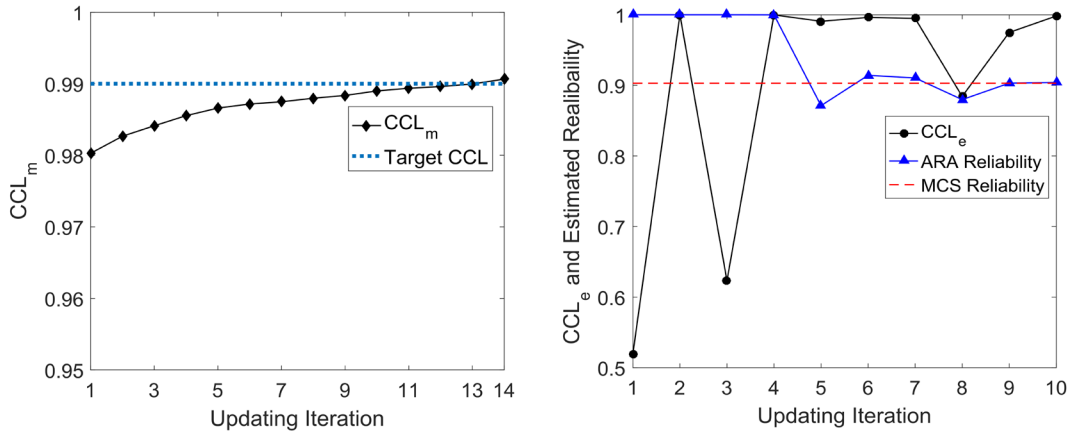

Figure 6.9: CCL_e and Estimated reliability history during ARA in a) phase I and b) phase II

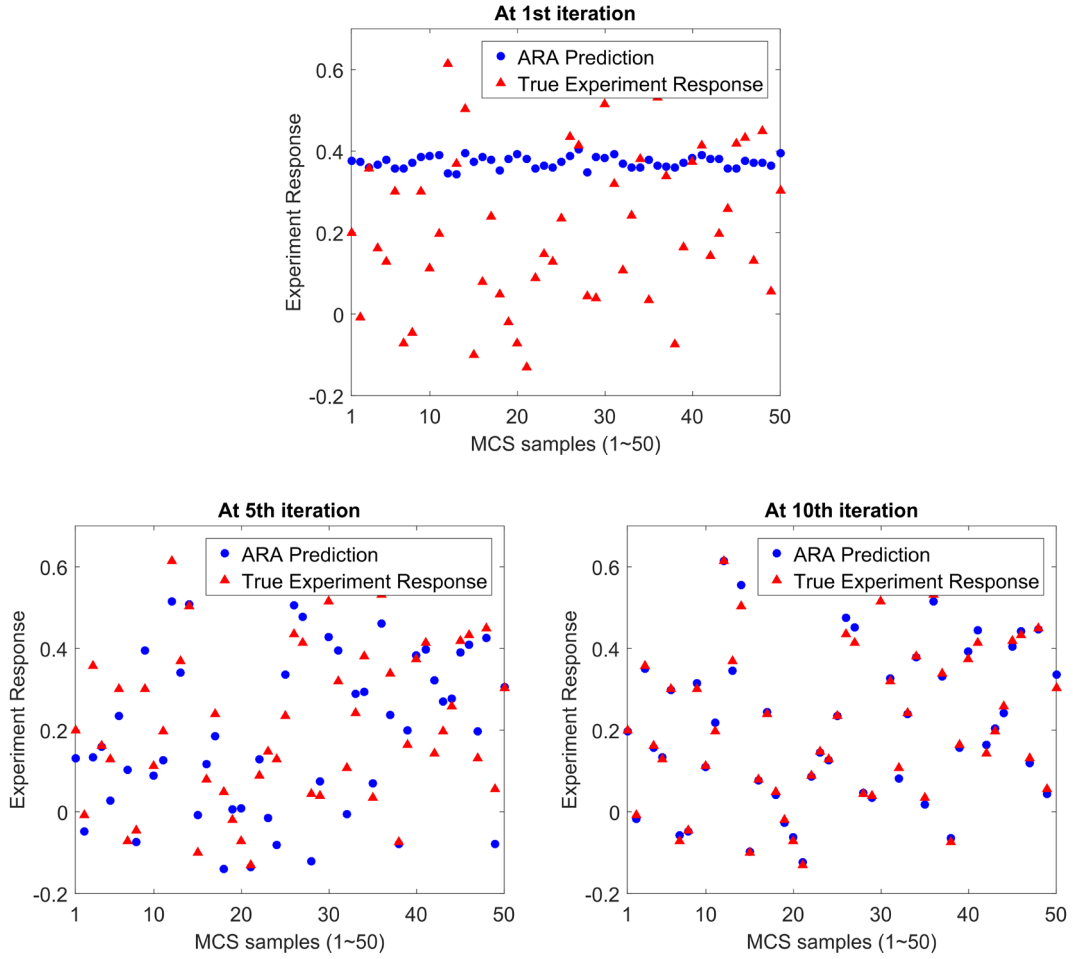

Figure 6.10: Comparison between true experiments and ARA predictions at 1) first, 2) 5^{th}, and 3) 10^{th} iterations

To demonstrate the effectiveness of the proposed approach, the first 50 MCS samples are evaluated by the actual experimental limit state function G^e, and then treated as validation data. Note the model bias correction is iteratively performed along with the updating process in phase II of ARA. At each iteration, there is an enhanced GP model that constructed based on the current simulation and experimental data sets. At the 1^{st}, 5^{th}, and 10^{th} iteration of phase II, the enhanced GP models are used to predict the experiment responses of the first 50 MCS samples. As shown in Fig. 6.10, by iteratively updating the experimental data using ARA, the estimated experiment responses are getting closer to the actual experimental responses that evaluated by G^e. The enhanced GP model constructed at the last iteration is capable of providing accurate predictions, thus, the resultant reliability prediction is ensured to be accurate.

To test the stability of the proposed approach, ARA has been performed 30 times by using different layout of the initial simulation data set. The average of the total number of simulations and experiments that identified at each run is given as 78 and 15, respectively. For comparison purpose, conventional model bias correction approach is employed for reliability analysis of the same problem, while the Latin hypercube sampling method is used for generating the random samples of both simulations and experiments. By fixing the number of simulations at 78, four different scenarios have been introduced by varying the number of experiments as 15, 20, 25, and 30. For each scenario, the model bias correction and reliability analysis are repeated 30 times (the location of simulations and

experiments are totally different). Figure 6.11 shows the box plots of the estimated probability of failure from 30 repetitive runs using the proposed ARA, conventional method, and MCS method. As indicated by the box length, the accuracy of reliability analysis using conventional approach can be improved by increasing the number of experiments. However, the box length and length of whiskers for the proposed approach is much shorter than conventional methods, which can demonstrate the robustness of the ARA approach. Therefore, the results prove that the proposed ARA approach can reduce the costs while ensuring an accurate reliability assessment.

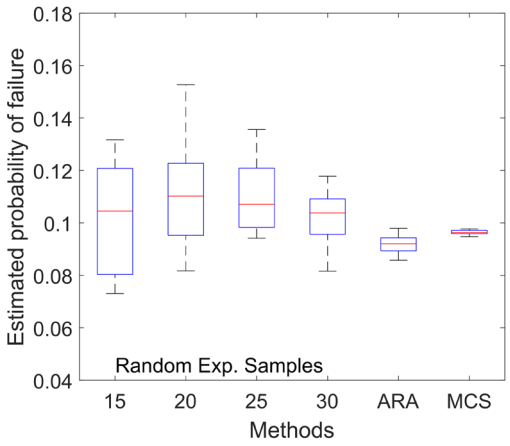

Figure 6.11: Comparison of estimated P_f for 30 repetitive runs using different methods

To investigate the performance of ARA for problems with smaller probability of failure, the input variables of vehicle disc brake system have been modified as shown in Table 6.5, where smaller standard deviations are applied for h_1, h_2, and h_3. Both the simulation model (G_m) and experimental limit state function (G_e) remain the same, and the probability of failure evaluated based on the actual G_e are calculated as 0.0184. By employing the ARA approach, 60 LHS samples are generated for the initial simulation data set. During the ARA process, 10 simulation and 16 experimental samples have been iteratively selected and

evaluated in Phase I and II, respectively. Figure 6.12 shows the iterative CCL_m, CCL_e, and estimated reliability history during ARA, and Table 6.6 details the updating history in Phase II of ARA. Similarly, in Figure 6.13, the effectiveness of the proposed approach has been demonstrated by using the fist 50 MCS samples as validation data. The results show that the proposed ARA approach can be successfully applied for reliability analysis with small probability of failure.

Table 6.5: Properties of input variables for high reliability target

Variable	Distribution Type	Mean	Standard Deviation
h_1	Normal	14.5 mm	0.3 mm
h_2	Normal	15 mm	0.5 mm
h_3	Normal	12 mm	0.4 mm
μ	Normal	0.35	0.01
p	Normal	0.5 MPa	0.02 MPa

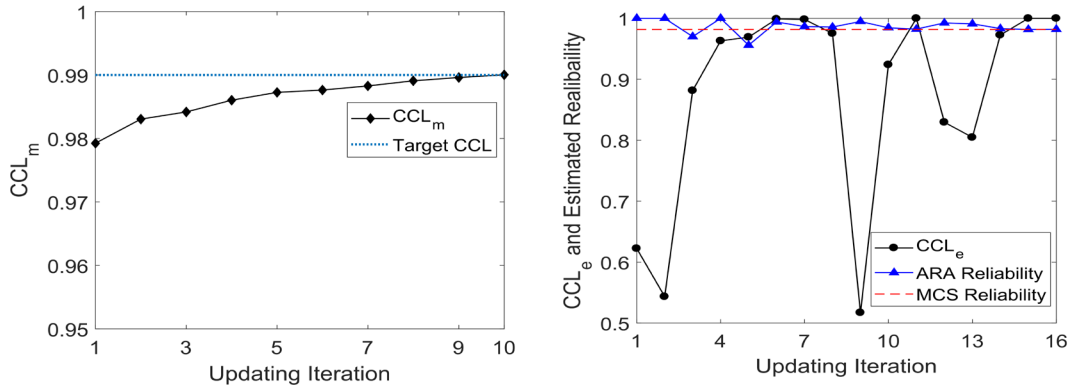

Figure 6.12: CCL_m, CCL_e, and Estimated reliability history during ARA in a) phase I and b) phase II

Table 6.6: ARA history in phase II

Ite.	Experiment Input	Exp. Response	Estimated P_f
1	[14.5438, 15.2228, 11.4309, 0.3619, 0.5126]	0.1708	0.0000
2	[14.5268, 14.5984, 11.9205, 0.3498, 0.5024]	0.2578	0.0000
3	[14.3940, 15.1249, 12.0357, 0.3509, 0.4839]	0.1398	0.0301
4	[14.5549, 15.1524, 12.5316, 0.3505, 0.4996]	0.2688	0.0000
5	[14.3886, 15.0761, 11.7609, 0.3617, 0.4729]	0.0573	0.0441
6	[14.0435, 15.1363, 11.8999, 0.3526, 0.4894]	0.1044	0.0060
7	[14.2318, 15.6373, 11.4171, 0.3539, 0.4727]	-0.0422	0.0135
8	[14.7424, 15.8375, 11.7295, 0.3563, 0.4686]	0.0129	0.0143
9	[14.3445, 15.2938, 11.6727, 0.3441, 0.4610]	-0.0006	0.0051
10	[14.5140, 15.1942, 11.8991, 0.3446, 0.5061]	0.2219	0.0155
11	[14.1827, 14.8199, 12.0749, 0.3338, 0.4887]	0.1859	0.0177
12	[14.1248, 15.5177, 12.0744, 0.3571, 0.4643]	0.0029	0.0076
13	[14.5539, 15.1321, 12.0189, 0.3573, 0.5066]	0.2327	0.0090
14	[14.8613, 15.1764, 11.8231, 0.3489, 0.4865]	0.1716	0.0169
15	[14.3654, 13.8820, 12.0541, 0.3447, 0.4933]	0.2886	0.0183
16	[14.1035, 14.0750, 10.9629, 0.3506, 0.4641]	0.0029	0.0181

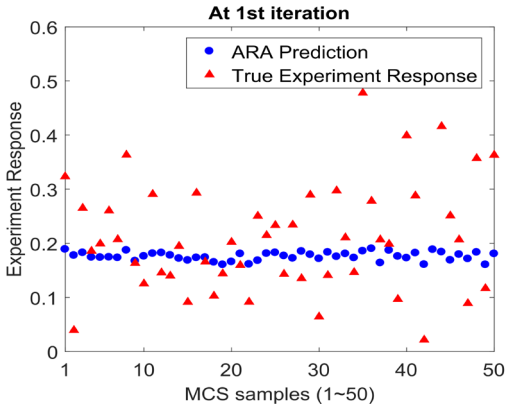

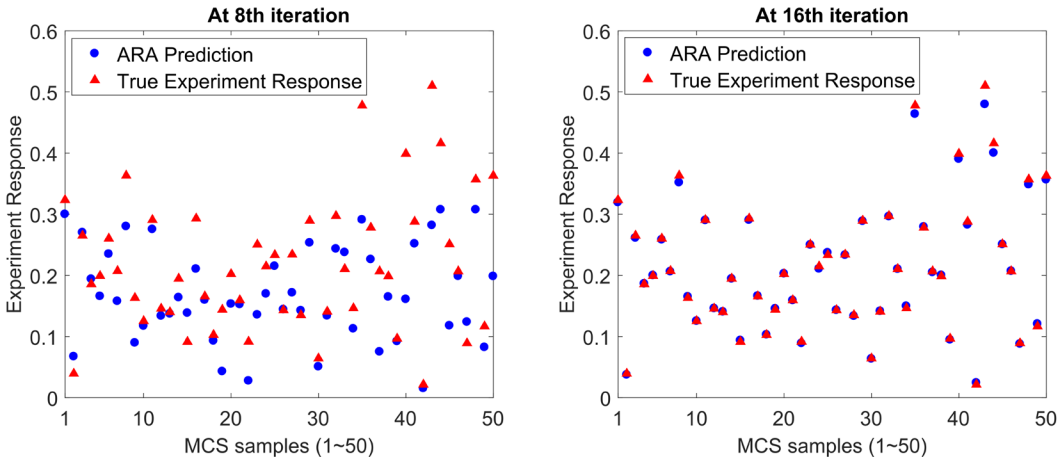

Figure 6.13: Comparison between true experiments and ARA predictions at 1) first, 2) 8th, and 3) 16th iterations

6.3.3 Case Study III: Vehicle Side Impact

This case study considers a vehicle side impact problem, where a total number of six random variables are involved as introduced in Table 6.7. For ensuring the safety of passengers, vehicle systems must meet regulated side impact requirements, and the dummy's response and the velocity of door are the quantity of interest according to the European Enhanced Vehicle-Safety Committee (EEVC) side impact procedure. In this study, the limit state function of the lower viscous criteria is determined explicitly as

$$
\begin{aligned}
&G^m(\mathbf{x}) = 0.32 - (0.74 - 0.61x_2 - 0.163x_3x_5 + 0.001232x_1x_3 - 0.166x_4x_6 + 0.227x_2^2)\\
&G^e(\mathbf{x}) = G^m(\mathbf{x}) + \delta(\mathbf{x});\\
&\delta(\mathbf{x}) = 0.003(x_2x_3x_4 + 0.12x_1 + \frac{x_5}{x_6})
\end{aligned}
\tag{6.31}
$$

It should be mentioned that the bias function is only proposed for demonstrating the effectiveness of the ARA approach, which may not be able to reflect the differences between simulation models and true experiments of the lower viscous criteria. Following

the procedure introduced in subsection 6.2.4, 10^6 MCS samples are first generated according to the input randomness, and 80 LHS samples are generated and evaluated as the initial simulation data set. By using the ARA approach, 18 simulations and 13 experiments have been evaluated for resources allocation of both simulations and experiments. The CCL_m and CCL_e history are provided in Fig. 6.14, which shows that the accuracy of GP models $\hat{G}^m$ and $\hat{g}^e$ can be increased by sequentially adding more training samples. Detailed iterative information in phase II is summarized in Table 6.8, which clearly shows the convergence of the estimated reliability. The reliability analysis result obtained by employing the direct MCS on the actual limit state function G^e is given as 0.0486, which indicates that an accurate reliability assessment can be achieved by using the ARA approach.

Table 6.7: Properties of input variables for car side impact

Variable	Distribution	Mean	Standard Deviation
x_1(Barrier height)	Normal	0	10
x_2(B-pillar reinforce)	Normal	0.75	0.03
x_3(Floor side inner)	Normal	1.2	0.03
x_4(Roof rail)	Normal	1	0.03
x_5(Mat. B-pillar inner)	Normal	0.3	0.006
x_6(Mat. floor side inner)	Normal	0.3	0.006

Table 6.8: ARA history for updating experiments

Ite.	Experiment Input	Exp. Response	Estimated P_f
1	[6.8472, 0.7273, 1.1768, 1.0010, 0.3005, 0.2944]	0.0083	0.0655
2	[1.4086, 0.7502, 1.2159, 0.9854, 0.3006, 0.3012]	0.0228	0.0732
3	[2.9775, 0.7638, 1.1701, 0.9970, 0.3005, 0.3028]	0.0234	0.0652
4	[12.0846, 0.7366, 1.2051, 1.0076, 0.293, 0.3011]	0.0062	0.0658
5	[3.9040, 0.7784, 1.2052, 0.9973, 0.2973, 0.2972]	0.0263	0.0644
6	[9.0206, 0.7306, 1.1870, 0.9615, 0.2944, 0.2988]	0.0047	0.0603
7	[-7.9398, 0.7333, 1.2026, 1.0079, 0.2989, 0.3012]	0.0288	0.0554
8	[14.7941, 0.7325, 1.1869, 1.0392, 0.3031,0.3002]	0.0049	0.0513
9	[15.2205, 0.7233, 1.2108, 0.9913, 0.3042,0.3011]	0.0004	0.0587
10	[-1.8346, 0.7548, 1.2335, 1.0107, 0.2997, 0.2988]	0.0295	0.0553
11	[-7.5288, 0.7558, 1.1848, 0.9881, 0.3006,0.2981]	0.0323	0.0495
12	[8.6931, 0.7246, 1.2087, 0.9390, 0.2993, 0.3027]	0.0046	0.0495
13	[3.9127, 0.6971, 1.1937, 0.9947, 0.3008, 0.3008]	0.0043	0.0492

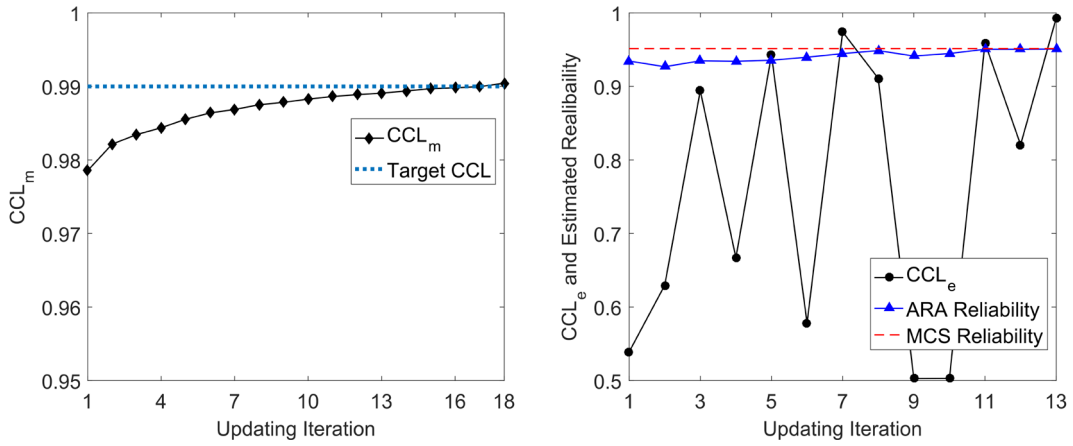

Figure 6.14: Updating history in a) phase I and b) phase II of ARA

To visualize the effectiveness of the proposed approach, the first 50 MCS samples are treated as validation data, and Fig. 6.15 shows the comparisons of true bias and bias

prediction at 1st, 6th, and 13th iterations in phase II of ARA. Similarly, the comparisons of actual experiment responses and predictions from enhanced models constructed at 1st, 6th, and 13th iterations are depicted in Fig. 6.16. The results show that the bias function can be accurately modeled by using the ARA approach. Since the simulation response can be accurately predicted based on the determined simulation data, the accuracy of predicted experiment responses is then guaranteed by using the updated simulation and experimental data set. To compare the proposed approach with conventional random sampling approach, the ARA approach has been performed 30 times while the averaging numbers of updated simulation data and experimental data are given as 102 and 18, respectively. By fixing the number of simulations at 102, conventional methods using random sampling of simulations and experiments are used for model bias correction and reliability analysis. The comparison results are shown in Fig. 6.17, where the box plot obtained by performing 30 times direct MCS method is treated as a reference. As indicated by the shape of the boxes, the proposed approach outperforms the conventional approach as ARA can always achieve accurate reliability estimations with less number of experiments.

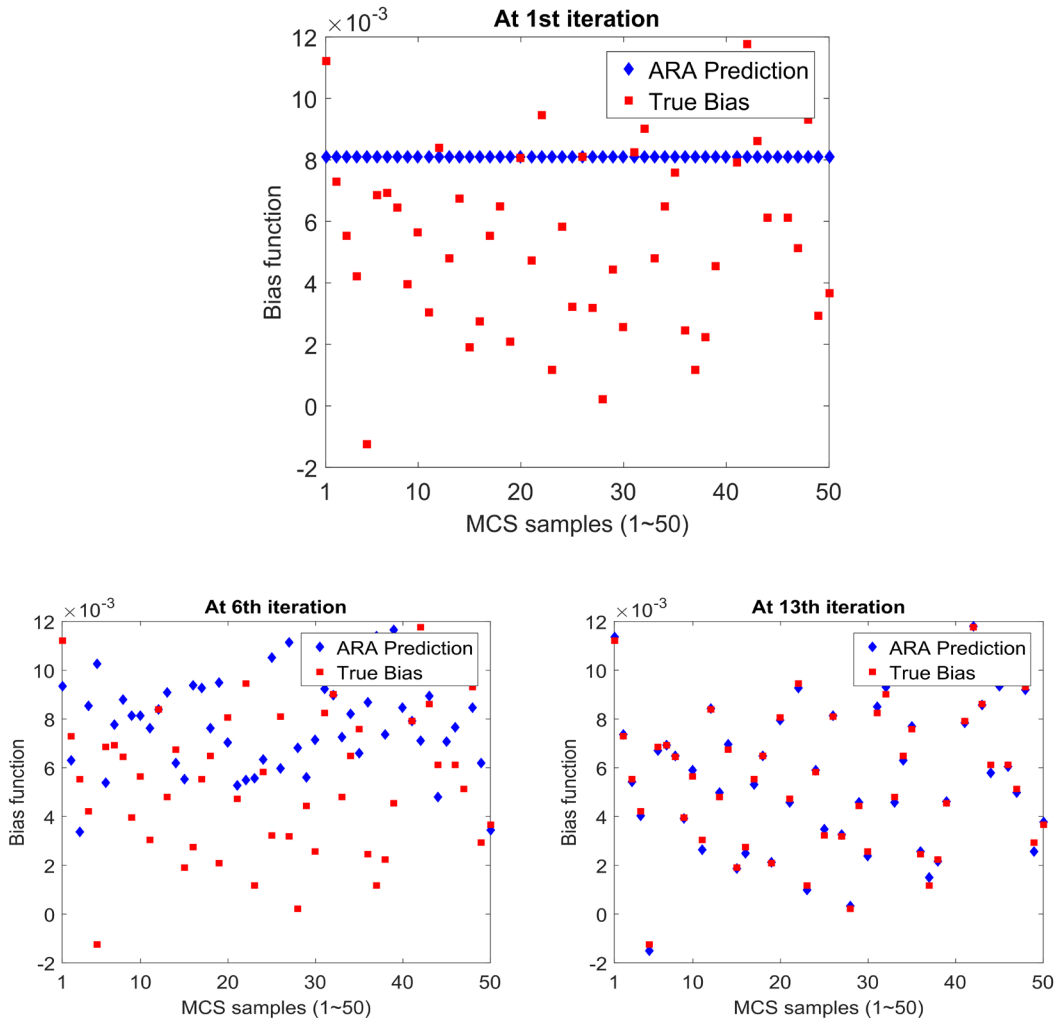

Figure 6.15: Comparison between true bias and ARA predictions at 1) first, 2) 6th, and 3) 13th iterations

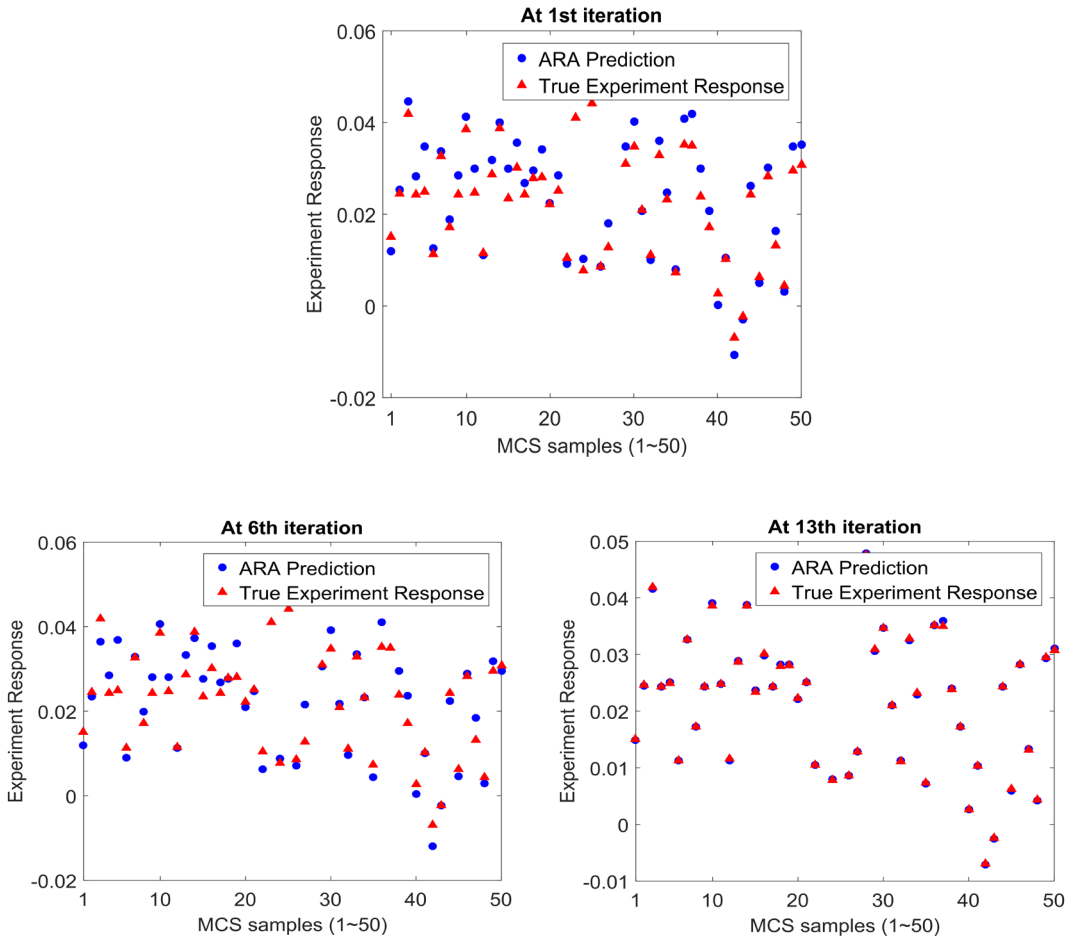

Figure 6.16: Comparison between true experiments and ARA predictions at 1) first, 2) 6th, and 3) 13th iterations

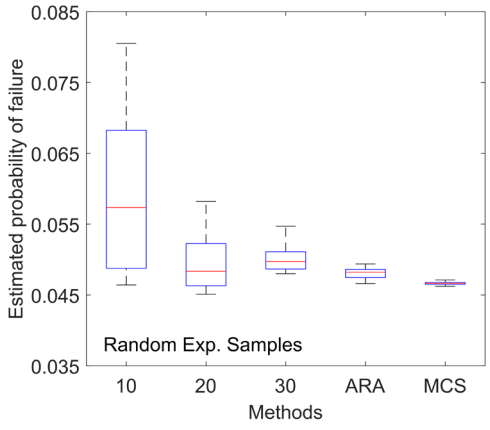

Figure 6.17: Comparison of estimated P_f for 30 repetitive runs using different methods (case study III)

6.3.4 Case Study IV: A Cantilever Beam Example

To demonstrate the proposed ARA approach for reliability analysis with model bias correction, a cantilever beam shown in Fig. 6.18 is considered as a numerical example in the section. The beam is fixed on the wall while a static load F is applied at one of the corners. The length L, width b, thickness h, and external load F has been treated as four random variables, and the statistical information are detailed in Table. 6.9.

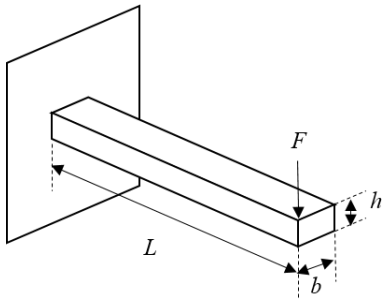

Figure 6.18: Geometry of the cantilever beam

Table 6.9: Properties of random variables for the cantilever beam

Variable	Distribution	Mean	Standard Deviation
Length, L	Normal	40 cm	0.2 cm
Width, b	Normal	7 cm	0.01 cm
Height, h	Normal	4 cm	0.01 cm
Load, F	Normal	1000 N	4 N

The Young's modulus of the beam is treated as a constant E = 70 GPa, and a high-fidelity 3D model is developed in ANSYS APDL for static analysis, where the element

type is selected as *solid185*, and a total number of 1080 elements have been generated for evaluation. The response of this example is the maximum deformation of the beam, and the results obtained by the 3D model is treated as the experimental responses. Thus the limit state function G^e is formulated as

$$G^e(\mathbf{x}) = 0.1 - D_{FEA}(\mathbf{x}) \tag{6.32}$$

In this study, the failure is defined as the maximum deformation is greater than a threshold 0.1 mm. By assuming the load is applied on the midpoint of the right edge, the problem can be simplified, and the maximum deformation can be calculated by using Euler–Bernoulli beam theory, expressed as

$$D = \frac{4PL^3}{Ebh^3} \tag{6.33}$$

The responses computed by Eq. (6.33) is treated as the output of simulation model, and the simulation limit state function is expressed as

$$G^m(\mathbf{x}) = 0.1 - D \tag{6.34}$$

By setting the target *CCL* at 0.99, the ARA approach is performed to estimate the reliability at the given input. Starting from 20 initial simulations obtained by Latin hypercube sampling, 11 simulation and 5 experimental data have been collected in phase I and II, respectively. The iterative updating process in phases I and II are depicted in Fig. 6.19, while Table 6.10 details the updated information in phase II, including the experiment inputs, actual experiment responses, and estimated P_f.

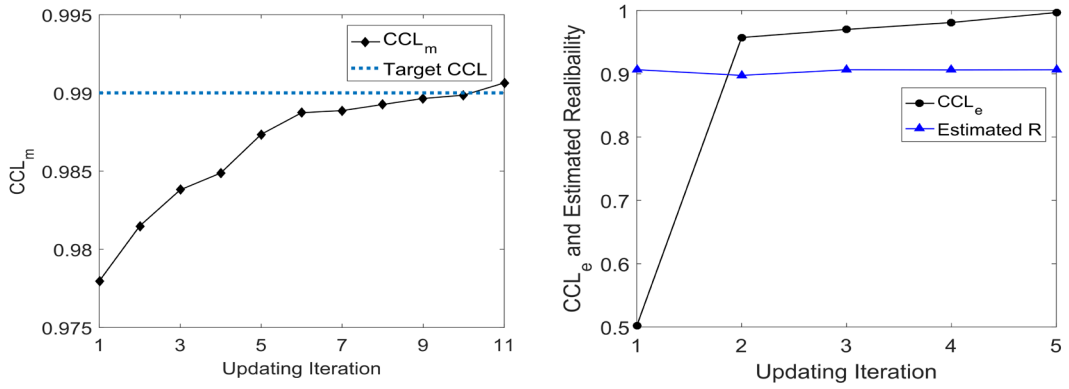

Figure 6.19: Updating history in ARA phase I and phase II

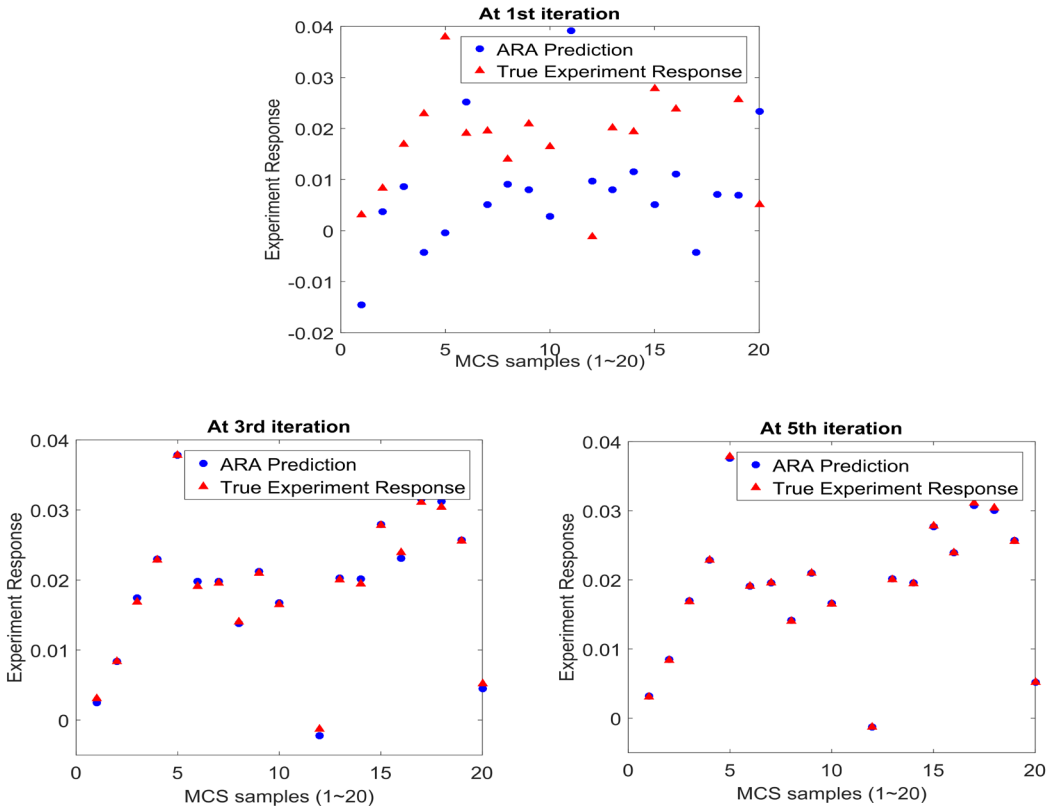

Figure 6.20: ARA predicted responses vs. true experiment responses for the validation points

To demonstrate the effectiveness of the proposed approach, the actual experiment responses of the first 20 MCS samples are evaluated by the 3D model for validation. Figure

6.20 shows the comparison between predicted responses and actual responses at 1st, 3rd, and 5th iterations, which clearly indicates that the predicted responses converge to the true one by iteratively updating the experiments in phase II. Considering the high cost of running the finite element analysis, it is computational prohibitive to directly employ MCS on the 3D model for validating the results of reliability analysis using ARA approach. However, the accuracy of the reliability assessment can be guaranteed since the experiment responses can be accurately predicted after model bias correction using the ARA approach. The ANSYS APDL is performed at the given input to calculate the maximum deformation (m), and the contour plot is shown in Fig. 6.21.

Table 6.10: ARA history for updating experiments

Ite.	Experiment Input	Exp. Response (mm)	Estimated P_f
1	[4.2881, 0.7082, 0.3987, 995.5499]	0.0015	0.0936
2	[3.9190, 0.6980, 0.4005, 1000.0198]	0.0232	0.1026
3	[4.2039, 0.6941, 0.3938, 1002.0745]	0.0010	0.0937
4	[4.1393, 0.7006, 0.3849, 998.2543]	0.0002	0.0940
5	[4.2285, 0.7090, 0.3919, 1001.2111]	0.0001	0.0938

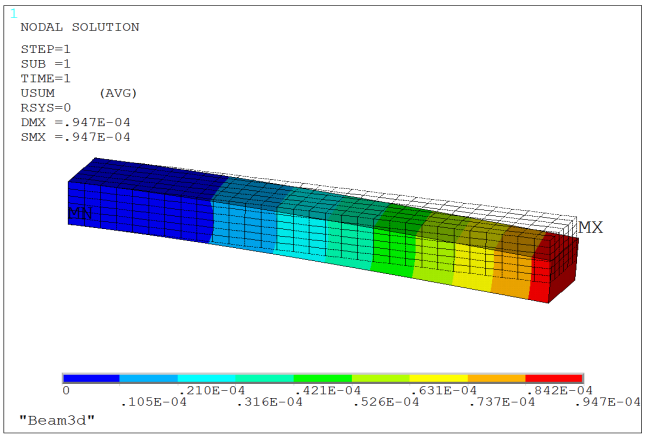

Figure 6.21: ANASYS results of maximum deformation (unit: m)

6.4 Conclusion

In simulation-based reliability analysis, significant errors can be introduced due to the existence of model bias. This work presents an active resource allocation (ARA) approach for reliability analysis with model bias correction, which aims at maintaining an accurate reliability estimation while reducing the costs incurred in running simulations and conducting experiments. In this study, a successive two-phase updating scheme is developed to identify the most important points for allocating both computational and experimental resources. Then the two data sets are fused to construct an enhanced surrogate model for predicting the response of the actual system. In the proposed ARA approach, the adaptive sampling scheme is closely integrated with model bias correction to enable the saving of both computational and experimental costs. The procedure of active resource allocation will be performed until the stop rule is satisfied. Finally, the resultant enhanced surrogate model will be integrated with Monte Carlo simulation (MCS) to calculate the probability of failure. The results of comparison studies have demonstrated that the ARA

approach is capable of providing accurate reliability assessment while maintain a high level of cost efficiency.

7 RELIABILITY-BASED MULTI-FIDELITY OPTIMIZATION USING ADAPTIVE HYBRID LEARNING[101]

7.1 Introduction

Most of the existing reliability-based design optimization (RBDO) are not capable of analyzing data from multi-fidelity sources to improve the confidence of optimal solution while maintaining computational efficiency. In this work, we propose a novel reliability-based multi-fidelity optimization (RBMO) framework that adaptively integrates both low- and high-fidelity data for achieving reliable optimal designs. The Gaussian process (GP) modeling technique is first utilized to build a hybrid surrogate model by fusing data sources with different fidelity levels. To reduce the number of low- and high-fidelity data, an adaptive hybrid learning (AHL) algorithm is then developed to efficiently update the hybrid model. The updated hybrid surrogate model is used for reliability and sensitivity analysis in solving a RBDO problem, which provides a pseudo optimal solution in the RBMO framework. An optimal solution that meets the reliability targets can be achieved by sequentially performing the adaptive hybrid learning at the iterative pseudo optimal designs and solving RBDO problems. The effectiveness of the proposed framework is demonstrated through three case studies.

7.2 Reliability-Based Multi-Fidelity Optimization

As a substitution of real physical process, low-fidelity simulation model is capable of capturing some fundamental features of the underlying physics. Most existing reliability analysis and RBDO methods are performed using only simulation models, which are assumed to be perfectly accurate for representing the real physical process. Though

surrogate modeling techniques have been extensively utilized for reducing the computational costs in RBDO process, the achieved optimal design may not be trustworthy due to the ignorance of the differences between low- and high-fidelity model outputs. As a result, conventional RBDO methods may not be applicable for practical engineering design problems since they lack the capability of handling design problems with multiple fidelity data sources. In this work, a reliability-based multi-fidelity optimization (RBMO) framework is proposed to efficiently integrate both low- and high-fidelity data in probabilistic design optimization, which can be formulated as

$$
\begin{aligned}
&\textit{Minimize}: \quad \textit{Cost}(\mathbf{d}) \\
&\textit{subject to}: \quad P_f^i = \Pr\left[G_i(\mathbf{x}) \le 0) \right] \le \Phi(-\beta_t^i) = 1 - R_t^i, \quad i = 1, ..., nc; \\
&\qquad\qquad \mathbf{x} = [\mathbf{x}_{non}, \mathbf{d}]; \\
&\qquad\qquad \mathbf{d}^{\mathrm{L}} \le \mathbf{d} \le \mathbf{d}^{\mathrm{U}}, \quad \mathbf{x} \in R^{nr} \text{ and } \mathbf{d} \in R^{nd} \qquad (7.1) \\
&\textit{where} \\
&\qquad\qquad G(\mathbf{x}) = y^h(\mathbf{x}) - \textit{threshold}; \\
&\qquad\qquad y^h(\mathbf{x}) = y^l(\mathbf{x}) + \delta(\mathbf{x})
\end{aligned}
$$

where $\mathrm{x} = [\mathrm{x}_{non}, \mathrm{d}]$ represents the overall random variables, x_{non} and d represent the vector of non-design random variables and design variables, respectively; *Cost*(d) represents the objective function that needs to be minimized; $G_i(\mathrm{x})$ is the i^{th} limit state function and $\Pr[G_i(\mathrm{x}) \le 0]$ denotes the corresponding probability of failure, where the failure event occurs when the limit state function response is smaller than zero; d^{L} and d^{U} represent the lower and upper boundaries of the design variables; $\Phi(\cdot)$ is standard normal cumulative distribution function; β_t^i and R_t^i is the target reliability index and the target reliability of the i^{th} probabilistic constraint, respectively; and *nc*, *nr*, and *nd* are the number of probabilistic constraints, random variables, and design variables, respectively. In Eq. (1), the term y^l and

y^h represents low- and high-fidelity models, respectively.

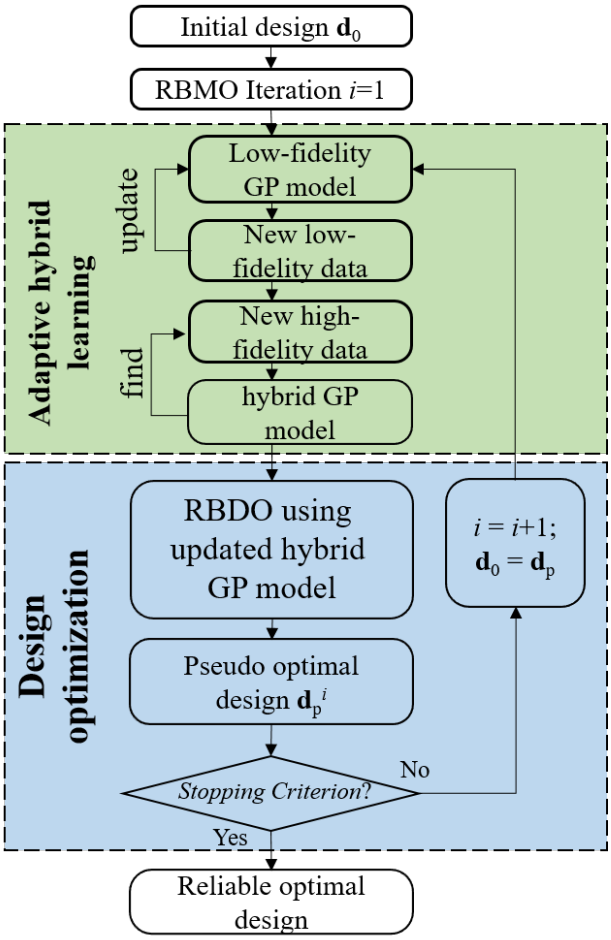

Figure 7.1: Sketch of the RBMO using adaptive hybrid learning.

For a given random variables x, $y^h(\mathrm{x})$ denotes the observations from a high-fidelity model, $y^l(\mathrm{x})$ represents the response evaluated by using the low-fidelity model, and $\delta(\mathrm{x})$ represents the bias function that is referred to as the model discrepancy between the low- and high- fidelity model. In general, the high-fidelity models require more expensive costs but can provide more accurate results than the low-fidelity models. However, the computational costs of running low-fidelity models cannot be ignored when a significant number of low-fidelity data is required for dealing with complex structural designs.

Therefore, how to efficiently learn from the multi-fidelity models and ensure a reliable optimal design are the main targets of the proposed approach. The flowchart of the RBMO framework is shown in Fig. 7.1. Starting from an initial design point, Latin hypercube sampling (LHS) method is first utilized for obtaining the initial low-fidelity data set. To smartly determine the layout of the low- and high-fidelity data, the Gaussian process-based multi-fidelity data fusion technique is employed to build hybrid GP models by fusing the low- and high-fidelity data, where the adaptive hybrid learning algorithm is performed for sequentially identifying new samples. The resultant updated hybrid GP model is then utilized for reliability and sensitivity analysis in solving a RBDO problem, which provides a "pseudo optimal design". The term "pseudo" is used to emphasize that this solution may not be the final optimal solution. The pseudo optimal design will be served as a new initial design for the next iteration in RBMO. Instead of updating the hybrid GP model over the whole design domain, the AHL algorithm only focuses on the critical region of the iterative pseudo optimal designs for efficiently reducing the costs of collecting both low- and high-fidelity data. Thus, a new pseudo optimal design will be achieved at each iteration of RBMO. The iterative process stops until the new pseudo optimal solution is validated as reliable. Though multiple RBDOs are performed during the RBMO framework, the computational costs are neglectable as the reliability and sensitivity analysis are purely conducted based on the updated hybrid GP models.

7.3 Gaussian Process-Based Multi-Fidelity Data Fusion

Surrogate models are attractive tools in reliability analysis since the computational costs are much less than running low- and high-fidelity models. Compared to other

surrogate models, GP models can provide not only the prediction value but also an estimation of the uncertainty due to the lack of training data, which is useful for finding additional training samples. In this work, Gaussian process model is employed for surrogate modeling, where the limit state function $G(\mathrm{x})$ is considered as a realization of a Gaussian process, expressed as

$$G(\mathbf{x}) \sim GP\left(\mathbf{h}(\mathbf{x})\boldsymbol{\beta}, \sigma^2 R(\mathbf{x}, \mathbf{x}')\right) \tag{7.2}$$

where $\mathrm{h}(\mathrm{x})\beta$ represents the mean function and $R(\mathrm{x}, \mathrm{x}')$ is the correlation function, and σ is a hyperparameter needs to be determined. The term $\mathrm{h}(\mathrm{x})$ is a vector of polynomial functions and β represents the vector of corresponding coefficients. The polynomial term $\mathrm{h}(\mathrm{x})$ is assumed to be a constant in this work as it is sufficient for engineering applications. The covariance function $V(\mathrm{x}, \mathrm{x}')$ can be expressed as

$$V(\mathbf{x}, \mathbf{x}') = \sigma^2 R(\mathbf{x}, \mathbf{x}') = \sigma^2 \exp\left[-\sum_{p=1}^{k} \omega_p \left| \mathbf{x}_p - \mathbf{x}_p' \right|^2 \right] \tag{7.3}$$

where k is the dimension of the input variable x; $\omega = [\omega_1, \omega_2, \ldots, \omega_k]$ is the vector of roughness parameters that captures the nonlinearity of the process. As shown in Eqs. (7.2) and (7.3), the unknown hyperparameters β, ω, and σ^2 fully characterize the GP model. Given a training data set $\mathrm{D} = [\mathrm{X}, \mathrm{Y}]$, where X denotes the vector of N_t training samples and Y represents the vector of training responses, the values of these hyperparameters can be estimated by using Maximum Likelihood Estimation (MLE) with a log likelihood function given as

$$likelihood = -\frac{1}{2}\left[N_t \ln(2\pi) + N_t \ln \sigma^2 + \ln|\mathbf{V}| + \frac{1}{2\sigma^2}(\mathbf{Y} - \mathbf{H}\boldsymbol{\beta})\mathbf{V}^{-1}(\mathbf{Y} - \mathbf{H}\boldsymbol{\beta}) \right] \tag{7.4}$$

where Hβ represents the mean vector that H = [$h^T(x_1)$, …, $h^T(x_{Na})$], and V is the covariance matrix. Note H is a unit vector as the constant mean 1 is adopted for replacing the h(.) functions. With the training data set, the hyperparameters can be determined by maximizing Eq. (7.4), then the GP model can be used to predict response at any different point x'. The prediction follows a normal distribution with mean μ(x') and variance v(x') as,

$$\mu(\mathbf{x}') = \mathbf{h}(\mathbf{x}')\boldsymbol{\beta} + \mathbf{r}^T\mathbf{V}^{-1}(\mathbf{Y} - \mathbf{H}\boldsymbol{\beta}) \tag{7.5}$$

and

$$v(\mathbf{x}') = \sigma^2\left\{1 - \mathbf{r}^T\mathbf{V}^{-1}\mathbf{r} + \left[\mathbf{h}(\mathbf{x}') - \mathbf{H}^T\mathbf{V}^{-1}\mathbf{r}\right]^T\left(\mathbf{H}^T\mathbf{V}^{-1}\mathbf{H}\right)^{-1}\left[\mathbf{h}(\mathbf{x}') - \mathbf{H}^T\mathbf{V}^{-1}\mathbf{r}\right]\right\} \tag{7.6}$$

where r represents the correlation vector between the input point x' and the training samples. The prediction variance is also known as the mean squared error, which is treated as an estimation of the prediction accuracy at the point x'.

To perform the hybrid learning using multi-fidelity data, the high-fidelity response is treated as the sum of low-fidelity result and bias function as shown in Eq. (7.1). Characterization of bias function is of critical importance in validating the low-fidelity model, and the goal is to construct a predictive model that can predict the high-fidelity response at any input site. Therefore, the GP modeling technique [102] is further utilized for bias correction using both low- and high-fidelity data. The low-fidelity model y^l(x) and bias function δ(x) are first replaced by GP models, expressed as

$$\begin{aligned} y^l(\mathbf{x}) &\sim GP\left(\mathbf{h}^l(\mathbf{x})\boldsymbol{\beta}^l, \sigma_l^2 R^l(\mathbf{x}, \mathbf{x}')\right) \\ R^l(\mathbf{x}, \mathbf{x}') &= \exp\left[-\sum_{p=1}^{k}\omega_p^l\left|\mathbf{x}_p - \mathbf{x}_p'\right|^2\right] \end{aligned} \tag{7.7}$$

and

$$\delta(\mathbf{x}) \sim GP\left(\mathbf{h}^{\delta}(\mathbf{x})\boldsymbol{\beta}^{\delta}, \sigma_{\delta}^{2} R^{\delta}(\mathbf{x}, \mathbf{x}')\right)$$
$$R^{\delta}(\mathbf{x}, \mathbf{x}') = \exp\left[-\sum_{p=1}^{k} \omega_{p}^{\delta} \left|\mathbf{x}_{p} - \mathbf{x}_{p}'\right|^{2}\right] \tag{7.8}$$

where $\boldsymbol{\phi}^{l} = [\beta^{l}, \omega^{l}, \sigma_{l}^{2}]$ is the vector of the hyperparameters for the GP model $\hat{g}^{l}$, and $\boldsymbol{\phi}^{\delta} = [\beta^{\delta}, \omega^{\delta}, \sigma_{\delta}^{2}]$ is the vector of the hyperparameters for the bias GP model $\hat{g}^{\delta}$. By assuming the low-fidelity model and the bias function are statistically independent, a hybrid GP model $\hat{g}^{hy}$ for high-fidelity response $y^{h}(\mathrm{x})$ can be built through the combination of $\hat{g}^{l}$ and $\hat{g}^{\delta}$, written as

$$y^{hy}(\mathbf{x}) \sim GP\left(\mathbf{h}^{l}(\mathbf{x})\boldsymbol{\beta}^{l} + \mathbf{h}^{\delta}(\mathbf{x})\boldsymbol{\beta}^{\delta}, \sigma_{hy}^{2} R^{hy}\left(\mathbf{x}, \mathbf{x}'\right)\right)$$
$$\sigma_{hy}^{2} R^{hy}\left(\mathbf{x}, \mathbf{x}'\right) = \sigma_{l}^{2} R^{l}\left(\mathbf{x}, \mathbf{x}'\right) + \sigma_{\delta}^{2} R^{\delta}\left(\mathbf{x}, \mathbf{x}'\right) \tag{7.9}$$

As shown in Eq. (7.9), the GP model $\hat{g}^{hy}$ is constructed based on the hyperparameters $\boldsymbol{\phi}^{l}$ and $\boldsymbol{\phi}^{\delta}$, which can be estimated based on both low- and high-fidelity data sets. Considering that N_l low-fidelity data and N_h high-fidelity data have been respectively collected, denoted as

$$\mathbf{D}^{l} = [\mathbf{X}^{l}, \mathbf{Y}^{l}]$$
$$\mathbf{X}^{l} = [\mathbf{x}_{1}^{l}, ..., \mathbf{x}_{Nl}^{l}]; \mathbf{Y}^{l} = [y^{l}(\mathbf{x}_{1}^{l}), ..., y^{l}(\mathbf{x}_{Nl}^{l})] \tag{7.10}$$

and

$$\mathbf{D}^{h} = [\mathbf{X}^{h}, \mathbf{Y}^{h}]$$
$$\mathbf{X}^{h} = [\mathbf{x}_{1}^{h}, ..., \mathbf{x}_{Nh}^{h}]; \mathbf{Y}^{h} = [y^{h}(\mathbf{x}_{1}^{h}), ..., y^{h}(\mathbf{x}_{Nh}^{h})] \tag{7.11}$$

The responses data $\mathrm{Y}^{lh} = [\mathrm{Y}^{l}, \mathrm{Y}^{h}]$ follows a multivariate normal distribution according to Eqs. (7.7), (7.8), and (7.9), given as

$$\mathbf{Y}^{lh} = \begin{bmatrix} y^l(\mathbf{x}_1^l) \\ \vdots \\ y^l(\mathbf{x}_{Nl}^l) \\ y^h(\mathbf{x}_1^h) \\ \vdots \\ y^h(\mathbf{x}_{Nh}^h) \end{bmatrix} \sim N\left(\mathbf{H}_{l\delta}\boldsymbol{\beta}_{l\delta}, \mathbf{V}_{lh}\right) \tag{7.12}$$

where the mean function is given as

$$\mathbf{H}_{l\delta} = \begin{bmatrix} \mathbf{H}^l(\mathbf{X}^l) & 0 \\ \mathbf{H}^l(\mathbf{X}^h) & \mathbf{H}^\delta(\mathbf{X}^h) \end{bmatrix}, \boldsymbol{\beta}_{l\delta} = \begin{bmatrix} \boldsymbol{\beta}^l \\ \boldsymbol{\beta}^\delta \end{bmatrix}, \tag{7.13}$$

where $H^l(.)$ and $H^\delta(.)$ are unit vectors as a constant polynomial function is adopted in this work. The covariance matrix V_{lh} can be expressed as

$$\mathbf{V}_{lh} = \begin{bmatrix} \mathbf{V}^l\left(\mathbf{X}^l, \mathbf{X}^l\right) & \mathbf{V}^l\left(\mathbf{X}^h, \mathbf{X}^l\right)^T \\ \mathbf{V}^l\left(\mathbf{X}^h, \mathbf{X}^l\right) & \mathbf{V}^l\left(\mathbf{X}^l, \mathbf{X}^l\right) + \mathbf{V}^\delta\left(\mathbf{X}^h, \mathbf{X}^h\right) \end{bmatrix} \tag{7.14}$$

where $V^l(.,.) = \sigma_l^2 R^l(.,.)$ and $V^\delta(.,.) = \sigma_\delta^2 R^\delta(.,.)$ represents the covariance functions of the simulation GP model $\hat{g}^l$ and bias function GP model $\hat{g}^\delta$, respectively. It should be mentioned that the correlation function $R^l(.,.)$ and $R^\delta(.,.)$ are not the same since the roughness parameters are different. A likelihood function of the hyperparamters $\phi^{l\delta} = [\phi^l, \phi^\delta]$ can be formulated as

$$\begin{aligned} &L(\mathbf{Y}^{lh} \left| \phi^{l\delta}\right.) = p(\phi^{l\delta} \left| \mathbf{Y}^{lh}\right.) \propto \\ &\left|\mathbf{V}_{lh}\right|^{-1/2} \left|\mathbf{H}_{l\delta}^T \mathbf{V}_{lh}^{-1} \mathbf{H}_{l\delta}^T\right|^{-1/2} \exp\left[-\frac{1}{2}\left(\mathbf{Y}^{lh} - \mathbf{H}_{l\delta}^T \boldsymbol{\beta}_{l\delta}\right)^T \mathbf{V}_{lh}^{-1}\left(\mathbf{Y}^{lh} - \mathbf{H}_{l\delta}^T \boldsymbol{\beta}_{l\delta}\right)\right] \end{aligned} \tag{7.15}$$

Then the MLE method can be employed for maximizing the log-likelihood function, expressed as

$$\max_{\phi^{l\delta}} \quad \log L(\mathbf{Y}^{lh} \middle| \phi^{l\delta})$$

where

$$\log L(\mathbf{Y}^{lh} \middle| \phi^{l\delta}) = -\frac{1}{2}\log\left|\mathbf{V}_{lh}\right| + \frac{1}{2}\log\left|\mathbf{H}_{l\delta}^{T}\mathbf{V}_{lh}^{-1}\mathbf{H}_{l\delta}^{T}\right| - \frac{1}{2}\left(\mathbf{Y}^{lh} - \mathbf{H}_{l\delta}^{T}\boldsymbol{\beta}_{l\delta}\right)^{T}\mathbf{V}_{lh}^{-1}\left(\mathbf{Y}^{lh} - \mathbf{H}_{l\delta}^{T}\boldsymbol{\beta}_{l\delta}\right) \tag{7.16}$$

The genetic algorithm is employed in this work for estimating the hyperparameters. As a result, the three GP models $\hat{g}^{l}$, $\hat{g}^{\delta}$, and $\hat{g}^{hy}$ can be obtained accordingly. For any given input, these GP models can be used for predicting the low-fidelity response, model discrepancy, and high-fidelity response, respectively.

7.4 Adaptive Hybrid Learning Scheme

In the presented work, the adaptive hybrid learning process is performed at the iterative pseudo optimal designs for reducing the total costs. The first priority of the AHL is to reduce the number of high-fidelity data since the costs of running high-fidelity models is much more expensive than obtaining low-fidelity data. Therefore, the low-fidelity data will be first updated, and the pseudo code of the AHL algorithm is presented in Algorithm 7.1. Starting from the initial design point d_0, a set of N_{li} initial samples X^{li} is first generated by using the Latin hypercube sampling, and the low-fidelity model is used for evaluating the responses of these initial samples, denoted as Y^{li}. Then a surrogate GP model $\hat{G}^{l}$ can be constructed accordingly, where the hyperparameters are purely estimated based on the training data set [X^{li}, Y^{li}]. Note that the GP model $\hat{G}^{l}$ may be inaccurate due to the lack of data. Therefore, a confidence-based adaptive sampling method [99] is employed to iteratively identify new low-fidelity training data for updating the GP model. Based on the

statistical information of the random variables and the initial design variable d_0, N random realizations can be generated by using the Monte Carlo simulation method, which are denoted as $X_m = [x_{m,1}, x_{m,2}, \ldots, x_{m,N}]$. For each MCS sample, an indicator function is introduced to classify this sample into two states, expressed as

$$I_f(\mathbf{x}_{m,i}) = \begin{cases} 1, & \mu_l(\mathbf{x}_{m,i}) < 0 \quad (failure) \\ 0, & otherwise \quad (safe) \end{cases} \tag{7.17}$$

where $\mu_l(x_{m,i})$ is the $\hat{G}^l$ prediction mean for the i^{th} MCS sample. As shown in Eq. (7.17), a failure sample is defined as the prediction mean is less than zero. It should be mentioned that the response predictions from the GP model $\hat{G}^l(x)$ may lack accuracy when the training data is limited. As a result, the sign of the actual low-fidelity response at $x_{m,i}$ can be different from the prediction $\mu_l(x_{m,i})$. Thus, the confidence level $CL_l|d_0$ of the prediction at a MCS point is defined as the probability of making correct classification, which means that the sign of the actual response of the low-fidelity model is identical with the sign of the prediction. The mean $\mu_l(x_{m,i})$ and standard deviation $\sigma_l(x_{m,i})$ of the prediction are used to calculate the CL_l, expressed as

$$CL_l\left(\mathbf{x}_{m,i}\right)\Big|\mathbf{d}_0 = \Phi\left(\frac{\left|\mu_l(\mathbf{x}_{m,i})\right|}{\sigma_l(\mathbf{x}_{m,i})}\right) \tag{7.18}$$

where $\Phi(.)$ is the standard normal cumulative distribution function. A cumulative confidence level $CCL_l|d_0$ quantifies the prediction accuracy of the GP model $\hat{G}^l(x)$ at design point d_0 and can be obtained by averaging the confidence levels of the N MCS samples, expressed as

$$CCL_l\Big|\mathbf{d}_0 = \frac{1}{N}\sum_{i=1}^{N} CL_l(\mathbf{x}_{m,i})\Big|\mathbf{d}_0 \tag{7.19}$$

A higher $CCL_l|d_0$ indicates that the MCS samples are more likely to be correctly classified. Therefore, the critical part of updating the GP model is to add new low-fidelity data to increase the $CCL_l|d_0$. For each MCS sample, a potential improvement PI_l of the $CCL_l|d_0$ is calculated as

$$PI_l(\mathbf{x}_{m,i}) = (1 - CL_l(\mathbf{x}_{m,i})) * f_x(\mathbf{x}_{m,i}) * \sigma^l(\mathbf{x}_{m,i}) \tag{7.20}$$

where $f_x(.)$ is the joint probability density function of input variables x. Since CL_l represents the probability of correct classification, the first term in Eq. (7.20) represents the potential confidence level improvement. The multiplication of the first two terms represents how likely the potential improvement can be achieved. It is known that the prediction variance of the GP model near a point $x_{m,i}$ will be reduced if $x_{m,i}$ is added as a new training sample. Therefore, the last term is added and sample points with larger prediction variance are more likely to have larger PI_l values. By evaluating all the MCS samples using Eq. (7.20), the sample point with the largest PI_l is considered as the most useful sample that can maximally improving the cumulative confidence level $CCL_l|d_0$. After obtaining the low-fidelity response of the selected sample, the new training data is added into the training data set for updating $\hat{G}^l(x)$. The updating process will be repeated until the $CCL_l|d_0$ is greater than a pre-defined target CCL_t. By using Eq. (7.20) as the sampling criterion, the identified most useful samples tends to be sparsely located within the local domain of the given point x.

Once an accurate GP model $\hat{G}^l$ is achieved through adding new low-fidelity data, the next step is to construct a hybrid GP model by fusing both the low- and high-fidelity data. In the proposed approach, the last identified low-fidelity sample will be treated as the input for collecting the first high-fidelity data. With the available low- and high-fidelity data, the

GP-based multi-fidelity data fusion is performed to build a hybrid GP model $\hat{g}^{hy}$ according to Section 7.3. As shown in Algorithm 7.1, the hybrid GP model needs to be updated by iteratively identifying the most useful high-fidelity samples. Similarly, the confidence level CL_{hy} of the hybrid GP model prediction at a MCS point can be calculated as

$$CL_{hy}(\mathbf{x}_{m,i})\left|\mathbf{d}_0 = \Phi\left(\frac{\left|\mu_{hy}(\mathbf{x}_{m,i})\right|}{\sigma_{hy}(\mathbf{x}_{m,i})}\right)\right. \tag{7.21}$$

where $\mu_{hy}(.)$ and $\sigma_{hy}(.)$ represents the mean and standard deviation of the prediction from the hybrid GP model. Then the cumulative confidence level $CCL_{hy}|\mathrm{d}_0$ can be obtained by averaging the CL_{hy} for all the MCS samples, which quantifies the prediction accuracy at the design point d_0. For each MCS sample, the potential improvement PI_{hy} of the $CCL_{hy}|\mathrm{d}_0$ needs to be calculated, which is expressed as

$$PI_{hy}(\mathbf{x}_{m,i}) = (1 - CL_{hy}(\mathbf{x}_{m,i})) * f_x(\mathbf{x}_{m,i}) * \sigma^{\delta}(\mathbf{x}_{m,i}) \tag{7.22}$$

where $\mathrm{x}_{m,i}$ represents the i^{th} MCS sample. It should be mentioned that the accuracy of predicting the bias function is of critical importance in determining the best location of the new high-fidelity data. Therefore, the bias prediction obtained by the GP model $\hat{g}^{\delta}(.)$ is used as the last term in Eq. (7.22). The sample point with larger $\sigma^{\delta}(.)$ indicates that the bias prediction is less accurate, which tends to result in larger PI_{hy} value. After evaluating all the MCS samples, the point with largest PI_{hy} will be selected as the new sample for computing the high-fidelity response. Then a new hybrid GP model can be constructed with the updated high-fidelity data set and available low-fidelity data. The iterative updating process will be repeated until the target cumulative confidence level is achieved.

Algorithm 7.1: Adaptive hybrid learning

Initialization:
Initial design point, d_0
Target confidence level, CCL_t
Size of the Monte Carlo simulations N
Initial low-fidelity data set, $[X^{li}, Y^{li}]$

(AHL first identifies most useful low-fidelity data)
$sp = 0$;
While $sp = 0$ do
  Construct GP model $\hat{G}^l$ based on current low-fidelity data set
  for i= 1 to N do
  Evaluate $CL_l(x_{m,i})$ using Eq. 18
  Evaluate $PI_l(x_{m,i})$ using Eq. 20
  end for
  compute $CCL_l|d_0$ using Eq. 19
  If $CCL_l|d_0 < CCL_t$ then
    $\mathbf{x}_{new} = \arg\max(PI_l)$; $\mathbf{y}_{new} = y^l(\mathbf{x}_{new})$
    Update D^l
  else if
    $sp = 1$
  end if
end while
(Then AHL identifies most useful high-fidelity data)
$sp = 0$;
While $sp = 0$ do
  Construct hybrid GP model $\hat{g}^{hy}$ based on current low- and high-fidelity data set D^l and D^h
  for i= 1 to N do
  Evaluate $CL_{hy}(x_{m,i})$ using Eq. 21
  Evaluate $PI_{hy}(x_{m,i})$ using Eq. 22
  end for
  compute $CCL_{hy}|d_0$ by averaging $CL_{hy}(x_{m,i})$
  If $CCL_{hy}|d_0 < CCL_t$ then
    $\mathbf{x}_{new} = \arg\max(PI_{hy})$; $\mathbf{y}_{new} = y^h(\mathbf{x}_{new})$
    Update D^h
  else if
    $sp = 1$
  end if
end while

7.5 RBMO Using Hybrid GP Model

To ensure a reliable optimal design while reducing the number of both low- and high-fidelity data, the AHL and RBDO are sequentially performed at each iteration of RBMO. As introduced in Section 7.2, a RBDO problem will be solved for obtaining the pseudo optimal design once the updated hybrid GP model is achieved. The typical form of the

RBDO can be formulated as

$$\begin{aligned} &Minimize: \quad Cost(\mathbf{d}) \\ &subject\ to: \quad P_f^i = \Pr\left[\hat{g}_{hy}^i(\mathbf{x}) \le 0)\right] \le 1 - R_t^i, \quad i = 1, ..., nc \\ &\qquad\qquad \mathbf{d}^{\mathbf{L}} \le \mathbf{d} \le \mathbf{d}^{\mathbf{U}}, \quad \mathbf{x} \in R^{nr} \text{ and } \mathbf{d} \in R^{nd} \end{aligned} \tag{7.23}$$

where $\hat{g}_{hy}$ represents the updated hybrid GP model that characterizes the limit state functions $G(\mathrm{x})$. In this study, the prediction mean $\mu_{hy}(.)$ is treated as the estimated response from $\hat{g}_{hy}$. In the RBDO, the design objective is to minimize the cost function while ensuring the probabilistic constraints are satisfied at the pseudo optimal design. Based on the updated hybrid GP model, the MCS approach is used to estimate the probability of failure, which can be expressed as

$$P_f \approx \Pr\left[\hat{g}_{hy}(\mathbf{X}) < 0\right] = \int_{\Omega_f} I_f(\mathbf{x}) f_x(\mathbf{x}) d\mathbf{x} = E[I_f(\mathbf{x})] \tag{7.24}$$

where $f_x(\mathrm{x})$ is the joint probability density function of the random variables, Ω_f denotes the failure region, $E[.]$ is the expectation operator, and $I_f(.)$ is an indicator function to classify failure and safe samples. At the given design point, a number of N MCS samples are generated for random realizations as introduced in Section 7.4, and each MCS sample are evaluated by the indicator function $I_f(.)$, given as

$$I_f(\mathbf{x}_{m,i}) = \begin{cases} 1, & \mu_{hy}(\mathbf{x}_{m,i}) < 0 \quad (failure) \\ 0, & otherwise \quad\quad (safe) \end{cases} \tag{7.25}$$

where $\mu_{hy}(\mathrm{x}_{m,i})$ is the hybrid GP model prediction mean for the i^{th} MCS sample. After evaluating all the N MCS samples, the probability of failure of the given design point can be calculated based on the number of failure samples to the number of total MCS samples, expressed as

$$Pf = \frac{\sum_{i=1}^{N} I_f(\mathbf{x}_{m,i})}{N} = \frac{N_f}{N} \tag{7.26}$$

In RBDO, the sensitivity information of the probability of failure with respect to the design variables is required in searching for pseudo optimal solutions. In this work, the first-order score function method [103] is adopted due to its high efficiency, where the sensitivity can be directly approximated based on the updated hybrid GP model and the generated MCS samples. According to Eq. (7.26), the partial derivative of the probability of failure with respect to the i^{th} design variable d_{i} is thus derived as

$$\frac{\partial P_f}{\partial d_i} = \frac{\partial}{\partial d_i}\int_{\Omega} I_f(\mathbf{X}) f_x(\mathbf{X}) d\mathbf{X} = \mathrm{E}\left[I_f(\mathbf{X}) \frac{\partial \ln f_x(\mathbf{X})}{\partial d_i} \right] \tag{7.27}$$

where the partial derivative of the log function of the joint PDF f_x(X) with respect to the design variable d_i is known as the first-order score function. For independent random variables, the joint probability density function of X is expressed as multiplication of its marginal PDFs, written as

$$f_x(\mathbf{X}) = \prod_{i=1}^{nr} f_{x_i}(x_i) \tag{7.28}$$

where *nr* is the dimension of random variables X. Therefore, the sensitivity information of the probability of failure with respect to design variables can be efficiently approximated without incurring extra computational costs. With the capability of performing reliability and sensitivity analysis, the sequential quadratic programming (SQP) method is selected for solving the RBDO problem in Eq. (7.23).

Since there is no adaptive learning process involved during the RBDO process, the prediction from the hybrid model at the pseudo optimal design may not be accurate. As

introduced in Section 7.2, the RBMO process will be continued once the pseudo optimal solution is achieved. Therefore, a stopping criterion of the RBMO is proposed as

$$\begin{cases} CCL_{hy}\left|\mathbf{d}_p \geq CCL_t \right. \\ P_f\left|\mathbf{d}_p \leq 1-R_t \right. \end{cases} \tag{7.29}$$

where $CCL_{hy}|\mathrm{d_p}$ represents the cumulative confidence level of the hybrid GP model at the pseudo optimal design $\mathrm{d_p}$, $\mathrm{P_f}|\mathrm{d_p}$ represents the estimated probability of failure, and CCL_t is a user-defined target. If the obtained $CCL_{hy}|\mathrm{d_p}$ is higher than the target CCL, it means the latest hybrid GP model also possess a high prediction accuracy at the pseudo optimal design point, thus the achieved $\mathrm{d_p}$ tends to be trustworthy. A reliable RBMO optimal solution can be obtained once the stopping criterions in Eq. (7.29) are satisfied. The overall procedure of performing the RBMO is summarized in Algorithm 7.2.

Algorithm 7.2: RBMO using adaptive hybrid learning

Initialization:
Initial design for optimization, $\mathrm{d_0}$
Target reliability level R_t
Generate N MCS samples that follows standard normal distribution.
Specify the boundaries for design variables d, and use LHS for obtaining the initial low-fidelity data set [X^{li}, Y^{li}].
ite = 0 (RBMO iteration number)
RBMO_stop == 0 (logic variable for RBMO process)
RBDO_stop == 0 (logic variable for RBDO process)

while *RBMO_stop* == 0 do
  if *ite* == 1 do
  initial design $\mathrm{d_0}$
  else if
  $\mathrm{d_0} = \mathrm{d_p}$
  end if
    Map the initial MCS sample based on statistical information of $\mathrm{d_0}$
  Perform AHL as shown in Algorithm 1
  (Employ RBDO to provide pseudo optimum)
    while *RBDO_stop* == 0 do
      for i = 1 to N do
        $\mu_{hy}(\mathrm{x}_{m,i})$ from the hybrid GP prediction $\hat{g}_{hy}(\mathbf{x}_{m,i})$
        classify this sample into failure or safe using Eq. (25)

end for
calculated the estimated reliability based on Eq. (26)
compute the sensitivity according to Eq. (27)
calculate the cost function value and derive the sensitivity.
provide reliability estimation, sensitivities for probabilistic constraints and cost function to the SQP optimizer.
if Achieve new design point d' do
$d_0 = d'$
else if
achieve optimal solution, $d_p=d_0$, *RBDO_stop* = 1
end if
Map the initial MCS sample based on statistical information of d_0
end while
(RBDO complete)
check the stopping criterion in Eq. (29)
If satisfied do
RBMO optimal $d_{opt} = d_p$
else if
RBMO_stop = 0; ite = ite + 1
end if
(RBMO Iteration number)
end while

7.6 Case Studies

In this section, three design problems will be solved to demonstrate the effectiveness of the proposed RBMO framework.

7.6.1 Case Study I: Mathematical Example

In the first case study, a benchmark 2D mathematical design problem [104] is considered for testing the performance of the proposed RBMO framework. The two design variables d = [μ_{X1}, μ_{X2}] are both normally distributed with standard deviation std = [0.3464, 0.3464]. The design optimization problem involves three probabilistic constraints, which can be formulated as

$$
\begin{aligned}
&\text{Minimize}: \; Cost = 10 - \mathbf{d}_1 + \mathbf{d}_2 \\
&\text{subject to}: \; \mathrm{P}_f^i = \Pr\left(G_i(\mathbf{X}) \le 0\right) \le 1 - R_t^i, i = 1 \sim 3 \\
&\qquad\qquad \mathbf{d} \;=\; [\mu_{X_1}, \mu_{X_2}], \mathbf{X} = [X_1, X_2]; \\
&\qquad\qquad 0 \le \mathbf{d}_1 \,\&\, \mathbf{d}_2 \le 10 \\
&\text{where} \qquad G_1 = \frac{X_1^{\,2} X_2}{20} - 1 \\
&\qquad\qquad G_2^l = \frac{(X_1 + X_2 - 5)^2}{30} + \frac{(X_1 - X_2 - 12)^2}{120} - 1 \\
&\qquad\qquad G_2^h = G_2^l + \delta; \;\; \delta = 0.05 X_1 X_2 \\
&\qquad\qquad G_3 = -0.05 X_1^2 - X_1 - X_2 + 14
\end{aligned}
\tag{7.30}
$$

As shown in Eq. (7.30), the limit state functions G_1 and G_3 remains the same while two data sources are available for the second constraint, where the low-fidelity (LF) and high-fidelity (HF) model are denoted as G_2^l and G_2^h respectively. The term $\delta(.)$ represents the bias function that quantifies the differences between low- and high- fidelity responses. The target reliability is set to 0.985 for all the three constraints, and the target for cumulative confidence level is set to 0.99.

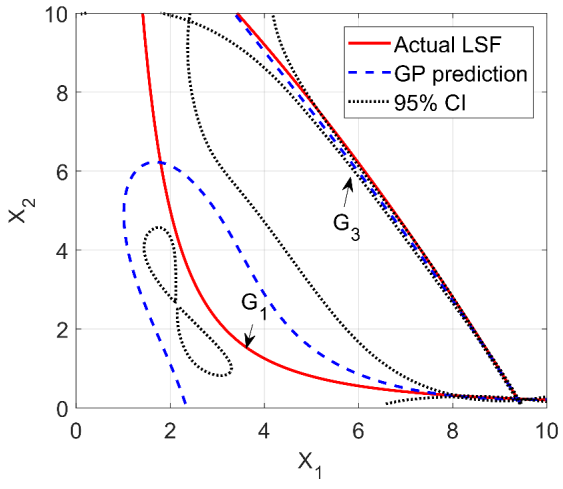

Figure 7.2: Approximated limit state functions for G_1 and G_3

The RBMO framework is employed to solve the optimization problem by using 10^5 MCS samples. Given the boundaries of the two design variables, the initial design point is selected as $d_0 = [5, 5]$. Within the design domain, the Latin hypercube sampling (LHS) algorithm is employed to generate six initial training samples, where the limit state functions G_1, G_2^l, and G_3 are evaluated for obtaining the initial training data sets. Therefore, three GP models can be constructed accordingly. Since the proposed approach focuses on the adaptive hybrid learning for multi-fidelity data, the updating process for GP models of G_1 and G_3 is skipped in this work, where the approximated limit state functions are shown in Fig. 7.2. Following the procedure introduced in Section 7.2, the AHL and RBDO are sequentially performed for achieving the RBMO optimal solution. After two iterations in RBMO, an optimal solution is obtained as $d_{opt} = [7.7344, 1.6650]$.

In the 1st iteration of RBMO, the AHL algorithm determines that there is no need to update the GP model $\hat{G}^l$ that constructed using 6 low-fidelity data, and three high-fidelity sample are sequentially identified for updating the hybrid GP model. With the hybrid GP model constructed using 6 low- and 3 high-fidelity data, a RBDO problem is solved for providing the pseudo optimal design as introduced in Section. 7.4. The design history of the 1st RBDO is shown in Table 7.2, including the design points, estimated probability of failure and the value of cost function. The 1st pseudo optimal solution $d_p^1 = [8.0739, 1.0594]$ failed to satisfy the stopping criterion as the $CCL_{hy}|d_p$ is calculated as 0.9234, which is less than the target *CCL* 0.99. Thus, in the 2nd iteration of RBMO, the AHL and RBDO are performed with the pseudo optimal design d_p^1, where two low- and two-high-fidelity data have been collected for updating the hybrid GP model. As shown in Fig. 7.3, the GP model constructed using the 8 low-fidelity samples can accurately reflect the failure surface of the

low-fidelity model within the critical region. In Fig. 7.4, the effectiveness of adding the fourth and fifth high-fidelity data can be demonstrated by comparing the approximated limit state function with the actual limit state function G_2^h. For the lasted hybrid GP model, the corresponding hyperparameters are given as β^l = 14.4097, ω^l = [0.1619 0.1605], σ_l = 9.9984, β^δ = -1.4899, ω^δ = [0.4184, 0.2801], σ_δ = 3.2624, respectively. Table 7.3 shows the information of all the identified low- and high-fidelity data during the overall RBMO process, and the design history in the 2nd RBDO is included in Table 7.4. The design history of the RBMO is depicted in Fig. 7.5, which clearly shows the convergences during the two RBDOs.

Table 7.2: Design history in the 1st RBDO

Ite.	Input	R1	R2	R3	Cost
1	[5.0000, 5.0000]	1.0000	1.0000	1.0000	10.0000
2	[6.0000, 4.0000]	1.0000	1.0000	0.9988	8.0000
3	[9.9572, 0.0000]	0.2732	1.0000	0.1156	0.0428
4	[7.8362, 0.8361]	0.9276	1.0000	0.9990	2.9999
5	[7.9881, 0.9669]	0.9703	1.0000	0.9932	2.9788
6	[8.1170, 1.0349]	0.9823	1.0000	0.9815	2.9179
7	[8.0745, 1.0576]	0.9846	1.0000	0.9851	2.9831
8	[8.0740, 1.0593]	0.9849	1.0000	0.9850	2.9853
9	[8.0739, 1.0594]	0.9850	1.0000	0.9850	2.9855

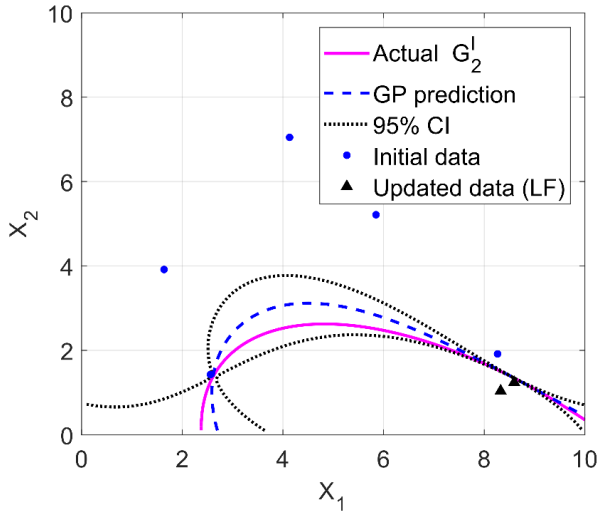

Figure 7.3: Approximated limit state function (LF) at the 2nd iteration of RBMO

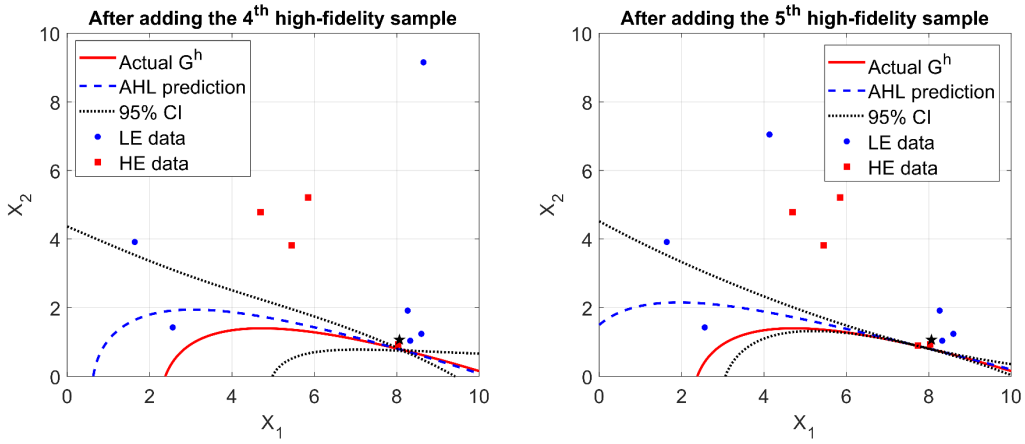

Figure 7.4: Adaptive hybrid learning for high-fidelity data at the 2nd iteration of RBMO

For comparison purpose, the design problem has been solved by using conventional RBDO methods: 1) an adaptive GP model [99] constructed using only low-fidelity data, denoted as GP(LF), and 2) an adaptive GP model [99] constructed using only high-fidelity data, denoted as GP(HF). To maintain the consistency, the approximated limit state functions for G_1 and G_3 remains the same. Moreover, direct MCS method has been applied

for the design problems using the high-fidelity model. To validate the optimal designs obtained by different methods, direct MCS with 10^5 samples are used to evaluate the actual reliability of the probabilistic constraints G_2^h. The optimal results obtained by using different methods are shown in Table 7.5, which includes the number of function evaluations for G_2^l and G_2^h. As shown in Fig. 7.6, the optimal designs obtained by GP(HF) and RBMO are close to the MCS optimal design. When GP(LF) is used for design optimization, the optimal design completely falls into the failure region. It proves that the ignorance of the difference between low- and high-fidelity data may yield infeasible solutions. Though GP model constructed with only high-fidelity data can be used for providing reliable optimal solution, 10 high-fidelity samples are evaluated, which is the twice of the high-fidelity samples used by the proposed approach. The results demonstrate that the RBMO framework is capable of providing reliable optimal solutions with less total costs.

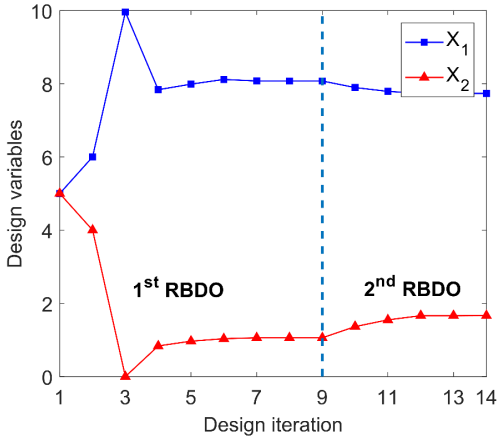

Figure 7.5: RBMO design history

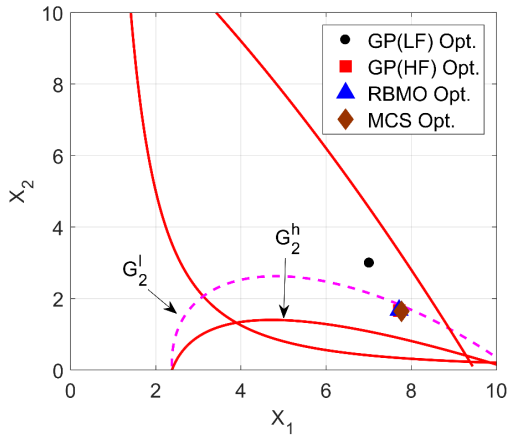

Figure 7.6: Optimal solutions obtained by using different methods

Table 7.3: Low- and high-fidelity data identified by AHL

	Ite.	Input	Sim./Exp. Response	CCL_m /CCL_e	Updated at
Updated LF data	1	[8.3273, 1.0371]	-0.1803	0.9810	2nd ite. RBMO
	2	[8.5958, 1.2381]	-0.0415	0.9917	2nd ite. RBMO
Updated HF data	1	[5.8489, 5.2127]	2.8254	0.9593	1st ite. RBMO
	2	[4.6915, 4.7793]	2.0050	0.9876	1st ite. RBMO
	3	[5.4476, 3.8158]	1.5411	0.9997	1st ite. RBMO
	4	[8.0301, 0.9262]	0.0934	0.9737	2nd ite. RBMO
	5	[7.7389, 0.8960]	0.0088	0.9968	2nd ite. RBMO

Table 7.4: Design history in the 2nd RBDO

Ite.	Input	R1	R2	R3	Cost
1	[8.0739, 1.0594]	0.9850	0.7663	0.9850	2.9855
2	[7.8948, 1.3670]	0.9991	0.9260	0.9854	3.4722
3	[7.7906, 1.5496]	0.9999	0.9686	0.9855	3.7590
4	[7.7349, 1.6646]	0.9999	0.9848	0.9851	3.9297

5	[7.7345, 1.6649]	0.9999	0.9850	0.9850	3.9304
6	[7.7344, 1.6650]	0.9999	0.9850	0.9850	3.9306

Table 7.5: Optimal solutions obtained from different methods

Methods	Design points	Actual P_f	No. of Sim. + Exp.	Cost
GP(LF)	[7.0147, 2.9898]	0	10 + 0	5.9751
GP(HF)	[7.7160, 1.6625]	0.0142	0 + 10	3.9465
RBMO	[7.7344, 1.6650]	0.0134	8 + 5	3.9306
MCS_RBDO	[7.7707, 1.6409]	0.0150	$0 + 10^5$	3.8702

7.6.2 Case Study II: Vehicle Brake Disc Design

To model a vehicle disc brake system, a 3D finite element model using 26,125 elements and 37,043 nodes is constructed according to Xia et al. [100]. The disc brake system consists of a brake disc and a pair of brake pads, and the failure occurs if the damping ratio of the vibration is less than a threshold -0.01. Based on the finite element model, a quadratic polynomial response surface approximation model is developed for expressing the limit state function of the damping ratio. Therefore, the design optimization problem can be formulated as

$$
\begin{aligned}
&\text{Minimize}: \; Cost = \mathbf{d}_3 \\
&\text{subject to}: \; \mathrm{P}_f = \Pr\left(G(\mathbf{d},u,p) \le 0\right) \le 1 - R_t \,, \\
&\qquad\qquad \mathbf{d} \;=\; [\mu_{h_1}, \mu_{h_2}, \mu_{h_3}], \\
&\text{where} \qquad G^l(\mathbf{d},u,p) = 0.046287 + 0.20458u - 0.059821p - 0.00036549h_1 \\
&\qquad\qquad - 0.010037h_2 + 0.013836h_3 + 0.24308up - 0.0037884uh_1 \\
&\qquad\qquad + 0.0023358uh_2 - 0.016918uh_3 + 0.029287ph_1 - 0.015872ph_2 \\
&\qquad\qquad - 0.0028333ph_3 + 0.0007175h_1h_2 - 0.00046158h_1h_3 - 0.0003648h_2h_3 \\
&\qquad\qquad - 0.39076u^2 - 0.015968p^2 - 0.0011936h_1^2 + 0.000269h_2^2 \\
&\qquad\qquad + 0.00062638h_3^2 + 0.01; \\
&\qquad\qquad G^h(\mathbf{d},u,p) = G^l(\mathbf{d},u,p) + \delta(\mathbf{d},u,p); \quad \delta(\mathbf{d},u,p) = 0.25h_1p - 1.15\frac{h_2}{h_3} - u
\end{aligned}
$$

(7.31)

where the three design variables are the mean of the friction material thickness h_1, disc thickness h_2, and back plate thickness h_3. Two non-design random variables are involved, including the friction coefficient u and brake pressure p. As shown in Eq. (7.31), an artificial bias function $\delta(.)$ is used to distinguish the low- and high-fidelity model, where the quadratic polynomial response surface approximation model is treated as the low-fidelity model. The properties of the design and random variables are detailed in Table 7.6. Since the lightweight is an important target in vehicle design, the thickness of the back plate μ_{h3} is treated as the objective function that needs to minimize. In this study, the target CCL and the reliability target are set to 0.99 and 0.985, respectively.

Table 7.6: Properties of the random variables

Variable	Distribution Type	Mean	Standard Deviation	Design Boundaries
h_1	Normal	μ_{h1} mm	0.9 mm	[14.5, 15.5]

h_2	Normal	μ_{h2} mm	0.9 mm	[19.5, 20.5]
h_3	Normal	μ_{h3} mm	0.9 mm	[12, 20]
μ	Normal	0.35	0.01	/
p	Normal	0.5 MPa	0.02 MPa	/

Starting from an initial design d_0 = [15, 20, 15], the RBMO framework is employed to achieve a reliable optimal design. The Latin hypercube sampling method is utilized to generate 50 initial samples, and a GP model $\hat{G}^l$ can be constructed after evaluating the low-fidelity responses of these initial samples. By performing the adaptive hybrid learning, 82 low-fidelity samples and 19 high-fidelity samples are collected at the first iteration of RBMO, where Fig. 7.7 shows the CCL_l and CCL_{hy} history during the AHL process. The updated hybrid GP model is used to solve a RBDO problem as introduced in Section 7.4, where the history of the design points and the estimated probability of failure are shown in Table 7.7. At the 2nd iteration of RBMO, the AHL process is repeated and three high-fidelity data have been identified for enhancing the prediction accuracy within the critical region. Figure 7.8 shows the CCL_{hy} achieves the target after adding the third high-fidelity data. The design history of the 2nd RBDO is summarized in Table 7.8, where the new pseudo optimal solution is validated as the RBMO optimal design, given as d_{opt} = [15.5000, 19.5000, 17.4284]. The design history of RBMO is shown in Fig. 7.9, where 132 low- and 22 high-fidelity data are collected during the overall RBMO process. To validate the optimal solution, 10^5 MCS samples are used for calculating the actual reliability based on the high-fidelity model G^h, which is given as 0.9829.

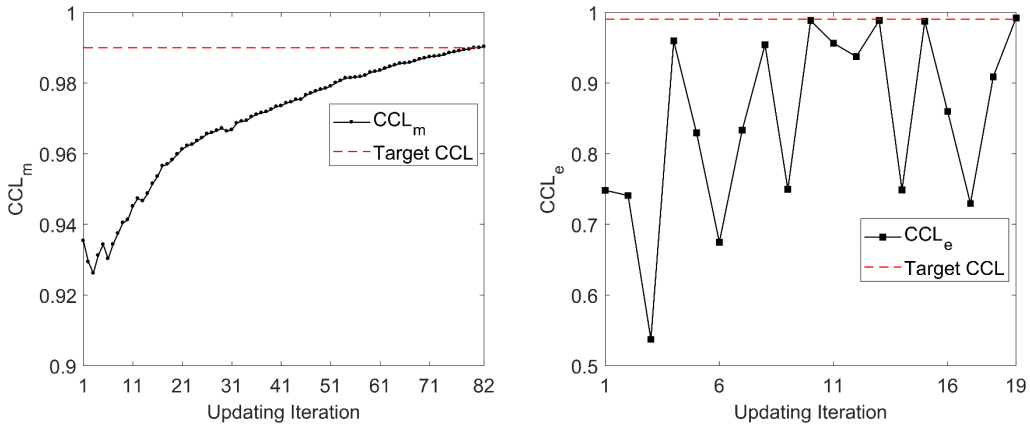

Figure 7.7: Adaptive hybrid learning in the 1st iteration of RBMO

Table 7.7: Design history in the 1st RBDO

Iterations in RBDO	Design points	Estimated P_f	Cost
1	[15.0000, 20.0000, 15.0000]	0.4727	15.0000
2	[15.5000, 19.5000, 15.9799]	0.1124	15.9799
3	[15.5000, 19.5000, 16.8457]	0.0445	16.8457
4	[15.5000, 19.5000, 17.4120]	0.0224	17.4120
5	[15.5000, 19.5000, 17.6665]	0.0156	17.6665
6	[15.5000, 19.5000, 17.6958]	0.0151	17.6958
7	[15.5000, 19.5000, 17.7011]	0.0151	17.7011
8	[15.5000, 19.5000, 17.7011]	0.0150	17.7011

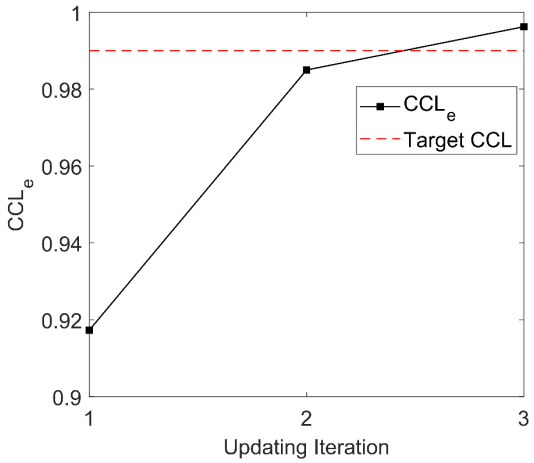

Figure 7.8: Adaptive hybrid learning in the 2nd iteration of RBMO

Table 7.8: Design history in the 2nd RBDO

Iterations in RBDO	Design points	Estimated P_f	Cost
1	[15.5000, 19.5000, 17.7011]	0.0970	17.7011
2	[15.5000, 19.5000, 17.3589]	0.0169	17.3589
3	[15.5000, 19.5000, 17.4333]	0.0149	17.4333
4	[15.5000, 19.5000, 17.4271]	0.0150	17.4271
5	[15.5000, 19.5000, 17.4284]	0.0150	17.4284

To demonstrate the effectiveness of the proposed RBMO framework, the same design problem has been solved by three different methods, including 1) GP(LF), 2) GP(HF), and 3) RBDO using hybrid GP model with randomly generated sample points, denoted as (hybrid GP) approach. For the latest method, the number of low-fidelity data is fixed at 132, which is the total number of low-fidelity samples that utilized by the proposed approach. Moreover, three different combinations are considered where different numbers (30/40/50) of high-fidelity samples are used for the hybrid GP approach. The optimal

solutions obtained using different methods are detailed in Table 7.9, where the corresponding accurate reliabilities are calculated by directly using 10^5 MCS samples. The results clearly indicate that the optimal design failed to satisfy the reliability requirement if the problem is solved by only using low-fidelity data. GP(HF) method can ensure a reliable optimal solution, however, the number of high-fidelity samples is given as 168, indicating the cost efficiency is much lower than the RBMO framework. For the hybrid GP approach, the performance can be improved by increasing the number of high-fidelity data. However, the hybrid GP model approach using 30 random high-fidelity samples provides an untrustworthy solution as the reliability 0.9362 failed to satisfy the target. Compared to hybrid GP model constructed using randomly generated samples, the proposed AHL can provide reliable optimal solutions with less number of function evaluations.

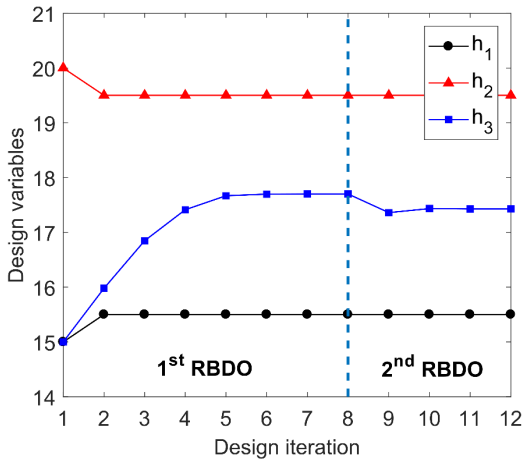

Figure 7.9: Design iterations during RBMO

Table 7.9: Optimal solutions obtained from different methods

Methods	Design points	Actual R	No. of LF + HF
GP(low-fidelity)	[15.5000, 19.5000, 16.0610]	0.8940	132+0

GP(high-fidelity)	[15.5000, 19.5000, 17.5176]	0.9841	0+168
Hybrid GP	[15.5000, 19.5000, 17.5938]	0.9362	132+30
Hybrid GP	[15.5000, 19.5000, 17.4596]	0.9817	132+40
Hybrid GP	[15.5000, 19.5000, 17.6792]	0.9879	132+50
RBMO	[15.5000, 19.5000, 17.4284]	0.9828	132+22
MCS_RBDO	[15.5000, 19.5000, 17.5450]	0.9850	$0+10^5$

7.6.3 Case Study III: Cantilever Beam Example Design

In case study III, a cantilever beam is considered as an example for testing the performance of the RBMO framework. The beam is made of aluminum with Young's modulus 69 GPa. As shown in Fig. 7.10, the left end of the beam is fixed on the wall while a load F is applied at the corner of the right end. The design objective is to minimize the volume while satisfying the design requirement on the maximum total deformation, the RBMO problem can be formulated as

$$\begin{aligned} &\text{Minimize}: \ Cost = d_1 \cdot d_2 \cdot d_3 \\ &\text{subject to}: \ \mathrm{P}_f = \Pr\left(G(\mathbf{d}, E, F) \le 0\right) \le 1 - R_t; \\ &\qquad\qquad h < b; \\ &\qquad\qquad \mathbf{d} \ = \ [\mu_l, \mu_h, \mu_b] \\ &\text{where} \qquad G^l\left(\mathbf{d}, E, F\right) = 0.1 - \frac{4PL^3}{Ebh^3}; \\ &\qquad\qquad G^h\left(\mathbf{d}, E, F\right) = 0.1 - D_{FEA}\left(\mathbf{d}, E, F\right); \end{aligned} \tag{7.32}$$

In this example, the mean of the length l, width b, and thickness h are considered as three design variables, while the Young's modulus E and external load F are two random variables. The statistical information of the random variables is summarized in Table 7.10. In Eq. (7.32), a failure occurs if the maximum deformation is greater than a threshold 0.1

mm. The low-fidelity model G^l is derived based on the Euler- Bernoulli beam theory, where the load is assumed to be applied on the midpoint of the right edge. On the other hand, a high-fidelity 3D model using 1080 elements is developed in ANSYS APDL for static analysis, and the results are treated as high-fidelity model $D_{FEA}(.)$. The target reliability for the optimization problem is set to 0.985.

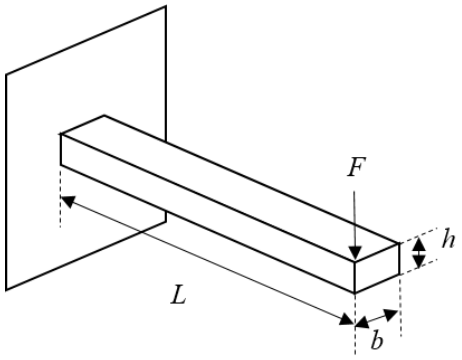

Figure 7.10: Geometry of the cantilever beam

Table 7.10: Properties of random variables for the cantilever beam

Variable	Distribution	Mean	Standard Deviation	Design Boundaries
Length, L	Normal	μ_L dm	0.4 dm	[3, 5]
Width, b	Normal	μ_b dm	0.02 dm	[0.4, 0.8]
Height, h	Normal	μ_h dm	0.02 dm	[0.3, 0.6]
Young's Modulus, E	Normal	69 GPa	1 GPa	/
Load, F	Normal	1000 N	4 N	/

The RBMO framework is employed to solve the optimization problem with an initial design d_0 = [4, 0.6, 0.45] and 50 initial samples generated by LHS. An optimal design d_{opt}

= [3.0000, 0.4000, 0.4542] is obtained after two iterations in RBMO. Therefore, the AHL process and RBDO have been performed twice for achieved the optimal solution. The iterative design history during the 1st and 2nd RBDO are summarized in Table 7.11 and 7.12, respectively, and Figures. 7.11 and 7.12 depicts the iterative design points and the reliability history during the RBMO. After achieving the 1st pseudo optimal design, the RBMO continues as the stopping criterion is not satisfied. Therefore, in the 2nd iteration of RBMO, the AHL algorithm is reused to update the hybrid GP model at the 1st pseudo optimal design, leading to two different estimated reliabilities in Fig. 12.

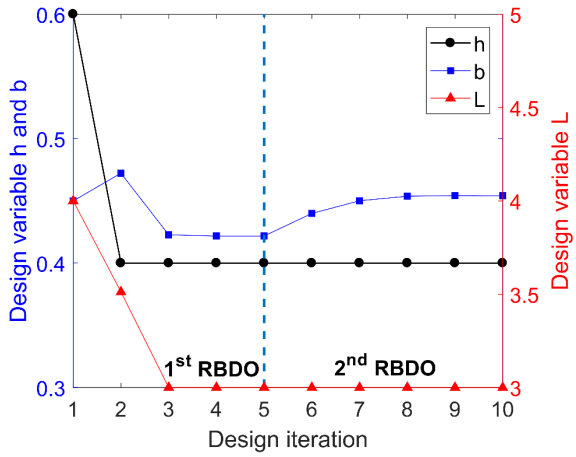

Figure 7.11: Design iterations during the RBMO

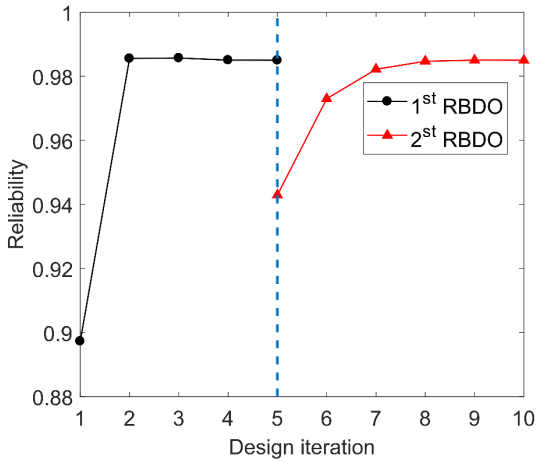

Figure 7.12: Reliability history during the RBMO

At the 1st iteration of RBMO, 42 low- and 8 high-fidelity data have been selected for updating the hybrid GP model, while 1 low- and 2 high-fidelity data have been identified at the 2nd iteration of RBMO. Therefore, a total number of 93 low- and 10 high-fidelity data are used for deriving the optimal solution. The ANSYS APDL is performed at the optimal solution to calculate the maximum deformation (m), and the contour plot is shown in Fig. 7.13.

Table 7.11: Design history at the 1st iteration of RBMO

Iterations in RBDO	Design points	Estimated P_f	Cost
1	[4.0000, 0.6000, 0.4500]	0.1027	1.0800
2	[3.5119, 0.4000, 0.4723]	0.0144	0.6634
3	[3.0000, 0.4000, 0.4227]	0.0143	0.5072
4	[3.0000, 0.4000, 0.4218]	0.0150	0.5062
5	[3.0000, 0.4000, 0.4218]	0.0150	0.5061

Table 7.12: Design history at the 2nd iteration of RBMO

Iterations in RBDO	Design points	Estimated P_f	Cost
1	[3.0000, 0.4000, 0.4218]	0.0571	0.5061
2	[3.0000, 0.4000, 0.4399]	0.0270	0.5279
3	[3.0000, 0.4000, 0.4501]	0.0178	0.5402
4	[3.0000, 0.4000, 0.4538]	0.0153	0.5446
5	[3.0000, 0.4000, 0.4542]	0.0150	0.5451
6	[3.0000, 0.4000, 0.4542]	0.0150	0.5450

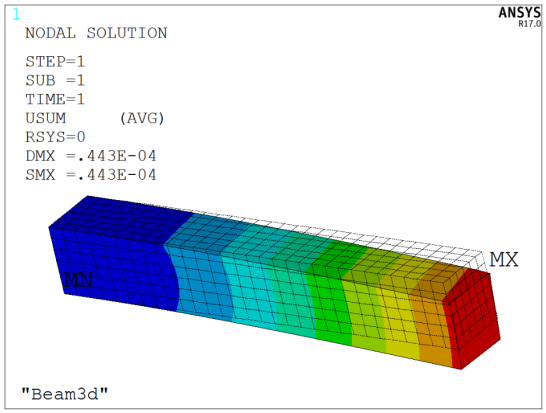

Figure 7.13: ANASYS results of maximum deformation (unit: m)

7.7 Conclusion

In this work, a reliability-based multi-fidelity design optimization framework was developed for ensuring reliable optimal design while reducing the number of low- and high-fidelity data. To provide more accurate response predictions, data from both sources are integrated for constructing a hybrid GP model. At each iteration of the RBMO, the adaptive hybrid learning is first performed to iteratively identify new low- and high-fidelity samples for updating the hybrid GP model, then a RBDO problem is solved for providing

a pseudo optimal solution. The RBMO process will be repeated until the new pseudo optimal solution is validated as a reliable optimal design. In RBMO, the layout of the low- and high-fidelity data is smartly designed by the AHL algorithm, which can reduce the total costs as well as providing the most useful information to achieve the optimal solution. Moreover, the multiple RBDO strategy that embedded in the RBMO framework can further reduce the costs as the updating scheme only needs to be performed at the critical region, which moves towards to the final optimal solution. The results from three case studies show that RBMO outperforms RBDO methods that purely based on one data source. Through the comparison study, it proves that RBMO is capable of providing a reliable optimal design while reducing the costs of collecting both high-fidelity and low-fidelity data.

8 BAYESIAN MIXTURE MODELING FOR RELIABILITY-BASED DESIGN OPTIMIZATION UNDER HETEROGENEOUS UNCERTAINTIES[105]

8.1 Introduction

Heterogeneous uncertainties due to model imperfection, lack of training data, and input variations coexist in practical simulation-based design applications. In this work, a Bayesian mixture modeling (BMM) approach is developed to handle heterogeneous uncertainties concurrently in reliability-based design optimization. To account for model-form uncertainty, a Bayesian model inference approach is first employed to calibrate high fidelity simulation models by using Gaussian process (GP) regression. Then a validated Bayesian model is constructed based on a set of simulation data and experimental observations to predict the response of the actual physical system. By using the Monte Carlo simulation (MCS), the resultant Bayesian model predictions are utilized to form a

Gaussian mixture model (GMM) for propagating heterogeneous uncertainties concurrently in system reliability analysis. An aggregative reliability index (ARI) is then defined based on GMM to approximate the probability of failure under heterogeneous uncertainties. The proposed BMM approach is further integrated with RBDO framework to search for optimal system designs. The effectiveness of the proposed approach is demonstrated through three case studies.

8.2 Heterogeneous Uncertainty Aggregation Using Bayesian Mixture Modeling

8.2.1 Heterogeneous Uncertainties in Simulation-based Design

In simulation-based design, heterogeneous uncertainties can be categorized into three different types as shown in Fig. 8.1, including 1) model-form uncertainty, 2) data uncertainty, and 3) input variations. Model form uncertainty is introduced when high-fidelity simulation models are built through idealizations and simplifications of real physical processes or systems. Similarly, data uncertainty occurs if low-fidelity surrogate models is constructed to replace the high-fidelity simulation models based on a set of simulations runs. The input variation, also known as aleatory uncertainty, inherently exists in practical engineering system such as material properties, and manufacturing batch to batch variations, which can be characterized by statistical modeling methods.

A general formulation for quantifying the model form uncertainty is expressed as [1, 97]

$$y^e(\mathbf{x}) = y^m(\mathbf{x},\boldsymbol{\theta}) + \delta(\mathbf{x}) + \varepsilon \tag{8.1}$$

where $y^e(x)$ denotes the actual observations of a physical process, $y^m(x, \theta)$ represents the simulation model response as a function of inputs x and unknown parameters θ, which is also referred to as calibration parameter, θ_{ture} is the vector of true values for the unknown parameters, $\delta(x)$ represents the bias or discrepancy function that characterize the differences between simulation and experiment output, and ε stands for the experimental errors, which is often assumed to follow a normal distribution ~ $N(0, \lambda)$. As shown in Eq. (1), two main sources of model form uncertainties can be identified as: 1) the model parameters that fixed in real physics but is unknown in simulation model and 2) model discrepancy due to flawed understanding of the system. Inappropriate managing model form uncertainty may introduce significant errors in predicting system responses, resulting in inaccurate reliability assessment and untrustworthy optimal designs. Surrogate models can be constructed based on simulations and experimental data to further reduce the computational costs. However, the data uncertainty is introduced due to the limited number of training. As a result, errors are inevitable when using surrogates to predict the actual performance of the physical system.

To efficiently quantify the heterogeneous uncertainties, the Bayesian mixture modeling (BMM) approach is proposed as shown in Fig. 8.1. The proposed BMM first addresses the model form uncertainties using Bayesian calibration with both simulation results and experimental observations. Then a validated Bayesian model can be constructed as a better surrogate of physical processes. Due to the lack of both simulation results and experimental data, the data uncertainty should be taken into account in RBDO while using the validated Bayesian model to predict the system response. Therefore, the response prediction is treated as normal distributions instead of a constant. By using the Monte Carlo

simulation for random realizations of the inputs, and predicted responses are utilized to form a Gaussian mixture model, which accounts for all the heterogeneous uncertainties. Eventually, a new measure, referred to as "aggregative reliability index", is defined to propagate the heterogeneous uncertainties for reliability assessment.

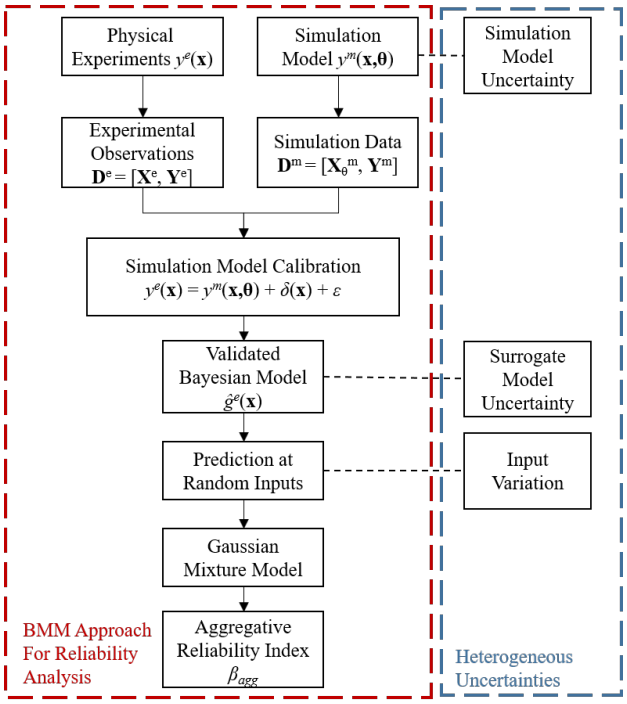

Figure 8.1: Flowchart of the Bayesian mixture modeling approach dealing with heterogeneous uncertainties

8.2.2 Bayesian Inference for Model Calibration and Bias Correction

In this section, a Bayesian model inference approach [35] is employed to quantify the model form uncertainties, where the Gaussian process (GP) regression technique is employed for building surrogates. Below we first introduce a brief review of the GP modeling and then details the Bayesian inference approach to calibrate the unknown model parameters and capture model bias. .

Assume a performance function $G(z)$ is characterized by a GP model, the response is treated as a single realization of a Gaussian process, given as

$$\hat{g}(\mathbf{z}) \sim GP\left(\mathbf{h}(\mathbf{z})\boldsymbol{\beta}, \sigma^2 R(\mathbf{z}, \mathbf{z}')\right) \tag{8.2}$$

where z is a general formulation represents the inputs, h(z) is a vector of regression functions, and β represents a vector of coefficients. In this work, the prior mean h(z)β is assumed to be a constant. In Eq. (8.2), σ^2 is an unknown constant and $R(.,.)$ is the correlation function that characterize the relationship between the responses at input z_i and z_j, expressed as

$$R(\mathbf{z}_i, \mathbf{z}_j) = \exp\left[-\sum_{p=1}^{k} \omega_p \left|\mathbf{z}_{i,p} - \mathbf{z}_{j,p}\right|^2\right] \tag{8.3}$$

where k is the dimension of input z; $\omega = [\omega_1, \omega_2, \ldots, \omega_k]$ is the vector of roughness parameters that capture the nonlinearity of the process. Therefore, the unknown hyperparameters β, ω, and σ^2 fully characterize the GP model, and these values can be approximated by using Maximum Likelihood Estimation (MLE) with a log likelihood function given as

$$likelihood = -\frac{1}{2}\left[N_a \ln(2\pi) + N_a \ln\sigma^2 + \ln\left|\mathbf{V}\right| + \frac{1}{2\sigma^2}(\mathbf{Y} - \mathbf{H}\boldsymbol{\beta})\mathbf{V}^{-1}(\mathbf{Y} - \mathbf{H}\boldsymbol{\beta})\right] \tag{8.4}$$

where $Y = G(Z)$ represents the vector of responses and $Z = [z_1, z_2, \ldots, z_{Na}]$ represents the N_a input sites, Hβ represents the mean vector where $H = [h^T(x_1), \ldots, h^T(x_{Na})]$, and $V = \sigma^2 R(.,.)$ stands for the covariance matrix. Numerical optimization algorithms such as genetic algorithm and simulated annealing method can be used to solve the MLE based on training data D = [Z, Y]. The prediction at any input x is assumed to follow a Gaussian

distribution with mean $\mu(z)$ and variance $v(z)$ as,

$$\mu(\mathbf{z}) = \mathbf{h}(\mathbf{x})\boldsymbol{\beta} + \mathbf{r}^T\mathbf{V}^{-1}(\mathbf{Y} - \mathbf{H}\boldsymbol{\beta}) \tag{8.5}$$

and

$$v(\mathbf{z}) = \sigma^2\left\{1 - \mathbf{r}^T\mathbf{V}^{-1}\mathbf{r} + \left[\mathbf{h}(\mathbf{z}) - \mathbf{H}^T\mathbf{V}^{-1}\mathbf{r}\right]^T\left(\mathbf{H}^T\mathbf{V}^{-1}\mathbf{H}\right)^{-1}\left[\mathbf{h}(\mathbf{z}) - \mathbf{H}^T\mathbf{V}^{-1}\mathbf{r}\right]\right\} \tag{8.6}$$

where r is the correlation vector between the input x and all training sample points in Z.

With the GP modeling technique, a GP model $\hat{g}^e$ for experimental response can be formed by assuming the simulation model, bias function, and experimental errors are statistically independent, expressed as

$$\begin{aligned} &\hat{g}^e(\mathbf{x}) \sim GP\left(\mathbf{h}^m(\mathbf{x},\boldsymbol{\theta})\boldsymbol{\beta}^m + \mathbf{h}^\delta(\mathbf{x})\boldsymbol{\beta}^\delta, \sigma_e^2 R^e\left[(\mathbf{x},\boldsymbol{\theta}),(\mathbf{x}',\boldsymbol{\theta}')\right]\right) \\ &\sigma_e^2 R^e\left[(\mathbf{x},\boldsymbol{\theta}),(\mathbf{x}',\boldsymbol{\theta}')\right] = \sigma_m^2 R^m\left[(\mathbf{x},\boldsymbol{\theta}),(\mathbf{x}',\boldsymbol{\theta}')\right] + \sigma_m^2 R^\delta(\mathbf{x},\mathbf{x}') + \lambda \end{aligned} \tag{8.7}$$

where x represents the inputs of the physical system. As indicated by Eq. (8.7), the GP model $\hat{g}^e$ consists of GP models of simulation model and bias function. For a given set of simulation data $D^m = [X_\theta^m, Y^m]$, the simulation model can be replaced by a GP model $\hat{g}^m(X_\theta^m) \sim GP(H^m\beta^m, \sigma_m^2 R^m(.,.))$, where $X_\theta^m = [X^m, \theta]$ represents the inputs of simulation model that consists of the vector of random variables X^m and the vector of unknown parameters θ. The hyperparameters of the GP model $\hat{g}^m$ can be estimated by only using the simulations data D^m. Based on the simulation data and the experimental observations $D^e = [X^e, Y^e]$ that collected at *Ne* input sites, the bias function can be modeled by fitting another GP model $\hat{g}^\delta(X^e) \sim GP(H^\delta\beta^\delta, \sigma_\delta^2 R^\delta(.,.))$. To estimate the hyperparameters of the bias function, Kennedy and O'Hagan [31] developed the likelihood function based on the hyperparameters from simulation GP model and prior distribution of the unknown parameter. Then the mean function and the covariance matrix V^e of the GP model $\hat{g}^e$ can

be expressed by augmenting the N_e input sites X^e of the experimental observations with the unknown parameter θ, denoted as $X_\theta{}^e = \{[x_1{}^e, \theta], \ldots, [x_{Ne}{}^e, \theta]\}$. The term H^e can be written as

$$\mathbf{H}^e = \begin{bmatrix} \mathbf{H}^m(\mathbf{X}_\theta^m) & 0 \\ \mathbf{H}^m(\mathbf{X}_\theta^e) & \mathbf{H}^\delta(\mathbf{X}^e) \end{bmatrix} \tag{8.8}$$

and the variance matrix V^e can be expressed as

$$\mathbf{V}^e = \begin{bmatrix} \mathbf{V}^m(\mathbf{X}_\theta^m, \mathbf{X}_\theta^m) & \mathbf{V}^m\left\{\mathbf{X}_\theta^m, \mathbf{X}_\theta^e\right\}^T \\ \mathbf{V}^m\left\{\mathbf{X}_\theta^m, \mathbf{X}_\theta^e\right\} & \lambda\mathbf{I} + \mathbf{V}^m\left\{\mathbf{X}_\theta^e, \mathbf{X}_\theta^e\right\} + \mathbf{V}^\delta\left\{\mathbf{X}^e, \mathbf{X}^e\right\} \end{bmatrix} \tag{8.9}$$

where λ is the standard deviation of the experimental error and I is an identity matrix. The covariance matrix $V^\delta(.,.)$ is expressed as

$$\mathbf{V}^m(\mathbf{X}^e, \mathbf{X}^e) = \begin{bmatrix} \sigma^\delta R^\delta(\mathbf{x}_1, \mathbf{x}_1) & \cdots & \sigma^\delta R^\delta(\mathbf{x}_1, \mathbf{x}_{Ne}) \\ \vdots & \ddots & \vdots \\ \sigma^\delta R^\delta(\mathbf{x}_{Ne}, \mathbf{x}_1) & \cdots & \sigma^\delta R^\delta(\mathbf{x}_{Ne}, \mathbf{x}_{Ne}) \end{bmatrix} \tag{8.10}$$

and the covariance matrix $V^m(.,.)$ is written as

$$\mathbf{V}^m(\mathbf{A}, \mathbf{B}) = \begin{bmatrix} \sigma^m R^m(A_1, B_1) & \cdots & \sigma^m R^m(A_1, B_{kb}) \\ \vdots & \ddots & \vdots \\ \sigma^m R^m(A_{ka}, B_1) & \cdots & \sigma^m R^m(A_{ka}, B_{kb}) \end{bmatrix} \tag{8.11}$$

where *ka* and *kb* represent the maximum indices for matrix A and matrix B, respectively; they are equal to N_m for $X_\theta{}^m$ and N_e for X^e and $X_\theta{}^e$. It should be mentioned that the covariance matrix V^m and V^δ are calculated by using the hyperparameters of the simulation model GP $\hat{g}^m$ and the bias function GP $\hat{g}^\delta$, respectively.

Clearly, the unknown parameter θ exists in the simulation model and it affects the GP modeling of experimental response. Therefore, the Bayesian inference method is utilized

to estimate the posterior distribution of the unknown parameter θ. By integrating the simulation data set and experimental observations, the overall responses are obtained as $Y^{all} = [Y^m, Y^e]$, and the posterior distribution of θ can be approximated as

$$p(\boldsymbol{\theta}\left|\mathbf{Y}^{all},\phi\right.) \propto p(\mathbf{Y}^{all}\left|\boldsymbol{\theta},\phi\right.)p(\boldsymbol{\theta}) \tag{8.12}$$

where $p(\theta)$ is the prior of the calibration parameters and ϕ represents all the estimated hyperparameters during the GP modeling of simulation model and bias function. The likelihood function $p(Y^{all} \mid \theta, \phi)$ can be written as

$$\begin{aligned} &p(\mathbf{Y}^{all}\left|\boldsymbol{\theta},\phi\right.) = \\ &\left|\mathbf{V}^e\right|^{-1/2}\left|\mathbf{W}\right|^{1/2}\exp\left[-\frac{1}{2}\left\{\mathbf{Y}^{all}-\mathbf{H}^e\boldsymbol{\beta}^e\right\}^T\mathbf{V}_e^{-1}\left\{\mathbf{Y}^{all}-\mathbf{H}^e\boldsymbol{\beta}^e\right\}\right] \end{aligned} \tag{8.13}$$

where W is expressed as

$$\mathbf{W} = \left[\mathbf{H}_e^{\,T}\mathbf{V}_e^{-1}\mathbf{H}^e\right]^{-1} \tag{8.14}$$

The details of calculating the posterior distribution of the calibration parameter can be found in the ref. [97]. After estimating the posterior distribution of the calibration parameter by the Bayesian inference, the actual response for any new point x' can be predicted by the GP model $\hat{g}^e$(x'), referred to as validated Bayesian model, where the prediction mean is given as

$$\mu(\mathbf{x}') = \mathbf{h}(\mathbf{x}',\boldsymbol{\theta})\boldsymbol{\beta}^e + \mathbf{T}^T\mathbf{V}_e^{-1}\left[\mathbf{Y}^{all}-\mathbf{H}^e\boldsymbol{\beta}^e\right] \tag{8.15}$$

where the correlation matrix T can be written as

$$\mathbf{T} = \begin{bmatrix} \mathbf{V}^m\{(\mathbf{x}',\boldsymbol{\theta}),\mathbf{X}_\theta^m\} \\ \mathbf{V}^m\{(\mathbf{x}',\boldsymbol{\theta}),\mathbf{X}_\theta^e\} + \mathbf{V}^\delta(\mathbf{x}',\mathbf{X}^e) \end{bmatrix} \tag{8.16}$$

The covariance function at the given point x' can be calculated as

$$v(\mathbf{x}') = \mathbf{V}^m\{(\mathbf{x}',\boldsymbol{\theta}),(\mathbf{x}',\boldsymbol{\theta})\} + \lambda\mathbf{I} - \mathbf{T}^T\mathbf{V}_e^{-1}\mathbf{T} + \left(\mathbf{h}(\mathbf{x}',\boldsymbol{\theta}) - \mathbf{H}_e{}^T\mathbf{V}_e^{-1}\mathbf{T}\right)^T \square \\ \mathbf{W}\left(\mathbf{h}(\mathbf{x}',\boldsymbol{\theta}) - \mathbf{H}_e{}^T\mathbf{V}_e^{-1}\mathbf{T}\right) \tag{8.17}$$

Therefore, we can make inference about the experimental response by integrating Eqs. (8.15) and (8.17) with respect to the posterior distribution of θ in Eq. (8.12), which can be done by using numerical computation methods such as Gauss-Legendre quadrature. By employing the Bayesian model inference approach, the model form uncertainty has been quantified through integrating both the simulation results and experimental observations, and a validated Bayesian model can be obtained for predicting the response of the actual physical system.

8.2.3 Reliability Analysis under Heterogeneous Uncertainties

Reliability is a fundamental attribute for the safe operation of engineering systems, and reliability analysis aims at the quantification of the probability of failure under various sources of uncertainties. Considering a limit state function $G(\mathrm{x})$, which is generally a simulation model of a real physical process, a system failure is defined as the limit state value is less than zero. Then the probability of failure P_f is a multi-dimensional integral given as

$$P_f = \Pr\left[G(\mathbf{x}) < 0\right] = F_G(0) = \int\cdots\int_{G(\mathbf{x})<0} f_x(\mathbf{x})d\mathbf{x} \tag{8.18}$$

where $f_x(\mathrm{x})$ represents the joint probability density function of the input variables x, and $F_G(.)$ represents the cumulative distribution function of $G(\mathrm{x})$. However, it is extremely difficult to analytically compute the probability of failure by directly using Eq. (8.18). Moreover, only the input variation is considered when assessing the reliability using Eq. (8.18). In practical engineering applications, heterogeneous uncertainties need to be taken

into account in reliability analysis as the simulation model has to be calibrated by experimental observations and data uncertainty should be addressed when the validated Bayesian model is used as the representative of the real physical process. Therefore, the Bayesian mixture model is proposed in this subsection for propagating heterogeneous uncertainties in reliability analysis.

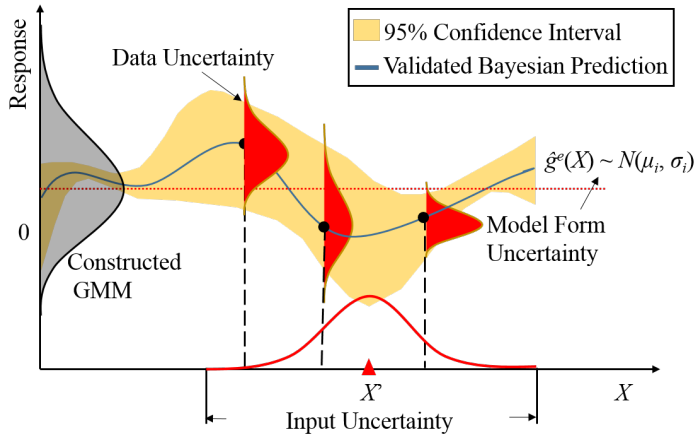

Figure 8.2: Gaussian mixture model for heterogeneous uncertainties aggregation

A validated Bayesian model can be constructed by calibrating the simulation model, and the experimental response at any input site can be predicted using the validated Bayesian model. The model form uncertainty can be addressed by replacing the limit state function $G(\mathrm{x})$ with the validated Bayesian model $\hat{g}^e(\mathrm{x})$, and the estimated probability of failure can be written as

$$\Pr\left[G(\mathbf{x})<0\right] \approx \Pr\left[\hat{g}^e(\mathbf{x})<0\right] = F_{\hat{g}(\mathbf{x})}(0) = \int_{-\infty}^{0} p(\hat{g}^e(\mathbf{x}))d\hat{g}^e(\mathbf{x}) \qquad (8.19)$$

where $F_{\hat{g}e(\mathrm{x})}(.)$ represents the estimated cumulative distribution function of the predicted experimental response using the validated Bayesian model, $p(.)$ represents the probability density function, and x is the input vector contains nr random variables x_i, $i = 1, 2, \ldots, nr$.

To propagate the input variation to the system response, Monto Carlo simulations method is directly utilized for random realizations of the input x. In MCS, N samples are generated according to the randomness of the input variables x, denoted as $\mathrm{X_m} = [\mathrm{x}_{m,1}, \mathrm{x}_{m,2}, \ldots, \mathrm{x}_{m,N}]$. For each MCS sample, the validated Bayesian model is used for experimental response prediction, given as $\hat{g}^e(\mathrm{x}_{m,i}) \sim N(\mu_i,\sigma_i)$, $i = 1, 2, \ldots, N$, where the prediction mean and standard deviation for the i^{th} distribution are denoted as $\mu_i = \mu(\mathrm{x}_{m,i})$ and $\sigma_i = v(\mathrm{x}_{m,i})^{1/2}$ for simplicity. It should be mentioned that the prediction variance is also known as the mean squared error, which is used as a measurement for quantifying the prediction accuracy. Therefore, the prediction at any MCS sample point is actually a normally distributed random variable, which results in a point-to-normal distribution mapping relationship between the MCS sample and response predictions. After predicting the response of all the MCS samples by the validated Bayesian model, a family of normal distributions are readily obtained to yield the stochastic system response with the consideration of the heterogeneous uncertainties.

As shown in Fig. 8.2, simulation results and experimental observations are used for constructing the validated Bayesian model for representing the real physical process. Within the range of the input variation, MCS is employed for random realizations and the predicted responses are treated as component normal distributions to form a Gaussian mixture model (GMM). As the means and variances of the component normal distributions can be directly obtained by the validated Bayesian model, the probability density function of the GMM is then expressed as

$$p(GMM) = \sum_{i=1}^{N} \pi_i p\left[\hat{g}^e(\mathbf{x}_{m,i})\right] = \sum_{i=1}^{N} \pi_i N\left(\mu_i, \sigma_i\right) \tag{8.20}$$

where x_i represents the i^{th} MCS sample, π_i is the weight of the i^{th} component normal distribution, and the summary of π_i is equal to one. The MCS samples are equally important since they are simultaneously generated according to the randomness of the given input x. Therefore, the weight π_i of each component normal distribution of the GMM has the same value $1/N$. According to Eq. (8.20), the mean μ_{GMM} and standard deviation σ_{GMM} of the GMM can be directly calculated based on the known statistical moments of the N component normal distributions, expressed as

$$\mu_{GMM} = \frac{1}{N}\sum_{i=1}^{N}\mu_i \tag{8.21}$$

$$\sigma_{GMM} = \sqrt{v_{GMM}} = \sqrt{\frac{1}{N}\sum_{i=1}^{N}\left(v_i + \mu_i^2\right) - \left(\frac{1}{N}\sum_{i=1}^{N}\mu_i\right)^2} \tag{8.22}$$

where v_i represents the prediction variance of the i^{th} MCS sample. By assuming that the GMM follows a normal distribution with mean μ_{GMM} and variance v_{GMM}, the probability of failure can be estimated through the integration over the area of the failure region, expressed as

$$\Pr\left[G(\mathbf{x}) < 0\right] \approx \Pr\left[GMM < 0\right] = \Phi\left(\frac{-\mu_{GMM}}{\sigma_{GMM}}\right) \tag{8.23}$$

Apparently, the three different types of uncertainties have been concurrently incorporated in Eq. (8.23), and thus the proposed BMM approach is capable of aggregating the heterogeneous uncertainties in reliability analysis. To facilitate the RBDO process, an aggregative reliability index β_{agg} is defined as $\frac{\mu_{GMM}}{\sigma_{GMM}}$, and the reliability can be approximated as

$$R \approx \hat{R} = \Phi(\beta_{agg}) \tag{8.24}$$

8.3 Reliability Based Design Optimization Framework

Reliability-based design optimization aims at finding optimal system designs that minimize cost while satisfying a high level of reliability requirement. By using the proposed BMM approach, heterogeneous uncertainties including three different types have been taken into account for ensuring reliable reliability assessment. By integrating with the BMM, the RBDO problem is reformulated as

$$
\begin{aligned}
&\textit{Minimize}: \quad \textit{Cost}(\mathbf{X}) \\
&\textit{subject to}: \quad \beta_{agg}^{i} = \Phi^{-1}\left[\Pr\left(GMM_i \geq 0\right)\right] = \frac{\mu_{GMM}^{i}}{\sqrt{v_{GMM}^{i}}}, \quad i = 1,....,nc; \\
&\qquad\qquad \beta_t^i = \Phi^{-1}(R_t^i); \quad \beta_{agg}^{i} \geq \beta_t^i; \\
&\qquad\qquad \mathbf{X}^{\mathbf{L}} \leq \mathbf{X} \leq \mathbf{X}^{\mathbf{U}}, \quad \mathbf{X} \in R^{nd} \\
&\textit{where} \\
&\qquad\qquad G_i^e(\mathbf{X}) = G_i^m(\mathbf{X}, \boldsymbol{\theta}) + \delta(\mathbf{X}) + \varepsilon; \\
&\qquad\qquad \hat{g}_i^e(x_j) \sim N(\mu_j, \sigma_j), j = 1, \ ..., N; \\
&\qquad\qquad GMM_i = \sum_{j=1}^{N} \frac{1}{N} \hat{g}_i^e(x_j);
\end{aligned}
\tag{8.25}
$$

where $\beta_{agg}{}^{i}$ represents the aggregative reliability index of the i^{th} limit state function $G_i^e(\mathrm{X})$; β_t^i represents the corresponding reliability target; $\hat{g}_i^e(\mathrm{X})$ represents the validated Bayesian model for the i^{th} limit state function; *Cost*(d) represents the objective function; GMM_i stands for the constructed GMMs; X is the vector of random variables; and *nc*, *nd* are the number of constraints and design variables, respectively. Validated Bayesian models are first built by integrating both simulation results and experimental observations, and GMMs are then constructed to simultaneously address the heterogeneous uncertainties in iterative reliability analysis.

For an engineering design application, the procedure of RBDO using the proposed BMM approach is summarized in Fig. 8.3. The first step is to calibrate the simulation model by using the Bayesian model inference method. For a simulation model y^m, N_m random samples are first generated by using Latin hypercube sampling (LHS), denoted as $X_\theta^m = [X^m, \theta^m]$. With the evaluated simulation responses at these input points, a Gaussian process model can be constructed based on the data set $D^m = [X_\theta^m, Y^m]$. Similarly, N_e experiment observation are collected at random sample X^e generated by LHS method. Based on the overall responses $Y^{all} = [Y^m, Y^e]$ and prior distributions of unknown parameter θ, a validated Bayesian model that used to predict the actual response can be achieved as introduced in subsection 8.2.2. It should be mentioned that the model calibration process only needs to be conducted once during the RBDO process. Staring at an initial design d_0, the RBDO will be performed iteratively. To provide a reliable optimum design with heterogeneous uncertainties, the proposed reliability analysis approach is employed to estimate the reliability in each design iteration. In reliability analysis, N Monte Carlo samples are first generated according to the randomness of the current design point, denoted as $X_m = [x_{m,1}, x_{m,2}, \ldots, x_{m,N}]$. By using the validated Bayesian model, the predicted response for each MCS sample is treated as a normally distributed random variable, where the prediction mean and variance can be calculated as shown in Eq. (8.15) and (8.17). After collecting all the N normal distributed predictions, a Gaussian mixture model can be constructed accordingly. The GMM is assumed to follow a normal distribution with mean μ_{GMM} and standard deviation σ_{GMM}, which can be easily computed by using Eq. (8.21) and (8.22). Consequently, an aggregative reliability index β_{agg} can be calculated as the ratio of μ_{GMM} to σ_{GMM}. To determine the next design point, the finite difference method is employed

for calculating the sensitivity of β_{agg} with respect to design variables, and the sequential quadratic programming (SQP) technique is served as the optimizer in RBDO. The iterative RBDO process will be repeated until it converges to an optimum design.

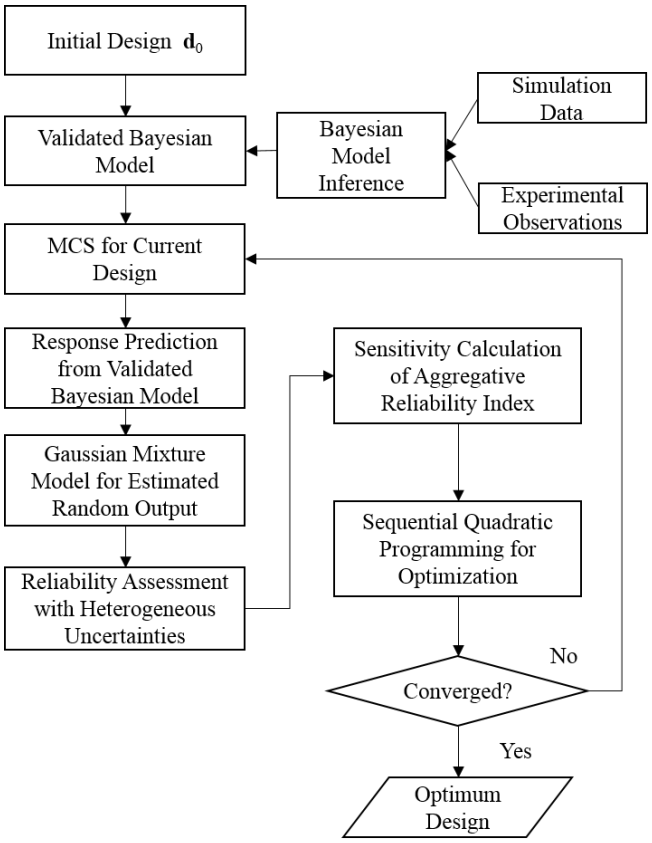

Figure 8.3: Flowchart of BMM-RBDO framework

8.4 Case Studies

In this section, three RBDO problems will be solved to demonstrate the effectiveness of the proposed Bayesian mixture modeling method.

8.4.1 Case Study I: A Mathematical Design Problem

In the first case study, two random design variables X_1 and X_2 are both normally distributed as $X_1 \sim N(\mu_1, 0.3464^2)$ and $X_2 \sim N(\mu_2, 0.3464^2)$. The RBDO problem is

formulated as

$$
\begin{aligned}
&\text{Minimize}: \ Cost = 10 - X_1 + X_2 \\
&\text{subject to}: \ \beta_{agg}^i \geq \beta_t^i, \ \ i = 1 \sim 3 \\
&\qquad \beta_{agg}^i = \Phi^{-1}\left(\Pr\left(G(\mathbf{d}) \geq 0\right)\right) \\
&\qquad \mathbf{d} \ = \ [\mu_1, \mu_2] \\
&\qquad 0 \leq \mu_1 \ \& \ \mu_2 \leq 10 \\
&\text{where} \\
&\qquad G_1 = \frac{X_1^{\,2} X_2}{20} - 1 \\
&\qquad G_2^m(x_1, x_2, \theta) = \frac{(X_1 + X_2 - \theta)^2}{30} + \frac{(X_1 - X_2 - 12)^2}{120} - 1 \\
&\qquad G_2^e = G_2^m(x_1, x_2, \theta_{true}) + \delta(X_1, X_2) + \varepsilon; \ \ \delta(X_1, X_2) = -0.05 X_1 X_2 \\
&\qquad G_3 = -0.05 X_1^2 - X_1 - X_2 + 14
\end{aligned}
$$

(8.26)

where the second constraint has been modified with an unknown calibration parameter θ and a bias function $\delta(X_1, X_2)$, the experimental error is assumed to be neglectable. The prior of calibration parameter is assumed to follow a normal distribution as $\theta_{prior} \sim N(8, 2)$ while the true value of θ is set to 5. In this study, the design objective is to minimize the cost function and ensures reliability requirements are satisfied. The target reliability level is set to 0.985 for all the three constraints, thus the target reliability index β_t can be calculated as 2.1701.

As outline in Section 3, the first step is to calibrate the simulation model with the consideration of unknown parameter and bias function. Note the functions G_1 and G_3 have not been modified to distinguish the differences between simulation and experimental model, they are assumed to be accurate experimental functions and 12 Latin hyper cube samples are generated to construct the GP models. As shown in Fig. 8.4, two high-fidelity

GP models for G_1 and G_3 are constructed, thus we can avoid significant influences caused by these two limit state functions on the performance of RBDO. For G_2 function, 25 total samples are generated according to Latin hyper cube sampling. Among these sample points, 20 simulation responses are collected with random values of θ while 5 experimental responses are collected with the true calibration parameter. As introduced in subsection 8.2.2, a validated Bayesian model for G_2^e can be obtained after simulation model calibration based on the simulation data and experimental observations. The posterior distribution of the unknown parameter θ is approximated as $\theta_{post} \sim N(8.2376, 1.2383)$. Figure 8.5a shows the comparison of estimated and origin simulation model G_2^m and 8.5b shows the comparison of estimated and origin limit state functions of G_2^e. Due to the identifiability problem and the lack of data, the estimation of posterior distribution of θ is not accurate, leading to significant errors in predicting the simulation model G_2^m at the true θ value. However, the limit state function predicted by the validated Bayesian model is close to the actual one since the validation process considers both unknown parameter and bias function.

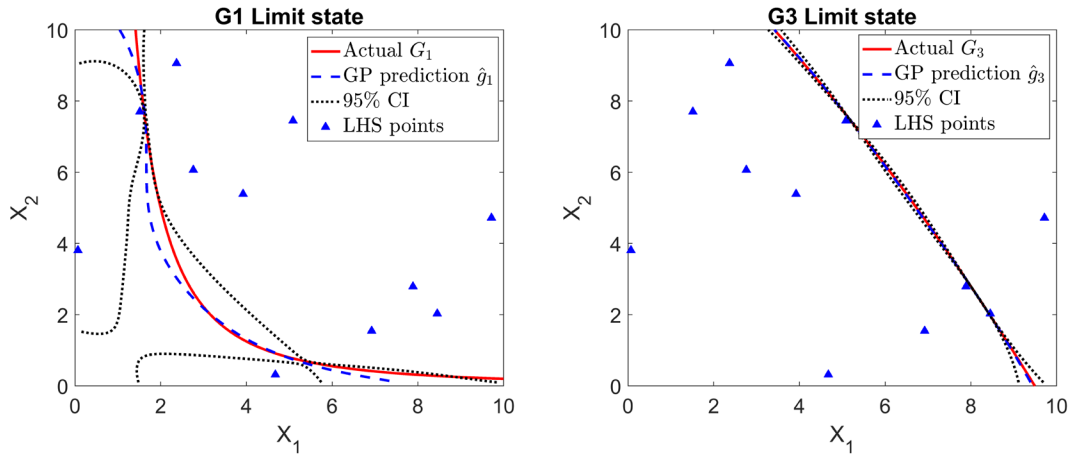

Figure 8.4: Actual LSFs of G_1 and G_3 vs. estimated LSFs using GP models

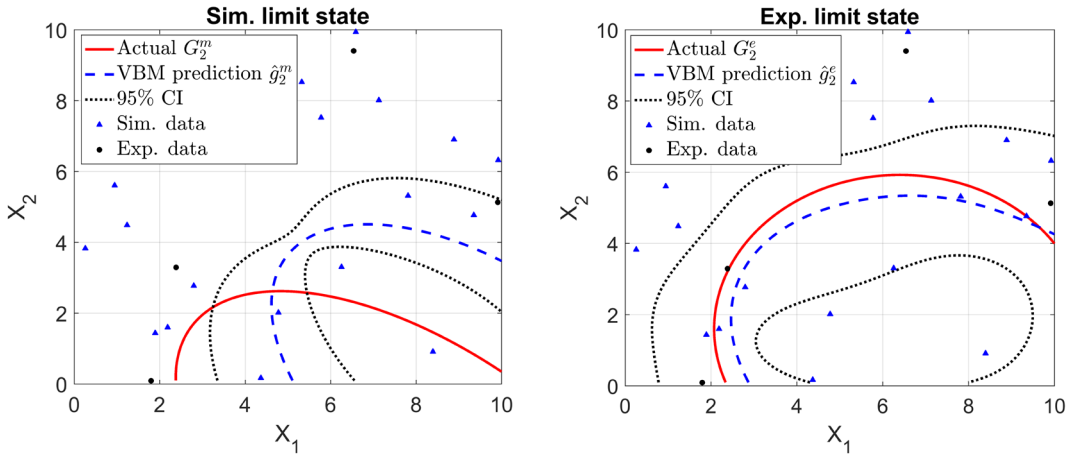

Figure 8.5: Validated Bayesian model prediction of a) simulation model G_2^m, and b) experimental response G_2^e

To solve the RBDO problem, the proposed reliability analysis method is employed for iterative reliability assessment. In each design iteration, 10^5 MCS samples are generated according to the randomness of the current design point. For each constraint, the reliability is approximated based on the GMM that constructed by the predicted responses at MCS samples. Starting from the initial design d_0 = [5, 5], the optimum design d_{opt} = [4.8312, 6.6407] is obtained after 9 iterations. The iterative design history of deigns points, reliabilities estimated by the GP models, and cost function values are listed in Table 8.1. Figure 8.6 shows the iterative design history for design variable X_1 and X_2, and Figure 8.7 shows the estimated reliabilities of three limit state functions during the RBDO process.

Table 8.1: Design history for case study I

Iteration	Design Point	$\hat{\mathbf{R}}^1$	$\hat{\mathbf{R}}^2$	$\hat{\mathbf{R}}^3$	Cost
1	[5.0000, 5.0000]	1.0000	1.0000	0.4784	10.0000
2	[4.7352, 6.0202]	1.0000	0.9997	0.8392	11.2850

3	[4.6737, 6.7401]	1.0000	0.9920	0.9940	12.0664
4	[4.6600, 6.7149]	1.0000	0.9935	0.9927	12.0549
5	[4.7505, 6.6658]	1.0000	0.9902	0.9885	11.9153
6	[4.8101, 6.6523]	1.0000	0.9863	0.9865	11.8422
7	[4.8303, 6.6424]	1.0000	0.9850	0.9852	11.8121
8	[4.8311, 6.6409]	1.0000	0.9850	0.9850	11.8098
9	[4.8312, 6.6407]	1.0000	0.9850	0.9850	11.8095

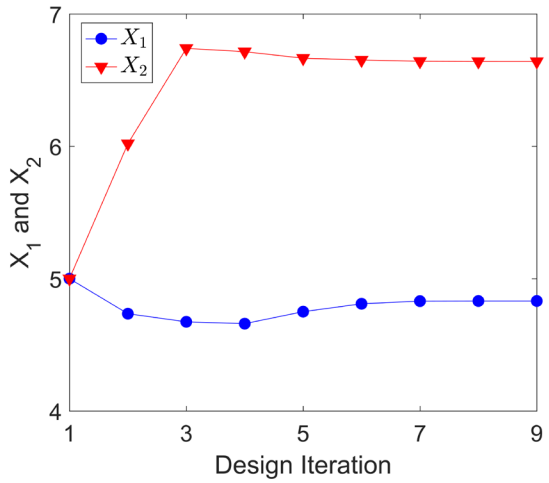

Figure 8.6: RBDO history of design variables

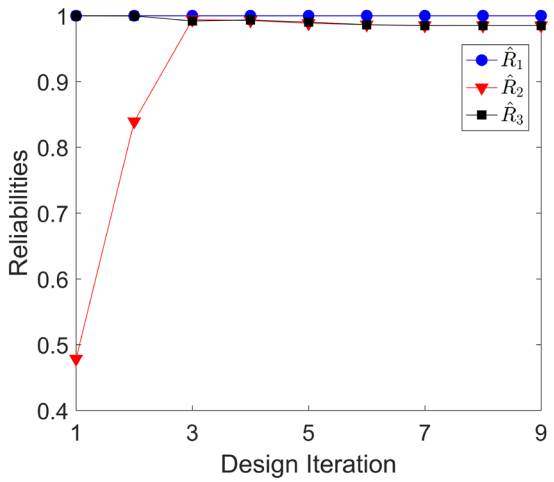

Figure 8.7: Reliabilities estimation at each design iteration

In the proposed BMM approach, the RBDO problem is solved with the consideration of three different types of uncertainties. To demonstrate the effectiveness of the proposed approach, the RBDO problem are solved under other two different conditions: 1) the validated Bayesian model $\hat{g}_2^m$ is used for reliability analysis while the bias function has been ignored, denoted as "Sim. Only", and 2) the validated Bayesian model $\hat{g}_2^e$ is directly employed for reliability analysis which means the data uncertainty is ignored, denoted as "RBDO". All the optimal results are shown in Table 8.2, while the reliabilities have been validated by direct MCS with 10^6 samples. As shown in Fig. 8.8, without the consideration of bias function, the optimal design completely falls in the failure region while the reliability of G_2^e is 0.0231. Similarly, an optimal design near to the failure surface is obtained when the data uncertainty is not addressed, and the reliability of G_2^e is given as 0.6735. On the contrary, by aggregating the three different types of uncertainties in reliability analysis, the proposed BMM approach can provide a reliable optimum design that all the three probabilistic constraints are satisfied.

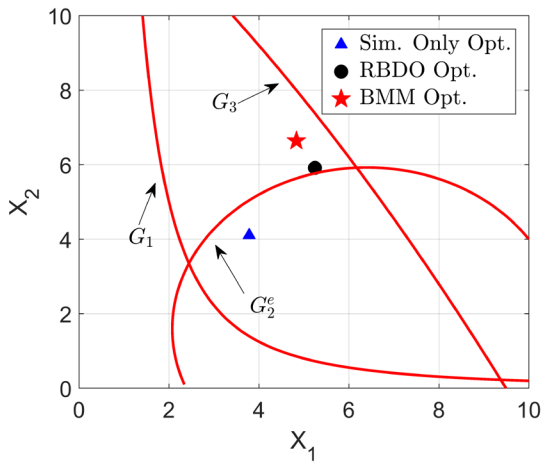

Figure 8.8: Optimal designs obtained by using different methods

Table 8.2: Comparison of optimal results

	Optimum	R1	R2	R3	Cost
Sim. Only	[3.7843, 4.1126]	1	0.0231	1	10.3283
RBDO	[5.2454, 5.9145]	1	0.6735	0.9891	10.6691
BMM	[4.8312, 6.6407]	1	0.9974	0.9852	11.8095

8.4.2 Case Study II: A Highly Nonlinear Problem

The bench mark example with 2 statistically independent random variables x = [x_1, x_2] has been tested by the proposed BMM approach. The random variables are assumed to follow normal distributions as $x_1 \sim N(d_1, 0.1)$ and $x_2 \sim N(d_2, 0.1)$, respectively. The RBDO problem is then formulated as

$$\begin{aligned}
&\text{Minimize}: \ Cost(\mathbf{d}) = (d_1 - 3.7)^2 + (d_2 - 4)^2 \\
&\text{subject to:} \ \ \beta^i_{agg} \geq \beta^i_t; \\
&\qquad \beta^i_{agg} = \Phi_t^{-1}\left[\Pr\left(\hat{g}^i(\mathbf{d}) \geq 0\right)\right], i = 1, 2 \\
&\qquad \mathbf{d} \ = \ [d_1, d_2], \\
&\qquad 0 \leq d_1 \leq 3.7, \ \ 0 \leq d_2 \leq 4 \\
&\text{where} \\
&\qquad G_1 = x_1 + x_2 - 3 \\
&\qquad G_2^m(x_1, x_2, \theta) = -x_1 \sin(\theta x_1) - 1.1 x_2 \sin(2x_2) \\
&\qquad G_2^e = G_2^m(x_1, x_2, \theta_{ture}) + \delta(x_1, x_2) + \varepsilon; \ \ \delta(x_1, x_2) = 0.5(x_1 - x_2)
\end{aligned} \tag{8.27}$$

where an unknown calibration parameter θ is added in the second constraint while the prior distribution is given as $\theta_{prior} \sim N(6, 1)$ and the true value is set to 4; the experimental error is assumed to be neglectable.

The target reliability for both constraints are set to 0.985, thus the target reliability index is approximated as 2.1701. Due to the high nonlinearity, 50 simulation and 12

experimental sample points are generated by Latin hypercube sampling scheme for simulation model validation of G_2^e, and 8 samples are used for constructing GP model for G_1. In this study, 10^5 MCS samples are used for reliability analysis during RBDO process. Starting from an initial design $d_0 = [2.5, 2.5]$, an optimum design $d_{opt} = [2.7078, 2.2965]$ is obtained after twelve iterations.

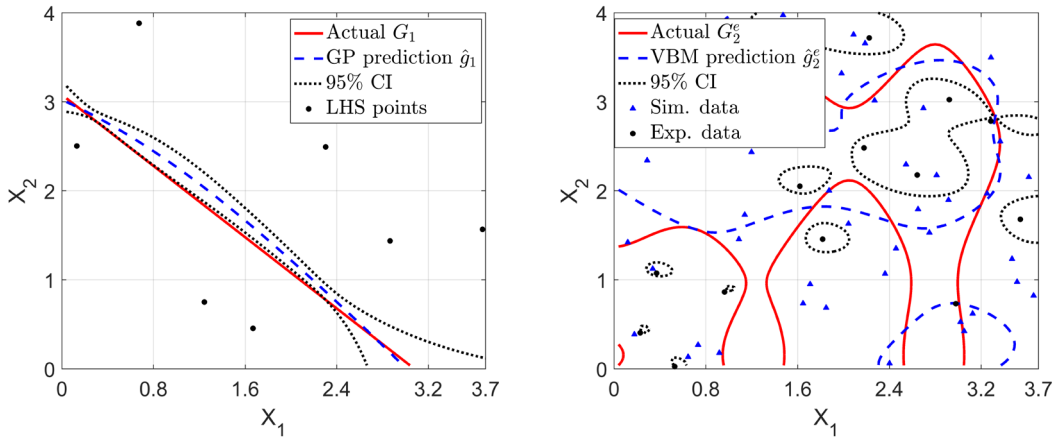

Figure 8.9: Actual LSF of G_1 and G_2 vs. estimated LSF using a) GP model, and b) validated Bayesian model

Table 8.3: Design history for case study II

Iteration	Design Point	$\hat{\mathbf{R}}^1$	$\hat{\mathbf{R}}^2$	Cost
1	[2.5000, 2.5000]	1.0000	0.9207	3.6900
2	[2.7091, 2.2251]	1.0000	0.9954	4.1321
3	[2.8073, 2.3334]	1.0000	0.9605	3.5744
4	[2.7474, 2.2543]	1.0000	0.9906	3.9549
5	[2.7367, 2.2659]	1.0000	0.9893	3.9351
6	[2.7078, 2.3075]	1.0000	0.9825	3.8491
7	[2.7127, 2.2887]	1.0000	0.9864	3.9032

8	[2.7062, 2.3004]	1.0000	0.9843	3.8764
9	[2.7078, 2.2954]	1.0000	0.9853	3.8902
10	[2.7073, 2.2971]	1.0000	0.9849	3.8854
11	[2.7076, 2.2964]	1.0000	0.9851	3.8871
12	[2.7078, 2.2965]	1.0000	0.9850	3.8863

The contour plot of origin and predicted limit state functions are depicted in Fig. 8.9, which indicates the high nonlinearity of the performance function G_2^e. Figure 8.10 shows the impact of simulation model uncertainties due to the unknown parameter and model discrepancy. It shows that the limit state function of G_2^m differs from the true one if the calibration parameter is not at its true value or the bias term is ignored. These limit state functions are not trust-worthy and underestimated or overestimated optimal designs can be achieved when they are directly applied for RBDO. This brings up the importance of validating simulation model in design under uncertainties.

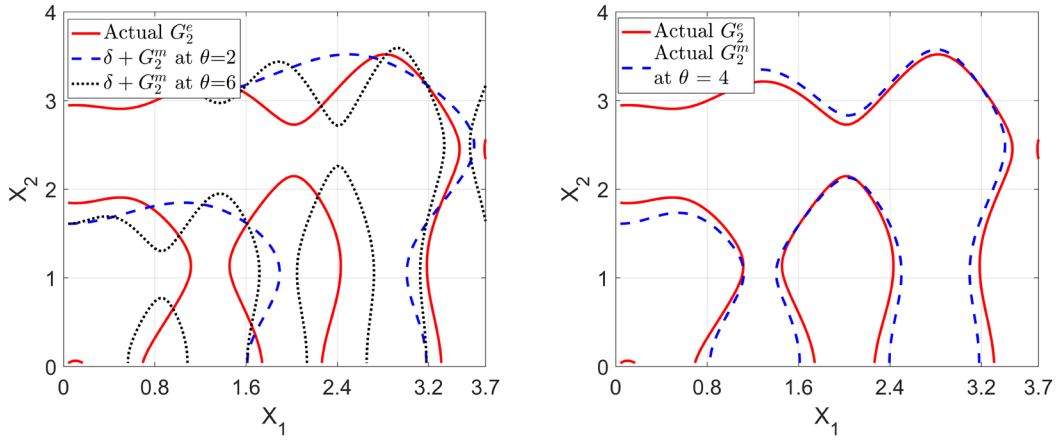

Figure 8.10: Model form uncertainties introduced by a) unknown parameter, and b) bias function

The RBDO history of design variables, estimated reliabilities, and cost function values are detailed in Table 8.3 and Fig. 8.11 and 8.12. To validate the optimal design obtained by the proposed BMM approach, direct MCS with 10^6 samples are employed based on G_2^e function with the true calibration parameter and bias term, and the reliability is given as 0.9996. To demonstrate the effectiveness of simulation model validation, the BMM approach is performed with 120 simulation and 40 experimental samples. By increasing the number of training data points, a more accurate predicted limit state function can be obtained as shown in Fig. 8.13. Moreover, the data uncertainty can be significantly reduced as indicated by the 95% confidence interval. By constructing a validated Bayesian model, the same RBDO problem is solved and an optimal design is obtained as d_{opt} = [2.8046, 3.2765] which is close to the actual optimum [2.8163, 3.2677] that obtained based on the actual experimental limit state functions. The results demonstrate that the proposed reliability analysis approach is applicable when the data uncertainty is not significant.

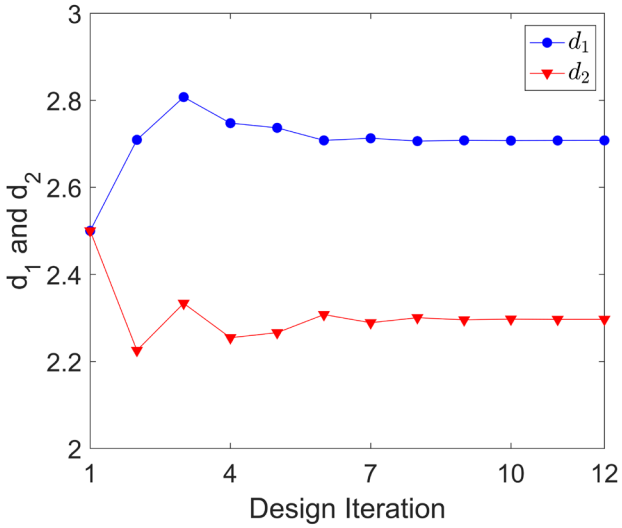

Figure 8.11: RBDO history of design variables

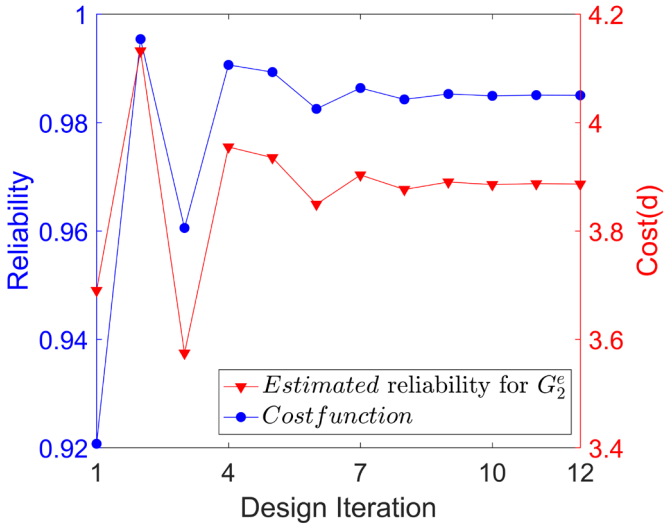

Figure 8.12: Reliabilities estimation in each design iteration

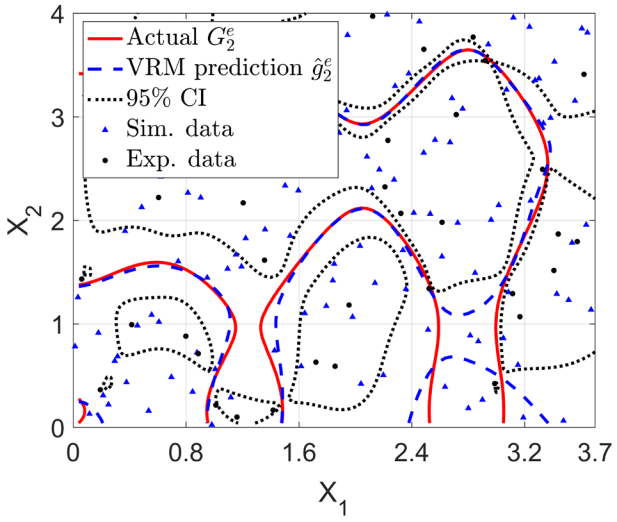

Figure 8.13: High fidelity of the validated Bayesian model for G_2^e with sufficient data points

8.4.3 Case Study III: Short Column Design

This case study considers a design problem of a short column with rectangular cross-section. The column is subjected to normal force F and biaxial bending moments M_1 =

250kNm and $M_2 = 125kNm$. The dimensions of the cross-section are denoted as h and b, receptively, which are assumed to be normally distributed with a variance of 25 mm, denoted as $\mathbf{d} = [b, h]$. The following RBDO formulation is used for the short column design:

$$
\begin{aligned}
&\text{Minimize}: && \text{Cost}(\mathbf{d}) = \mu_b \mu_h \\
&\text{subject to}: && \beta_{agg} \geq \beta_t \\
& && \beta_{agg} = \Phi^{-1}\left(\Pr\left(\hat{g}(\mathbf{d}) \geq 0\right)\right) \\
& && 0.5 \leq \mu_b / \mu_h \leq 2 \\
& && \mathbf{d} = [\mu_b, \mu_h] \\
& && 100\text{mm} \leq b \leq 1000mm \\
& && 100\text{mm} \leq h \leq 1000mm
\end{aligned}
\tag{8.28}
$$

where

$$
G^m(\mathbf{d}, F) = 1 - \frac{4M_1}{bh^2 f_y} - \frac{4M_2}{b^2 h f_y} - \frac{F^2}{(bhf_y)^2}
$$

$$
G^e = G^m(\mathbf{d}, F_{true}) + \delta(\mathbf{d}) + \varepsilon;\ \ \delta(\mathbf{d}) = 0.0009(b - h)
$$

where $f_y = 40$ MPa is the yield strength, the experimental error is assumed to be neglectable and the force F is treated as the unknown parameter with a normal prior distribution $F_{prior} \sim N(4000kN, 1000kN)$ while the true value is given as $2500kN$. The design objective is to minimize the cross-section area of the column with a reliability requirement 0.985.

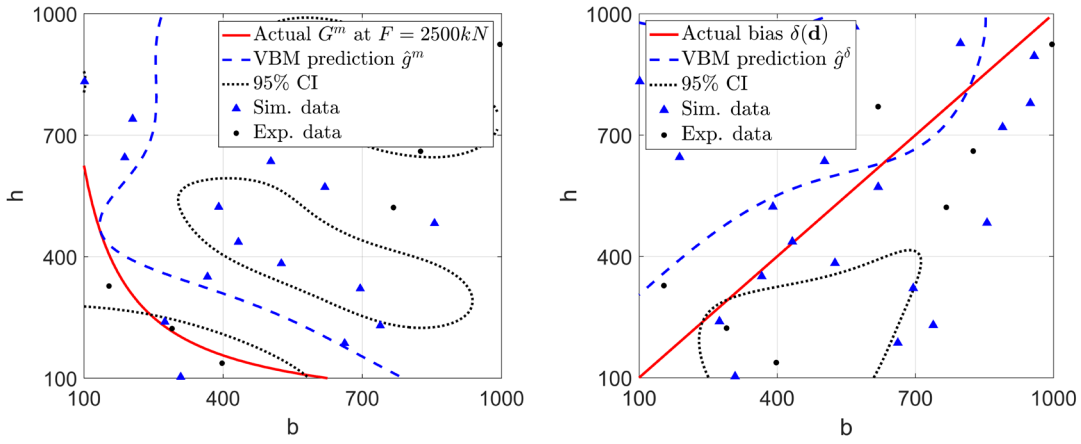

Figure 8.14: Validated Bayesian model prediction of a) simulation model, and b) bias function

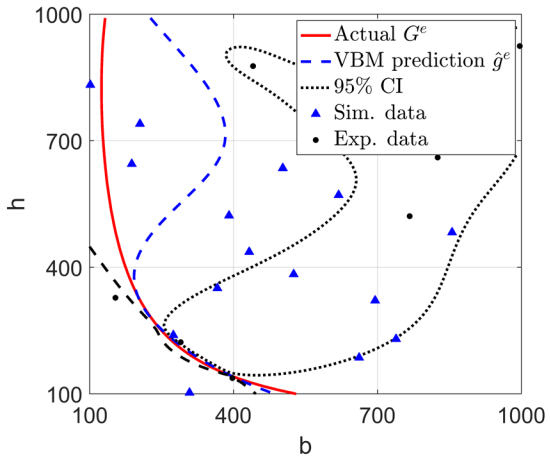

Figure 8.15: Approximated LSF by validated Bayesian model vs. actual LSF of G^e

To solve the design problem, 28 total samples are generated by using Latin hypercube sampling, including 22 simulation data obtained with random calibration parameter and 6 experimental observations. Following the procedure introduced in Section 8.3, a validated Gaussian process model is first built based on the overall data set and the prior information of the calibration parameter. The posterior distribution is obtained as $F_{post} \sim N(3834kN, 933kN)$, which is quite similar with the prior distribution. The reason is because of the identifiability problem when considering both bias function and calibration parameters. Figure 8.14 shows the GP predictions of simulation model G^m at zero and bias function $\delta(.)$ at zero, respectively. Though the GP models $\hat{g}^m$ and $\hat{g}^\delta$ cannot accurately model the actual simulation model and bias function, the validated Bayesian model $\hat{g}^e$ can provide better approximations of the actual experimental function as shown in Fig. 8.15.

Starting from an initial design point d_0 = [600, 600], the RBDO using the proposed approach is performed and an optimal solution d_{opt} = [359.0247, 178.8203] is obtained after

22 iterations. The iterative design history is depicted in Fig. 8.16, which shows that the design variables converge to the optimal solution after the 15^{th} iteration. By using 10^5 Monto Carlo simulation samples, the proposed BMM approach is employed for addressing the model form, data uncertainty, and input variation in reliability analysis during RBDO. The reliability history and the objective function values are shown in Fig. 8.17. The actual reliability at the optimal design is evaluated by 10^6 MCS samples based on the performance function with true calibration parameter and bias function, given as 0.9982. The result demonstrates that the proposed BMM approach can provide reliable optimal designs by aggregating the three different types of uncertainties.

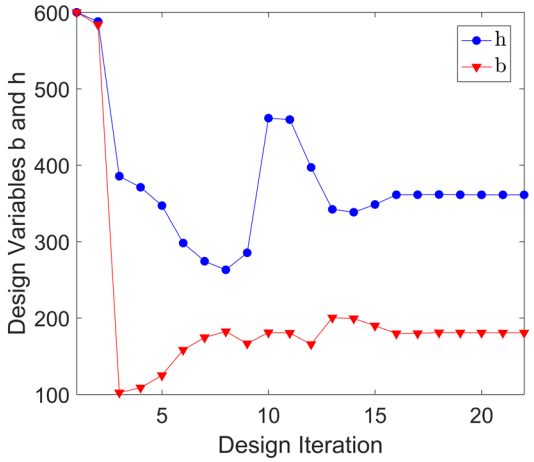

Figure 8.16: RBDO history of design variables

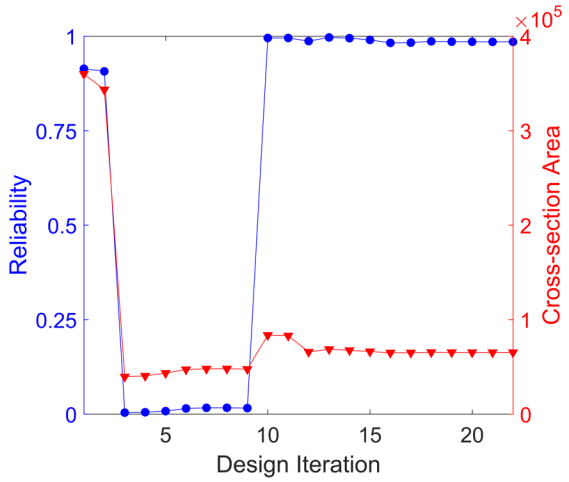

Figure 8.17: RBDO history of reliability and objective function

8.5 Conclusion

This work presents a Bayesian mixture modeling approach for solving RBDO problems with the consideration of heterogeneous uncertainties. To characterize the stochastic behavior of a physical process, a number of experimental observations are used to refine its simulation model by using the Bayesian inference method and GP modeling technique. With the validated Bayesian model, the response predictions are obtained for a large number of random sample point in Monte Carlo simulation, and then readily formed to a Gaussian mixture model for propagating the heterogeneous uncertainties. To approximate the probability of failure under heterogeneous uncertainties, an aggregative reliability index is defined based on the first two statistical moments of the Gaussian mixtures to calculate the probability density function of the stochastic system response. The proposed BMM approach is then integrated into RBDO framework for system design under heterogeneous uncertainties, and three case studies are solved to demonstrate the effectiveness. The results indicate that the proposed BMM approach can successfully

manage the heterogeneous uncertainties, and thus is capable of suggesting more reliable optimum designs by taking the three different types of uncertainties into account in RBDO.

9 CONCLUSION AND FUTURE WORK

This dissertation presents a series research on heterogeneous uncertainty quantification for reliability analysis and RBDO. By using machine learning and deep learning techniques, new reliability analysis and design techniques are presented to effectively address the challenges of dealing with different types of uncertainties.

In Chapter 3, the results from two examples demonstrate that LSTM is capable of predicting the response at each time instant. By using the LSTMs, a large number of artificial data can be achieved without evaluating the actual time-dependent responses, which can significantly reduce the computational costs. With a large scale data set, the DFN is used to effectively account for both the uncertainties due to random variables and stochastic process. The proposed framework also develops a strategy to determine the best architecture of the DFN in terms of the number of neurons in the hidden layers, which can effectively prevent over-fitting issue and thus enhance the performance of the time-dependent reliability analysis. The results from Chapter 4 demonstrate that the proposed sequential Kriging model algorithm can obtain accurate optimum solutions, and the required computational costs are less than existing methods. The major contribution of these work lies in developing a simulation-based framework for efficiently handling the complexity and high dimensionality of generic stochastic processes in time-dependent reliability analysis and time- dependent reliability-based design optimization.

Although surrogate modeling techniques have been successfully employed for reliability-based design optimization, the performances of such methods for complex engineering applications is severely limited due to the expensive costs of collecting

sufficient training data. When the training data is limited, most of existing surrogate-based RBDO methods lack the capability to provide reliable optimum designs due to the ignorance of surrogate model uncertainty. Chapter 5 introduces a new RBDO framework to compensate the surrogate model uncertainty, where the sensitivity of the equivalent reliability index is derived and thus facilitate the optimization process. As a result, the overestimation of reliability is avoided and the results demonstrate that the proposed approach can efficiently handle surrogate model uncertainty and thus provide reliable optimum solutions by balancing the trade-off between the cost and the risk of the overestimation of reliability.

In Chapter 6 and 7, one reliability analysis method and one RBDO algorithm are developed to account for simulation model uncertainties. By employing the Gaussian process regression technique, surrogate models are constructed for simulation model and experiments, respectively. The model discrepancy is addressed by updating the hyperparameters of the experimental GP model with existing simulation and experimental data. To enhance the model fidelity, critical simulation results and experimental observations are sequentially collected, which ensures an accurate reliability estimation. A multi-fidelity design optimization strategy is then proposed to provide reliable optimal solutions. In Chapter 8, a Bayesian mixture modeling technique is developed to aggregate the heterogeneous uncertainties in RBDO, where Bayesian inference techniques are employed to deal with the unknown parameters in the simulation models. By addressing the heterogeneous uncertainties into an aggregative reliability index, the derived optimal solution is ensured to avoid underestimation. The results from case studies and comparisons demonstrate the effectiveness of the proposed approaches.

In Chapter 3, the proposed approach reveals the advantage of using the LSTM, which can accurately make time-dependent response predictions based on only one time-series data. Future work will focus on improving the data efficiency and accuracy of reliability approximation. For example, starting from a less number of training data sets, adaptive sampling schemes can be applied to sequentially build new LSTM models. Critical samples will be iteratively identified until the reliability approximation converges. As a result, the stability can be enhanced while the computational costs can be further reduced. Instead of designing the width of the DFN, accounting for both depth and width of the network may improve the accuracy of minimum response predictions. Methods such as Bayesian optimization will be investigated in future. Moreover, the presented work will be further extended to dynamic systems, where the system response at current time step is related to previous actions and outputs.

10 REFERENCE

[1] Liu, F., Bayarri, M., Berger, J., Paulo, R., and Sacks, J., 2008, "A Bayesian analysis of the thermal challenge problem," Computer Methods in Applied Mechanics and Engineering, 197(29-32), pp. 2457-2466.

[2] Chojaczyk, A., Teixeira, A., Neves, L. C., Cardoso, J., and Soares, C. G., 2015, "Review and application of artificial neural networks models in reliability analysis of steel structures," Structural Safety, 52, pp. 78-89.

[3] Hu, Z., and Mahadevan, S., 2016, "A single-loop kriging surrogate modeling for time-dependent reliability analysis," Journal of Mechanical Design, 138(6), p. 061406.

[4] Kang, F., Xu, Q., and Li, J., 2016, "Slope reliability analysis using surrogate models via new support vector machines with swarm intelligence," Applied Mathematical Modelling, 40(11-12), pp. 6105-6120.

[5] Wang, S., Chen, W., and Tsui, K.-L., 2009, "Bayesian validation of computer models," Technometrics, 51(4), pp. 439-451.

[6] ZHOU, Z.-b., DONG, D.-d., and ZHOU, J.-l., 2006, "Application of Bayesian Networks in reliability analysis [J]," Systems Engineering-Theory & Practice, 6, pp. 95-100.

[7] Hu, Z., and Du, X., 2015, "Mixed efficient global optimization for time-dependent reliability analysis," Journal of Mechanical Design, 137(5), p. 051401.

[8] Wang, Z., and Chen, W., 2016, "Time-variant reliability assessment through equivalent stochastic process transformation," Reliability Engineering & System Safety, 152, pp. 166-175.

[9] Schöbi, R., Sudret, B., and Marelli, S., 2016, "Rare event estimation using polynomial-chaos kriging," ASCE-ASME Journal of Risk and Uncertainty in Engineering Systems, Part A: Civil Engineering, 3(2), p. D4016002.

[10] Bourinet, J.-M., 2016, "Rare-event probability estimation with adaptive support vector regression surrogates," Reliability Engineering & System Safety, 150, pp. 210-221.

[11] Balesdent, M., Morio, J., and Brevault, L., 2016, "Rare event probability estimation in the presence of epistemic uncertainty on input probability distribution parameters," Methodology and Computing in Applied Probability, 18(1), pp. 197-216.

[12] Keshtegar, B., and Meng, Z., 2017, "A hybrid relaxed first-order reliability method for efficient structural reliability analysis," Structural Safety, 66, pp. 84-93.

[13] Wang, G., and Ma, Z., 2017, "Hybrid particle swarm optimization for first-order reliability method," Computers and Geotechnics, 81, pp. 49-58.

[14] Lim, J., Lee, B., and Lee, I., 2014, "Second-order reliability method-based inverse reliability analysis using Hessian update for accurate and efficient reliability-based design optimization," International Journal for Numerical Methods in Engineering, 100(10), pp. 773-792.

[15] Lim, J., Lee, B., and Lee, I., 2016, "Post optimization for accurate and efficient reliability-based design optimization using second-order reliability method based on importance sampling and its stochastic sensitivity analysis," International Journal for Numerical Methods in Engineering, 107(2), pp. 93-108.

[16] Piric, K., 2015, "Reliability analysis method based on determination of the performance function's PDF using the univariate dimension reduction method," Structural safety, 57, pp. 18-25.

[17] Acar, E., Rais-Rohani, M., and Eamon, C. D., 2010, "Reliability estimation using univariate dimension reduction and extended generalised lambda distribution," International Journal of Reliability and Safety, 4(2-3), pp. 166-187.

[18] Liang, H., Cheng, L., and Liu, S., 2011, "Monte Carlo simulation based reliability evaluation of distribution system containing microgrids," Power System Technology, 10, pp. 76-81.

[19] Miao, F., and Ghosn, M., 2011, "Modified subset simulation method for reliability analysis of structural systems," Structural Safety, 33(4-5), pp. 251-260.

[20] Bichon, B. J., Eldred, M. S., Swiler, L. P., Mahadevan, S., and McFarland, J. M., 2008, "Efficient global reliability analysis for nonlinear implicit performance functions," AIAA journal, 46(10), pp. 2459-2468.

[21] Du, X., 2008, "Unified uncertainty analysis by the first order reliability method," Journal of mechanical design, 130(9), p. 091401.

[22] Adams, B. M., Bohnhoff, W., Dalbey, K., Eddy, J., Eldred, M., Gay, D., Haskell, K., Hough, P. D., and Swiler, L., 2009, "DAKOTA, a multilevel parallel object-oriented framework for design optimization, parameter estimation, uncertainty quantification, and sensitivity analysis: version 5.0 user's manual," Sandia National Laboratories, Tech. Rep. SAND2010-2183.

[23] Youn, B. D., and Choi, K. K., 2004, "A new response surface methodology for reliability-based design optimization," Computers & structures, 82(2-3), pp. 241-256.

[24] Zaman, K., and Mahadevan, S., 2017, "Reliability-based design optimization of multidisciplinary system under aleatory and epistemic uncertainty," Structural and Multidisciplinary Optimization, 55(2), pp. 681-699.

[25] Song, L.-K., Fei, C.-W., Wen, J., and Bai, G.-C., 2017, "Multi-objective reliability-based design optimization approach of complex structure with multi-failure modes," Aerospace Science and Technology, 64, pp. 52-62.

[26] Youn, B. D., and Wang, P., 2008, "Bayesian reliability-based design optimization using eigenvector dimension reduction (EDR) method," Structural and Multidisciplinary Optimization, 36(2), pp. 107-123.

[27] Gunawan, S., and Papalambros, P. Y., "A bayesian approach to reliability-based optimization with incomplete information," Proc. ASME 2006 International Design Engineering Technical Conferences and Computers and Information in Engineering Conference, American Society of Mechanical Engineers, pp. 1157-1168.

[28] Youn, B., and Wang, P., "Bayesian reliability based design optimization under both aleatory and epistemic uncertainties," Proc. 11th AIAA/ISSMO Multidisciplinary Analysis and Optimization Conference, p. 6928.

[29] Zhuang, X., Pan, R., and Du, X., 2015, "Enhancing product robustness in reliability-based design optimization," Reliability Engineering & System Safety, 138, pp. 145-153.

[30] Shahraki, A. F., and Noorossana, R., 2014, "Reliability-based robust design optimization: a general methodology using genetic algorithm," Computers & Industrial Engineering, 74, pp. 199-207.

[31] Lee, I., Choi, K., Du, L., and Gorsich, D., 2008, "Dimension reduction method for reliability-based robust design optimization," Computers & Structures, 86(13-14), pp. 1550-1562.

[32] Hu, Z., and Du, X., 2016, "Reliability-based design optimization under stationary stochastic process loads," Engineering Optimization, 48(8), pp. 1296-1312.

[33] Yu, S., and Wang, Z., "Time-Dependent Reliability-Based Robust Design Optimization via Extreme Value Moment Method," Proc. ASME 2018 International Design Engineering Technical Conferences and Computers and Information in Engineering Conference, American Society of Mechanical Engineers, pp. V02BT03A056-V002BT003A056.

[34] Lee, I., Choi, K., Du, L., and Gorsich, D., 2008, "Inverse analysis method using MPP-based dimension reduction for reliability-based design optimization of nonlinear and multi-dimensional systems," Computer Methods in Applied Mechanics and Engineering, 198(1), pp. 14-27.

[35] Agarwal, H., and Renaud, J. E., 2006, "New decoupled framework for reliability-based design optimization," AIAA journal, 44(7), pp. 1524-1531.

[36] Zou, T., and Mahadevan, S., 2006, "A direct decoupling approach for efficient reliability-based design optimization," Structural and Multidisciplinary Optimization, 31(3), pp. 190-200.

[37] Jeong, S.-B., and Park, G.-J., 2017, "Single loop single vector approach using the conjugate gradient in reliability based design optimization," Structural and Multidisciplinary Optimization, 55(4), pp. 1329-1344.

[38] Jiang, C., Qiu, H., Gao, L., Cai, X., and Li, P., 2017, "An adaptive hybrid single-loop method for reliability-based design optimization using iterative control strategy," Structural and Multidisciplinary Optimization, pp. 1-16.

[39] Wang, Y., Zeng, S., and Guo, J., 2013, "Time-dependent reliability-based design optimization utilizing nonintrusive polynomial chaos," Journal of Applied Mathematics, 2013.

[40] Singh, A., Mourelatos, Z. P., and Li, J., 2010, "Design for lifecycle cost using time-dependent reliability," Journal of Mechanical Design, 132(9), p. 091008.

[41] Li, J., Chen, J.-b., and Fan, W.-l., 2007, "The equivalent extreme-value event and evaluation of the structural system reliability," Structural Safety, 29(2), pp. 112-131.

[42] Zhang, J., and Du, X., 2011, "Time-dependent reliability analysis for function generator mechanisms," Journal of Mechanical Design, 133(3), p. 031005.

[43] Chen, J.-B., and Li, J., 2007, "The extreme value distribution and dynamic reliability analysis of nonlinear structures with uncertain parameters," Structural Safety, 29(2), pp. 77-93.

[44] Hu, Z., and Du, X., 2012, "Time-dependent reliability analysis by a sampling approach to extreme values of stochastic processes," ASME Paper No. DETC2012-70132.

[45] Li, C.-C., and Der Kiureghian, A., 1995, "Mean out-crossing rate of nonlinear response to stochastic input," Proceedings of ICASP-7, Balkema, Rotterdam, pp. 295-302.

[46] Sudret, B., 2008, "Analytical derivation of the outcrossing rate in time-variant reliability problems," Structure and Infrastructure Engineering, 4(5), pp. 353-362.

[47] Kuschel, N., and Rackwitz, R., 2000, "Time-variant reliability-based structural optimization using SORM," Optimization, 47(3-4), pp. 349-368.

[48] Andrieu-Renaud, C., Sudret, B., and Lemaire, M., 2004, "The PHI2 method: a way to compute time-variant reliability," Reliability Engineering & System Safety, 84(1), pp. 75-86.

[49] Singh, A., Mourelatos, Z. P., and Nikolaidis, E., "An importance sampling approach for time-dependent reliability," Proc. Proceedings of the ASME 2011 International Design Engineering Technical Conferences and Computers and Information in Engineering

Conference, IDETC/CIE, pp. 28-31.

[50] Wang, Z., and Chen, W., 2017, "Confidence-based adaptive extreme response surface for time-variant reliability analysis under random excitation," Structural Safety, 64, pp. 76-86.

[51] Majcher, M., Mourelatos, Z. P., Geroulas, V., Baseski, I., and Singh, A., 2015, "An efficient method to calculate the failure rate of dynamic systems with random parameters using the total probability theorem," ARMY TANK AUTOMOTIVE RESEARCH DEVELOPMENT AND ENGINEERING CENTER WARREN MI.

[52] Li, M., and Wang, Z., "Sequential kriging optimization for time-variant reliability-based design involving stochastic processes," Proc. ASME 2017 International Design Engineering Technical Conferences and Computers and Information in Engineering Conference, American Society of Mechanical Engineers, pp. V02AT03A042-V002AT003A042.

[53] Hu, Z., Mahadevan, S., and Du, X., 2016, "Uncertainty Quantification of Time-Dependent Reliability Analysis in the Presence of Parametric Uncertainty," ASCE-ASME Journal of Risk and Uncertainty in Engineering Systems, Part B: Mechanical Engineering, 2(3), p. 031005.

[54] Wang, Z., and Wang, P., 2015, "A double-loop adaptive sampling approach for sensitivity-free dynamic reliability analysis," Reliability Engineering & System Safety, 142, pp. 346-356.

[55] Hu, Z., and Du, X., 2015, "First order reliability method for time-variant problems using series expansions," Structural and Multidisciplinary Optimization, 51(1), pp. 1-21.

[56] Rice, S. O., 1944, "Mathematical analysis of random noise," Bell System Technical

Journal, 23(3), pp. 282-332.

[57] Wang, Z., and Wang, P., 2012, "A nested extreme response surface approach for time-dependent reliability-based design optimization," Journal of Mechanical Design, 134(12), p. 121007.

[58] Jones, D. R., Schonlau, M., and Welch, W. J., 1998, "Efficient global optimization of expensive black-box functions," Journal of Global optimization, 13(4), pp. 455-492.

[59] Simpson, T., Mistree, F., Korte, J., and Mauery, T., "Comparison of response surface and kriging models for multidisciplinary design optimization," Proc. 7th AIAA/USAF/NASA/ISSMO Symposium on Multidisciplinary Analysis and Optimization, p. 4755.

[60] Queipo, N. V., Haftka, R. T., Shyy, W., Goel, T., Vaidyanathan, R., and Tucker, P. K., 2005, "Surrogate-based analysis and optimization," Progress in aerospace sciences, 41(1), pp. 1-28.

[61] Zhuang, X., and Pan, R., 2012, "A sequential sampling strategy to improve reliability-based design optimization with implicit constraint functions," Journal of Mechanical Design, 134(2), p. 021002.

[62] Deng, J., Gu, D., Li, X., and Yue, Z. Q., 2005, "Structural reliability analysis for implicit performance functions using artificial neural network," Structural Safety, 27(1), pp. 25-48.

[63] Chau, K.-W., 2007, "Reliability and performance-based design by artificial neural network," Advances in Engineering Software, 38(3), pp. 145-149.

[64] Cheng, J., Li, Q., and Xiao, R.-c., 2008, "A new artificial neural network-based response surface method for structural reliability analysis," Probabilistic Engineering

Mechanics, 23(1), pp. 51-63.

[65] Tan, X.-h., Bi, W.-h., Hou, X.-l., and Wang, W., 2011, "Reliability analysis using radial basis function networks and support vector machines," Computers and Geotechnics, 38(2), pp. 178-186.

[66] Orr, M. J., 1996, "Introduction to radial basis function networks," Technical Report, Center for Cognitive Science, University of Edinburgh.

[67] Hurtado, J. E., and Alvarez, D. A., 2001, "Neural-network-based reliability analysis: a comparative study," Computer methods in applied mechanics and engineering, 191(1), pp. 113-132.

[68] Yang, X., Liu, Y., Mi, C., and Tang, C., 2018, "System reliability analysis through active learning Kriging model with truncated candidate region," Reliability Engineering & System Safety, 169, pp. 235-241.

[69] Zhang, L., Lu, Z., and Wang, P., 2015, "Efficient structural reliability analysis method based on advanced Kriging model," Applied Mathematical Modelling, 39(2), pp. 781-793.

[70] Echard, B., Gayton, N., Lemaire, M., and Relun, N., 2013, "A combined importance sampling and kriging reliability method for small failure probabilities with time-demanding numerical models," Reliability Engineering & System Safety, 111, pp. 232-240.

[71] Zhao, H., Li, S., and Ru, Z., 2017, "Adaptive reliability analysis based on a support vector machine and its application to rock engineering," Applied Mathematical Modelling, 44, pp. 508-522.

[72] Sun, Z., Wang, J., Li, R., and Tong, C., 2017, "LIF: A new Kriging based learning function and its application to structural reliability analysis," Reliability Engineering &

System Safety, 157, pp. 152-165.

[73] Abbiati, G., Schöbi, R., Sudret, B., and Stojadinovic, B., "Structural Reliability Analysis Using Deterministic Hybrid Simulations and Adaptive Kriging Metamodeling," Proc. Proceedings of the 16th World Conference on Earthquake Engineering (16WCEE).

[74] Xue, G., Dai, H., Zhang, H., and Wang, W., 2017, "A new unbiased metamodel method for efficient reliability analysis," Structural Safety, 67, pp. 1-10.

[75] Deng, J., 2006, "Structural reliability analysis for implicit performance function using radial basis function network," International Journal of Solids and Structures, 43(11), pp. 3255-3291.

[76] Dubourg, V., Sudret, B., and Bourinet, J.-M., 2011, "Reliability-based design optimization using kriging surrogates and subset simulation," Structural and Multidisciplinary Optimization, 44(5), pp. 673-690.

[77] Picheny, V., 2009, "Improving accuracy and compensating for uncertainty in surrogate modeling," University of Florida.

[78] Acar, E., Kale, A., and Haftka, R., 2007, "Comparing effectiveness of measures that improve aircraft structural safety," Journal of Aerospace Engineering, 20(3), pp. 186-199.

[79] Starnes Jr, J. H., and Haftka, R. T., 1979, "Preliminary design of composite wings for buckling, strength, and displacement constraints," Journal of Aircraft, 16(8), pp. 564-570.

[80] Sjöstedt-de Luna, S., 2003, "The bootstrap and kriging prediction intervals," Scandinavian Journal of Statistics, 30(1), pp. 175-192.

[81] Zhao, L., Choi, K. K., Lee, I., and Gorsich, D., 2013, "Conservative surrogate model using weighted Kriging variance for sampling-based RBDO," Journal of Mechanical Design, 135(9), p. 091003.

[82] Viana, F. A., Picheny, V., and Haftka, R. T., 2010, "Using cross validation to design conservative surrogates," Aiaa Journal, 48(10), p. 2286.

[83] Li, M., Bai, G., and Wang, Z., 2018, "Time-variant reliability-based design optimization using sequential kriging modeling," Structural and Multidisciplinary Optimization, 58(3), pp. 1051-1065.

[84] Sakamoto, S., and Ghanem, R., 2002, "Simulation of multi-dimensional non-Gaussian non-stationary random fields," Probabilistic Engineering Mechanics, 17(2), pp. 167-176.

[85] Sakamoto, S., and Ghanem, R., 2002, "Polynomial chaos decomposition for the simulation of non-Gaussian nonstationary stochastic processes," Journal of engineering mechanics, 128(2), pp. 190-201.

[86] Saul, L. K., and Jordan, M. I., 1999, "Mixed memory markov models: Decomposing complex stochastic processes as mixtures of simpler ones," Machine learning, 37(1), pp. 75-87.

[87] Zhang, D., Han, X., Jiang, C., Liu, J., and Li, Q., 2017, "Time-dependent reliability analysis through response surface method," Journal of Mechanical Design, 139(4), p. 041404.

[88] Zhang, J., and Ellingwood, B., 1994, "Orthogonal series expansions of random fields in reliability analysis," Journal of Engineering Mechanics, 120(12), pp. 2660-2677.

[89] Stein, M., 1988, "Asymptotically efficient spatial interpolation with a misspecified covariance function," Ann. Statist, 16, pp. 55-63.

[90] Nocedal, J., and Wright, S. J., 2006, Sequential quadratic programming, Springer.

[91] Hu, Z., Li, H., Du, X., and Chandrashekhara, K., 2013, "Simulation-based time-dependent reliability analysis for composite hydrokinetic turbine blades," Structural and

Multidisciplinary Optimization, 47(5), pp. 765-781.

[92] Li, M., and Wang, Z., 2019, "Surrogate model uncertainty quantification for reliability-based design optimization," Reliability Engineering & System Safety, 192, p. 106432.

[93] Chan, K.-Y., Skerlos, S. J., and Papalambros, P., 2007, "An adaptive sequential linear programming algorithm for optimal design problems with probabilistic constraints," Journal of Mechanical Design, 129(2), pp. 140-149.

[94] Ahn, J., Kim, S., and Kwon, J.-H., 2005, "Reliability-based wing design optimization using trust region-sequential quadratic programming framework," Journal of aircraft, 42(5), pp. 1331-1336.

[95] Lee, I., Choi, K., and Zhao, L., 2011, "Sampling-based RBDO using the stochastic sensitivity analysis and Dynamic Kriging method," Structural and Multidisciplinary Optimization, 44(3), pp. 299-317.

[96] Li, M., and Wang, Z., 2019, "Active resource allocation for reliability analysis with model bias correction," Journal of Mechanical Design, 141(5).

[97] Kennedy, M. C., and O'Hagan, A., 2001, "Bayesian calibration of computer models," Journal of the Royal Statistical Society: Series B (Statistical Methodology), 63(3), pp. 425-464.

[98] Arendt, P. D., Apley, D. W., and Chen, W., 2012, "Quantification of model uncertainty: Calibration, model discrepancy, and identifiability," Journal of Mechanical Design, 134(10), p. 100908.

[99] Wang, Z., and Wang, P., 2014, "A maximum confidence enhancement based sequential sampling scheme for simulation-based design," Journal of Mechanical Design,

136(2), p. 021006.

[100] Xia, B., Lü, H., Yu, D., and Jiang, C., 2015, "Reliability-based design optimization of structural systems under hybrid probabilistic and interval model," Computers & Structures, 160, pp. 126-134.

[101] Li, M., and Wang, Z., 2020, "Reliability-Based Multifidelity Optimization Using Adaptive Hybrid Learning," ASCE-ASME J Risk and Uncert in Engrg Sys Part B Mech Engrg, 6(2).

[102] Jiang, Z., Chen, W., Fu, Y., and Yang, R.-J., 2013, "Reliability-based design optimization with model bias and data uncertainty," SAE International Journal of Materials and Manufacturing, 6(3), pp. 502-516.

[103] Lee, I., Choi, K. K., Noh, Y., Zhao, L., and Gorsich, D., 2011, "Sampling-based stochastic sensitivity analysis using score functions for RBDO problems with correlated random variables," Journal of Mechanical Design, 133(2), p. 021003.

[104] Li, M., and Wang, Z., 2018, "Confidence-Driven Design Optimization Using Gaussian Process Metamodeling With Insufficient Data," Journal of Mechanical Design, 140(12), p. 121405.

[105] Li, M., and Wang, Z., 2020, "Heterogeneous uncertainty quantification using Bayesian inference for simulation-based design optimization," Structural Safety, 85, p. 101954.

APPENDIX: COPYRIGHT DOCUMENTATION

A. Springer copyright document for chapter 4

SPRINGER NATURE LICENSE
TERMS AND CONDITIONS

Aug 06, 2020

This Agreement between Dr. Mingyang Li ("You") and Springer Nature ("Springer Nature") consists of your license details and the terms and conditions provided by Springer Nature and Copyright Clearance Center.

License Number	4881421126468
License date	Aug 03, 2020
Licensed Content Publisher	Springer Nature
Licensed Content Publication	Structural and Multidisciplinary Optimization
Licensed Content Title	Time-variant reliability-based design optimization using sequential kriging modeling
Licensed Content Author	Mingyang Li et al
Licensed Content Date	Mar 21, 2018
Type of Use	Thesis/Dissertation
Requestor type	non-commercial (non-profit)
Format	electronic
Portion	full article/chapter
Will you be translating?	no
Circulation/distribution	1 - 29
Author of this Springer Nature content	yes
Title	HETEROGENEOUS UNCERTAINTY QUANTIFICATION FOR RELIABILITY-BASED DESIGN OPTIMIZATION
Institution name	Michigan Technological University
Expected presentation date	Aug 2020
Requestor Location	Dr. Mingyang Li Woodmar Drive Apartment C Houghton, MI 49931 United States Attn: Dr. Mingyang Li
Total	**0.00 USD**
Terms and Conditions	

Springer Nature Customer Service Centre GmbH
Terms and Conditions

This agreement sets out the terms and conditions of the licence (the **Licence**) between you and **Springer Nature Customer Service Centre GmbH** (the **Licensor**). By clicking 'accept' and completing the transaction for the material (**Licensed Material**), you also confirm your acceptance of these terms and conditions.

1. Grant of License

1. 1. The Licensor grants you a personal, non-exclusive, non-transferable, world-wide licence to reproduce the Licensed Material for the purpose specified in your order only. Licences are granted for the specific use requested in the order and for no other use, subject to the conditions below.

1. 2. The Licensor warrants that it has, to the best of its knowledge, the rights to license reuse of the Licensed Material. However, you should ensure that the material you are requesting is original to the Licensor and does not carry the copyright of another entity (as credited in the published version).

1. 3. If the credit line on any part of the material you have requested indicates that it was reprinted or adapted with permission from another source, then you should also seek permission from that source to reuse the material.

B. ASME copyright document for chapter 6

Copyright Clearance Center Marketplace™

American Society of Mechanical Engineers ASME - License Terms and Conditions

This is a License Agreement between Mingyang Li ("You") and American Society of Mechanical Engineers ASME ("Publisher") provided by Copyright Clearance Center ("CCC"). The license consists of your order details, the terms and conditions provided by American Society of Mechanical Engineers ASME, and the CCC terms and conditions.

All payments must be made in full to CCC.

Order Date	12-Aug-2020	Type of Use	Republish in a thesis/dissertation
Order license ID	1055065-1	Publisher	AMERICAN SOCIETY OF MECHANICAL ENGINEERS,
ISSN	1050-0472	Portion	Chapter/article

LICENSED CONTENT

Publication Title	Journal of mechanical design	Country	United States of America
Author/Editor	AMERICAN SOCIETY OF MECHANICAL ENGINEERS.	Rightsholder	American Society of Mechanical Engineers ASME
Date	01/01/1990	Publication Type	Journal
Language	English		

REQUEST DETAILS

Portion Type	Chapter/article	Rights Requested	Main product
Page range(s)	051413	Distribution	Worldwide
Total number of pages	13	Translation	Original language of publication
Format (select all that apply)	Print, Electronic	Copies for the disabled?	No
Who will republish the content?	Academic institution	Minor editing privileges?	Yes
Duration of Use	Life of current and all future editions	Incidental promotional use?	No
Lifetime Unit Quantity	Up to 499	Currency	USD

NEW WORK DETAILS

Title	HETEROGENEOUS UNCERTAINTY QUANTIFICATION FOR RELIABILITY-BASED DESIGN OPTIMIZATION	Institution name	Michigan Technological University
Instructor name	Mingyang Li	Expected presentation date	2020-08-10

ADDITIONAL DETAILS

Order reference number	N/A	The requesting person / organization to appear on the license	Mingyang Li

REUSE CONTENT DETAILS

Title, description or numeric reference of the portion(s)	Active Resource Allocation for Reliability Analysis With Model Bias Correction	**Title of the article/chapter the portion is from**	Active Resource Allocation for Reliability Analysis With Model Bias Correction
Editor of portion(s)	N/A	**Author of portion(s)**	AMERICAN SOCIETY OF MECHANICAL ENGINEERS.
Volume of serial or monograph	141	**Issue, if republishing an article from a serial**	5
Page or page range of portion	13	**Publication date of portion**	2019-01-11

PUBLISHER SPECIAL TERMS AND CONDITIONS

Permission is granted for the specific use of the ASME paper as stated herein and does not permit further use of the materials without proper authorization. As is customary, we request that you ensure proper acknowledgment of the exact sources of this material, the authors, and ASME as original publisher.

CCC Republication Terms and Conditions

1. Description of Service; Defined Terms. This Republication License enables the User to obtain licenses for republication of one or more copyrighted works as described in detail on the relevant Order Confirmation (the "Work(s)"). Copyright Clearance Center, Inc. ("CCC") grants licenses through the Service on behalf of the rightsholder identified on the Order Confirmation (the "Rightsholder"). "Republication", as used herein, generally means the inclusion of a Work, in whole or in part, in a new work or works, also as described on the Order Confirmation. "User", as used herein, means the person or entity making such republication.

2. The terms set forth in the relevant Order Confirmation, and any terms set by the Rightsholder with respect to a particular Work, govern the terms of use of Works in connection with the Service. By using the Service, the person transacting for a republication license on behalf of the User represents and warrants that he/she/it (a) has been duly authorized by the User to accept, and hereby does accept, all such terms and conditions on behalf of User, and (b) shall inform User of all such terms and conditions. In the event such person is a "freelancer" or other third party independent of User and CCC, such party shall be deemed jointly a "User" for purposes of these terms and conditions. In any event, User shall be deemed to have accepted and agreed to all such terms and conditions if User republishes the Work in any fashion.

3. Scope of License; Limitations and Obligations.

    3.1. All Works and all rights therein, including copyright rights, remain the sole and exclusive property of the Rightsholder. The license created by the exchange of an Order Confirmation (and/or any invoice) and payment by User of the full amount set forth on that document includes only those rights expressly set forth in the Order Confirmation and in these terms and conditions, and conveys no other rights in the Work(s) to User. All rights not expressly granted are hereby reserved.

    3.2. General Payment Terms: You may pay by credit card or through an account with us payable at the end of the month. If you and we agree that you may establish a standing account with CCC, then the following terms apply: Remit Payment to: Copyright Clearance Center, 29118 Network Place, Chicago, IL 60673-1291. Payments Due: Invoices are payable upon their delivery to you (or upon our notice to you that they are available to you for downloading). After 30 days, outstanding amounts will be subject to a service charge of 1-1/2% per month or, if less, the maximum rate allowed by applicable law. Unless otherwise specifically set forth in the Order Confirmation or in a separate written agreement signed by CCC, invoices are due and payable on "net 30" terms. While User may exercise the rights licensed immediately upon issuance of the Order Confirmation, the license is automatically revoked and is null and void, as if it had never been issued, if complete payment for the license is not received on a timely basis either from User directly or through a payment agent, such as a credit card company.

    3.3. Unless otherwise provided in the Order Confirmation, any grant of rights to User (i) is "one-time" (including the editions and product family specified in the license), (ii) is non-exclusive and non-transferable and (iii) is subject to any and all limitations and restrictions (such as, but not limited to, limitations on duration of use or circulation) included in the Order Confirmation or invoice and/or in these terms and conditions. Upon completion of the licensed use, User shall either secure a new permission for further use of the Work(s) or immediately cease any new use of the Work(s) and shall render inaccessible (such as by

C. ASME copyright document for chapter 7

Copyright Clearance Center Marketplace™

American Society of Mechanical Engineers ASME - License Terms and Conditions

This is a License Agreement between Mingyang Li ("You") and American Society of Mechanical Engineers ASME ("Publisher") provided by Copyright Clearance Center ("CCC"). The license consists of your order details, the terms and conditions provided by American Society of Mechanical Engineers ASME, and the CCC terms and conditions.

All payments must be made in full to CCC.

Order Date	06-Aug-2020	Type of Use	Republish in a thesis/dissertation
Order license ID	1053792-1		
Series ISSN	2332-9017	Publisher	ASME
		Portion	Chapter/article

LICENSED CONTENT

Publication Title	ASCE-ASME Journal of Risk and Uncertainty in Engineering Systems, Part B. Mechanical Engineering	Publication Type	Other
		URL	http://risk.asmedigitalcollection.asme.org/journal.aspx?journalid=170
Rightsholder	American Society of Mechanical Engineers ASME		

REQUEST DETAILS

Portion Type	Chapter/article	Rights Requested	Main product
Page range(s)	12	Distribution	Worldwide
Total number of pages	12	Translation	Original language of publication
Format (select all that apply)	Electronic	Copies for the disabled?	No
Who will republish the content?	Academic institution	Minor editing privileges?	Yes
Duration of Use	Current edition and up to 5 years	Incidental promotional use?	No
Lifetime Unit Quantity	Up to 499	Currency	USD

NEW WORK DETAILS

Title	HETEROGENEOUS UNCERTAINTY QUANTIFICATION FOR RELIABILITY-BASED DESIGN OPTIMIZATION	Institution name	Michigan Technological University
		Expected presentation date	2020-08-05
Instructor name	Mingyang Li		

ADDITIONAL DETAILS

Order reference number	N/A	The requesting person / organization to appear on the license	Mingyang Li

REUSE CONTENT DETAILS

Title, description or numeric reference of the portion(s)	Reliability-Based Multifidelity Optimization Using Adaptive Hybrid Learning	Title of the article/chapter the portion is from	N/A
Editor of portion(s)	N/A	Author of portion(s)	N/A
Volume of serial or monograph	6	Issue, if republishing an article from a serial	2
Page or page range of portion	12	Publication date of portion	2020-03-30

PUBLISHER SPECIAL TERMS AND CONDITIONS

Permission is granted for the specific use of the ASME paper as stated herein and does not permit further use of the materials without proper authorization. As is customary, we request that you ensure proper acknowledgment of the exact sources of this material, the authors, and ASME as original publisher.

CCC Republication Terms and Conditions

1. Description of Service; Defined Terms. This Republication License enables the User to obtain licenses for republication of one or more copyrighted works as described in detail on the relevant Order Confirmation (the "Work(s)"). Copyright Clearance Center, Inc. ("CCC") grants licenses through the Service on behalf of the rightsholder identified on the Order Confirmation (the "Rightsholder"). "Republication", as used herein, generally means the inclusion of a Work, in whole or in part, in a new work or works, also as described on the Order Confirmation. "User", as used herein, means the person or entity making such republication.

2. The terms set forth in the relevant Order Confirmation, and any terms set by the Rightsholder with respect to a particular Work, govern the terms of use of Works in connection with the Service. By using the Service, the person transacting for a republication license on behalf of the User represents and warrants that he/she/it (a) has been duly authorized by the User to accept, and hereby does accept, all such terms and conditions on behalf of User, and (b) shall inform User of all such terms and conditions. In the event such person is a "freelancer" or other third party independent of User and CCC, such party shall be deemed jointly a "User" for purposes of these terms and conditions. In any event, User shall be deemed to have accepted and agreed to all such terms and conditions if User republishes the Work in any fashion.

3. Scope of License; Limitations and Obligations.

   3.1. All Works and all rights therein, including copyright rights, remain the sole and exclusive property of the Rightsholder. The license created by the exchange of an Order Confirmation (and/or any invoice) and payment by User of the full amount set forth on that document includes only those rights expressly set forth in the Order Confirmation and in these terms and conditions, and conveys no other rights in the Work(s) to User. All rights not expressly granted are hereby reserved.

   3.2. General Payment Terms: You may pay by credit card or through an account with us payable at the end of the month. If you and we agree that you may establish a standing account with CCC, then the following terms apply: Remit Payment to: Copyright Clearance Center, 29118 Network Place, Chicago, IL 60673-1291. Payments Due: Invoices are payable upon their delivery to you (or upon our notice to you that they are available to you for downloading). After 30 days, outstanding amounts will be subject to a service charge of 1-1/2% per month or, if less, the maximum rate allowed by applicable law. Unless otherwise specifically set forth in the Order Confirmation or in a separate written agreement signed by CCC, invoices are due and payable on "net 30" terms. While User may exercise the rights licensed immediately upon issuance of the Order Confirmation, the license is automatically revoked and is null and void, as if it had never been issued, if complete payment for the license is not received on a timely basis either from User directly or through a payment agent, such as a credit card company.

   3.3. Unless otherwise provided in the Order Confirmation, any grant of rights to User (i) is "one-time" (including the editions and product family specified in the license), (ii) is non-exclusive and non-transferable and (iii) is subject to any and all limitations and restrictions (such as, but not limited to, limitations on duration of use or circulation) included in the Order Confirmation or invoice and/or in these terms and conditions. Upon completion of the licensed use, User shall either secure a new permission for further use of the Work(s) or immediately cease any new use of the Work(s) and shall render inaccessible (such as by deleting or by removing or severing links or other locators) any further copies of the Work (except for copies printed on paper in accordance with this license and still in User's stock at the end of such period).